THE
PHYSICAL REVIEW
A Journal of Experimental and Theoretical Physics Established by E. L. Nichols in 1893
VOL. 57, NO. 10 MAY 15, 1940 SECOND SERIES

Intensity and Rate of Production of Mesotrons in the Stratosphere

MARCEL SCHEIN, WILLIAM P. JESSE AND E. O. WOLLAN
The University of Chicago, Chicago, Illinois
(Received February 23, 1940)

Two free balloon flights have been made with a coincidence-counter apparatus designed to record the vertical mesotron intensity and also the number of mesotrons produced in a 2-cm lead block by a non-ionizing radiation. The results show that the mesotron intensity at first increases with elevation and reaches a maximum at a pressure at about 6.6 cm Hg where the intensity is about 11 times that at sea level. Above this altitude the intensity falls off until at the lowest pressure reached (3.6 cm Hg) the intensity has decreased to about 8 times the sea-level value. Between $p=8$ cm and 50 cm Hg the mesotron intensity decreases almost exponentially with the mass of air traversed from which we obtain a constant "absorption coefficient" $\mu=1.2\times10^{-3}$ g^{-1} cm^{-2} for the mesotrons in this range. The production of mesotrons in the lead block becomes noticeable at about 35 cm pressure and increases with altitude at about the same rate as does the soft component. This is evidence that the photons are the agents responsible for a large part of the observed creation in the lead and on this assumption we calculate a cross section for the creation process $\sigma_{p\text{Pb}}=0.7\times10^{-27}$ cm^{-2} per nuclear particle in lead.

INTRODUCTION

DURING the past six months two free-balloon flights have been made for the purpose of determining the intensity and rate of production of mesotrons as a function of altitude. A counter train for threefold coincidences was used to measure the vertical intensity with 8 cm of lead inserted in the path of the particles to eliminate any soft radiation. Simultaneously measurements were made of the rate of production of mesotrons by non-ionizing radiation in a lead block of 2 cm thickness. Similar attempts to obtain penetrating secondaries from a non-ionizing soft radiation have been made by Rossi[1] and by Hsiung[2] at sea level and by Shonka[3] at an elevation 4300 meters with negative results. Positive evidence of such mesotron production was obtained by Schein and Wilson[4] in an airplane flight at an altitude of 7600 meters. A bibliography of previous work is given in the last named paper.

APPARATUS

The detailed arrangement of the counter set is shown in Fig. 1. Counters 1, 2 and 3 represent one coincidence set, and counters 2, 3 and 4 constitute another set. Since a particle which passes through either set of counters must penetrate at least 8 cm of lead, the coincidences registered here must be due to penetrating particles, i.e., to mesotrons. The top set of counters can be actuated only by mesotrons which have originated outside the apparatus, whereas the lower set can be set off either by a mesotron entering from the outside or by one

[1] B. Rossi, Zeits. f. Physik **82**, 151 (1933).
[2] D. S. Hsiung, Phys. Rev. **46**, 653 (1934).
[3] F. Shonka, Phys. Rev. **55**, 24 (1939).
[4] M. Schein and V. C. Wilson, Rev. Mod. Phys. **11**, 292 (1939).

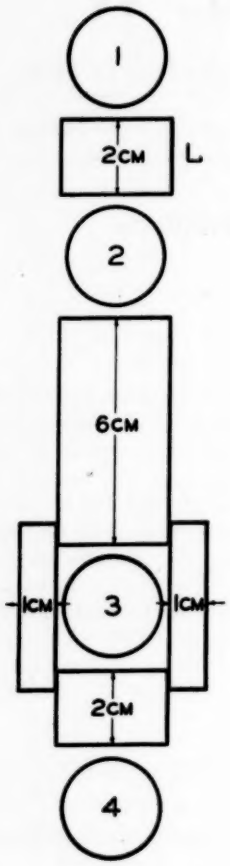

FIG. 1. Arrangement of counter apparatus.

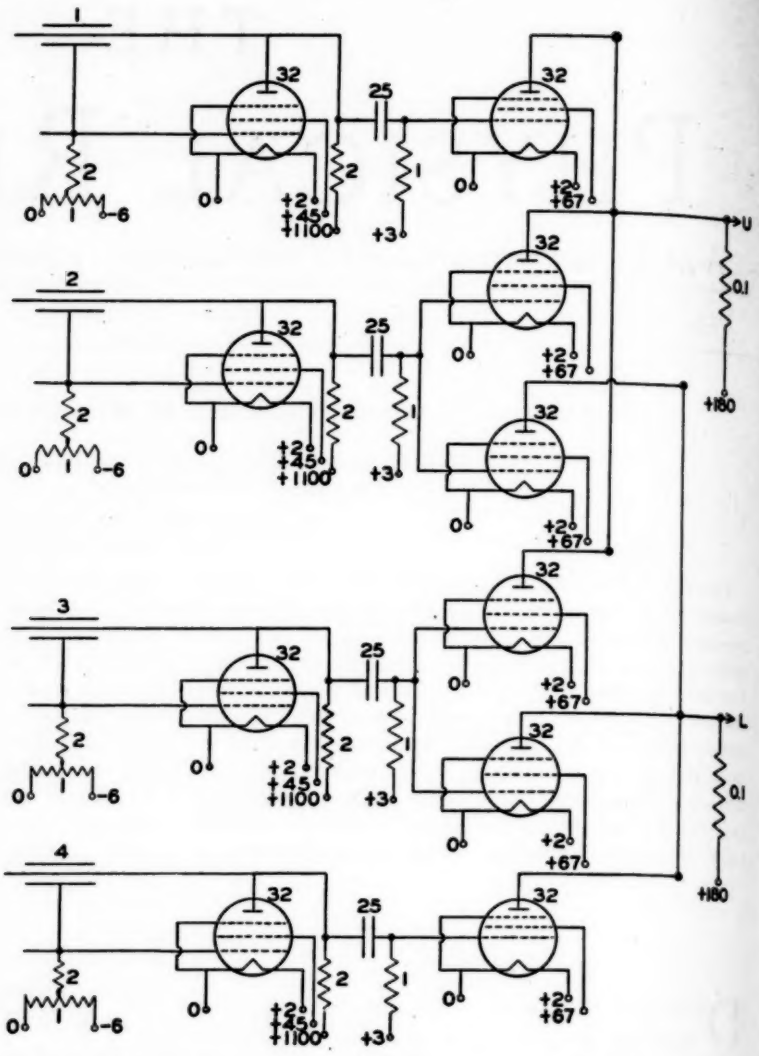

FIG. 2. Diagram of connections for the first two stages in the two threefold coincidence circuits. Capacities are given in microfarads, resistances in megohms and potentials in volts.

which is produced in the lead block L. If there is such a production of mesotrons in the lead block L by a non-ionizing radiation, one should observe a greater number of counts in the lower set of counters than in the upper set. Thus the difference in the counting rate between the two sets represents the rate of production of mesotrons in the 2-cm lead block.[5] In order to reduce the effect of softer particles originating from horizontal air showers, a shield of 1 cm of lead was placed on the sides of counter 3.

Each Geiger-Mueller tube was 10 cm in length and 2.5 cm in diameter, and was made according to the technique of Shonka.[3] The cut-off voltage for each of these tubes was approximately the same (about 850 volts) and the plateau for constant counting rate extended over a range of several hundred volts. The actual voltage used on all counter tubes was the same and was approximately 1100 volts.

The arrangement of the coincidence circuits is shown in Fig. 2. The discharges in each counter

[5] Because of the absorption of the incident mesotron in the last 2-cm block of lead, a correction amounting to about one percent of the rate for the upper coincidence train is to be added to the production rate as thus calculated. A similar minor correction has to be made for those mesotrons which are produced in different parts of the 2-cm lead block and which have not sufficient energy to traverse the lower counter train.

tube are quenched by an RCA 32 tube in a Neher-Harper circuit.[6] Since counter tubes 2 and 3 are common to both coincidence sets (Fig. 1), the pulse from each tube was divided at the output of the Neher-Harper tube and fitted into two different mixing circuits (U and L) by means of two 32 tubes. Careful tests by means of chance coincidences proved the complete independence of these two coincidence circuits. In each mixing circuit the pulse was first lengthened and then used to operate a Western Electric B 1003 relay which actuated a shutter for a light beam. The mesotron counts were thus registered on a photographic film. This film was wound on a cylinder which was rotated by clock work at the rate of one rotation per hour. By means of a helical screw the cylinder was also advanced in the direction of its axis by a distance equal to one millimeter per hour. Such a recorder gives a very compact record. On a film $30\times2\frac{1}{2}$ cm a record for a ten-hour flight was obtained with complete data from the two counter sets. A portion of the film from one of the flights which gives only the data from the lower counter set is shown in Fig. 3. The number of spots per cm, which is proportional to mesotron intensity, is observed to increase rapidly on passing from row to row, then to remain constant for a long period, and finally to decline slowly. This corresponds to the rapid rise of the apparatus, to the final equilibrium position, and considerably later to the initial stages of the descent.

A continuous record of the barometric pressure was obtained throughout the flight on a second drum which was driven at a slower rate by the same clock. The barometric capsule consisted of an evacuated metallic bellows inside which was placed a very stiff steel spring. Such an arrangement practically eliminates all hysteresis effects. Ground tests of the pressure device gave an average random error of about 1 mm of mercury. This barometric device has been in use in this laboratory for over a year and has given satisfactory results in some fifteen balloon flights. The temperature in the apparatus was also recorded throughout the flight by a device consisting essentially of a bimetallic strip.

The total weight of the equipment was 17 kilograms, the lead alone weighing $5\frac{1}{2}$ kilograms. Two flights were made with this apparatus, the first on August 14 and the second on October 20, 1939. The length of each flight was about twelve hours. In the first flight, 15 balloons were used and the minimum pressure reached was 6.6 cm of mercury. In the second flight with twenty-one balloons the minimum pressure was 3.5 cm. Altitude-time curves for both flights are given[7] in Fig. 4. It is interesting to note that in both cases the balloons reach an equilibrium position in the stratosphere where they remain at a constant altitude for four or five hours. Under these conditions the mesotron intensity can be determined for the corresponding pressure with very good accuracy.

Because of the rapid increase of the soft component of cosmic rays with altitude, the counting rate of each individual G-M tube also increases rapidly. This will result in a decreased efficiency in recording coincidences unless the resolving

[6] H. V. Neher and W. W. Harper, Phys. Rev. **49**, 940 (1936).

[7] Where, for convenience, altitudes have been given in this paper they have been taken from conversion tables in Humphreys' *Physics of the Air* (McGraw-Hill, 1929).

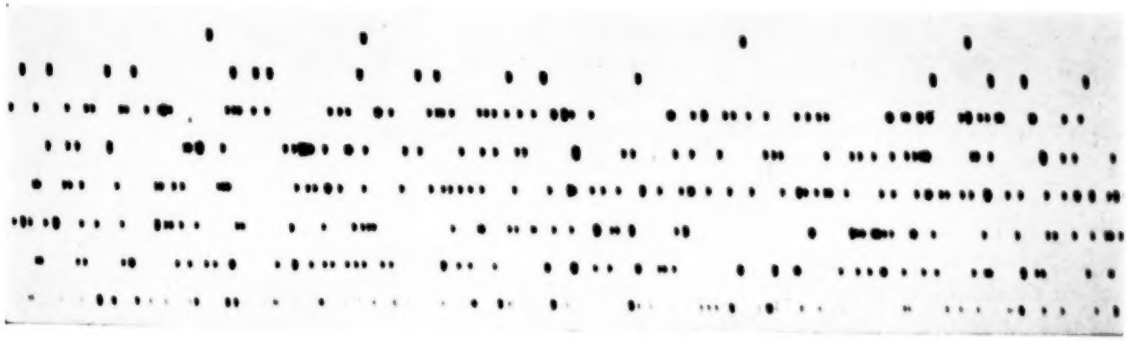

FIG. 3. A reproduction of part of the film showing a portion of each hour's record for threefold coincidence counts.

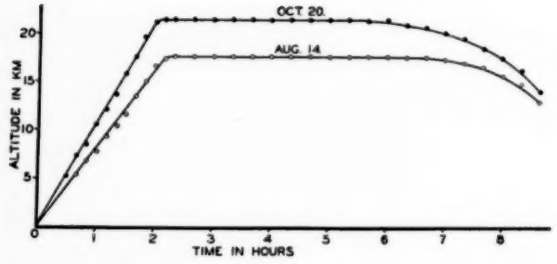

FIG. 4. Altitude time curves for the two flights. The balloons descended after nightfall and the cooling of the gas in the balloons accounts for the nonlinear character of the descent curve.

power of the tubes and circuits involved is sufficiently high.[4] Therefore the resolving time of each G-M tube alone and also the resolving time of each tube with its corresponding circuit was determined with a cathode-ray oscillograph. By this method and also by the method of chance coincidences the resolving time of each of the four different counter-tube circuits was found to be between 1 and 2×10^{-4} second. A further test was made by bringing a radium source near the apparatus while the coincidence set was counting vertical mesotrons. Even when the radium was brought so near that the counting rate in each individual G-M tube was greater than that expected in the stratosphere, no decrease in the efficiency of recording threefold coincidence counts was observed.

EXPERIMENTAL RESULTS

The combined results from the two flights are represented by the curve in Fig. 5. Curve *B*, which gives the number of coincidences recorded in the upper counter set (G-M tubes 1, 2 and 3), and yields directly the number of mesotrons as a function of the barometric pressure or of the altitude. Curve *A*, which corresponds to the number of coincidences recorded in the lower counter set (G-M tubes 2, 3 and 4), gives in addition to the number of mesotrons present at each altitude those which are produced by a non-ionizing radiation in the 2-cm lead block below the first G-M tube. Curve *C*, which is the difference between curves *A* and *B*, represents as a function of altitude the number of those mesotrons which are produced in the lead block by a non-ionizing radiation.

From curve *B* one sees that the mesotron intensity increases with altitude and reaches a maximum value at about 17.6 km (6.6 cm Hg). The intensity at the maximum is about 11 times that at sea level and, although from this point on, the intensity decreases with altitude, it is still about 8 times[8] the sea level value at 21.3 km (3.6 cm Hg). The vertical lines at the measured points represent the probable errors. At low altitudes the percentage errors are rather large, but they become less at higher altitudes where the counting rate is greater and where the equipment remained for a longer time. The top point from the first flight (at 6.6 cm Hg) represents the point at which the apparatus leveled off and remained for several hours with the result that several thousand counts were recorded. So few coincidences were recorded at altitudes below 4.5 km that reliable results could not be obtained with our equipment. Therefore, for this part of the curve we have used data obtained by Rossi, Hilberry and Hoag,[9] who have made a more extensive study of the mesotron intensity with about the same lead shield at points between sea level and the top of Mt. Evans.

From curve *C*, which gives as a function of altitude the number of mesotrons produced in

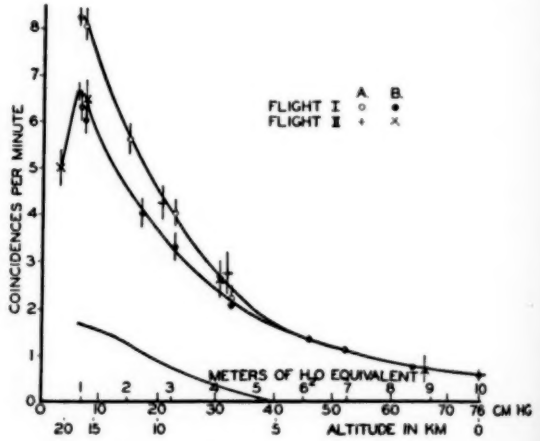

FIG. 5. The plot represents, (*A*—upper curve) coincidence altitude curve for lower counter set, (*B*—center curve) same for upper counter set (mesotron intensity as a function of altitude), (*C*—lower curve) difference between *A* and *B* (created mesotrons as a function of altitude).

[8] The point at 3.6 cm Hg was obtained on the second flight, for which part of the record was damaged and for this reason the accuracy is not as good as for the top point from the first flight.

[9] B. Rossi, H. Van N. Hilberry and J. B. Hoag, Phys. Rev. **56**, 837 (1939).

the 2-cm lead block, one sees that the production begins noticeably at about 6 km and increases with altitude attaining a value of about 25 percent of the total mesotron intensity at the maximum. Since our second flight did not give a complete record for the lower counter set our production curve extends to only 17.6 km which corresponds to the maximum altitude reached in the first flight.

In Fig. 6 is plotted the log of the intensity *vs.* the pressure. The fact that this curve is approximately a straight line between a pressure of 8 cm Hg and about 50 cm Hg shows that the mesotron intensity decreases in this range almost exponentially with the mass of air traversed. From this curve we obtain a constant absorption coefficient $\mu=1.2\times10^{-3}$ g^{-1} cm^{-2} in the range $p=8$ cm Hg to 50 cm Hg. From $p=50$ cm Hg to sea level the absorption coefficient changes from the above value to a value $\mu=0.7\times10^{-3}$ g^{-1} cm^{-2} at sea level as given by Wilson.[10]

Discussion

Variation of mesotron intensity with altitude

The first measurements of cosmic rays in the stratosphere with shielded equipment were made by Compton and Stephenson[11] in the "Century of Progress" balloon flight manned by Commander T. G. W. Settle and Lieutenant C. L. Fordney. They used an ionization chamber shielded with 6 cm lead and they reached an altitude corresponding to a pressure of about 5 cm Hg. Their results can be compared with those obtained by a vertical counter arrangement only after they have been reduced by a Gross transformation. If we should consider their reduced measurements as giving a mesotron curve to be directly comparable with ours, we find that the ratio of the intensity at the altitude of 17 km to that at sea level is much larger in their case than in ours. For comparison we have plotted their reduced curve together with ours in Fig. 7. We have arbitrarily fitted their curve to the top of our curve *A* of Fig. 5. We have considered their data more comparable with curve *A* than with curve *B* since their equipment would also be expected to record mesotrons which are produced in the lead shield. When their curve *C* and *S* and our curve *A* are fitted at the top one sees that except for a large hump in their curve the two give the same increase in intensity over the upper half of the atmosphere. In the lower half of the atmosphere ionization measurements with lead shields in general give a more rapid increase of intensity than is obtained with vertical counter arrangements, a fact which may be due to the inadequacy of the Gross transformation.[12]

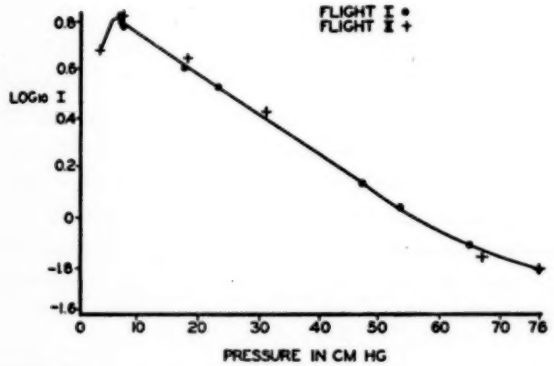

Fig. 6. The plot gives the logarithm of mesotron intensity as a function of pressure.

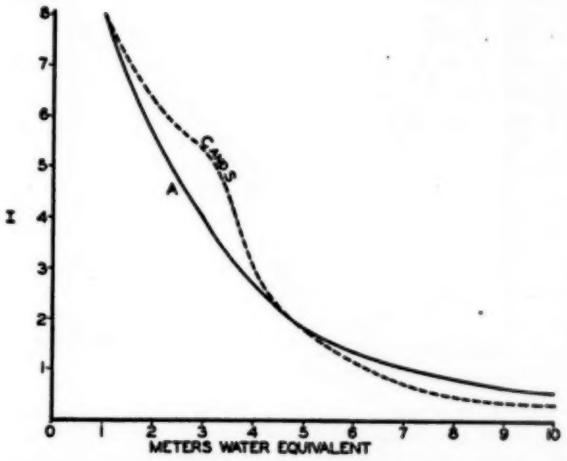

Fig. 7. Comparison of curve *A* of Fig. 5 with the shielded ionization chamber measurements of Compton and Stephenson reduced by means of the Gross transformation.

It is possible that at least part of the large hump in the *C* and *S* curve at an altitude of

[10] V. C. Wilson, Phys. Rev. **53**, 337 (1938).
[11] A. H. Compton and R. J. Stephenson, Phys. Rev. **45**, 441 (1934).
[12] Also, since *C* and *S* used 6 cm of lead whereas in curve *A* 10 cm were used, *C* and *S* will observe more slow mesotrons, which are relatively abundant at higher altitudes.

about 9 km arises from large showers which are known to increase rapidly with altitude.[13]

It seems that a more reliable measurement of the vertical mesotron intensity can be obtained with coincidence counters than with a shielded ionization chamber since in the latter case large showers will contribute much to the total ionization while with counters a large shower appears as a single coincidence. In our counter set such

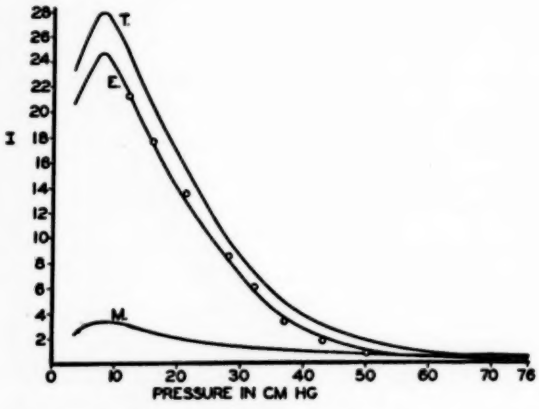

FIG. 8. The plot represents as a function of pressure, (T) the total vertical intensity as measured by Pfotzer, (M) vertical mesotron intensity from present experiments, (E) the difference between curves T and M which should give the vertical electron intensity. The open circles which represent the shower intensity as measured by Regener and Ehmert are seen to follow very closely curve E.

showers will be most effective from the sides which are not sufficiently shielded.[14]

Since the appearance of our first paper[15] on this subject a preliminary report of measurements of the intensity of the penetrating component by means of a vertical coincidence counter arrangement shielded by 10 cm of lead has been published by Dymond.[16] From three flights in which he used the radio method of transmitting the counts he finds that the mesotron intensity reaches a maximum at about 16 km at which altitude the intensity is about 9 times that at sea level. In this respect his measurements are in qualitative agreement with ours, but since he gives no curve for the dependence of mesotron intensity on altitude no exact comparison between his results and ours can be made. Dymond carried out his measurements at a geomagnetic latitude of about 59°N whereas ours were made at 52.5°N. The above-mentioned agreement between the two measurements indicates that, as is the case for the total intensity,[17] no appreciable latitude effect of the mesotron intensity in the stratosphere can be expected between 52.5°N and 59°N.

It is interesting to note the relative proportion of the soft and penetrating components of the cosmic rays as a function of altitude. A direct measurement of the total vertical intensity has been made by Pfotzer[18] with coincidence counters. His results for the total vertical intensity (curve T) are plotted together with our curve for the penetrating component (curve M) in Fig. 8. The difference between these two curves (curve E) should give the vertical electron intensity (soft component).

The shower intensity as a function of altitude has been measured by Regener and Ehmert[19] down to a pressure of 12.3 cm Hg and more accurately at lower altitudes by Johnson.[20] Their measurements are represented by the circles fitted to the soft component curve at the top point. One sees that the shower intensity curve follows very closely that of the soft component.

At the maximum of curve $T(p=8$ cm Hg) the mesotrons represent about 12 percent and the electrons about 88 percent of the total vertical intensity, while at sea level about 75 percent of the total vertical intensity consists of mesotrons and only the remaining 25 percent of electrons. The area under the mesotron curve from the top of the atmosphere down to sea level is about 10 percent of the area under the total vertical intensity curve.

[13] P. Auger and collaborators, Rev. Mod. Phys. **11**, 288 (1939).

[14] In a recent counter experiment carried out in an aeroplane up to an altitude of 8.5 km, measurements of the effect of lateral showers have been made with an arrangement similar to the one described above but in which one of the counters was moved out of line. A correction at this altitude for the effect of lateral showers was found to be not more than about three percent. A note on this experiment will be published in the near future by Schein, Wollan and Groetzinger. See also T. H. Johnson and J. G. Barry, Phys. Rev. **57**, 245 (1940).

[15] M. Schein, W. P. Jesse and E. O. Wollan, Phys. Rev. **56**, 613 (1939).

[16] E. G. Dymond, Nature **144**, 782 (1939).

[17] I. S. Bowen, R. A. Millikan and H. V. Neher, Phys. Rev. **53**, 855 (1938); H. Carmicheal and E. G. Dymond, Proc. Roy. Soc. **A171**, 321 (1939).

[18] G. Pfotzer, Zeits. f. Physik **102**, 23 (1936).

[19] E. Regener and A. Ehmert, Zeits. f. Physik **111**, 501 (1939).

[20] T. H. Johnson, Phys. Rev. **47**, 318 (1935).

Created Mesotrons

Curve *C* (Fig. 5), as we have mentioned above, gives as a function of altitude the number of mesotrons which are created by a non-ionizing radiation in the 2-cm lead block. Any mesotrons which are created with energies less than 1.2×10^{8} ev would not be recorded by our apparatus since they would not be able to penetrate the 8-cm lead shield. Also, if mesotrons are created in multiples,[21] the number recorded would be less than those created in the lead block since each multiple process would be recorded as a single event.

Since we are dealing here with mesotrons created by a non-ionizing radiation, it is reasonable as a first assumption to associate the production in the 2-cm lead block with photons, which we know are present in large quantities at high altitudes where the creation process becomes important. The photons as a source of mesotron creation has been suggested by several investigators.[22] A test of this hypothesis can to some extent be made by calculating the ratio of the created mesotrons to the number of incident photons under the assumption that the photon spectrum does not change appreciably in the range of altitudes between 7 km and 18 km. This ratio N_y/N_s at various altitudes is plotted in Fig. 9. N_y gives our values of the number of mesotrons produced in the lead block (Fig. 1) and N_s represents the intensity of the soft component as obtained by Regener and Ehmert.[19] Although, as is to be expected, the errors are large, the results are suggestive of a constant value for the ratio of created mesotrons to the number of incident photons. This lends support to the hypothesis that photons are responsible for the excess mesotrons which we observe in our lower counter set. On the basis of this result we calculate a cross section σ_{ph} for the creation process by photons[4] and obtain a value $\sigma_{ph}=0.7\times10^{-27}$ cm² per nuclear particle in lead.

The question arises whether the great number of mesotrons observed in the stratosphere and represented by curve *B* (Fig. 5) can be explained as a result of a similar creation process by photons in air. The observed value of the mesotron intensity (Fig. 5) at an altitude of 21.3 km (3.6 cm Hg) indicates that in an air layer corresponding to ½ meter water equivalent 8 times as many mesotrons have to be produced as are present at sea level. Hence either the cross section for mesotron production by photons at the top of the atmosphere must be considerably greater than the value $\sigma_{ph}=10^{-27}$ cm² estimated by Nordheim and Hebb,[21] from the mesotron intensity at sea level or part of the mesotrons must be produced by some other primary radiation,[23] probably by protons.[24] Both possibilities have been discussed by Nordheim,[25] who showed that in both cases a serious difficulty for the theory arises if one considers the great penetration and hardening of the mesotrons observed at great depths.[10] From this fact it follows that the nuclear cross section for the absorption of mesotrons must be considerably smaller (by a factor of about 100) than the cross section for the creation of a mesotron by a photon or proton. This conclusion follows rather directly from the presence of the great number of mesotrons in the atmosphere (large creation cross section) in contrast to the great penetrating power of the mesotrons in great depths (small

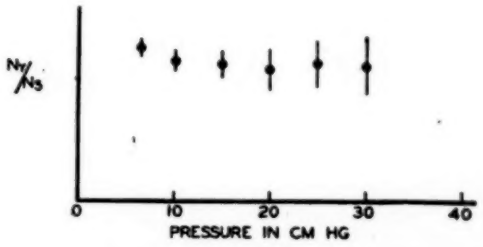

Fig. 9. The plot shows the approximate constancy of the ratio in purely arbitrary units of Ny to N_S where Ny is the number of mesotrons produced in the 2-cm lead block and N_S is the intensity of the soft component as measured by Regener and Ehmert.

[21] L. W. Nordheim and M. H. Hebb, Phys. Rev. **56**, 494 (1939).

[22] H. T. Bhabha, Proc. Roy. Soc. **A164**, 257 (1938); W. Heitler, Proc. Roy. Soc. **A166**, 529 (1938); M. Kobayasi and T. Okayama, Proc. Phys. Math. Soc. Japan **21**, 1 (1939).

[23] Since the energy of the primary electrons at the top of the atmosphere is considerably higher than at the peak of the transition curve (16.6 km) there is a possibility that primary electrons produce energetic photons in the lead of the counter train which can then create mesotrons somewhere in the lead. Such a process would give rise to a coincidence in both counter sets and could be partly responsible for the great number of mesotron counts measured in the upper counter set at an altitude corresponding to 3.6 cm Hg.

[24] T. H. Johnson, Rev. Mod. Phys. **11**, 208 (1939).

[25] L. W. Nordheim, Phys. Rev. **56**, 502 (1939).

absorption cross section). In this respect mesotrons seem to behave quite differently from high energy electrons where the cross section for pair creation by photons is of the same order of magnitude as that of the production of a photon by an electron.

Recalling the evidence brought forward by Bowen, Millikan and Neher[26] that the number of primary cosmic-ray particles is about 10 percent of the number of ionizing particles at the peak of the altitude ionization curve, it will be seen from Fig. 8 that the number of mesotrons at the maximum is likewise greater than the number of primary particles. This means, of course, that on the average there corresponds to each primary ray approximately one produced mesotron.

The Energy of the Mesotrons

In Fig. 6 where the log of the mesotron intensity is plotted against the pressure we see that the absorption coefficient remains approximately constant over the range from 50 cm Hg to 8 cm Hg. From this we can conclude that the average energy of the mesotrons in this altitude range remains approximately constant. In order that this can be the case the loss of mesotrons and the change of the energy spectrum by absorption must be nearly balanced by mesotrons which are added by creation.

Since at sea level the maximum of the energy spectrum[27] between 1 and 2×10^9 ev corresponds to an absorption coefficient of 0.7×10^{-3} g^{-1} cm^{-2}, the observed coefficient of 1.2×10^{-3} g^{-1} cm^{-2} above 5 km indicates that the energy maximum should occur at a value not greater than 10^9 ev.[28] Many of the produced mesotrons in the stratosphere must be of an energy considerably lower than 10^9 ev in order to maintain an approximately constant value of the mean energy of the mesotrons.

The energy of the primary cosmic-ray particles entering the earth's atmosphere as determined by Bowen, Millikan and Neher[17] has its maximum at about 6×10^9 ev. Taking into account that for primary electrons a considerable reduction of their energy takes place by cascade processes in the atmosphere,[29] one finds that the mean energy of the photons at the peak of the transition curve for the soft component (8 cm Hg) should be about 10^9 ev, which is of the same order of magnitude as the mean energy of the mesotrons estimated from the absorption curve of Fig. 6.

The result that at least the great majority of the mesotrons in the stratosphere must have energies around 10^9 ev is a direct proof of their secondary origin. This follows from the fact that no singly charged particles with energies smaller than about 3×10^9 ev can penetrate through the barrier of the earth's magnetic field at a geomagnetic latitude of 52.5°N.[30]

The writers wish to express to Professor A. H. Compton at whose suggestion this whole series of experiments was initiated, their appreciation of his continued interest.

[26] I. S. Bowen, R. A. Millikan and H. V. Neher, Phys. Rev. **53**, 217 (1938).
[27] H. Jones, Rev. Mod. Phys. **11**, 235 (1939).
[28] This conclusion is supported by measurements recently made by M. Schein, E. O. Wollan and G. Groetzinger, who found by absorption measurements in lead that at 8.5 km altitude about 30 percent of the mesotrons have their energies between 2×10^8 and 5×10^8 ev.
[29] J. F. Carlson and J. R. Oppenheimer, Phys. Rev. **50**, 493 (1937); R. Serber, Phys. Rev. **54**, 311 (1938).
[30] G. Lemaître and M. S. Vallarta, Phys. Rev. **50**, 493 (1936).

Energy Release from $Be^9(d,\alpha)Li^7$ and the Production of Li^{7*}

ELIZABETH RIDDLE GRAVES
Ryerson Physical Laboratory, University of Chicago, Chicago, Illinois
(Received March 4, 1940)

The α-particles from $Be^9(d,\alpha)Li^7$ have been investigated with a variable air pressure absorption cell, ionization chamber and linear amplifier. It has been established that there are two groups of α-particles differing at 760 mm pressure and 15°C by 3.08±0.10 mm range reduced to zero bombarding voltage. The groups have been shown to be associated with the production of Li^7 in the ground state and in an excited state. At 239 kv bombarding voltage, the excited state is formed 1.7 times as often as the ground state. The energy balance, Q, associated with the production of the ground state has been determined to be 7.093±0.022 Mev. The energy of the excited level has been determined to be 494±16 kev. The total yield curve for α-particles has been investigated from 235 kv to 390 kv bombarding voltage. The measured value for the energy of the excited level in Li^7 is discussed in connection with values from other reactions in which Li^7 is an end product and with γ-ray measurements of the level.

INTRODUCTION

IT has been shown that Li^7 is formed partially in an excited state of relatively low energy in the reactions

$$Li^6+H^2\rightarrow Li^7+H^1+Q_1,^{1-3} \quad (1)$$

$$B^{10}+n\rightarrow Li^7+He^4+Q_2.^{4-7} \quad (2)$$

The estimates of the energy of the excitation level, however, have diverged widely. It is to be expected that Li^7 might also be formed in an excited state in the process

$$Be^9+H^2\rightarrow Li^7+He^4+Q_3, \quad (3)$$

particularly since the intermediate nucleus, B^{11}, and the end products, Li^7+He^4, are identical with those of (2). Reaction (3) has been investigated by Williams, Haxby and Shepherd[8] with thick targets. They found only a single group of α-particles giving a value for Q_3 of 6.95 Mev. Since the most recent energy release measurements on other reactions performed in this laboratory[9] predict a value of 7.04±0.06 Mev, it seemed appropriate to perform a similar investigation with thin targets to redetermine Q_3 and to ascertain whether any structure might appear in the α-particle spectrum indicating the formation of Li^{7*}.

APPARATUS

The Cockcroft Walton circuit previously described[10] was used to accelerate deuterons pulled by a probe from a low voltage arc source to energies of from 200 to 350 kev. The beam was magnetically analyzed and collimated through 0.794-cm apertures by an aluminum tube 16.5 cm long. The target was mounted to allow for preheating by a platinum filament. A negative potential of 300 volts to prevent entrance of secondaries from the collimating tube was applied to the target chamber which was insulated as a Faraday cage. Beams which measured from 15 to 20 microamperes at the target were used. The current integrator which tripped the counter was adjusted so that about 75 to 100 counts were included in the counting period. The disintegration products emitted at 90°±2° 15′ were counted after passage through the variable air pressure absorption cell described by Smith.[9] Thin windows (about 2 mm air equivalent) of

[1] L. H. Rumbaugh and L. R. Hafstad, Phys. Rev. **50**, 681 (1936).
[2] J. H. Williams, W. G. Shepherd and R. O. Haxby, Phys. Rev. **52**, 390 (1937).
[3] L. H. Rumbaugh, R. B. Roberts and L. R. Hafstad, Phys. Rev. **54**, 657 (1938).
[4] O. Haxel, Zeits. f. Physik **104**, 7–8, 540 (1937).
[5] C. O'Ceallaigh and W. T. Davies, Proc. Roy. Soc. London **A167**, 81 (1938).
[6] M. S. Livingston and J. G. Hoffman, Phys. Rev. **53**, 227 (1938).
[7] W. Maurer and J. B. Fisk, Zeits. f. Physik **112**, 7–8 436 (1939).
[8] J. H. Williams, R. O. Haxby and W. G. Shepherd, Phys. Rev. **52**, 1031 (1937).
[9] N. M. Smith, Jr., Phys. Rev. **56**, 548 (1939); S. K. Allison, L. S. Skaggs and N. M. Smith, Jr., Phys. Rev. **57**, 550 (1940), a correction to previously published Q_3 for $Be^9(p,\alpha)Li^6$.
[10] G. T. Hatch, Phys. Rev. **54**, 165 (1938).

Newskin were mounted at each end of the cell on copper microphone screening of transmission coefficient 0.315. In order to use the cell at less than atmospheric pressures, the window facing the ionization chamber was mounted on the outside of the cell. The entire cell, insulated from the target chamber by a Bakelite bushing, was raised by batteries to a potential of 225 volts and formed the front cap of an ionization chamber 3 mm deep. The collecting button of the ionization chamber connected directly to the grid of a 954 acorn tube in the first stage of a linear amplifier.

The pulses from the linear amplifier were recorded through a scale-of-sixteen dividing circuit by a Cenco mechanical counter. The bias voltage on the scaling circuit was read with a voltmeter and frequently checked and adjusted if necessary. The output of the amplifier was also fed into a 5-inch cathode-ray oscillograph so that conditions could be checked visually. It was found that with these large beams, secondaries from the target striking the front of the absorption cell caused a bad disturbance in the background. This was eliminated by deflecting the secondaries with a small electromagnet.

Thin targets were made by vaporizing BeF_2 from a platinum wire in an oxygen flame. The BeF_2 vapor was condensed on a cold nickel button placed in the tip of the flame for a few seconds. This process was repeated many times in order to obtain targets of sufficient strength. Two thin targets were used for the data reported. One was roughly three or four times as strong as the other, but both yielded thin target curves as judged by comparison with curves from a thin Po source.

Experimental Procedure

The type of number-*vs.*-range curve which is obtained from the bombardment of a thin target depends upon the bias voltage used to select the threshold of ionization which shall be recorded as a count. If the bias is set at a low voltage so that small amounts of ionization will be recorded, a plateau curve which falls to zero in several mm of range is obtained for a single group of α-particles. The point of steepest slope differs from the mean range of the group by a small constant equal to the depth of penetration into the chamber necessary to produce a count. If there are two groups of α-particles separated by a small range difference, the front of the curve will have a hump in it and two points of maximum slope corresponding to the two mean ranges. Also if, as in this reaction, longer range particles whose ionization is fairly constant over the part of the curve in question are present, they will produce a background which is subject to statistical fluctuations which add to the fluctuations of the shorter range groups. Thus, it may become impossible under such conditions of bias to resolve two groups of α-particles whose ranges differ by only a small amount. The bias voltage may be increased until a peaked curve is obtained which runs fairly constant at some low value, then rises rapidly to a maximum and falls to zero with a half-width at half-maximum of about 1 mm. Under these conditions, fluctuations from the lower ionization groups are eliminated and the resolving power is greatly increased. Two distinct α-particle groups then produce a curve which is the sum of two such peaked curves of similar shape. Since range is directly proportional in our experiment to cell pressure, the number *vs.* cell pressure curve corresponds to the number *vs.* range curve.

In making these measurements, a series of curves (number-*vs.*-cell pressure) were taken at various bias voltages with a thin Po source. That voltage was selected which gave the narrowest peaked curve without too great a sacrifice of maximum height. With higher bias voltage, the height was cut down and the half-width of the curve was hardly changed at all. This bias voltage was then used for the Be+D run. Since the amplification changed from day to day with charging of batteries etc., the correspondence of bias voltage with threshold of ionization could only be relied upon during the few hours consumed in a particular run. Consequently, this selection of bias voltage had to be made anew for each run. For two of the determinations of Q_3, the Po run and the Be target run were made consecutively. For the other two, the Be curves were compared with Po curves of corresponding threshold of ionization taken through identical cell windows but obtained on

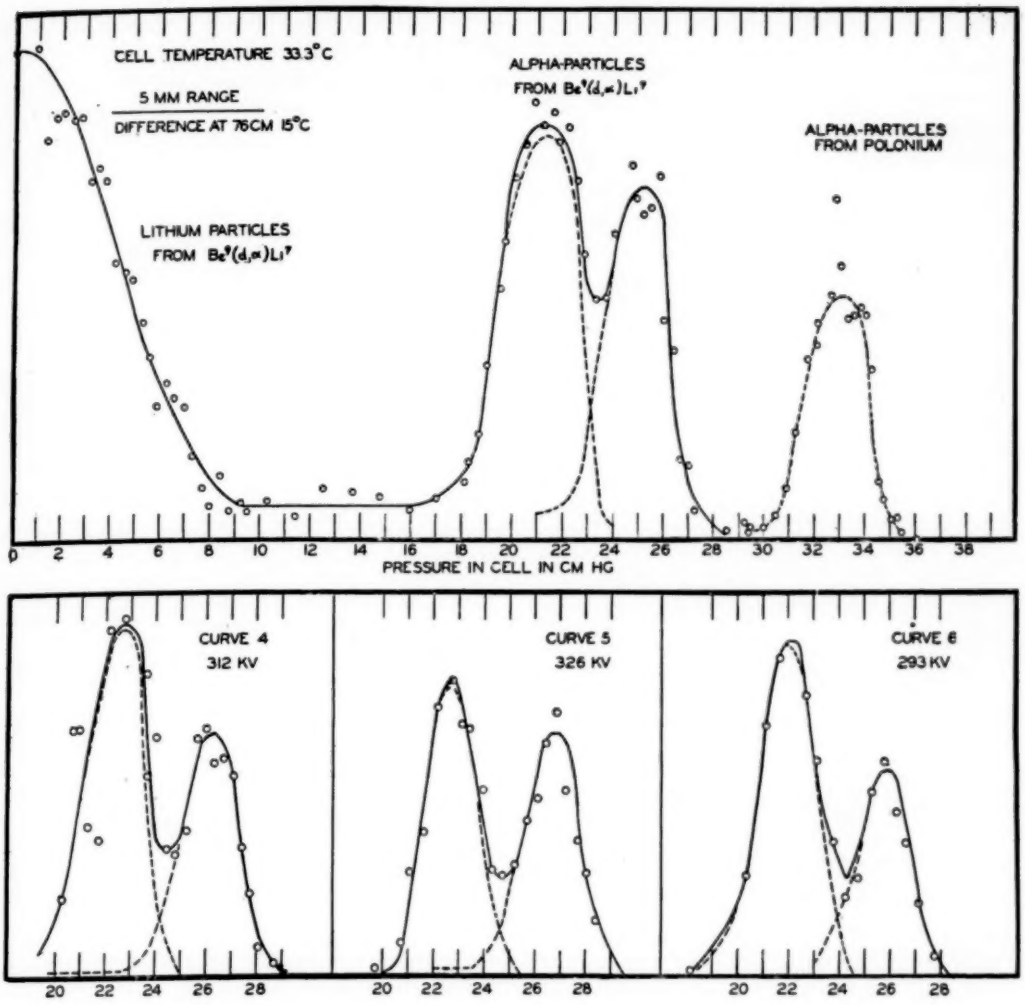
CELL TEMPERATURE 33.3°C
5 MM RANGE
DIFFERENCE AT 76CM 15°C
LITHIUM PARTICLES FROM $Be^9(d,\alpha)Li^7$
ALPHA-PARTICLES FROM $Be^9(d,\alpha)Li^7$
ALPHA-PARTICLES FROM POLONIUM
0 2 4 6 8 10 12 14 16 18 20 22 24 26 28 30 32 34 36 38
PRESSURE IN CELL IN CM HG
CURVE 4
312 KV
CURVE 5
326 KV
CURVE 6
293 KV
20 22 24 26 28
20 22 24 26 28
20 22 24 26 28

FIG. 1. Analysis of disintegration products from beryllium under deuteron bombardment, showing particles of ranges under 4 cm. The points at the peak of the longest range artificial alpha-particle group represent the counting of about 150 particles.

different days. Consequently, weights of 10 and 5, respectively, have been used in averaging. The BeF_2 targets were heated before and during bombardment to prevent deposition and carbonization of oil, and the Po source was also heated. In every case the cell temperature was read frequently, and the barometer was watched for change. Cell pressure was read on an open end manometer connected directly to the cell. The reading after the cell had been pumped out thoroughly with a Cenco Hyvac pump was taken as the zero of pressure. CO_2 and H_2O were removed from room air before it was admitted to the cell. Sample curves are shown in Fig. 1.

Eleven curves are used for the determination of the energy difference between the two groups of α-particles. Po curves were not taken to establish the bias for all of them because after a little experience it was easy to select the proper bias by quickly running over the curve and adjusting for the heights of the maxima and minimum. Then a run was made with the bias voltage carefully kept constant throughout. Runs were taken with NaF and C targets to eliminate the possibility that α-particle groups from F or from carbon contamination might account for either of the groups in the doublet.

Resolution of the Doublet and Results

Each doublet curve was resolved in the following manner. The Po curves for various biases were reduced to the height of the high energy peak, and the Po curve which best fitted it with regard to front slope and width was drawn as the high energy component. Where consecutive Be and Po runs were made, the best curve was, of course, the corresponding Po curve. The curve representing the complete doublet joined the high energy component somewhere between the minimum and the second maximum. The low energy component was then derived by subtraction. This procedure gave components whose half-widths at half-maximum agreed in seven cases to within 0.1 mm range in about 1.1 mm. Now let P=critical pressure in cm Hg corresponding to center of peak measured at half-maximum, L=length of path in air in cell in cm, T=temperature of cell in degrees absolute, R=mean range in cm at 76.0 cm pressure, 15 degrees centigrade.

Then $$R=L\times P/76.0\times 288/T+c$$

where c is the sum of the air equivalents of the windows (about 2 mm each) and the penetration depth for counting which is a function of the threshold of ionization. Hence, the difference in range between two groups whose critical pressures, P_1 and P_2, have been measured is

$$\Delta R=R_1-R_2$$
$$=L\times 288/76.0\times(P_1/T_1-P_2/T_2)+c_1-c_2.$$

Table I. *Q_3 and ΔQ_3 from experimental data. (± values are root mean square deviations.) Weighted average $Q_3=7.093\pm0.022$ Mev; weighted average $\Delta Q_3=0.494\pm0.016$ Mev; range difference between two groups at $E_d=0$, (760 mm; 15°C), $\Delta R=3.08\pm0.10$ mm.*

E_d Mev	Curve No.	$R_{Po}-R_\alpha$ 15°C; 760 mm	Q_3 (Mev)	Wt.	ΔQ_3 (Mev)	Wt.	Av. I_{Li}^*/I_{Li}
0.351	1	0.658 cm	7.105	10	0.501	8	1.15
0.326	2	0.695	7.067	5	0.473	10	
	5				0.514	6	1.40
	11				0.509	10	
0.312	3	0.675	7.108	5	0.490	4	1.39
	4	0.699	7.066	10	0.487	9	
	6				0.500	4	
	7				0.531	2	1.69
	8				0.471	8	
	9				0.520	5	
0.254	10				0.487	8	1.72

If the same windows and threshold of ionization have been used in measuring P for each group, then $c_1-c_2=0$. Since both windows bulge in the same direction by the same amount, L is the length of the cell=6.699 cm. Because of the method of biasing and the proximity of the Po range and the artificial α-particle ranges, no significant corrections have to be applied.

From curves 1, 2, 3, 4, range differences between Po and the artificially produced α-particles are calculated for each of the two groups, and the corresponding energy differences, are taken from the 1938 Cornell range-energy curve for α-particles. The absolute energy for Po is taken to be 5.298 Mev from Lewis and Bowden[11] corrected according to Briggs'[12] new determination of $H\rho$ for RaC′ which was used as a standard for the Po energy determination. E_α is 5.298 Mev minus the measured energy difference. From the derived values of E_α, and the values of the deuteron energies E_d, the reaction energy Q_3 for the reaction

$$Be^9+H^2\rightarrow Li^7+He^4+Q_3$$

may be determined from the expression

$$Q_3=\left(1+\frac{4.00386}{7.01814}\right)E_\alpha-\left(1-\frac{2.01473}{7.01814}\right)E_d.$$

The numerical values in this expression are the masses of He^4, H^2, and Li^7, and the expression assumes conservation of energy and momentum at right angles to the deuteron beam.

If ΔE_α is the energy difference between the two alpha-particle groups, the decrement ΔQ_3 in the reaction energy corresponding to the production of the excited state of Li^7 is given with sufficient accuracy by

$$\Delta Q_3=(11/7)\Delta E_\alpha.$$

No polonium curves were taken with curves 5 to 11 to establish the absolute energy of either group. For these curves ΔR was computed by the method of resolution into components outlined above. The energy of the ground state group was computed theoretically using the ob-

[11] W. B. Lewis and B. V. Bowden, Proc. Roy. Soc. London **A145**, 235 (1934).
[12] G. H. Briggs, Proc. Roy. Soc. London **A157**, 183 (1936).

served Q_3 from curves 1, 2, 3, 4 and the bombarding voltage. This value was used as a reference point on the range energy curve from which to read the ΔE_α corresponding to ΔR.

The values obtained for Q_3 and ΔQ_3 are summarized in Table I. The weighted average for Q_3 of 7.093 ± 0.022 Mev lies within the range of predicted values, which is 7.04 ± 0.06 Mev, and establishes the higher energy group as the ground state group. The average intensity ratio I_{Li^8}/I_{Li} decreases gradually with increasing bombarding voltage.

The total yield curve from a thick target was investigated from 235 kv to 390 kv and is shown in Fig. 2. The plot $\log_{10} N$ against E_d gives a straight line which, if extrapolated to 210 kv, gives a yield of about 1×10^{-9} alpha-particle per deuteron. Since certain auxiliary experiments showed that the mass 2 spot of the deuteron beam contained over 90 percent deuterium, no correction for beam composition was made. The yield at 210 kv agrees with the experiments of Williams, Haxby and Shepherd[8] who found 1×10^{-9} alpha-particle per deuteron at 212 kv.

It is possible to derive Q_2 for

$$B^{10}+n\rightarrow Li^7+He^4+Q_2 \qquad (2)$$

from fundamental measurements considering the following chain of reactions in conjunction with (2):

$$Be^9+H^2\rightarrow Li^7+He^4+Q_3, \qquad (3)$$

$$B^{10}+H^2\rightarrow Be^8+He^4+Q_4, \qquad (4)$$

$$Be^9+h\nu\rightarrow Be^8+n+Q_5, \qquad (5)$$

where

$$Q_3=7.093\pm0.022 \text{ Mev},$$
$$Q_4=17.80\pm0.15 \text{ Mev},^{13,14}$$
$$Q_5=-1.63\pm0.02 \text{ Mev}.^{15}$$

Thus

$$Q_2=-(2H^2-He^4)+Q_3+Q_4-Q_5.$$

Bainbridge and Aston have independently measured the doublet $(2H^2-He^4)$ with comparable results.[16] Using Bainbridge's value, 0.02561 ±0.00004 mass unit, we calculate

$$Q_2=2.68\pm0.17 \text{ Mev}.$$

Aston's value for the doublet, 0.02551 ± 0.00008 mass unit, gives

$$Q_2=2.78\pm0.17 \text{ Mev}$$

($\pm$ value is $[\Sigma \text{ (r.m.s. deviation)}^2]^{\frac{1}{2}}$). A weak point in the chain of reactions is $Q_4=17.80$ Mev with an uncertainty of 0.15 Mev. As pointed out by Allison,[14] however, any error in Q_4 is likely to be such as to reduce its value. Therefore, any error in Q_2 introduced by Q_4 will be more likely to cause a lower value than a higher one.

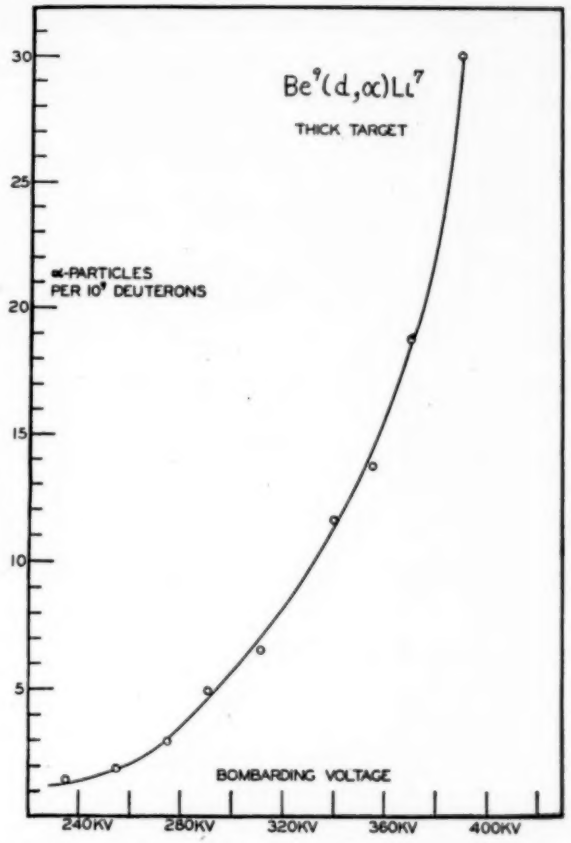

FIG. 2. Total yield of alpha-particles from bombardment of a thick target of metallic beryllium with deuterons.

DISCUSSION

Evidence for the production of an excited state of Li^7 has now been found in connection with

[13] J. D. Cockcroft and W. B. Lewis, Proc. Roy. Soc. London **A154**, 246 (1936).
[14] S. K. Allison, Phys. Rev. **55**, 626 (1939).
[15] L. S. Skaggs, Phys. Rev. **56**, 24 (1939). By considering a correction to the calculations on the electrostatic analyzer (see S. K. Allison, L. S. Skaggs and N. M. Smith, reference 9) the value -1.62 ± 0.02 Mev given in this reference has been lowered to -1.63 ± 0.02 Mev.
[16] M. S. Livingston and H. A. Bethe, Rev. Mod. Phys. **9**, 370 (1937).

TABLE II. *Summary of measurements on* $B^{10}(n, \alpha)Li^7$. *Where only one range group has been found, it is tabulated under* $Range_1$. *Where an additional group has been found, it is tabulated under* $Range_2$. *In rows 1 to 7, column 5 contains* Q_2 *calculated from* $Range_1$, *and column 6 contains* ΔQ_2 *calculated from* $Range_1 - Range_2$. *In row 8, column 5 contains the five energy groups reported by Maurer and Fisk, and column 6 contains the corresponding* ΔQs.

AUTHOR	METHOD	$Range_1$	$Range_2$	Q_2 (MEV)	ΔQ_2
Walen[17]	R_α by ioniz. ch.	8.5 mm		2.54	
Rotblat[18]	R_α by ioniz. ch. + Hoffman electrometer	8.18 mm		2.44	
Fünfer[19]	R_α by prop. counter + linear amplifier	8.6 mm		2.57	
Haxel[4]	R_α by variable pressure counter	9.4 mm	6.4 mm	2.80	0.92
Bower, Bretscher and Gilbert[20]	Total $R_\alpha + R_{Li}$ from Boric acid methyl ester in cloud ch.	7.0 mm		2.08	
O'Ceallaigh and Davies[5]	R_α from amorphous B on foil in cloud ch.	8.9 mm	7.15 mm	2.66	0.54
Livingston and Hoffman[6]	R_α by ioniz. ch. + linear amplifier	8.5 mm	7.15 mm	2.53	0.47
Maurer and Fisk[7]	Total E by ioniz. ch. + linear amplifier and oscillograph			$Q = 2.90$ $Q' = 2.70$ $Q'' = 2.49$ $Q''' = 2.26$ $Q'''' = 2.06$	 0.200 0.410 0.640 0.840

the following reactions:

$$Li^6 + H^2 \rightarrow Li^7 + H^1, \quad (1)$$

$$B^{10} + n \rightarrow Li^7 + He^4, \quad (2)$$

$$Be^9 + H^2 \rightarrow Li^7 + He^4, \quad (3)$$

$$Li^7 + He^4 \rightarrow Li^{7*} + He^4, \quad (6)$$

$$Li^7 + H^1 \rightarrow Li^{7*} + H^1, \quad (7)$$

$$Be^7 \rightarrow Li^7. \quad (8)$$

Reaction (1), investigated by Williams *et al.*[2] and by Rumbaugh *et al.*,[3] has been shown to yield two groups of protons separated by about 4.3 cm range. The energy level in Li^7 is computed to be 455 ± 15 kev. This is to be compared with our value of 494 ± 16 kev corresponding to an α-particle group separation at zero bombarding voltage of 3.08 ± 0.10 mm. However accurate the range difference measurements may be in each case, the energy level must be derived from the range energy curves for protons and α-particles. The energy correction necessary to bring the α-particle range difference into agreement with the proton range difference is $-7/11 \times 40$ kev $= -25$ kev, or that to bring the proton difference into agreement with the α-particle difference is $7/8 \times 40$ kev $= 35$ kev. A correction of this type necessitates a change in slope of the range energy curve. According to Holloway and Livingston,[21] the 1938 Cornell curve for α-particles is fitted experimentally between 2.5 cm and 2.8 cm range where it is known with good accuracy and again at the Po point of 3.840 cm range. If the curve is revised by connecting the 2.8-cm point and the 3.840-cm point by a straight line, this change is sufficient to reduce ΔQ_3 to 477 kev and changes Q_3 to 7.067 ± 0.020 Mev. It may be pointed out, however, that to reduce ΔQ_3 further by adjusting the range energy curve is not consistent with a constantly decreasing slope but would require putting a hump in the curve. Reducing ΔQ_3 to 477 kev in this manner would leave only a correction of $7/8 \times 20$ kev to be made in the proton difference. Since the data of Rumbaugh *et al.* extend over a bombarding voltage range of 200 kv, the slope change would

[17] R. J. Walen, Comptes rendus **202**, 1500 (1936).
[18] J. Rotblat, Nature **138**, 202 (1936).
[19] E. Fünfer, Ann. d. Physik **29**, 1 (1937).
[20] J. C. Bower, E. Bretscher and C. W. Gilbert, Proc. Camb. Phil. Soc. **34**, 290 (1938).
[21] M. G. Holloway and M. S. Livingston, Phys. Rev. **54**, 30, 37 (1938).

have to extend from about 24 cm to 32 cm range. It is fairly obvious that no such change can be made. Hence, it must be concluded that the value 455 kev from the proton difference cannot be changed appreciably by adjusting the range energy curve. Since agreement cannot be reached between the two values in this manner, we leave the value from the α-particle range difference at 494 kev and the corresponding Q_3 at 7.093 Mev. Either some unseen correction must be applied or the levels represented are not the same.

An excellent summary of the methods used and the results obtained up to 1938 for reaction (2) has been made by O'Ceallaigh and Davies[5] using the 1937 Cornell range energy curve for α-particles and its revision according to Blewett and Blewett. In Table II we have summarized the recent work, recalculating Q_2 from the published ranges by means of the revised 1938 Cornell curve which supersedes the others. The ranges published by Livingston and Hoffman[6] have been raised slightly by a recalculation of the ionization chamber penetration depth from the new range energy curve. Because the older mass values predicted $Q_2=2.99$ Mev, it was previously suggested that Walen,[17] Rotblat[18] and Fünfer[19] were probably observing the α-particles associated with the production of Li^{7*}. Estimates of the energy level were made on this basis. We have derived $Q_2=2.68\pm0.17$ Mev using Bainbridge's doublet measurement, and $Q_2=2.78\pm0.17$ Mev using Aston's doublet measurement. In view of this derived Q_2 and the work of O'Ceallaigh and Davies and of Livingston and Hoffman, Walen, Rotblat and Fünfer were probably observing the ground state group. If the range energy curve in the low energy region is reliable, the lower value $Q_2=2.68$ Mev is in better agreement with experiment.

Maurer and Fisk interpret their results as indicating four excitation levels in Li^7. We find, as shown in curve 1, no evidence for any other α-particle groups of comparable intensity between 1.9-cm range and the full range group. We can, therefore, say that no other excited states of comparable intensity are evident up to 1.8 Mev. Using the partition ratio found by Bower, Bretscher and Gilbert[20] for shorter range Li^7+He^4, $R_\alpha/R_{Li}=1.62$, we calculate roughly that the Li particles should have a range of about 1.6 cm. This range is represented on curve 1 by 5.6 cm cell pressure. The wider peak from 0 to 9 cm pressure is then ascribed to Li particles and its greater width is probably due to higher ionization in the chamber, to variation of charge, and to lack of resolution of the two range groups.

Because of the difficulty in making measurements on short range α-particles, the results from the $B^{10}(n,\alpha)Li^7$ reaction are more uncertain than the results from the $Li^6(d,p)Li^7$ and the $Be^9(d,\alpha)Li^7$ reactions. Therefore, comparison can be made only in a general way.

Li^{7*} should revert to the ground state with the emission of a γ-ray. Table III summarizes the most recent work on γ-rays in the low energy region from the bombardment of Li and the decay of Be^7. $Be+H^2$ bombardment has been investigated[22,23] for γ-rays of higher energy arising from excited states of B^{10}, but measurements have not been carried to a sufficiently low energy region to detect the γ-ray expected from Li^{7*}. The γ-ray measurements in general

TABLE III. *Summary of related γ-ray measurements.*

SOURCE	AUTHOR	METHOD OF E_γ MEAS.	E_γ(MEV.)
Li^6+d	Williams *et al.*[3]	Abs'n coeff. in Pb	0.400 ± 0.025
$Li^7+\alpha$	Webster[24]	Abs'n coeff. in Pb	0.600 ± 0.100
	Savel[25]	Abs'n coeff. in Pb	0.500
	Bothe[26]	β-ray spectrograph	0.390 and 0.590
	Speh[27]	Abs'n coeff. in Pb	0.700 ± 0.070
Li^7+p	Fowler and Lauritsen[28]	Abs'n coeff. compared with N^{13} rad'n	0.495 ± 0.025
$Be^7\rightarrow Li^7$	Rumbaugh *et al.*[3]	Abs'n coeff. compared with N^{13} rad'n	0.425 ± 0.025

are not reliable enough to compare critically with the energy differences from particle range differ-

[22] H. R. Crane, L. A. Delsasso and W. A. Fowler, Phys. Rev. **47**, 782 (1935).
[23] H. R. Crane, J. Halpern and N. C. Oleson, Phys. Rev. **57**, 13 (1940).
[24] H. C. Webster, Proc. Roy. Soc. London **A136**, 428 (1932).
[25] P. Savel, Ann. de physique II **4**, 88 (1935).
[26] W. Bothe, Zeits. f. Physik **100**, 273 (1936).
[27] K. C. Speh, Phys. Rev. **50**, 689 (1936).
[28] W. A. Fowler and C. C. Lauritsen, Phys. Rev. **56**, 840 (1939).

ences. A direct comparison of the γ-rays from $Li^6(d,p)Li^7$ and $Be^9(d,\alpha)Li^7$ in the low energy region would be of interest.

The author wishes to express great appreciation to Professor Samuel K. Allison for his continued assistance and encouragement throughout this experiment, to Dr. Lester S. Skaggs for invaluable aid in taking data and to Mr. Leonard C. Miller for construction of the current integrator. The work was aided by a grant from the American Philosophical Society to Professor Allison.

MAY 15, 1940 PHYSICAL REVIEW VOLUME 57

Internal Scattering of Gamma-Rays

E. P. COOPER AND P. MORRISON
Department of Physics, University of California, Berkeley, California

(Received March 4, 1940)

If an element is irradiated with gamma-rays of sufficiently high energy, the upper limit of the Compton recoils is less than the minimum energy of photo- or conversion electrons from any shell. But electrons of energy between these two limits may be ejected in processes in which the momentum condition can be relaxed. Such processes are (1) the scattering of an external gamma-ray by a bound electron, where momentum can be taken up by the nucleus, (2) the internal scattering by the electrons of the radioactive atom itself, where the radiation field of the near-by nucleus can fulfill momentum conditions impossible for a plane wave. We consider the second case, for scattering of an electric dipole gamma-ray by s electrons. We use Dirac electron theory with Born approximation. The process is of order α compared to the internal conversion, as expected. Our small result indicates that most of the electrons observed in such a region—for instance from the 2.62-Mev gamma-ray of Th C″—are of instrumental origin. This is in agreement with the results of the latest experiments.

I. INTRODUCTION

IN the study of the electron energy spectrum of radioactive elements with the magnetic spectrograph, certain observers[1] found an unexpectedly large number of electrons in energy regions just below strong K-conversion lines. A particularly clear-cut case in point was that of the region 2.39–2.52 Mev in the spectrum of the thorium elements, in which really no electrons were expected. This is below the 2.62-Mev gamma-ray of ThC″, but near no other strong gamma-ray. Any electrons near 2.62 Mev and above the upper limit of the beta-ray spectrum at 2.25 Mev, must be indirectly produced by this gamma-ray.

The ordinary processes by which a gamma-ray can produce electrons are internal conversion, and photo-effect and Compton scattering in the material of the source. There is an upper limit to the energy that can be given a recoil electron in Compton scattering. In general this is $E_c=h\nu/(1+mc^2/2h\nu)$. The sharp K-conversion line sets a lower limit for both of the absorption processes: $E_K=h\nu-mc^2[1-(\alpha Z)^2]^{\frac{1}{2}}$. For any element E_K will be greater than E_c if only the gamma-ray energy, $h\nu$, is large enough. In the case mentioned this condition is fulfilled. In fact $E_K=2.52$ Mev and $E_c=2.39$ Mev. Thus, between 2.39 and 2.52 Mev, no electrons from these processes can appear. The problem was whether it was necessary to attribute the many electrons observed in the excluded region to unknown instrumental difficulties, or whether some other process for their production was actually involved.

Now, internal conversion and photo-effect are the only processes of first order in the interaction of matter and radiation; i.e., with a probability proportional to α, the fine structure constant. Any other process will be proportional to a higher power of α. Only one process seemed important here. This is internal scattering, which we shall

[1] Reported by Professor C. D. Ellis and F. Oppenheimer in discussion. Also W. J. Henderson, Proc. Roy. Soc. **A147**, 572 (1934).

define. It is of second order, proportional to α^2. It did not seem likely that this effect could account for all the observed electrons because α is only 1/137. We have calculated the probability of this effect in order definitely to decide about the instrumental origin of the unexpected electrons.

The two absorption processes internal conversion and photoelectric effect are closely related. Internal conversion is an analog to the photo-effect. However, the radiation is not a beam from an external source, but from the nucleus of the very atom whose electrons carry off the excitation energy which would otherwise go off as a gamma-quantum.[2] The chief difference between photo-effect and internal conversion is in the radiation field, which is a plane wave beam for photo-effect, but for internal conversion is the spherical wave of the nearby nuclear multipole. There is, of course, a process which differs from Compton scattering in the same way as internal conversion differs from photo-effect. This we call internal scattering. Here the excitation energy is not carried off by an electron alone, but is shared between an electron and a quantum. Just as the probability of Compton scattering is proportional to one higher power of the fine structure constant than the photo-effect, so internal scattering is related to conversion. Internal scattering has not previously been considered both because it is small compared to conversion, and because it does not yield any such direct information as do the sharp conversion lines, which give gamma-ray energies.

Internal scattering, unlike Compton effect, can give electrons in the energy range in question. The scattered quantum in the Compton effect cannot transfer an arbitrary fraction of its energy to the recoil electron because of the conservation of momentum. The incident plane wave has a well-defined momentum, and the electron is free. The total momentum must then be conserved between electron and quantum. The presence of a heavy body which can take up momentum without taking up energy will permit the transfer of any fraction of the gamma-ray energy to the recoil electron, and allow the emission of electrons in the excluded energy range. What we call internal scattering depends upon the absence of a unique momentum vector in the spherical field close to the nuclear multipole. Then the nucleus can take up momentum through the radiation field. We have not considered the effect of the Coulomb binding, which also allows the nucleus to take up momentum. That this omission of the binding is justified for a qualitative treatment of the internal scattering is shown by the experience with internal conversion, where calculations neglecting binding give a good estimate of the effect.

We have calculated the number of internally-scattered electrons as a function of electron energy for any gamma-ray energy, neglecting binding. We have considered scattering from s electrons only, since they have much the highest density at the nucleus. For gamma-ray energies safely above the threshold, the effect will be simply proportional to the electron density, and scattering from the s electrons in the K shell will give the bulk of the effect. We have found the formula only for electric dipole radiation. This is no essential restriction, since the dependence on multipole field is similar for scattering and conversion, this ratio, which is what is observed, will change little with multipole order. In the limit of high gamma-ray energy, $\nu\to\infty$, we get for the number of internally-scattered electrons in the range dE per electron internally converted in the K shell, for an electric dipole, neglecting binding:

$$\frac{N_E dE}{N_K}=\frac{\alpha}{\pi\nu^2}\left\{2\nu^2\left(\frac{\nu}{Q}-\frac{1}{\kappa}\right)+\frac{4}{\kappa}(2EQ-\nu^2)\ln\frac{\nu}{Q}-\frac{8E\nu}{\kappa}\ln\left[E-(E^2-1)^{\frac{1}{2}}\right]\right\}.$$

$Q=\nu-2E\kappa$. Where ν, κ and E are the energies of the initial and final quantum and the electron, respectively, in units of mc^2. We apply the above asymptotic formula to the example of ThC″. The gamma-ray is believed from conversion measurements to be an electric quadripole. The number of

[2] This should not be taken as an exact description of internal conversion. Actually each conversion electron represents, not the absorption of a gamma-ray, but an additional nuclear transition induced by the atomic electrons. The nucleus radiates essentially as though it were bare. Cf. H. M. Taylor and N. F. Mott, Proc. Roy. Soc. **A142**, 215–236 (1933).

internally scattered electrons turns out to be inappreciable. This is indeed in agreement with the absence of such electrons in the latest experiments.[3] The asymptotic expression gives about one electron scattered in the range in question for 30 in the K conversion. The exact formula gives half as many.

II. Calculations

We will find the rate of radiation of the emitted gamma-ray from the electron current in the transition from initial to final state. The energy radiated per second per unit solid angle with frequency $c\kappa/2\pi$ from a current distribution $\mathbf{S}(x, y, z, t)$ is:

$$R_\kappa d\Omega_\kappa = \frac{c\kappa^2}{2\pi}\left|\int d\tau \mathbf{S}_\perp \exp\left[i\boldsymbol{\kappa}\cdot\mathbf{r}\right]\right|^2 d\Omega_\kappa \tag{1}$$

where $\mathbf{S}_\perp = (\mathbf{S}-\mathbf{n}(\mathbf{S}\cdot\mathbf{n}))$; $\mathbf{n}$ is a unit vector in the direction of radiation, and $\mathbf{r}$ is the position vector (x, y, z). We take the relativistic form of the current, appropriate to the energy range considered:

$$\mathbf{S} = e\psi^+\boldsymbol{\alpha}\varphi. \tag{2}$$

Here α is the vector whose components are the Dirac velocity matrices. ψ and φ are Dirac wave functions depending on r, t and spin. φ represents the electron in the final state, and ψ represents the initial state. We shall take the states normalized in a unit volume. We are interested in the electron transitions to a group of states in the energy range dE, the momentum direction being in a solid angle $d\Omega_E$. The number of these states is $(pE/h^3)dEd\Omega_E$. Therefore the energy radiated in $d\Omega_\kappa$ for electron transitions to $dEd\Omega_E$ is:

$$R_\kappa' d\Omega_\kappa d\Omega_E dE = \frac{c\kappa^2}{2\pi}\left(\frac{pE}{h^3}\right)\left|\int d\tau \mathbf{S}_\perp \exp\left[i\boldsymbol{\kappa}\cdot\mathbf{r}\right]\right|^2 d\Omega_\kappa d\Omega_E dE. \tag{3}$$

We consider transitions through intermediate states which are plane waves. In the intermediate states the electron has energy E_1 and momentum $\hbar k_1$; in the final state, E and $\hbar k$. The wave functions are then:

$$\begin{aligned}\psi &= u_0 e^{-imc^2 t} + \sum \frac{H_{01}u_1 \exp\left[-i\tau_1 E_1 t + i\boldsymbol{\kappa}_1\cdot\mathbf{x}\right]}{(\hbar\nu + mc^2) - E_1},\\ \varphi &= u_f \exp\left[iEt + i\boldsymbol{\kappa}\cdot\mathbf{x}\right] + \sum \frac{H_{1f}u_1 \exp\left[-i\tau_1 E_1 t + i\boldsymbol{\kappa}_1\cdot\mathbf{x}\right]}{E - (\hbar\nu + E_1)},\end{aligned} \tag{4}$$

where τ_1 is the sign of the energy of the intermediate state, and the u's are wave amplitudes for a state defined by a given value of spin and τ. The normalization to unit volume means that $\Sigma|u_s|^2 = 1$ where the subscript s refers to the components of the Dirac wave functions. We use the Born approximation. We take u_0 as $e^{-r/a}/(\pi a^3)^{\frac{1}{2}}$; $a = \hbar/mc\alpha Z$, and we shall treat a as large. H_{01} and H_{1f} are matrix elements of the perturbing Hamiltonian: $H = e(\varphi - \boldsymbol{\alpha}\cdot\mathbf{A})$, where φ and $\mathbf{A}$ are the scalar and vector potentials of the multipole field. We take the radiation field as that of an electric dipole oscillator of angular frequency ν, and moment D. (D will not have to be determined):

$$\mathbf{A} = \left(0, 0, \frac{D}{r}\cos\left[\frac{\nu r}{c} - \nu t\right]\right), \quad \varphi = -\int dtc \operatorname{div}\mathbf{A} = -c\int \frac{\partial A_z}{\partial z}dt. \tag{5}$$

The matrix elements will contain integrals which are not simple δ-functions in momentum space as

[3] A. Alichanian and S. Nikitin, Comptes rendus de l'Acad. des Sciences U. S. S. R. 19, 337 (1938).

they are for a plane wave radiation field. There occur the integrals:

$$\lim_{a\to\infty}\int d\mathbf{r}A_z\exp\left[i\boldsymbol{\kappa}_1\cdot\mathbf{x}-r/a\right]=a_1(e^{i\nu t}+e^{-i\nu t}),\quad \lim_{a\to\infty}\int d\mathbf{r}\varphi\exp\left[i\boldsymbol{\kappa}_1\cdot\mathbf{x}-r/a\right]=b_1(e^{-i\nu t}-e^{i\nu t}), \tag{6}$$

where

$$a_1=\frac{4\pi D\nu}{(\nu^2-k_1^2)};\quad b_1=\frac{(k_1)_z}{\nu}a_1.$$

When we put these into the expression (4) for the wave functions, and form the current we find for

$$\left|\int d\mathbf{r}\mathbf{S}_\perp\exp\left[i\boldsymbol{\kappa}\cdot\mathbf{r}\right]\right|$$

two time-dependent terms:

$$\mathbf{q}_1e^{-i\nu t}+\mathbf{q}_2e^{i\nu t}.$$

In squaring to get the rate of radiation we will get the proper result only if we make the replacement[4]

$$\left|\int d\mathbf{r}\mathbf{S}_\perp\exp\left[i\boldsymbol{\kappa}\cdot\mathbf{r}\right]\right|^2\to 2\mathbf{q}_1\cdot\mathbf{q}_2.$$

Doing this we find

$$R_\kappa' d\Omega_\kappa d\Omega_E dE=\frac{c\kappa^2}{2\pi}\left(\frac{pE}{h^3}\right)\mathbf{I}^+\cdot\mathbf{I}^- d\Omega_\kappa d\Omega_E dE, \tag{7}$$

where

$$\mathbf{I}^+=e^2\sum\int d\mathbf{r}\left\{\exp\left[i(\mathbf{k}_1+\boldsymbol{\kappa})\cdot\mathbf{r}\right]\frac{\left[-a_1(u_0,\boldsymbol{\alpha}_\perp u_1)(u_1,\alpha_z u_f)-b_1(u_0,\alpha_\perp u_1)(u_1,u_f)\right]}{E-(\hbar\nu+E_1)}\right.$$

$$\left.+\exp\left[-i(\mathbf{k}_1-\mathbf{k}-\boldsymbol{\kappa})\cdot\mathbf{r}\right]\frac{\left[-a_1(u_0,\alpha_z u_1)(u_1,\boldsymbol{\alpha}_\perp u_f)+b_1(u_0,u_1)(u_1,\boldsymbol{\alpha}_\perp u_f)\right]}{(\hbar\nu+mc^2)-E_1}\right\}, \tag{8}$$

$$\mathbf{I}^-(a_1,b_1)=\mathbf{I}^+(a_1,-b_1).$$

From the expressions (6) we saw how the presence of the dipole field allows the relaxation of the momentum conditions in inducing transitions to the intermediate states. Here the space integrals are δ-functions and give for the first term in (8) $\mathbf{k}_1=-\boldsymbol{\kappa}$ and for the second $\mathbf{k}_1=\mathbf{k}+\boldsymbol{\kappa}$. This expresses the conservation of momentum in that step of the double transition in which the final quantum is emitted. The conservation of momentum then reduces the sum over intermediate states to a sum over spins and signs of energy for a given momentum. This sum is easily done using the completeness theorems for the u's.[5] We are then left with the rate of radiation for transitions to states with a given final spin component. We must sum over the final spins and over the spins of the two K electrons which can make the transitions. This we do by introducing the projection operators for initial and final states and summing over both spin components and signs of the energy, thus taking the trace of the resultant matrix products.[5] We integrate over the angles for both the electron and the final quantum. We obtain

$$\left(\int\int R_\kappa' d\Omega_\kappa d\Omega_E\right)dE=(2/\pi)\alpha\kappa D^2Z^3W_E dE$$

where W_E is an expression too long to be reproduced here, but whose asymptotic value, $\nu\to\infty$ is:

$$\lim_{\nu\to\infty}W_E=\frac{2}{3}\left\{2\nu^2\left(\frac{\nu}{Q}-\frac{1}{\kappa}\right)+\frac{4}{\kappa}(2EQ-\nu^2)\ln\frac{\nu}{Q}-\frac{8E\nu}{\kappa}\ln\left[E-(E^2-1)^{\frac{1}{2}}\right]\right\};\quad Q=\nu-2E\kappa$$

[4] W. Heitler, *The Quantum Theory of Radiation* (Oxford, The Clarendon Press, 1936), p. 106.
[5] W. Heitler, reference 4, pp. 149–154.

ν, κ and E are energies of the initial quantum, final quantum, and electron in units of mc^2 and α is the fine structure constant 1/137. We divide this by κ to get the number of scattered quanta per second. This is also, of course, the number of recoil electrons per second. It is given in terms of D which is unknown. But the total number of electrons internally converted in the K shell for a dipole transition is also given in terms of D. It is[6]

$$N_K=\frac{4}{3}\left(\frac{\nu+2}{\nu}\right)^{\frac{1}{2}}(\nu^2+2)D^2Z^3\alpha^4.$$

Dividing the above expression for the number of electrons scattered per second in the energy range dE by this gives:

$$\frac{N_E dE}{N_K}=\frac{3\alpha}{2\pi}\left(\frac{\nu}{\nu+2}\right)^{\frac{1}{2}}\frac{W_E}{\nu^2+2}dE,$$

i.e., the number of electrons scattered in dE per electron internally converted. The above asymptotic expression for W_E gives a number about twice as large as that calculated from the more exact formula in the energy range 2.39–2.52 Mev for the 2.62-Mev gamma-ray. The average magnitude of the exact form of W_E in this range is about 800. This gives about 1/60 for the number of electrons scattered in this range per electron internally converted.

The authors are grateful to Professor J. R. Oppenheimer for suggesting this problem and for his kind guidance throughout the work.

[6] S. Dancoff and P. Morrison, Phys. Rev. **55**, 122 (1939).

MAY 15, 1940 PHYSICAL REVIEW VOLUME 57

The Oppenheimer-Phillips Process

G. M. VOLKOFF*
Department of Physics, University of California, Berkeley, California

(Received March 7, 1940)

A critical study of the previous theoretical treatments of the process of neutron capture by heavy nuclei bombarded with deuterons shows that while the dependence of the transmutation function on the incident deuteron energy, W, has been given correctly, the energy distribution of the outgoing protons has not been satisfactorily estimated. In I, the application to the Oppenheimer-Phillips process of the usual formula for the cross section is shown to be justified for restricted values of the atomic number Z and of the deuteron energy. Bethe's method is used to express the partial cross section as a product of three factors: the penetrability of the potential barrier, the sticking probability of the neutron, and the energy transfer factor. In II, methods of obtaining the deuteron wave-function are discussed. Calculations of the transmutation function are extended to higher values of Z and W, and results obtained by using the O-P-Bethe and the Kapur methods are compared. In III, the proton energy distribution is discussed. A re-evaluation of the dependence of the transfer factor on the proton energy, K, leads to a result differing from Bethe's. The transfer factor is found to have a fairly sharp maximum, and to determine essentially the proton energy distribution. For high Z and low W the position and half-breadth of this maximum is given roughly by $K_0\sim W$ and $\Delta K_0\sim 3.3\ WZ^{-\frac{1}{2}}$. Lifshitz' and Kapur's treatments of proton energies are examined, and found to be unsatisfactory.

Introduction

A GENERAL theoretical treatment of the nuclear reactions induced by deuteron bombardment is made difficult by the fact that they are many-body processes to which ordinary perturbation methods are not applicable because of the strong short-range forces involved. An attempt to simplify the problem may be made by considering first the probabilities of the proton

* Royal Society of Canada Fellow.

and the neutron penetrating to the surface of the nucleus, and then treating the interaction of these particles with the nucleus schematically in terms of a "sticking probability." Such a method is useful in discussing a mechanism proposed by Oppenheimer and Phillips[1] to describe the process of neutron capture by heavy nuclei bombarded with deuterons. According to this mechanism the deuteron is polarized by the Coulomb field, the neutron penetrates to the surface of the nucleus where it is captured, while the proton is repelled by the Coulomb field without penetrating deeply into the potential barrier. This mechanism undoubtedly is important for describing neutron capture reactions in light as well as in heavy nuclei, and over a wide range of deuteron bombarding energies. However, the theoretical treatment of this process based on considering separately the penetrabilities and the "sticking probabilities" of the particles is shown to be justified only for deuteron energies considerably smaller than the Coulomb barrier of the nucleus involved in the reaction.

In this paper we consider only the neutron capture process occurring under bombardment with deuterons whose energy satisfies the above restriction. Oppenheimer and Phillips[1] first found the dependence of the transmutation function on the incident deuteron energy. Kapur[2] repeated the calculation using a different approximation for the deuteron wave-function obtained by a generalization of the W.K.B. method developed by Kapur and Peierls.[3] Lifshitz,[4] although starting from a point of view different from that of Kapur, arrives at results identical with those of Kapur for the dependence of the transmutation function on the incident deuteron energy. Finally, Bethe[5] expresses the cross section for this process in terms of the "sticking probability" of the neutron, and the penetrability of the potential barrier. Lifshitz,[4] Bethe[5] and Kapur[6] give discussions of the outgoing proton energies, but their methods of treating this question turn out to be unsatisfactory. However, Bethe's treatment needs modification in only one essential point, and is taken as the basis of the present discussion of proton energies.

The purpose of this paper is threefold: (a) to show under what restrictions the usual perturbation-theoretic formula for the cross section in terms of the square of the matrix element of the perturbing interaction is applicable to this problem where the perturbation is not small; (b) to extend the calculations of the transmutation function to higher Z and higher bombarding energies, comparing the results of the O-P-Bethe, and the Kapur methods; and (c) to give a qualitative discussion of the proton energy distribution with reference to previous theoretical treatments of this topic.

I. Derivation of the Cross Section for the O-P Process

Bethe's[5] derivation of the cross section for the O-P process is based on the application to this problem of the formula

$$\sigma=(2\pi/\hbar)\left|\int V_A(N,n)\chi_A^*(N)\varphi_W^*(p,n)\times\chi_B(N,n)\psi_K(p)dNdndp\right|^2, \quad (1)$$

where N, p, n denote the coordinates of the particles in the initial nucleus, A, and in the incoming deuteron, φ_W and ψ_K are properly normalized Coulomb-field wave functions of the incoming deuteron of energy, W, and the outgoing proton of energy, K, χ_A and χ_B are the internal wave functions for the initial and final nuclei, and V_A is the schematic interaction between the original nucleus and the neutron. The usual perturbation-theoretic derivation of (1) is based on considering transitions between orthogonal states under the action of a *small* perturbing potential V_A, so that terms of order V_A^2 in the matrix element may be neglected. The validity of applying (1) to the O-P process in which V_A is not small must therefore be examined. We make the restriction to sufficiently high Z and low W to make the probability of both the proton and the neutron penetrating to the surface of the nucleus much smaller than that for the neutron alone, so that the short range non-Coulomb interaction $V_A'(N,p)$ of the proton with the nucleus, and the effects of direct deuteron capture may be neglected. The O-P process may then be represented by transitions between two almost orthogonal states. In the initial state the system is well described by $\chi_A(N)\varphi_W(p,n)$ where the effects of the nuclear

[1] J. R. Oppenheimer and M. Phillips, Phys. Rev. **48**, 500 (1935).
[2] P. L. Kapur, Proc. Roy. Soc. **A163**, 553 (1937).
[3] P. L. Kapur and R. Peierls, Proc. Roy. Soc. **A163**, 606 (1937).
[4] E. Lifshitz, Physik. Zeits. d. Sowjetunion **13**, 324 (1938).
[5] H. A. Bethe, Phys. Rev. **53**, 39 (1938).
[6] P. L. Kapur, Ind. J. Phys. **13**, 87 (1939).

Coulomb potential $V_c(N, p)$ and of the proton-neutron interaction $V(n, p)$ are considered in calculating $\varphi_W(p, n)$, and $V_A(N, n)$ and $V_A'(N, p)$ are neglected. The final state of the system is represented by $\chi_B(N, n)\psi_K(p)$ where $\chi_B(N, n)$ takes into account the effect of $V_A(N, n)$, but the influence of only $V_c(N, p)$ on $\psi_K(p)$ is considered, the short-range interaction of the proton with the compound nucleus being neglected. These two states are not completely orthogonal since different parts of the total interaction are left out in obtaining them, but will approach orthogonality more and more closely as the deuteron energy W is reduced making the penetration of the proton to the surface of the nucleus less and less likely. Oppenheimer's[7] method of treating transitions between almost orthogonal states may be applied to this problem. It gives (1) for the first-order term in the cross section, while the second-order correction to the matrix element is of order VV_A instead of being of order V_A^2 as given by the usual perturbation theory for transitions between orthogonal states. Although both V and V_A are large, the matrix element of their product will be small for the states under consideration, as both interactions are of short range, differing from zero only in small practically non-overlapping regions if the above restriction on the deuteron energy is made. Since no correction terms in V_A^2 appear, and the term in VV_A is small, the partial cross section to any specified final state is given by (1), subject to the condition on Z and W.

If all the variables specifying the final state except the proton energy K are integrated out of (1), the energy distribution of the outgoing protons for a given W will be obtained, and another integral over K will then give the total cross section as a function of W, i.e. the transmutation function. Carrying out these integrations in accordance with the arguments given by Bethe,[5] we obtain as a rough approximation for the proton energy distribution, leaving out numerical factors independent of K and W,

$$\sigma(K, W)dK \sim |\varphi_W(p_0, R)|^2 T(K)\xi(E_B)dK. \quad (2)$$

The principal simplifying assumptions made in obtaining (2) include the following:

(a) In order to factor out the sticking probability ξ, it is assumed that the principal contribution to (1) comes from the positions of the neutron on the surface of the nucleus. Since the neutron-nucleus interaction is of short range, regions outside the nucleus will not contribute appreciably, and since the neutron does not penetrate deeply into the nucleus undisturbed, but rapidly shares its energy with the nuclear particles, the whole neutron-nucleus interaction may be throught of as confined to a region about the surface of the nucleus much smaller than the dimensions of the polarized deuteron, which are illustrated in Fig. 3.

(b) The effects of only the spherically symmetric partial waves for both the proton and the neutron are considered in (2). The effects of the higher partial waves are important for the determination of the angular distribution of the outgoing protons, or of the absolute value of the cross section, but do not introduce appreciable changes into the estimates of the transmutation function or the proton energy distribution. If the higher partial waves were taken into account, then the first two factors in (2) would be replaced by a sum of products of similar factors taken over the various values of the angular momenta allowed by the conservation laws. The general character of the dependence of each of these factors on K and W is shown in the following sections to be the same as for the one appearing in (2), so that the summation will affect the absolute value of the cross section, but not appreciably its dependence on K and W.

(c) The integrations over the angles of the proton and the neutron are assumed to introduce no factors dependent strongly on the distance of the proton from the nucleus or on the deuteron energy W. For a given nuclear radius and a given distance of the proton from the heavy nucleus the principal contribution in integrating over the angles will come from those positions of the proton and the neutron when they are very nearly in a straight line with the heavy nucleus. As the particles deviate from the straight line position, the center of mass moves in towards the nucleus and the proton-neutron distance increases. Both these effects tend to diminish the deuteron wave function. For high values of Z and low values of W to which we are restricted the wave function will fall off quite rapidly.

The first factor in (2) gives the dependence of the penetrability of the potential barrier on the incident deuteron energy, and determines essentially the tranmsutation function. $\varphi_W(p, R)$ is the spherically symmetric partial wave of the deuteron Coulomb-field wave function normalized to unit flux. It is calculated by methods described in the next section as a function of the proton coordinate with the proton, neutron and nucleus kept in the same straight line, and the neutron held fixed at the surface of the nucleus. p_0 is the value of the proton coordinate which makes $\varphi_W(p, R)$ a maximum, and will be referred to as "the most probable proton coordinate." R is the nuclear radius.

[7] J. R. Oppenheimer, Phys. Rev. **31**, 66 (1928).

The second factor describes the transfer of kinetic energy to the proton when its coupling to the neutron is suddenly terminated by the neutron being captured, and also takes into account the gain in energy by the liberated proton under the action of the Coulomb field. We shall refer to it as the "transfer" factor. It is given by

$$T(K)=K^{\frac{1}{2}}\left|\int p^2dpS(p)f_K(p)\right|^2\equiv K^{\frac{1}{2}}|I(K)|^2, \quad (3)$$

where $S(p)\equiv\varphi_W(p, R)/\varphi_W(p_0, R)$, and $f_K(p)$ is the spherically symmetric Coulomb-field partial wave for the proton as given for instance by Mott and Massey.[8] It is in the evaluation of this factor that we differ from Bethe. His rough estimate of it yields $T(K)\sim K^{-\frac{1}{2}}$, except at very low proton energies, so that he is led to the conclusion that compared to the sticking probability the transfer factor is slowly varying, and is not important in determining the proton energy distribution. However, our re-evaluation of this factor discussed in Section III shows it to be a peaked function of K essentially determining the proton energy distribution.

The last factor $\xi(E_B)$ is called by Bethe the modified neutron sticking probability, and is defined in terms of the level spacing and the neutron width of the levels of the compound nucleus. It is introduced to give an approximate averaged out result of the effect on the proton energy distribution of the various nuclear levels into which the neutron may be captured. The function ξ is assumed to be a function of the excitation energy E_B of the nucleus formed by neutron capture measured from the ground state of the compound nucleus. Through E_B and the conservation of energy

$$W-I-I_A=K-I_B+E_B. \quad (4)$$

Therefore ξ is a function of $W-K$. Here I_A and I_B are the binding energies of the ground states of the initial and final nuclei, while I is the binding energy of the deuteron. Little direct experimental information in regard to the sticking probability is available, but a plausible assumption seems to be that for low-lying and intermediate levels of the compound nucleus it is proportional to the level density, increasing until a value of nearly unity is reached, and then remaining approximately constant for the highly excited states of the compound nucleus. Actually, of course, the effect of nuclear levels will vary irregularly from level to level depending not only on the energy, but on the angular momentum and other characteristics of the individual levels. Therefore if the neutron is captured into low-lying levels (low values of E_B, hence high values of K) whose spacing is large compared to their breadth, so that effects due to individual levels must be considered, then this way of describing the process will fail. The energy distribution of protons may show group structure at high energies, and our only reliable information about the effect of sticking probability on the high energy part of the proton energy distribution curve will be the maximum possible value of K allowed by (4) corresponding to the neutron being captured into the ground level. However, if the neutron is captured into one of the highly excited levels of the compound nucleus in the region where the spacing of the levels is comparable with their breadth, then the function ξ giving the smeared out effect of a large number of levels will be a satisfactory way of describing the influence of nuclear structure on the low energy end of the proton energy distribution curve. The transfer factor is found to have quite a sharp maximum at values of K corresponding to the neutron being captured into the higher lying levels in the region in which the sticking probability gives a good schematized description of the interaction resulting in neutron capture. Moreover, for these high levels ξ probably varies only slowly with the energy, so that the proton energy distribution is determined essentially by the peaked transfer factor.

Integrating (2) over K, and retaining only the factor most strongly dependent on W we obtain for the transmutation function

$$\sigma(W)\sim|\varphi_W(p_0, R)|^2. \quad (5)$$

The Gamow transmutation function derived on the assumption that the deuteron is not polarized, and the proton and neutron both reach the surface of the nucleus, may be obtained from (5) by replacing the most probable proton coordinate p_0 by the nuclear radius R:

$$\sigma_G(W)\sim|\varphi_W(R, R)|^2. \quad (6)$$

[8] N. F. Mott and H. S. W. Massey, *The Theory of Atomic Collisions* (Oxford, 1933), p. 39.

II. The Deuteron Wave Function and the Transmutation Function

Oppenheimer and Phillips[1] used the adiabatic and W. K. B. approximations to calculate the spherically symmetric Coulomb-field partial wave for the straight line positions of the deuteron as a function of the proton and neutron coordinates. Kapur[2] avoids the use of the adiabatic approximation, and uses a two-dimensional extension of the W. K. B. method to evaluate this wave function only at the most probable proton coordinate when the neutron is held at the surface of the nucleus, thus determining the transmutation function. His method is easily extended to determine this wave function for other straight line positions of the proton, neutron and nucleus. Lifshitz[4] obtains the same result as Kapur for the transmutation function, and the relation of his work to the two other methods is discussed at the end of Section III. To facilitate comparison all results are stated in terms of Bethe's notation. R is the nuclear radius, p and n the proton and neutron coordinates, and $r=\frac{1}{2}(p+n)$ the coordinate of the center of mass. It is convenient to introduce the reduced dimensionless quantities $\rho=IR/Ze^2$, $x=Ip/Ze^2$, $y=In/Ze^2$, $\eta=Ir/Ze^2=\frac{1}{2}(x+y)$, $\epsilon=W/I$. Most of the results can be obtained in terms of these reduced quantities, and assumptions in regard to the magnitude of the nuclear radii have to be introduced only in the final stages of the calculations. We take the nuclear radii to be given by $R=R_0A^{\frac{1}{3}}$ with $R_0=1.4\times10^{-13}$ cm which makes $R=3.5\times10^{-13}$ cm for oxygen, and $R=8.7\times10^{-13}$ cm for uranium.

The adiabatic approximation used by Oppenheimer and Phillips[1] and Bethe[5] to separate the internal motion of the deuteron from the motion of its center of mass makes use of the fact that the effective time of collision of the deuteron with the nucleus is long compared to the period of the internal motion of the deuteron, so that the change in the external forces acting on the deuteron over a period of its internal motion may be neglected. The relative motion is approximately given by the solution of the wave equation when r, the distance of the center of mass of the deuteron from the nucleus, is held fixed. The center of mass moves in an effective potential which is the energy of the relative motion expressed as a function of r. The W. K. B. method is applied separately to the two resulting equations, and gives (for $p>n$)

$$\varphi_W(p,n)=\exp\left[-\frac{2Ze^2}{\hbar}\left(\frac{M}{I}\right)^{\frac{1}{2}}F_{OP}(\epsilon,x,y)\right], \quad (7)$$

where M is the proton mass, and

$$F_{OP}(\epsilon,x,y)=\int_\eta^x du\left(1+\frac{1}{u}-\frac{1}{\eta}\right)^{\frac{1}{2}} +\int_\eta^{1/\epsilon} ds\left(\frac{1}{s}-\epsilon\right)^{\frac{1}{2}} \quad (8)$$

$$=\epsilon^{-\frac{1}{2}}f(\epsilon\eta)+\eta^{\frac{1}{2}}|1-\eta|^{-\frac{1}{2}} \times\{f(1-\eta)-f(\{1-\eta\}\{2-y\eta^{-1}\})\} \quad (9)$$

$$f(\alpha)\equiv-\sinh^{-1}(-\alpha)^{\frac{1}{2}}-[(-\alpha)(1-\alpha)]^{\frac{1}{2}} \quad \alpha\leqq0$$

$$\equiv\cos^{-1}\alpha^{\frac{1}{2}}-[\alpha(1-\alpha)]^{\frac{1}{2}} \quad 0\leqq\alpha\leqq1. \quad (10)$$

This is imaginary for $\alpha>1$, and hence is neglected, as only the real part of F is of interest. The result is given in this form by Bethe,[5] and reduces on setting $y=0$ (zero nuclear radius) to that of Oppenheimer and Phillips.[1]

Kapur does not make the first adiabatic approximation, but directly substitutes $\varphi_W(p,n)=\exp[-1/\hbar S_K(W,p,n)]$ into the deuteron equation, and leaves out certain terms in the resulting expression. Whereas in the adiabatic approximation the variation of the relative-motion wave function with the coordinate of the center of mass is completely neglected in calculating the center-of-mass wave function, Kapur's procedure takes into account its variation with the magnitude, but not with the direction of the coordinate of the center of mass. If $S_K(W,p,n)=2Ze^2(M/I)^{\frac{1}{2}}F_K(\epsilon,x,y)$, then F_K satisfies the equation

$$F_x^2+F_y^2=\tfrac{1}{2}(1/x-\epsilon+1) \quad (11)$$

with the boundary condition (for $p>n$)

$$(F_x-F_y)_{x=y}=1. \quad (12)$$

This may be solved either by a process of minimization of a line integral as done by Kapur,[2] or by the method of characteristics. The latter method is more straightforward. The

characteristics are given by

$$dt=\frac{dx}{2F_x}=\frac{dy}{2F_y}=\frac{dF}{2(F_x^2+F_y^2)}$$
$$=-\frac{dF_x}{1/2x^2}=-\frac{dF_y}{O}. \quad (13)$$

$x=y=s$ is chosen as the initial line. The values of F_x and F_y along this line as obtained from (11) and (12) are:

$$F_x(s)=\tfrac{1}{2}[1-(1/s-\epsilon)^{\frac{1}{2}}],$$
$$F_y(s)=\tfrac{1}{2}[-1-(1/s-\epsilon)^{\frac{1}{2}}] \quad (14)$$

and the value of F along the initial line is given by

$$F(s)=\int_{1/\epsilon}^{s}F'(s)ds=\int_{s}^{1/\epsilon}\left(\frac{1}{s}-\epsilon\right)^{\frac{1}{2}}ds. \quad (15)$$

From (13) we see that the characteristics are the lines of steepest descent. Integration of (13) leads to

$$F_K(\epsilon, x, y_1)=2^{-\frac{1}{2}}\int_{x,\ y}^{x_1,\ x_1}dx\left(\frac{1}{x}-\epsilon+1\right)^{\frac{1}{2}}(1+y'^2)^{\frac{1}{2}}+\int_{x_1}^{1/\epsilon}\left(\frac{1}{s}-\epsilon\right)^{\frac{1}{2}}ds, \quad (16)$$

where the first integral is taken along the characteristic passing through the point (x, y) until it meets the initial line at the point (x_1, x_1). The slope of the characteristic at any point $(x\geqq y)$ is given by

$$y'=\pm\beta[2(1/x-\epsilon+1-\tfrac{1}{2}\beta^2]^{-\frac{1}{2}}, \quad (17)$$

where $+$ is taken for $\beta\geqq 2$, while $-$ is chosen for $1\leqq\beta<2$ along the initial line $x=y$, but changes to $+$ when the denominator of (17) vanishes in integrating along a characteristic. x_1 and β are determined in terms of ϵ, x and y by

$$(1/x_1-\epsilon)^{\frac{1}{2}}=\beta-1 \quad (18)$$

and

$$y-x_1=\int_{x_1}^{x}y'dx \quad (19)$$

taken along the characteristic. For $\epsilon\geqq\frac{1}{2}$, $(W\geqq\frac{1}{2}I)$ integration of (19) gives β as the root of

$$\tan^{-1}\frac{2-\beta}{(\beta^2-2+2\epsilon)^{\frac{1}{2}}}+y\frac{(\beta^2-2+2\epsilon)^{\frac{1}{2}}}{2\beta}-\frac{(\beta^2-2+2\epsilon)^{\frac{1}{2}}[\beta(\beta-1)+\epsilon-1]}{\beta[(\beta-1)^2+\epsilon]}=\pm G\left(\left[\frac{2}{x(\beta^2-2+2\epsilon)}-1\right]^{\frac{1}{2}}\right), \quad (20)$$

where $G(\alpha)\equiv\tan^{-1}\alpha+\alpha/(1+\alpha^2)$. The value of $\beta=1$ gives the characteristic which separates regions of real and complex values of F_K. In the latter region this method of obtaining F_K is inapplicable. The real values of $F_K(\beta\geqq 1)$ are given by:

$$F_K(\epsilon, x, y)=\frac{1}{\epsilon^{\frac{1}{2}}}\tan^{-1}\frac{\beta-1}{\epsilon^{\frac{1}{2}}}+\frac{\beta(\beta-1)+\epsilon-1}{\beta[(\beta-1)^2+\epsilon]}-y\frac{\beta^2+\epsilon-1}{\beta}\pm x(\beta^2+2\epsilon-2)^{\frac{1}{2}}\left[\frac{2}{x(\beta^2-2+2\epsilon)}-1\right]^{\frac{1}{2}}, \quad (21)$$

where the value of β and the sign are the same as in (20). Similar expressions are obtained for $\epsilon<\frac{1}{2}$, $(W<\frac{1}{2}I)$, but are not given here, as we are not interested in such low bombarding energies.

The difference between F_{OP} of (8) and F_K of (16) is that the paths of integration differ as shown in Fig. 1, and in the former $1/\eta\geqq\epsilon$ occurs instead of ϵ in the first integrand. We are interested primarily in $F(\epsilon, x, y)$ as a function of x for a fixed $y=\rho$. The graphs of both F_{OP} and F_K are given for a special case in Fig. 2. It is seen that the two are quite similar.

To obtain the transmutation function we must know the value of $F(\epsilon, x, \rho)$ at its minimum at $x_0=Ip_0/Ze^2$. The dependence of x_0 on ϵ for $F_{OP}(\epsilon, x, \rho)$ and a given ρ is obtained from $x_0=2\eta_0-\rho$, where η_0 is determined by $\partial F_{OP}/\partial\eta=0$ in the manner described by Bethe.[5] For $\rho<0.172$ (i.e. for those heavy nuclei whose radii satisfy the condition $R<0.172Ze^2/I=0.116Z\times10^{-13}$ cm) the

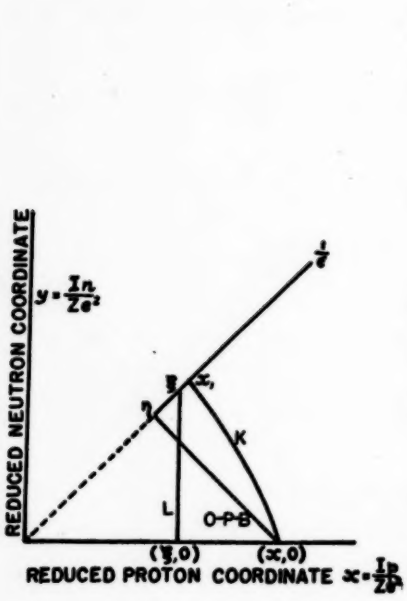

FIG. 1. Paths of integration for zero nuclear radius for the different approximations to the deuteron wave-function: O-P-B-Oppenheimer-Phillips-Bethe; K-Kapur; L-Lifshitz.

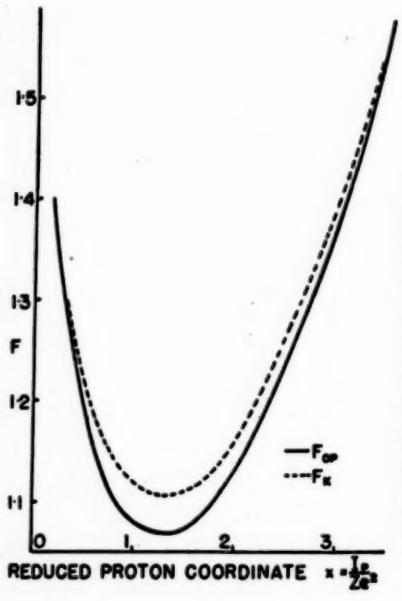

FIG. 2. Dependence of $F_{OP}(\epsilon, x, \rho)$ and $F_K(\epsilon, x, \rho)$ on the reduced proton coordinate $x=Ip/Ze^2$ for $\epsilon=0.5$, $\rho=0.17$.

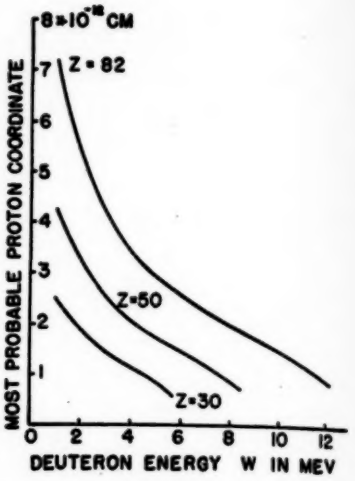

FIG. 3. Dependence on the deuteron energy W of the most probable proton coordinate $p_0=x_0 \cdot Ze^2/I$ when the neutron is at the surface of the nucleus, for different values of the atomic number Z.

minimum of $F_{OP}(\epsilon, x, \rho)$ at certain energies will lie in a region of complex values of F_{OP}, but since only the real part of F is of interest, all imaginary terms are left out whenever they appear in (9), (10) or $\partial F/\partial\eta=0$. The minimum in $F_K(\epsilon, x, \rho)$ occurs at the point where a characteristic (a line of steepest descent of F_K) is perpendicular to the line $y=\rho$. From (17) we find

$$x_0=2/(\beta_0^2-2+2\epsilon), \tag{22}$$

so that β_0 is determined as a function of ϵ for a given ρ by (20) with the right side set equal to zero. The dependence of x_0 on ϵ for a given ρ is then obtained from (22), and the result is found to be practically the same as the one for the O-P-Bethe method. As in the O-P-Bethe method, for heavy nuclei ($R<0.191Ze^2/I=0.129Z\times10^{-13}$ cm, $\rho<0.191$) the minimum of F_K at certain energies lies in the region of complex values of F_K. Since this method does not give a solution in that region, neither the most probable proton coordinate nor the value of the transmutation function at those energies can be obtained by this method. The dependence on Z and W of the most probable proton coordinate $p_0=x_0Ze^2/I$ when the neutron is kept at the surface of the nucleus is shown in Fig. 3, and illustrates the extent of the polarization of the deuteron by the Coulomb field. p_0 is roughly given by Ze^2/W, $(x_0=1/\epsilon)$. For a given Z the most probable proton coordinate decreases with increasing W until at $W_c=Ze^2/R-I=V_c-I$ it is found by both the O-P-Bethe and the Kapur method to be equal to the nuclear radius. W_c is thus the critical bombarding energy above which the O-P and the Gamow penetration functions coincide.

The transmutation functions of (5) and (6) are given by

$$\sigma(W)\sim|\varphi_W|^2=\exp\left[-\frac{4Ze^2}{\hbar}\left(\frac{M}{I}\right)^{\frac{1}{2}}F\right]$$
$$=\exp\left[-0.61ZF\right]. \tag{23}$$

Both $F_{OP}(\epsilon, x, \rho)$ and $F_K(\epsilon, x, \rho)$ reduce for $x=\rho$ (both proton and neutron at the surface of the nucleus) to the same value $F_G(\epsilon, \rho, \rho)=\epsilon^{-\frac{1}{2}}f(\epsilon\rho)$ which inserted in (23) gives the Gamow transmutation function. $F_G=0$ for $\epsilon=1/\rho$, $(W=Ze^2/R=V_c)$, i.e., when the deuteron bombarding energy is equal to the top of the nuclear Coulomb barrier, and increases with decreasing bombarding energy. Above the critical

value $\epsilon_c=1/\rho-1$, $(W_c=Ze^2/R-I)$, F_{OP} and F_K coincide with F_G. As ϵ decreases and x_0 becomes larger than ρ, F_{OP} and F_K become smaller than F_G, making the O-P penetrability larger than the Gamow penetrability. In Fig. 4, graphs of F_G-F_{OP} and F_G-F_K are given for several ρ. It is seen that the O-P-Bethe and the Kapur approximations yield slightly different results, the deviation being most pronounced for $\rho=0$ (zero nuclear radius), and quite small for the other values of ρ considered. The dependence of the ratio of the O-P penetrability to the Gamow penetrability on the bombarding energy for different Z is calculated by means of

$$\gamma=|\varphi_W(p_0, R)/\varphi_W(R, R)|^2 =\exp[0.61Z(F_G-F_{OP})] \quad (24)$$

and is plotted on a logarithmic scale in Fig. 5. The quantity $1/\gamma$ is a measure of the probability of both the proton and the neutron reaching the surface of the nucleus compared to that of the neutron penetrating alone. Since the theory of Section I applies only when $1/\gamma$ is small, it is seen that the calculations of this paper become increasingly less reliable as the bombarding energy approaches the critical energy $W_c=Ze^2/R-I$.

The approximation for the higher partial waves of the deuteron beam would have in the second integrand in (8) in addition to the Coulomb potential $1/s(=Ze^2/rI)$ a centrifugal potential term L/s^2 with

$$L=\frac{l(l+1)}{4Z^2}\left(\frac{\hbar c}{e^2}\right)^2\frac{I}{Mc^2}=10.7\frac{l(l+1)}{Z^2}.$$

The ratio of the centrifugal to the Coulomb potential is given by $L/s=10.7l(l+1)/Z^2s$. The important values of s are $s\sim\eta_0=\frac{1}{2}(x_0+\rho)\sim 1/2\epsilon+\rho/2$. For these values $L/s\leqq 21.4l(l+1)W/Z^2I$, so that the effect of the centrifugal potential is unimportant for $l(l+1)<Z^2I/20W$. This gives $l<6$ for 2-Mev deuterons on zinc, and $l<11$ for 5-Mev deuterons on lead. Thus both the absolute value and the shape of the first few deuteron partial waves considered as functions of the proton coordinate with the neutron kept at the surface of the nucleus will not be strongly dependent on l. The fact that several partial waves contribute appreciably to the cross section leads us to expect a nonisotropic angular distribution for the outgoing protons. However, in the present paper we do not attempt to give a discussion of this question.

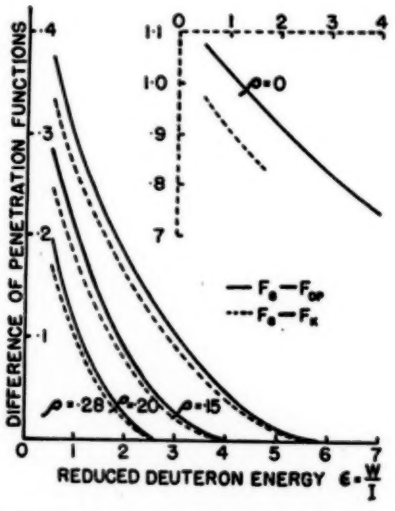

FIG. 4. Dependence on the reduced deuteron energy $\epsilon=W/I$ of $F_G(\epsilon, \rho, \rho)-F_{OP}(\epsilon, x_0, \rho)$ and $F_G(\epsilon, \rho, \rho)-F_K(\epsilon, x_0, \rho)$ for different values of the reduced nuclear radius $\rho=IR/Ze^2$.

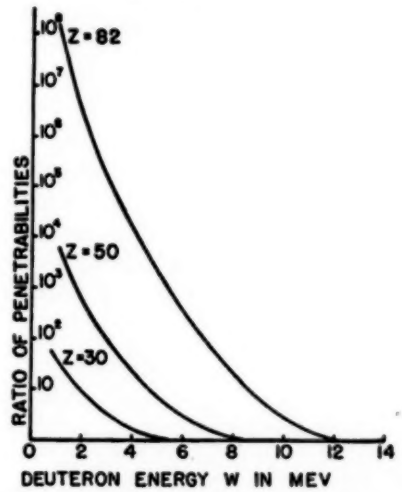

FIG. 5. Dependence on the deuteron energy W of the ratio of the Oppenheimer-Phillips to the Gamow penetrability for different values of the atomic number Z.

III. The Proton Energy Distribution

The transfer factor $T(K)$ in the proton energy distribution as given by (3) involves the integral $I(K)=\int p^2dpS(p)f_K(p)$. The dependence of this integral on K may be estimated as follows. $S(p)$ has a maximum at $p=p_0\sim Ze^2/W$. If it were sharp like a δ-function, $I(K)\sim p_0^2f_K(p_0)$. As a

function of K this starts out flat near the origin, reaches a maximum roughly at $K\sim Ze^2/p_0$, and then oscillates with an amplitude falling off as $K^{-\frac{1}{2}}$ for large K. Since actually $S(p)$ has quite a broad maximum, it will not resolve the oscillations of $f_K(p)$ as they crowd in with increasing K, so that after a few oscillations of rapidly decreasing amplitude $I(K)$ will fall off monotonically. The position of the maximum and the general shape of $S(p)$ is about the same for the first few deuteron partial waves, and the proton partial waves differ little from one another except for the relative positions of their maxima and minima. It is therefore expected that for low proton partial waves the general dependence on K of integrals of the type $I(K)$ will be roughly the same as of the one here calculated, while for higher proton partial waves these integrals will fall off in absolute value because of the more rapid oscillation of $f_K(p)$ with p for higher l, K being chosen to fix the first maximum of $f_K(p)$ at $p\sim p_0$.

An analytic estimate of $I(K)$ is obtained as follows. For any particular Z and W, $S(p)$ can be fitted quite well by a curve of the type

$$S(p)=(p+a)^m e^{-\alpha p}=\left(-\frac{d}{d\alpha}+a\right)^m e^{-\alpha p} \tag{25}$$

with suitably chosen a, α, and an integral value of m. Using the contour integral representation for $f_K(p)$ given by Mott and Massey,[8] and interchanging in $I(K)$ the order of contour integration and integration over the proton coordinate we obtain:

$$I(K)\sim\{K^{\frac{1}{2}}[1-\exp(-2\pi\delta K^{-\frac{1}{2}})]\}^{-1}J(K) \tag{26}$$

with

$$J(K)\sim\left(-\frac{d}{d\gamma}+\zeta\right)^m\left[\frac{1+\gamma/\delta}{(K+\gamma^2)^2}\exp\{-2\delta K^{-\frac{1}{2}}\tan^{-1}(\gamma K^{-\frac{1}{2}})\}\right]$$

$$\sim\frac{g_{m+2}(\gamma,K)}{(K+\gamma^2)^{m+2}}\exp\{-2\delta K^{-\frac{1}{2}}\tan^{-1}(\gamma K^{-\frac{1}{2}})\}. \tag{27}$$

Here $g_{m+2}(\gamma, K)$ is a polynomial of the mth degree in K with a nonzero constant term. It is obtained from $g_2(\gamma, K)\equiv 1+\gamma/\delta$ by an m-fold application of the recursion relation

$$g_{s+1}(\gamma,K)=\left[\left(1+\frac{\zeta}{2\delta}K\right)+\frac{s}{\delta}\gamma+\frac{\zeta}{2\delta}\gamma^2\right]g_s-\frac{K+\gamma^2}{2\delta}\frac{dg_s}{d\gamma}. \tag{28}$$

If K is measured in Mev, then δ defined by $n=Ze^2/\hbar v=\delta/K^{\frac{1}{2}}$ is given by $\delta=0.158Z$. γ and ζ are determined in terms of α and a of (25) by

$$\gamma=1.08\alpha/\delta \qquad \zeta=\delta a/1.08, \tag{29}$$

if a and α are expressed in terms of Ze^2/I taken as the unit of length.

The dependence of the partial cross section on proton energy for a given W is then given by

$$\sigma(K)dK\sim\xi K^{\frac{1}{2}}|I(K)|^2dK=\xi T(K)dK;$$

$$T(K)=[1-\exp(-2\pi\delta K^{-\frac{1}{2}})]^{-1}\frac{\exp[-4\delta K^{-\frac{1}{2}}\tan^{-1}(\gamma K^{-\frac{1}{2}})]}{(K+\gamma^2)^{2m+4}}\cdot|g_{m+2}(K)|^2$$

$$\equiv[1-\exp(-2\pi\delta K^{-\frac{1}{2}})]^{-1}G(K)g^2(K). \tag{30}$$

$G(K)$ is the dominant factor in $T(K)$ giving a pronounced peak. The first factor is practically unity over the range of K where $G(K)$ is appreciable. $g^2(K)$ describes the oscillations mentioned at the beginning of this section. The calculation of $g_{m+2}(K)$ by means of (28) is quite laborious for high

values of m. However, numerical calculations for particular cases show that for the values of Z and W considered the first zero of $g_{m+2}(K)$ comes at a much higher value of K than the peak of $G(K)$, so that $g_{m+2}(K)$ is slowly varying over the important range of values of K, and the position and half-breadth of the maximum of the transfer factor are determined essentially by $G(K)$.

For any particular Z and W the dependence of $G(K)$ on K may be found by substituting in (30) the values of m and γ obtained by fitting a curve of the type (25) to $S(p)$ numerically calculated for that case by methods of Section II. A very rough, but helpful estimate of the dependence on Z and W of K_0, the position of the maximum of $G(K)$, and its half-breadth ΔK_0, may be obtained as follows. We first estimate the dependence on Z and W of m and γ. If we write

$$F_{OP}(\epsilon, x, \rho)-F_{OP}(\epsilon, x_0, \rho)=X[(x-x_0)/x_0-\log (x/x_0)],$$

we find that over the range of Z and W (i.e., of ρ and ϵ) of interest to us X is practically a constant ~ 0.6. x_0 was shown to be given roughly by $1/\epsilon$. So we can take

$$S(p)\equiv\exp\left[-0.3Z\{F(x)-F(x_0)\}\right]\sim[xe^{-x}]^{0.18Z}$$

making $m=0.18Z$, $\gamma=1.08\times 0.18WZ/\delta I=0.57W$, $\zeta=0$. With these values $G(K)$ becomes

$$G(K)\sim\exp\left[-0.63ZK^{-\frac{1}{3}}\tan^{-1}(0.57WK^{-\frac{1}{3}})\right]/(K+0.325W^2)^{0.36Z+4}. \tag{31}$$

K_0 is determined by

$$G'(K_0)=0 \tag{32}$$

and ΔK_0 by

$$\Delta K_0=2[-G(K_0)/G''(K_0)]^{\frac{1}{2}}. \tag{33}$$

For W not too large we replace in (31) $\tan^{-1}\times(0.57WK^{-\frac{1}{3}})$ by its argument. Then (32) gives for K_0

$$K_0=W\left[\frac{1+\{1+1.3W(1+11.1/Z)\}^{\frac{1}{2}}}{2(1+11.1/Z)}\right],$$

which shows that $K_0\sim W$ for small W and large Z. Using $K_0\sim W$, and $G'(K_0)=0$, we obtain from (33)

$$\Delta K_0=2\left[\frac{0.72Z}{W^2}-\frac{0.36Z+4}{W^2(1+0.325W)^2}\right]^{-\frac{1}{2}}$$

$$=2WZ^{-\frac{1}{2}}\left[0.72-\frac{0.36+4/Z}{(1+0.325W)^2}\right]^{-\frac{1}{2}},$$

which shows that for small W and large Z, $\Delta K_0\sim 3.3WZ^{-\frac{1}{2}}$. These rough estimates give for

$Z=30$	$W=2$ Mev	$K_0\sim 2$ Mev	$\Delta K_0\sim 1.2$ Mev
$Z=82$	$W=1$ Mev	$K_0\sim 1$ Mev	$\Delta K_0\sim 0.36$ Mev.

More exact calculations using values of γ and m fitted to the above values of Z and W yield

$Z=30$	$W=2$ Mev	$K_0=1.9$ Mev	$\Delta K_0=1.4$ Mev
$Z=82$	$W=1$ Mev	$K_0=1.35$ Mev	$\Delta K_0=0.52$ Mev.

It should be emphasized again that the latter part of the above discussion of proton energies is only qualitative, and yields only the order of magnitude of K_0 and ΔK_0. However, it brings out the importance of the transfer factor in determining the proton energy distribution. Since $K_0\sim W$, the conservation of energy shows that for a proton to come off with this energy the neutron must be captured in a high lying state of the compound nucleus B with an excitation energy of $E_B\sim I_B-I_A-I\sim 6$ Mev above the ground level. For such states the "sticking probability" ξ is a valid way of describing the neutron-nucleus interaction and is expected to be roughly proportional to the level density in that region which, according to Weisskopf,[9] is given by $\omega(E_B)\sim\exp[2(E_B/a)^{\frac{1}{2}}]$ with a ~ 0.2 Mev. Since the half-breadth of the transfer factor is quite small, the sticking probability might vary by a factor of two or three over the breadth of the transfer factor, but the latter would still be the determining factor for the proton energy distribution.

We conclude with a reference to the work of Lifshitz[4] and Kapur.[6] Lifshitz sets out to evaluate the matrix element of the perturbing energy (really the scalar product of the initial and final wave-functions, as all non-exponential factors are left out) by using a semiclassical method (analogous to the W.K.B. approximation). In our present notation his expression for the transition probability

[9] V. Weisskopf, Phys. Rev. **52**, 295 (1937).

(using zero nuclear radius) is:

$$\sigma(\xi, W)\sim\exp\left[-\frac{4Ze^2}{\hbar}\left(\frac{M}{I}\right)^{\frac{1}{2}}F_{\mathrm{L}}(\epsilon, \xi)\right], \quad (34)$$

where

$$F_{\mathrm{L}}(\epsilon, \xi)=\frac{1}{2}\int_0^{\xi}(-2E_n)^{\frac{1}{2}}dy + \frac{1}{2}\int_{1/E_p}^{\xi}\left[2\left(\frac{1}{x'}-E_p\right)\right]^{\frac{1}{2}}dx' + \int_{\xi}^{1/\epsilon}\left(\frac{1}{s}-\epsilon\right)^{\frac{1}{2}}ds. \quad (35)$$

ξ is named by him the coordinate of the "transition point." E_n and E_p are interpreted by him as the energies of the neutron and the proton at "the instant of break-up" of the deuteron at the "transition point," the interpretation being based on a *classical* application of the energy and momentum conservation laws, and the use of the *classical* concept of the action function in a region *classically inaccessible* to the particles. E_n and E_p are given in terms of ϵ and ξ by

$$E_n=-\tfrac{1}{2}[1+(1/\xi-\epsilon)^{\frac{1}{2}}]^2$$
$$E_p=\epsilon-1+\tfrac{1}{2}[1+(1/\xi-\epsilon)^{\frac{1}{2}}]^2. \quad (36)$$

Since $1/\xi$ is connected by (36) with E_p Lifshitz interprets the variation of $\sigma(\xi, W)$ with ξ as describing the dependence of the cross section on the outgoing proton energy, and takes the transmutation function to be determined by $\sigma(\xi_0, W)$ where ξ_0 is the value of ξ which makes $\sigma(\xi, W)$ a maximum.

We compare $F_{\mathrm{L}}(\epsilon, \xi)$ of (35) with $F_{\mathrm{K}}(\epsilon, x, y)$ of (16) with $y=0$. The last integrals are of the same form. The first integral in (16) is taken along the characteristic through the point $(x, 0)$, and may be written as

$$\frac{1}{2}\int_{x,0}^{x_1,x_1}[2(1/x-E_n-E_p)]^{\frac{1}{2}}dt.$$

In (35) it is replaced by an integral along the x axis from a point $(x=1/E_p, 0)$ to $(\xi, 0)$, plus another integral along a vertical line from $(\xi, 0)$ to (ξ, ξ), as shown in Fig. 2. Thus formally F_{OP}, F_{K}, and F_{L} are very much alike. The paths of integration differ somewhat, the points at which the path of integration joins the line $x=y$ differ, but are in each case uniquely determined by the point $(x, 0)$ and the integrands along a part of the path differ, but the general dependence of any of these three functions on x is the same.

F_{K} is given explicitly by (20) and (21). The corresponding results for F_{L} are

$$F_{\mathrm{L}}(\epsilon, x, 0)=\frac{1}{\epsilon^{\frac{1}{2}}}\tan^{-1}\frac{\delta-1}{\epsilon^{\frac{1}{2}}} + \frac{1}{(\delta^2-2+2\epsilon)^{\frac{1}{2}}}\tan^{-1}\frac{2-\delta}{(\delta^2-2+2\epsilon)^{\frac{1}{2}}}, \quad (37)$$

where δ is given in terms of ϵ and x by

$$2/x=\delta^2-2+2\epsilon. \quad (38)$$

ξ is given by

$$(1/\xi-\epsilon)^{\frac{1}{2}}=\delta-1 \quad \text{(similar to (18))}. \quad (39)$$

The δ determined by (38) is in general different from the β determined by (20), so that ξ is different from x_1, and F_{L} is different from F_{K}. However, differentiation of F_{L} shows that its minimum is given by the same equation for δ_0 as is satisfied by β_0, i.e. by (20) with the right side equal to zero and $y=0$, and in that case it so happens that the positions of the minima, the values of F_{L} and F_{K} at that point, and the points ξ and x_1 fortuitously coincide, thus making Lifshitz' result for the transmutation function identical with Kapur's.

In view of the above it seems that Lifshitz' expression for the cross section (34) should be interpreted not as the square of the scalar product of the deuteron and proton wave functions given as a function of the outgoing proton energy, but rather as another approximation (analogous to the O-P-Bethe and Kapur approximations) to the square of the deuteron wave function considered as a function of the proton coordinate p with the neutron kept at the surface of the nucleus. Considered as a function of $E_p=Ze^2/p$ instead of p, (34) gives a measure of the probability of the deuteron penetrating into the classically inaccessible region and being so polarized by the Coulomb field that the proton is found at a point p where its Coulomb energy is given by $E_p=1/p$ while the neutron penetrates to the surface of the nucleus. The energy distribution of the outgoing protons, however, is determined not only by the energy gained by the proton from the Coulomb field, but also by the transfer of the kinetic energy to the proton when its connection with the neutron is severed. The two effects are taken into account in the transfer factor discussed above.

Kapur[6] interprets the process in a very classical way. Assuming the path of integration corresponding to the point (x_0, ρ) to be the *actual* path taken by the deuteron after penetrating the potential barrier he interprets the point (x_1, x_1) as the point at which the deuteron breaks up (analogous to Lifshitz' interpretation of the point ξ), and assumes the proton always to come out with an energy equal to its Coulomb energy at that point uniquely determined in terms of ρ and x_0. This interpretation is quite inconsistent, since it is based on describing the motion of the particles in terms of a well-defined classical trajectory in a region classically inaccessible to them.

The author takes great pleasure in expressing his gratitude to Professor J. R. Oppenheimer for suggesting the problem, and for continued guidance in the course of the work, and also wishes to thank Dr. L. I. Schiff and Mr. H. Snyder for helpful discussions. The grant by the Royal Society of Canada of a Research Fellowship under which this work was carried out is gratefully acknowledged.

The *K*-Absorption Edges of Br (35) and Kr (36)*

C. H. SHAW
Rowland Physical Laboratory, Johns Hopkins University, Baltimore, Maryland
(Received March 12, 1940)

The absorption of monochromatic x-rays as a function of the wave-length has been measured for gaseous krypton, bromine and hydrogen bromide in the region of the absorption edges. The data were taken with a double crystal spectrometer with a G-M counter to measure the x-ray intensities. The structure for krypton is considerably different from that previously obtained for argon. The data for Br_2 and HBr are of sufficient accuracy so that they may be used to check the Kronig-Petersen theory quantitatively.

FINE structure on the short wave-length side of the *K*-absorption edge of gaseous absorbers has been found to be of two kinds. The first is typified by argon, in which the structure is produced by transitions from the *K* state to discrete optical states allowed by the selection rules.[1] The second kind of structure is exhibited by polyatomic gases.[2] That the latter structure is a property of the molecule rather than the atom is demonstrated by the fact that the structure completely disappears when light atoms such as hydrogen are substituted for all but the absorbing atom in the molecule.

The present work is a quantitative determination of the shape and fine structure of the *K*-absorption edges of krypton and of bromine in Br_2 and in HBr. In the following paper comparisons are made with theory.

EXPERIMENTAL

The Societé Génevoise double crystal spectrometer has been described in a previous communication.[3] The accessories, with the exception of the intensity recorder, have remained essentially unchanged.

The x-ray intensity was recorded by a Geiger-Mueller counter especially designed for the purpose. The counter briefly described below is suitable for x-rays of wave-length between 0.7 and 2.5A. The cathode was of copper about 10 cm long and with an inside diameter of 2 centimeters. The thin entrance window was of the glass bubble type about 7 microns thick. It was placed at the end of the cathode so that the x-rays traversed the length of the counter and thus had ample chance for absorption. Since the central wire must be supported entirely from one end of the counter, it should be stiff enough to prevent undue sagging. A straight piece of ground tungsten wire 30 mils in diameter was selected and polished with crocus cloth until it was bright and smooth. Since it was not possible because of its large area to use the usual glass bead on the end of the counter wire, the end was merely rounded off carefully by grinding and likewise polished smooth. About one percent of the beam was intercepted by the wire. The rounded end of the central wire was allowed to approach within two or three millimeters of the glass window when the former was sealed into the glass envelope. The forward end of the cathode was kept about a centimeter away from the glass window to eliminate spurious discharges between the cathode and the end of the central wire. The counter was filled to about 45 centimeters of mercury pressure with 99.98 percent pure argon and 12 millimeters pressure of ethyl alcohol vapor.[4] The addition of the alcohol vapor, besides quenching metastable states in the argon gas, lowers the operating voltage of the counter considerably over those in which hydrogen or air is used. The counter operated at 1600 volts with about an 80-volt-wide plateau.

* This research was supported by a grant-in-aid made to Professor J. A. Bearden from the Penrose Fund of the American Philosophical Society.

[1] D. Coster and J. H. van der Tuuk, Zeits. f. Physik **37**, 367 (1926); J. D. Hanawalt, Phys. Rev. **37**, 715 (1931); L. G. Parratt, Phys. Rev. **56**, 295 (1939).

[2] A. E. Lindh, Dissertation, University of Lund, 1923; J. D. Hanawalt, Phys. Rev. **37**, 715 (1931); J. A. Prins, Physica **1**, 1174 (1934); D. Coster and G. H. Klamer, Physica **1**, 889 (1934); S. T. Stephenson, Phys. Rev. **50**, 790 (1936); B. Cioffari, Phys. Rev. **51**, 630 (1937); T. Drynski and R. Smoluchowski, Physica **6**, 929 (1939).

[3] J. A. Bearden and C. H. Shaw, Phys. Rev. **48**, 18(1935).

[4] A. Trost, Zeits. f. Physik **105**, 399 (1937).

Calculations show that about 80 percent of the radiation at 1.5A is absorbed in the counter. The residual background count was approximately 50 counts per minute. The Getting type of multivibrator,[5] thyratron scale of sixteen[6] and Cenco high impedance impulse counter were used to record the counts. The intensity recorder was linear to one or two percent up to 8000 random counts per minute. The intensities recorded in the present work were far below this—usually not more than 2500 per minute.

The Geiger counter has certain advantages and some disadvantages over the ionization chamber for measuring intensities. Statistical considerations indicate that 10,000 particles must be counted to bring the accuracy to ± 1 percent. Actually because of variations in the x-ray output from the tube, about 20,000 are needed. In recording absorption edges the intensity of the continuous spectrum using the double crystal spectrometer is rarely more than 2000 per minute, so that at least 30 minutes aggregate time must be spent for each point—twenty minutes with absorber in and ten minutes with absorber out. Of course, if plenty of intensity is available, this difficulty disappears, especially if a very fast counter and circuit are used.[7]

There are some rather impressive advantages of the counter over the ionization chamber and Pliotron tube. With the Pliotron tube circuit, there are always residual drifts in the base line which may change in magnitude from day to day inexplicably. This is especially true when high sensitivities are used, as is necessary when working with the continuous spectrum. The unsteadiness of the base line seems to always be more than the Brownian motion limit would indicate. This is probably due to variations in the high resistance leak, emission of positive ions from the filament and variations of the batteries. A long period galvanometer is oftentimes used to decrease the wanderings of the galvanometer spot due to statistical variations and alpha-particles from radioactive contamination of the ionization chamber. Sudden large deflections are produced, with a consequent loss of time and temper.

The counter is not subject to these limitations. It is stable and dependable over long periods of time. Since the action of the Geiger counter is a type of "trigger action" the effect of a highly ionizing alpha-particle is exactly the same as a weakly ionizing beta-particle. Both merely produce a count and the circuit has recovered in 10^{-4} second. The counter has been found to be simple in operation and more dependable than the Pliotron and galvanometer for the measurement of small x-ray intensities.

The calcite crystals used on the spectrometer were fairly good. The $(1-1)$ width at half-maximum was 3 or 4 percent wider than that for theoretically perfect crystals in the wavelength region used. Comparisons of $(1+1)$ and $(1-1)$ widths indicated that they were class I[8] crystals.

The absorption chambers were made by blowing a bubble glass window at either end of a glass tube about 15 mm in diameter. The actual length of the gas column was about 7 centimeters. A drop of liquid bromine was introduced into the tube, the end of the tube placed in a dry ice mixture to freeze the bromine, and the tube pumped out and sealed off. The vapor pressure of the bromine gas during the course of the experiment, then, was determined by its temperature. For this reason the ambient temperature was recorded to 0.1°C at short intervals while the absorption data were being taken. A similar cell contained spectroscopically pure krypton to approximately two-thirds atmospheric pressure.

In order to compare the absorption by the bromine molecule with that by the bromine atom the absorption of atomic bromine is required. The dissociation temperature of the bromine molecule is so high that it is not practical to observe the absorption in dissociated bromine gas. The alternative is to use a molecule composed of a bromine atom and another very light atom such as hydrogen. The interaction between the photoelectron ejected from the bromine atom and the hydrogen atom is negligible, so the absorption of this molecule is

[5] I. A. Getting, Phys. Rev. **53**, 103 (1938).
[6] J. Giarratana, Rev. Sci. Inst. **8**, 390 (1937).
[7] John Strong, *Procedures in Experimental Physics*, p. 270.
[8] L. G. Parratt, Rev. Sci. Inst. **6**, 387 (1935).

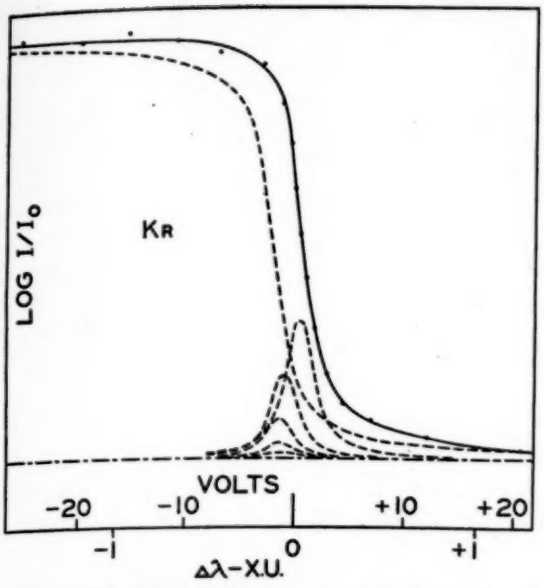

FIG. 1. Absorption in krypton as a function of x-ray wave-length near the absorption edge. The dots are experimental points; the broken lines are main absorption edge and absorption lines.

essentially the same as that of the bromine atom alone. Vapor from heated HBr solution was passed through phosphorus pentoxide, which removed most of the water vapor, and then into a liquid-air trap to which the absorption cell was connected and which had previously been exhausted. When dry ice and alcohol mixture was substituted for the liquid air, the HBr filled the cell, while the water and any Br_2 remained in the trap. The cell was thus filled to about 50 cm pressure with dry HBr.

The absorption cell was mounted on a slide between the crystals of the spectrometer in such a manner that it could be moved in and out of the x-ray beam. Because of the fact that the in-blown glass windows are curved, care was taken that the cell was always introduced into the x-ray beam accurately in the same position. The curvature of the window introduces an uncertainty in the actual length of the absorption path, but this was not serious in the present work, since the absolute values of the absorption coefficients were not of interest.

The procedure in taking data was then to record the number of counts with absorber removed in a two-minute period, the number of counts in four minutes with absorber in the beam. This was repeated four times and an average taken for each point on the curve. In the case of the bromine, the ambient temperature was then read. The whole curve was repeated three times, and parts four times to reduce the random error.

Since the temperature changed slowly from time to time, a correction due to the change in effective thickness of bromine gas was necessary. The absorption in the glass windows was measured. Allowance was made for both these factors in the accompanying plots of log I/I_0 *versus* wave-length.

RESULTS

Krypton

In Fig. 1 is shown a graph of log I/I_0 as a function of the wave-length. For convenience a voltage scale is also included. In contrast with the observations on argon,[9] it is apparent that no Kossel structure is resolved in the case of the krypton edge. However, the fact that the absorption edge is not symmetrical suggests that the structure may be present but washed out. Such washing out for krypton is to be expected when it is considered that the width of the K state in energy units is greater for krypton than for argon, and the separation in energy units of the p levels is less.

The theory of Richtmyer, Barnes and Ramberg[10] for the shape of an absorption edge unfortunately cannot be applied directly to the present observations. Ideally the arc tangent form of the absorption edge applies to the case where the electron is ejected into a continuum of energy states or into energy states which are close together and whose distribution on an energy scale is uniform. Neither of these conditions is satisfied even approximately for the first few empty p levels of krypton.

For energies of the ejected electron greater than that of the K-ionization potential, there is a continuum of energy states and the R.B.R. theory may be applied. A very rough estimate of the K-level width may be obtained in the usual way by measuring the width between $\frac{1}{4}$ and $\frac{3}{4}$ of the height of the limit. Such a measurement gives 2.07 volts, corrected for the resolving power of the crystals.[8] In dealing with problems

[9] L. G. Parratt, Phys. Rev. **56**, 295 (1939).
[10] Richtmyer, Barnes and Ramberg, Phys. Rev. **46**, 843 (1934).

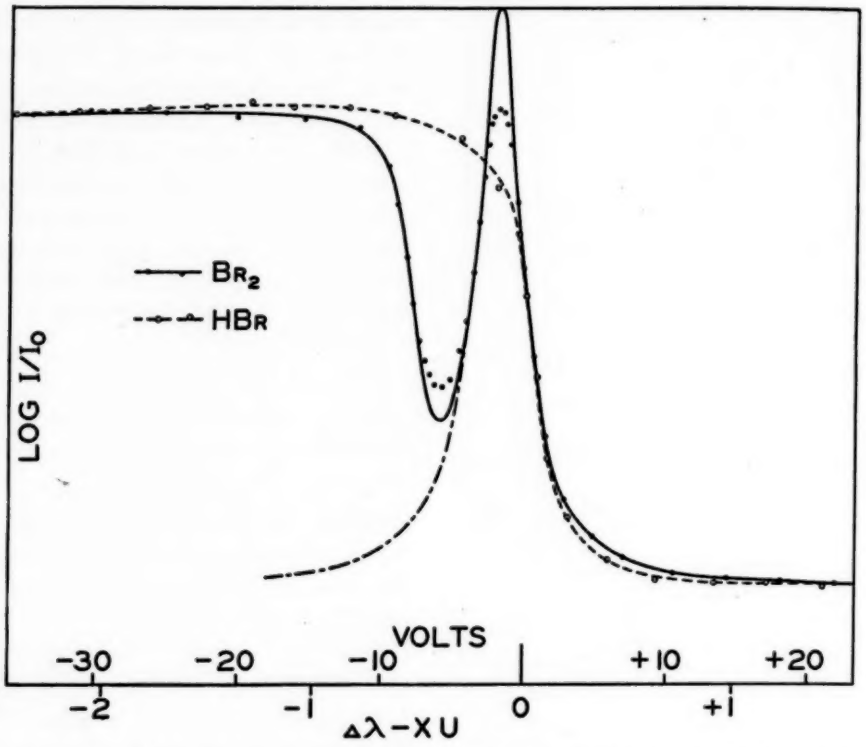

FIG. 2. Absorption in bromine gas (solid line) and HBr (broken line) near the absorption limit. Experimental points are indicated. The line — - — - — is the mirror image of the initial absorption edge used in correcting for the finite resolving power of the spectrometer.

of the present kind, it is convenient to make a distinction between the *initial* absorption edge as observed, in which absorption takes place to the first empty states allowed by the selection rules, and the *main* absorption edge, in which absorption takes place into a continuum of energy levels. This distinction has less meaning in the case of solids—particularly metals.

The position of the main absorption edge for krypton may be located approximately by adding the energy difference between the $5p$ level and the series limit for rubidium[11] (atomic number 37) to the energy corresponding to the position of the initial absorption edge. The unpredictable influence of the K-level width will make the position uncertain to perhaps half a volt.

The analysis into the component absorption lines can be done in the present case with only an indifferent degree of accuracy. Such a "reasonable" resolution into components is shown in the figure. In drawing the curves it was assumed that the intensity of the components would continually decrease as the main absorption edge is approached. Perhaps the most noteworthy feature is the difference in intensity of the first absorption line as compared to that for argon.[9]

Bromine

The two curves shown in Fig. 2 are for absorption in Br_2 and in HBr. The dots represent the experimental data. The solid line is the Br_2 curve as corrected for the resolving power of the crystals.[8] The most striking feature is the single sharp and intense region of high transmission to the high frequency side of the initial absorption edge for Br_2. The energy separation of this minimum from the absorption edge (the "position of the absorption edge" is here taken to be that of the inflection point in the initial absorption edge) is approximately 5.9 volts. The Kossel structure is completely washed out by the large width of the K state.

The previous observations by Cioffari[12] have indicated that the structure for Br_2 is limited to

[11] Bacher and Goudsmit, *Atomic Energy States*, p. 377.

[12] B. Cioffari, Phys. Rev. **51**, 630 (1937).

the one band of transmission and that within the limits of accuracy of the experiment there was no structure further from the edge. The present results show that the intensity of any remaining structure less than 50 volts from the initial absorption edge is not greater than 2 percent of the first absorption minimum.

This result is in sharp contrast with those of Coster and Klamer on $GeCl_4$.[13] Here several maxima and minima were observed of gradually decreasing intensity on the high frequency side of the initial absorption edge. As shown in the succeeding paper, the best theory[14] at the present time indicates that several maxima and minima should likewise be observed for bromine. As there suggested, some of the washing out may be due to molecular vibrations and the consequent variation of the interatomic distance. However, the calculations indicate that only part of the effect may be due to this factor. Since the Hartree fields and scattering phases have not been worked out for bromine, it was necessary to use those for krypton.[15] The several approximations and omissions from the theory including the above one introduce rather serious uncertainties, so the form of the theoretical intensity curve is subject to revision when these corrections are finally applied. For this reason the comparison with theory of such secondary characteristics as the width of the transmission band is meaningless.

The author wishes to express his appreciation to Professor J. A. Bearden for his interest during the progress of the work and his cooperation in the development of the Geiger counter.

[13] D. Coster and G. H. Klamer, Physica **1**, 889 (1934).
[14] H. Petersen, Zeits. f. Physik **80**, 258 (1933).
[15] J. Holtsmark, Zeits. f. Physik **66**, 49 (1930).

MAY 15, 1940 PHYSICAL REVIEW VOLUME 57

The Fine Structure of the X-Ray Absorption Limits of Bromine and Chlorine*

T. M. SNYDER AND C. H. SHAW
Rowland Physical Laboratory, Johns Hopkins University, Baltimore, Maryland

(Received March 12, 1940)

The ratio of the absorption coefficient of the bromine atom in Br_2 to that in HBr for monochromatic x-rays is calculated as a function of the x-ray wave-length in the region of the *K*-absorption edge according to the theory as given by Petersen. A predicted minimum at about 5.9 volts on the high frequency side of the absorption edge agrees satisfactorily with the experimental findings in position but not in intensity. A predicted broad maximum at about 15 volts from the absorption edge is not found experimentally. The structure for chlorine is recalculated from the Hartree self-consistent field for the chlorine atom and is compared with previous photographic measurements.

X-RAY absorption by an atom takes place when a deep-lying electron can be lifted past all the filled atomic levels into either an unoccupied discrete level or completely outside the atom into the continuum. As a result the x-ray absorption coefficient as a function of the frequency rises initially with a series of absorption lines extending to higher energies which converge to a series limit in a few volts. Absorption to still higher frequencies is continuous. Argon[1] and krypton[2] are excellent examples of this type of absorption.

In polyatomic gases, on the other hand, structure is found which extends for a distance of several hundred volts on the high frequency side of the absorption threshold. The explanation of this phenomenon was given by Kronig,[3] who called attention to the important rôle played by the ejected photoelectron because of its scattering by the partner atoms in the molecule.

* This research was supported by a grant-in-aid made to Professor J. A. Bearden from the Penrose Fund of the American Philosophical Society.

[1] L. G. Parratt, Phys. Rev. **56**, 295 (1939).
[2] C. H. Shaw, preceding paper.
[3] R. de L. Kronig, Zeits. f. Physik **75**, 468 (1932).

Interference between the direct and scattered electron wave at large distances from the molecule enhances or diminishes the chance of ejection of a photoelectron from the atom according to whether the interference is constructive or destructive. It is clear that the probability of the ejection of a photoelectron is the same as that of the absorption of an x-ray. Hence this interference process may cause either an increase or a decrease in the absorption coefficient over what would be found if the partner atoms in the molecule were not present.

In developing the theory for the variation of the absorption coefficient with frequency on the high frequency side of the absorption limit, Kronig[3] assumed the reverse of the actual process for purposes of convenience in calculation; i.e., instead of the absorption of a photon with the ejection of an electron from the K shell, he considered the emission of a photon when an incoming electron is captured by an atom with an empty K level. Fig. 1 represents a plane electron wave of energy E striking the diatomic gas molecule AB. The wave may be scattered by the atom B with change of phase δ. Assume, now, that the direct and scattered beams arrive at the K shell of the atom A, where there is an electron missing. The probability that the electron will be absorbed in the K shell and an x-ray quantum of wave-length λ emitted will depend upon the total amplitude of the wave at A and hence upon the phase difference between the direct and scattered electron waves, being a maximum for zero phase difference. Zero phase difference corresponds to a large transition probability and hence in the actual process to a high absorption coefficient for x-rays.

In general the phase difference between the direct and scattered electron waves at the absorbing atom depends upon four factors: (1) the interatomic distance ρ, (2) the change of phase δ upon scattering from the atom B, (3) the energy E of the electron (and hence the wave-length Λ of the associated de Broglie wave), and (4) the angle θ between the axis of the molecule and the direction of the incident electron wave. If the temperature of the gas under observation is kept so low that only a small percentage of the atoms have vibrational energy greater than the zero-point energy, ρ may be assumed to be

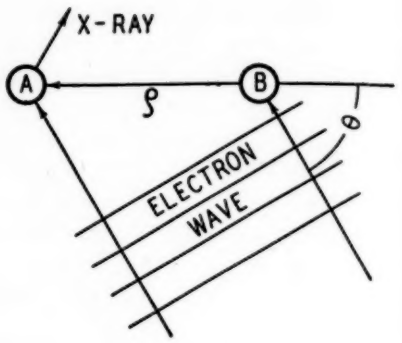

FIG. 1.

essentially a constant for all atoms, since the zero-point amplitude is so small as to be negligible in changing the interatomic distance. If the scattered wave is spherically symmetrical and if $\Lambda \ll \rho$ there will clearly be no x-ray structure, because for any given value of E and any chosen value of θ it will always be possible to select another value of θ such that the phase difference at A between the two scattered waves will be π and the structure will be eliminated. If Λ is of the same order of magnitude as ρ this is not necessarily true and structure may be present. This structure, however, will be confined to relatively small electronic energies (see Fig. 2). However, the electronic scattering is in fact highly directionally dependent, and the probability of a scattered wave of energy E arriving at A (and hence the total amplitude of the resultant electron wave) will depend upon θ for both of the above cases. It follows that the amplitude of the electron wave at the atom A for all possible angles θ depends upon the energy E of the incident electron. Thus certain energies of the incident electron will be favored over others to give constructive interference at the absorbing atom, i.e., the x-ray absorption coefficient will be greater for these values of the energy than for others. Calculations, based upon the above argument, show that the structure may extend several hundred volts from the absorption edge. This extent of structure has been verified experimentally.

THEORY

Kronig's theory[4] gives for the ratio $\chi(E)$ of the absorption coefficient of an atom bound in a

[4] R. de L. Kronig, Zeits. f. Physik **75**, 468 (1932).

diatomic molecule to that of the isolated atom

$$\chi(E)-1=\tfrac{1}{2}\int_0^{\pi}\sin\theta[(q+q^*)\cos\theta+qq^*]d\theta, \quad (1)$$

where

$$q=\frac{C(\rho,\theta)}{\rho}e^{i\tau(1-\cos\theta)},$$

in which ρ is the interatomic distance; θ is the angle between the molecular axis and the direction of the incident plane de Broglie wave of energy E; $C(\rho,\theta)/\rho$ is the ratio at the absorbing atom of the amplitude of the electron wave scattered from the partner atom to that of the incident de Broglie wave, $\tau=2\pi\rho(2E\mu)^{\frac{1}{2}}/h$; and μ is the mass of the electron. These quantities are conveniently measured in atomic units,[5] whereupon $\tau=(2E)^{\frac{1}{2}}\rho$.

To bring Eq. (1) into a form suitable for making calculations, the quantity q must be evaluated. This was done by Petersen[6] by a method similar to that used by Faxén and Holtsmark in their work on the Ramsauer effect.[7]

The scattered wave is considered as the sum of partial waves one for each (integral) value l of the angular momentum about the scattering atom. Each partial wave of order l is made up of the product of a combination of functions of the type f (see Eq. (2)) representing its radial dependence and the lth spherical harmonic representing the angular dependence. The amplitudes (and phases) of these waves are calculated in terms of the phase shifts of the partial waves at an infinite distance from the scattering atom. These phase shifts must be obtained by numerical integration of the radial equation for the incident and scattered wave in the field of the scattering atom.

The quantity q, then, is simply this composite wave altered in phase to take into account the finite separation of the two atoms in the molecule. The result of integrating Kronig's equation with this value of q is the equation obtained by Petersen:[6]

$$\chi(E)-1=\sum_{l=0}^{l=\infty}\{2\sin\delta_l[f_l(\tau)\cos\delta_l+(-1)^l f_{-l-1}(\tau)\sin\delta_l]\cdot[(l+1)f_{l+1}(\tau)-lf_{l-1}(\tau)]+(2l+1)[f_l^2(\tau)+f_{-l-1}^2(\tau)]\sin^2\delta_l\}. \quad (2)$$

In this expression δ_l is the phase shift of the partial scattered electron wave having angular momentum l in the field of the scattering atom B, and

$$f_l=(\pi/2\tau)^{\frac{1}{2}}J_{l+\frac{1}{2}}(\tau),$$

where $J_{l+\frac{1}{2}}(\tau)$ is the Bessel function of order $l+\frac{1}{2}$. The value of the quantity in brackets for any l gives the effect on the absorption coefficient of the lth partial scattered wave.

Bromine

For bromine the value of ρ was taken from Wierl[8] to be 2.28A or 4.30 atomic units.

The phase shifts for the bromine atom cannot be obtained directly by numerical integration because the self-consistent atomic field has not yet been calculated. However, the numerical integration has been performed for krypton[9] from the self-consistent field corrected for polarization of the scattering atom by the incident electron. Since the potential fields of krypton and bromine differ only slightly, the phase shifts so calculated for krypton should be acceptable approximations for the bromine atom. The calculation of χ as a function of E was first carried out with these phases. The result shows maxima in the absorption curve at 0.6, and 12 volts from the absorption edge, and minima at 4.6 and 47 volts (Fig. 4, vertical lines A, B, C).

If two atoms of different atomic numbers have fields accurately described by the Thomas-Fermi field,[10] the phase shifts for one may be obtained from those for the other by a simple equation[11] based on the WBJK method.[12] This equation was used to obtain the phases for bromine from those for krypton. The resulting phases as a function of τ shown in Fig. 2 should be somewhat more

[5] D. R. Hartree, R. de L. Kronig, H. Petersen, Physica **1**, 895 (1934).
[6] H. Petersen, Zeits. f. Physik **80**, 258 (1933).
[7] H. Faxén and J. Holtsmark, Zeits. f. Physik **45**, 307 (1927).
[8] R. Wierl, Ann. d. Physik **8**, 521 (1931).
[9] J. Holtsmark, Zeits. f. Physik **66**, 49 (1930).
[10] E. Fermi, Zeits. f. Physik **48**, 73 (1928).
[11] W. Henneberg, Zeits. f. Physik **83**, 555 (1933).
[12] See, for example, Rojansky, *Introductory Quantum Mechanics*, p. 186.

accurate than (but not greatly different from) the first set of phases.

Figure 3 shows the contributions to $\chi(E)-1$ due to the various partial waves, while the broken line in Fig. 4 is their sum or the total $\chi(E)-1$.

In comparing the experimental and theoretical results the *ratio* of the absorption of the molecule to that of the atom must be obtained. Since the scattering effect of the hydrogen atom in HBr is negligible, the absorption in HBr may be taken as that of atomic bromine. The absorption edges of bromine in Br_2 and HBr are shifted relative to one another because of a difference in the ionization potentials. Since this difference should not influence the *structure* of the absorption edge appreciably, the shift may be ignored and the ratio of absorption coefficients obtained with the two absorption edges superposed. The solid line in Fig. 4 is the ratio of the absorption per atom of bromine in Br_2 to that per atom of bromine in HBr according to the experimental findings.[2]

In agreement with experiment, the theory indicates a minimum at about 5.9 volts from the absorption edge. The predicted intensity of this minimum, however, is considerably smaller than that obtained experimentally. The predicted maximum to greater energies is not observed experimentally at all, while that at smaller energies is much weaker than the observed.

The lack of agreement between theory and experiment may be due not so much to faults in the fundamental assumptions of the theory as to failure to take into account all the influences producing the structure. Molecular vibration unquestionably affects the structure. Such effects may be brought about in three ways: First, by the change in the interatomic distance, ρ; second, by the change in the molecular field due to change in the overlapping of the two atomic fields; and third, by additional change in the molecular field due to variation of the polarization of the two atoms during the vibration. The third contribution is small enough to be neglected. In the region of low energies (<100 volts) where the structure for bromine is observed, the calculation of the second effect based on the assumption of a square well potential for each atom shows that this effect is negligible.

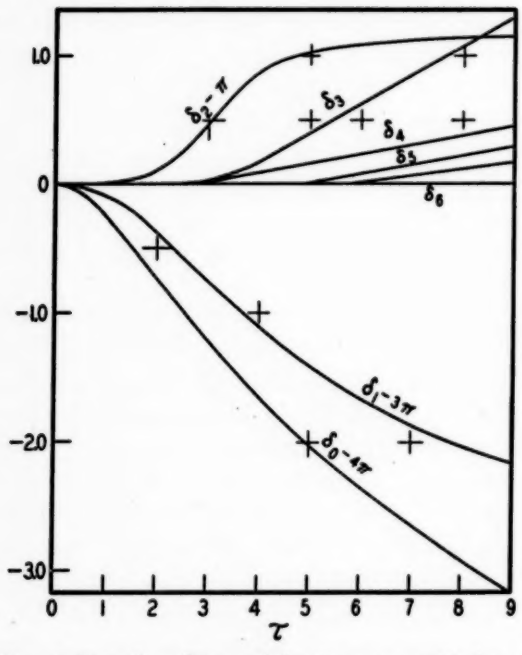

FIG. 2. Bromine. Phase shifts δ_l upon scattering as a function of $\tau=(2E)^{\frac{1}{2}}\cdot\rho$ for electronic waves of angular momentum l.

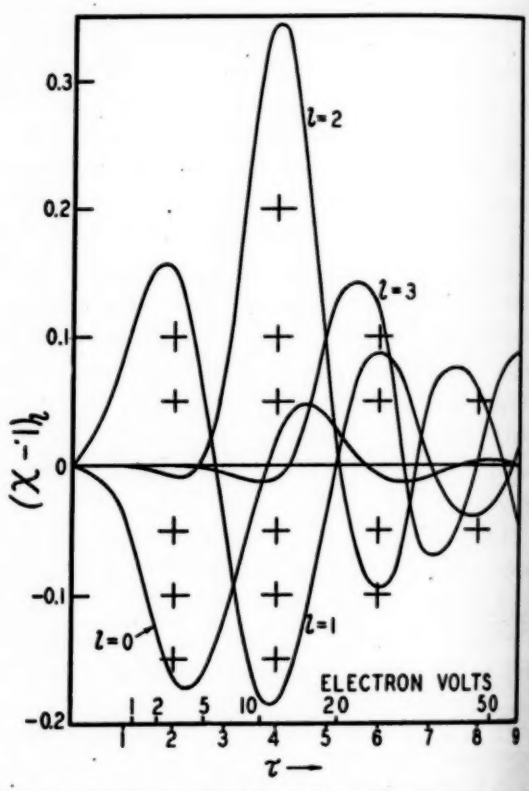

FIG. 3. Bromine. Contributions to the $\chi(E)-1$ curve by the partial scattered waves having various values of l.

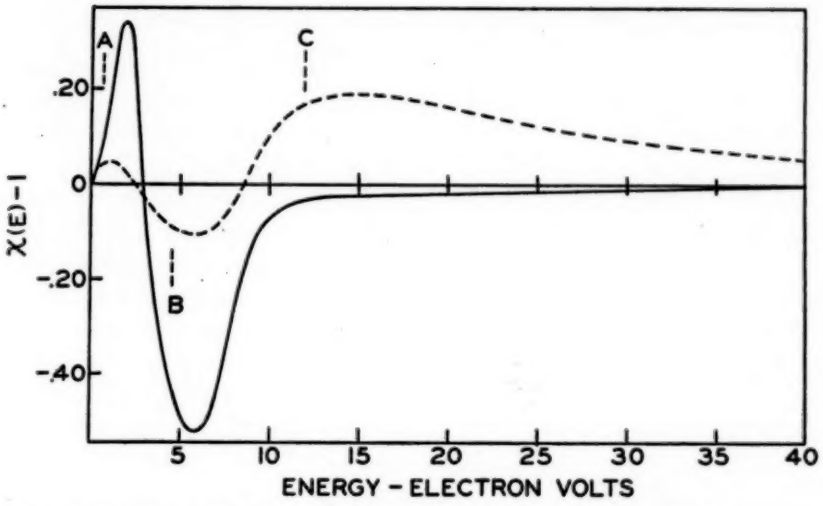

FIG. 4. Bromine. $\chi(E)-1$ as a function of the energy separation in electron volts from the absorption edge. Full line—experiment; broken line—theory. Vertical broken lines *A*, *B*, *C*—predicted positions of maxima and minima, using krypton phases.

The effect of the variation of atomic distance will be greatest at large energies. As an exaggerated case, all the atoms of bromine at room temperature were assumed to be in the first vibrational state. The amplitude of vibration in this state is 0.184 angstrom as calculated from the Morse potential. The structure predicted by Petersen's formula was calculated for the maximum and minimum atomic separations. When these curves are combined under the assumption that one-half the molecules has one of these values of ρ and the other half the remaining value, the resulting maximum at larger energies is reduced in magnitude by not more than ten percent. The conclusion, then, is that molecular vibration does not account for the absence of the predicted maximum at 15 volts from the absorption edge.

The lack of agreement in the magnitudes of the $\chi(E)-1$ curves at small energies may perhaps be explained by an error in δ_1. Hartree, Kronig and Petersen[5] have shown that in the case of the neutral chlorine atom the radial wave function for $l=1$, $\tau=0$ has only one node in place of the expected two because of the large difference in potential energy of the bound electron and incident electron at the same radius. This means that the value of δ_1 for zero energy is π instead of 2π. If such is likewise the case for bromine (which may be checked as soon as the self-consistent field is calculated for the bromine atom) then the value of δ_1 for $\tau=0$ would be 2π rather than 3π and the phase shift curve for δ_1 as a function of energy would drop sharply in the region of small energies.

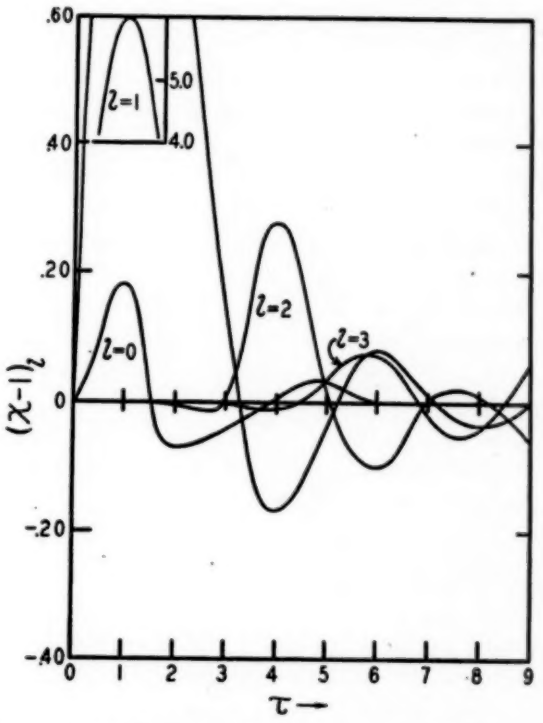

FIG. 5. Chlorine. Contributions to the $\chi(E)-1$ curve by the partial scattered waves having various values of l. The peak for $l=1$ is given in the inset.

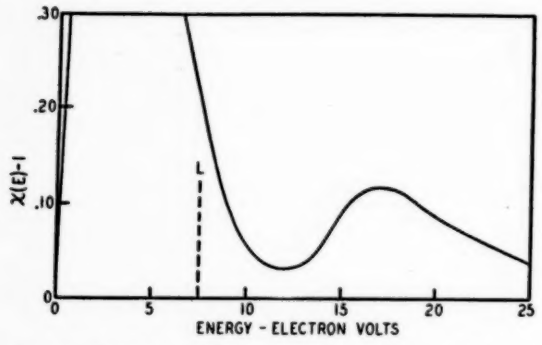

FIG. 6. Chlorine. $\chi(E)-1$ as a function of the energy separation in electron volts from the absorption edge. Full line—theory; vertical broken line, L—location of absorption minimum according to experiments by Lindh.

Thus the predicted $\chi(E)-1$ curve might easily rise to $+0.4$ in agreement with experiment. The effect of the choice of δ_1 at $\tau=0$ is illustrated both in the work on $GeCl_4$[5] and on chlorine in the present paper.

CHLORINE

Previous approximate calculations of the structure to be expected in the K-absorption edge of chlorine gas have been made by Petersen[13] using the values of δ_l computed for argon[14] instead of those for the chlorine atom. Since that time, however, the phase shifts for chlorine have been computed by Hartree, Kronig and Petersen.[5] From their phase shifts the structure for chlorine has been recomputed. Fig. 5 gives the partial $\chi(E)-1$ curves and Fig. 6 the final curve and the experimental results of Lindh.[15]

The huge peak at low energies is introduced by the fact that the phase shift δ_1 at $E=0$ is π rather than 2π. It is very doubtful that the absorption coefficient ratio actually is as great as this theory would indicate at low energies. The effect of the introduction of the new value of δ_1 is to shift the first predicted minimum to larger energies so that it now appears at 12 volts rather than the observed 7.5 volts.

[13] H. Petersen, Zeits. f. Physik **80**, 258 (1933).
[14] J. Holtsmark, Zeits. f. Physik **55**, 437 (1929).
[15] A. E. Lindh, dissertation, Lund., 1923.

CONCLUSIONS

In addition to the factors already discussed which introduce errors into the calculated absorption coefficients for bromine and chlorine, there are several others.

1. In the calculation of the scattered wave exchange scattering is neglected. However, in the calculation of the scattering of slow electrons by krypton, Holtsmark[9] likewise ignored exchange scattering and obtained good agreement with experiment. Hence this effect is small.

2. Multiple scattering between the two atoms in the molecule is neglected. This is justified at energies greater than a small fraction of a volt because of the small cross section for single scattering.[16]

3. The phase shifts used in the calculations may be in error by as much as 0.2 radian because of the uncertainty in the amount of polarization of the scattering atom by the incident electron, the inaccuracy of the Henneberg extrapolation at very low energies and the interpolation between the small number of points on the δ_l *vs.* τ curve given by Holtsmark.[9]

4. Kronig's theory replaces the molecular field by the superimposed Hartree fields of the atoms of the molecule.

In conclusion, then, it may be said that although Kronig's theory of the fine structure of x-ray absorption gives rather good agreement at large distances from the absorption limit, as illustrated by the results on $GeCl_4$, the approximations near the edge which are involved in making a numerical comparison between theory and experiment become increasingly serious. Thus a really good agreement between the two can no longer be expected, although the fundamental idea of electron scattering is still the predominant influence in producing the observed structure.

[16] Ramsauer and Kollath, Ann. d. Physik **87**, 259 (1928).

The Origin of Radio Fade-Outs and the Absorption Coefficient of Gases for Light of Wave-Length 1215.7A

WILLIAM M. PRESTON
Research Laboratory of Physics, Harvard University, Cambridge, Massachusetts

(Received March 9, 1940)

It has been suggested that the ionization in the *D* region which causes radio fade-outs is caused by radiation of the first line of the Lyman series of hydrogen, at 1215.7A, from solar eruptions. The actual absorption coefficients for this line, previously only roughly known, have been measured with the following results: oxygen 0.28, nitrogen $\leqslant 0.005$, carbon dioxide 2.01, water vapor 390 (all values reduced to NTP). Although it can probably penetrate to sufficiently low altitudes, it appears unlikely that this line can produce ionization and hence cause fade-outs. The possibility is considered that these may be due to higher Lyman series members, or to x-rays of around 2A wave-length.

RADIO fade-outs are characterized by the weakening or disappearance of reflections of high frequency radio waves from the *E* and *F* layers of the ionosphere. The effect is transient, lasting from a few minutes to an hour or more. The immediate cause is a sudden increase in the ionization in the *D* region, somewhere below an altitude of 100 km, where because of the relatively higher pressure the presence of free ions results in the absorption of short radio waves. Fade-outs have been definitely correlated with eruptions or localized disturbances of the sun's chromosphere.[1,2] The coincidence in time between the initial observation of a solar disturbance and the onset of a fade-out is close, and the fade-out occurs only over the daylight half of the earth, so we may assume that the ionization is caused by ultraviolet light rather than by charged corpuscles. This radiation must be in part at least of a frequency such that it can penetrate rather deeply into the earth's atmosphere and cause ionization where it is absorbed.

Study of these solar eruptions with the spectroheliograph has shown that they are characterized by the sudden appearance of exceptionally bright flocculi, in the neighborhood of sun-spots. The emission consists solely of an intense line spectrum in which the Balmer series of hydrogen and lines of He I and Ca II have been identified.[3] The intensity of Hα in emission is of the same order of magnitude as the intensity of the blackbody continuum in near-by areas. Since the emission of Hα is necessarily followed by the emission of Lyα (the first line of the Lyman series of hydrogen, at 1215.7A), and since the intensity of blackbody emission falls off very rapidly in the ultraviolet, it may be inferred that the intensity of Lyα is enormously greater than that of the blackbody continuum in the same wave-length region. In fact, Richardson estimates[4] that the emission from a single bright eruptive area of Lyα alone is equal to about 60 percent of the total blackbody radiation from the entire solar disk, in the wave-length range from 1100A to 1300A. Now Lyα lies in a region of comparatively great transparency of air,[5] a sort of "hole" between the strong continuous absorption of O_2 (1760–1350A) and the diffuse absorption bands of both O_2 and N_2 extending from 1000A to shorter wave-lengths. Martyn and his co-workers have suggested that Lyα-radiation, because it is emitted from solar eruptions and because of its penetrating power, may be responsible for fade-out ionization.[2]

The actual value of the absorption coefficient of air at this wave-length has been only roughly estimated, because of technical difficulties in measuring very small absorption coefficients by the ordinary method of introducing gas into a spectrograph connected directly to a discharge tube source, without an intervening window. In

[1] J. H. Dellinger, Terr. Mag. **42**, 49 (1937); R. G. Giovanelli and A. J. Higgs, Terr. Mag. **44**, 181 (1939).
[2] Martyn, Munro, Higgs and Williams, Nature **140**, 603 (1937).
[3] R. S. Richardson and R. Minkowski, Astrophys. J. **89**, 347 (1939).
[4] R. S. Richardson, Astrophys. J. **90**, 368 (1939).
[5] T. L. Lyman, Phys. Rev. **48**, 149 (1935).

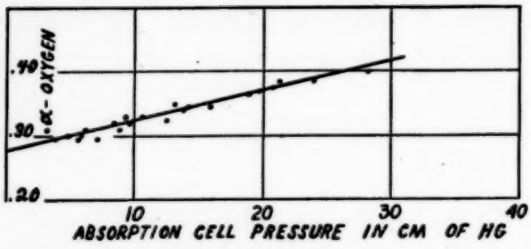

FIG. 1. The absorption coefficient α of oxygen, per centimeter path reduced to NTP, as a function of the pressure in the absorption cell.

view of a doubt expressed by Wulf and Deming[6] as to the ability of Lyα-radiation to penetrate the atmosphere much below 100 km, it appeared worth while to obtain a reasonably accurate value. It happened that an apparatus was available in this laboratory which, although built for a different purpose, was well suited for the problem.

EXPERIMENTAL PROCEDURE AND RESULTS

The source was a Wood-type hydrogen discharge tube. An absorption cell 21.8 cm long was closed at each end by a lens of lithium fluoride, which is satisfactorily transparent at this wave-length if properly handled.[7] Light from the discharge was rendered parallel by the first lens, passed through the absorption cell, and was brought to a focus on the slit of a one-meter grating vacuum spectrograph by the second lens. A second slit in the focal plane of the spectrograph isolated the light of Lyα, which then passed through a lithium fluoride window into an argon-filled photoelectric cell. The latter had a sensitive element made of platinum, which is insensitive to light of wave-length longer than 2500A, an advantage in reducing the background due to stray reflected light. High sensitivity and stability were obtained by measuring the photoelectric current with a balanced d.c. amplifier[8] and a sensitive galvanometer.

The intensity of Lyα was first measured when the absorption cell was evacuated. The gas to be studied was then quickly admitted from a storage bulb, to any desired pressure up to atmospheric, and the decreased intensity noted. The approximately linear relationship between light intensity and galvanometer deflection under the operating conditions was shown by the consistency of data obtained at different intensity levels and with different potentials on the photoelectric cell. The source discharge was largely "atomic," as shown by its crimson color. In a preliminary spectrogram Lyα was far more intense than any neighboring molecular line, and the dispersion of 8.3A/mm was sufficient so that no appreciable intensity of radiation other than Lyα could enter the photo-cell, even with a comparatively broad slit opening.

Tank oxygen was freed from water vapor and CO_2 by passing it slowly through tubes containing P_2O_5 and KOH. The results obtained are shown in Fig. 1, where the absorption coefficient α is plotted as a function of the pressure of O_2 in the absorption cell. Here α is defined by the equation $I=I_0e^{-\alpha l}$, where I_0 is the intensity measured with the absorption cell evacuated, I the intensity transmitted with gas in the cell, and l the path in centimeters of gas reduced to normal pressure and temperature. In the case of oxygen, α was measured over a pressure range of from 3 to 29 cm. In Fig. 1, the points represent individual determinations. It is seen that α increases linearly with the pressure; extrapolating to zero pressure, its value is 0.28.

The exact origin of this oxygen absorption is uncertain. The wave-length λ1215.7 is probably outside the range of the continuous absorption band with maximum at 1450A, carefully studied by Ladenburg,[9] which is already very weak at 1300A. Absorption in this band results in dissociation, with accompanying "clean-up" of oxygen. This effect was never measurable, although the source also radiated some energy in the molecular spectrum over a wide wave-length range. Spectrograms taken by Price and Collins[10] show a number of absorption bands within the range 1350 to 1000A. These are weak and diffuse, and increase in width with pressure of O_2. They probably approach as a limit the first ionization potential of O_2, near 1000A, and their diffuse character may arise from predissociation. One of these bands, in the above reference, has its

[6] O. R. Wulf and L. S. Deming, Terr. Mag. **43**, 283 (1938).
[7] E. Schneider, Phys. Rev. **49**, 341 (1936).
[8] D. B. Penick, Rev. Sci. Inst. **6**, 115 (1935).
[9] R. Ladenburg and C. C. Van Voorhis, Phys. Rev. **43**, 115 (1933).
[10] W. C. Price and G. Collins, Phys. Rev. **48**, 714 (1935).

long wave-length edge at 1211.8A, at a pressure of a fraction of a millimeter. The absorption of Ly_α may be due to an extension of this band at higher pressure, or to a weaker neighbor. Pressure broadening of the lines of a molecular band may account for the increase in α with O_2 pressure.

Tank nitrogen was freed of CO_2 and water vapor in a similar manner. Its absorption coefficient for Lyα was measured as 0.005 at 45 cm pressure. Because of the very small value of α and the possibility of a trace of impurities, this value should be taken only as an upper limit.

In the case of dry CO_2 free air, Fig. 2, the same type of increase in α with pressure was noted as with oxygen. The extrapolated absorption coefficients were $\alpha=0.063$ at zero pressure and $\alpha=0.152$ at atmospheric pressure. From the experimental values of α for O_2 and N_2, the calculated value of α for air (extrapolated to the limit at zero pressure) is $0.21\times0.28+0.78\times0.005=0.063$, in agreement with the measured value. (We have here assumed that the value of α for N_2 is independent of pressure, something not proved experimentally. Even if we neglect the absorption of N_2 completely, the computed value of α for air is in fair agreement.) At atmospheric pressure, a 4.5-cm path of dry, CO_2 free air will reduce the intensity of Lyα by a factor $\frac{1}{2}$; at pressures below 1 cm the equivalent path (reduced to NTP) would be 11 cm.

For dry CO_2, the value measured for α was 2.01; the mean variation of five readings over a pressure range in the absorption cell of from 8 mm to 6 cm was about 1 percent.

A side tube containing distilled water was attached to the absorption cell, and cooled in a dry ice—alcohol mixture to regulate the vapor pressure. The average value of α was 390, representing three readings at vapor pressures between 0.031 and 0.018 cm. The accuracy of this value is not great, because of the rapid change of vapor pressure with temperature. Rathenau has photographed the absorption spectrum of water vapor in this region.[11] Lyα falls within a strong diffuse band, one of a series probably leading to H+OH (excited) and showing evidence of predissociation.

[11] G. Rathenau, Zeits. f. Physik **87**, 32 (1932).

Discussion

We may now return to the problem of the possible connection between Lyα-radiation and radio fade-outs. To begin with, the location of the normal *D* region has been very uncertain. It is not known whether the ionization reaches a maximum at some altitude below the *E* layer, as it would if it were caused by monochromatic light with a definite absorption coefficient, or whether it is an ill-defined region extending with decreasing ion density from the *E* layer to lower altitudes. Also, we have no reason to assume that the fade-out ionization has the same distribution in altitude as the normal *D* region. However, recent measurements by Budden, Ratcliffe, and Wilkes have been made on the reflection of very long (16 kc) radio waves.[12] At angles of incidence between 30 and 60° these are normally reflected at a height of approximately 67 km, and they estimate the electron density to be about 300 electrons/cc at this altitude. Measurements made during solar disturbances associated with short wave fade-out indicated a small but definite decrease in the altitude at which these long waves were reflected. This shows definitely that the fade-out radiation must penetrate with appreciable intensity below 70 km. If we assume 9×10^{14} air molecules per cc at an altitude of 70 km,[13] the equivalent air path

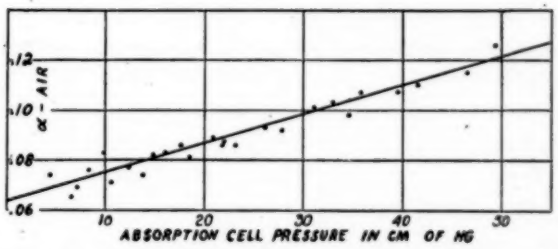

FIG. 2. The absorption coefficient α of air, per centimeter path reduced to NTP

at NTP for radiation penetrating to this level is about 20 cm.

If the absorption coefficient of air is taken as $\alpha=0.06$ for Lyα, and *if* we assume that the absorption above 70 km is due primarily to an equivalent path of 20 cm of *dry* air, then about

[12] Budden, Ratcliffe, and Wilkes, Proc. Roy. Soc. **171**, 188 (1939).

[13] O. R. Wulf and L. S. Deming, Terr. Mag. **41**, 299 (1936).

30 percent of the Lyα-radiation would penetrate below 70 km, and 8 percent below 65 km. The oxygen in the upper atmosphere is probably mostly in the molecular state below 80 km, and in the atomic state above 100 km.[6] Atomic oxygen in the normal state has no absorption line close to Lyα. Since the equivalent path at NTP above 80 km is only 5 cm, our estimate of the penetration of Lyα will not be greatly altered by the fact that some of the oxygen above 80 km is dissociated.

Because of its very high absorption coefficient ($\alpha=390$), an equivalent path at NTP of 0.1 mm of water vapor above 70 km (for example, a concentration of about 1 part in 2000 in the region between 70 and 80 km) would reduce the intensity of Lyα to about 2 percent at 70 km. The H_2O molecule is easily split up into H+OH (excited) by electron impact, and emission of the intense OH bands near 3100 results. Neither these bands nor the Balmer lines of hydrogen have been observed in the spectrum of the aurora or the night sky,[14] so that both hydrogen and water vapor must be present, if at all, in very small concentrations above 80 km. Some authors have suggested concentrations of water vapor of the order of 1 part in 10,000 in the *F* region[2,15] in order to maintain a reasonable temperature equilibrium. This would not greatly reduce the penetration of Lyα unless its presence in the *F* region could be shown to require a somewhat greater concentration between 70 and 80 km.[16]

Next we must consider whether the absorption of Lyα can produce ionization in any of the gases present in the upper atmosphere: N_2, O_2, O, O_3, and possibly H_2O. Their ionization potentials are as follows: N_2, 15.5 volts; O_2, 12.2 volts; O, 13.55 volts; H_2O, 12.56 volts;[17] O_3 unknown. None of these, with the possible exception of O_3, can be ionized in a single process by Lyα, whose quantum energy is 10.15 electron-volts. Martyn,[2] however, supposed that Lyα might ionize atomic oxygen in a manner suggested by Chapman and Price.[14] O I has a well-known metastable level, the $^1S_0$, (4.2 volts above the ground state) which is the initial state for the transition which produces the auroral green line. If metastable oxygen atoms are present, the following process might occur:

$$O(^1S_0)+h\nu\,(\lambda=1217.6\text{A})\rightarrow O(^1P_1).$$

The $^1P_1$ lever lies 0.75 volt above the ^4S ground state of singly ionized oxygen. There would be some possibility of a second kind collision as a result of which the $^1P_1$ atom would revert to the ^4S state, with the loss of an electron. However, if it can occur at all, this three-step process must be extremely rare at altitudes as low as 70 km. First, there seems to be no likely process at this altitude which results in the formation of $^1S_0$ metastable atoms. Since at 70 km the average time between collisions is about 5×10^{-6} second, metastable atoms would in any case have a low concentration because of their short lifetime, unless produced at a high rate. Second, the necessary wave-length for excitation to the $^1P_1$ level is 1217.6A, which differs from Lyα by 1.9A. The width of a spectrum line $\Delta\lambda$, due to temperature broadening, is proportional to the wave-length. If the width of Lyα were 3.8A, so that it overlapped the oxygen line, the width of Hα should be over 5 times as great. Richardson[4] gives a width of 2A for Hα in an eruptive area, and states that there is no large Doppler shift to indicate rapid motion of the source.[18] Finally, the lifetime of the $^1P_1$ state, which is not metastable, is probably short compared with the average time of 5×10^{-6} second between collisions, so

[14] S. Chapman and W. C. Price, Reports on Progress in Physics **3**, 42 (1936).

[15] G. H. Godfrey and W. L. Price, Proc. Roy. Soc. **163**, 228 (1937) and D. F. Martyn and O. O. Pulley, Proc. Roy. Soc. **154**, 455 (1936).

[16] The temperature in the *F* regions is probably high enough so that atoms as light as hydrogen have a fair chance of escaping from the earth's gravitational field. This would explain the absence of much hydrogen at great heights, and would also indicate a gradual loss of H_2O by dissociation and subsequent escape of the hydrogen. To maintain any concentration of H_2O, a replenishment by upward diffusion from lower altitudes is necessary.

[17] W. C. Price, J. Chem. Phys. **4**, 147 (1936).

[18] Richardson objects to the use of the word "eruption" to describe the exceptionally bright flocculi associated with fade-outs for just this reason, that in general there is no *large* radial velocity over the disturbed area. Protuberances frequently appear in the neighborhood of the bright flocculi, which consist of masses of gas moving with high velocity. At least in many cases, these appear dark in the light of *H*α against the bright background of the flocculi, and their emission of Lyα is consequently relatively small. For the excitation process under discussion, a *bright* protuberance moving *in* towards the sun with a velocity of about 500 km/sec. must be postulated; this motion would have to persist for the entire duration of the fade-out. Apparently, nothing of this sort has been observed.

that radiation rather than loss of energy in a second kind collision will be favored.[19]

Wulf and Deming have suggested the possibility that fade-outs may be caused by the ionization of ozone.[6] Although the maximum concentration of ozone in the atmosphere is known to occur near 25 km, they calculate that at 70 km there are still 6.35×10^7 molecules of O_3 per cc. Unfortunately, the ionization potential of O_3 is not known. In view of the small dissociation energy of O_3 (about 1 electron volt), it is unlikely to be much less than that of O_2 (12.2 volts, ~1010A). The hypothesis of Wulf and Deming that, by some unknown multiple process, the dissociation of ozone by light of comparatively long wave-length may lead to small amounts of ionization, must await experimental elucidation.

To summarize, Lyα will penetrate to an altitude of 67 km, at which fade-out ionization has been experimentally observed, unless the water vapor concentration in the region from 70–80 km is of the order of 1 part in 2000. However, there seems to be no known process by which it is likely to cause appreciable ionization.

The question next arises, whether any of the other radiation in the far ultraviolet, inferred from the visible spectrum of solar eruptions, may be the cause of fade-outs. Probably only the higher members of the Lyman series need to be considered.[20] These are:

2	1025.73	5	937.81
3	972.55	6	930.76
4	949.74	7	926.24

The ionization potential, 13.53 volts, corresponds to 911.76A. It is worth noting that the intensity of the higher members of the Balmer series is observed to fall off *far* less rapidly in these areas of solar disturbance, than in a laboratory discharge tube.[3] The third and higher members of the series lie above the first ionization potential of oxygen (at 1010A), in a region of weak continuous absorption.[14] In the same region are the strong Hopfield absorption bands, which show some evidence of pre-ionization. Takamine and Suga investigated qualitatively the absorption of the higher Lyman series members in oxygen,[21] and found that the third, sixth, and eighth members were completely absorbed by a path of less than 0.1 mm of oxygen at NTP; these lines coincide with bands of the Hopfield series, and would certainly be absorbed in the upper atmosphere at altitudes at which O_2 first appears. The remaining members of the series, numbers 4, 5, 7, 9 and some higher, have much smaller absorption coefficients in oxygen, and might therefore penetrate below the *E* region. However, N_2 also has some strong absorption bands in this neighborhood, although their accurate wave-lengths do not seem to have been published.[14] Until the actual absorption coefficients of these lines in oxygen and nitrogen have been determined experimentally, it will not be possible to decide whether they can penetrate to altitudes as low as 67 km, where they might produce fade-out ionization.

It happens that the Lyman series continuum largely overlaps the ionization continuum of atomic oxygen, which commences at 910.42A. It is therefore probable that radiation in the hydrogen continuous spectrum will be absorbed by atomic oxygen at relatively great altitudes, with the production of ionization.

Even if it could be shown that part of the Lyman series radiation from solar eruptions can produce ionization at sufficiently low altitudes to be a *possible* cause of radio fade-outs, certain general considerations seem to argue against this explanation. In order to estimate the intensity and spectral distribution of the solar radiation normally incident on the earth in the far ultraviolet, it was formerly customary to assume that it followed Planck's equation for a blackbody at about 6000°K. This predicts such a small intensity for wave-lengths shorter than 1000A,

[19] Martyn apparently assumed second kind collisions between excited $^1P_1$ oxygen atoms and *electrons* as responsible for transfer to the ^4S state. Possibly he confused the probability that a free electron will collide with a gas molecule, per unit time, with the probability that any particular gas molecule (in particular, an excited atom) will collide with a free electron. The former probability is relatively large, even at 70 km; the latter (which obviously depends on the free electron density) is entirely negligible at an electron density of the order of 10^3/cc.

[20] The $^1S_0-{}^1P_1$ series of He I, whose high intensity is to be inferred in the same manner as that of the Lyman series, commences at 584A, a region of such strong air absorption that penetration of more than a fraction of a millimeter at NTP is impossible. Ca II, the only other spectrum identified in spectroheliograms of eruptive areas by Richardson, has no lines in the far ultraviolet; its ionization potential is 11.8 volts.

[21] T. Takamine and T. Suga, Scientific Papers, Inst. of Phys. and Chem. Research, Tokyo **29**, 213 (1936).

which alone are capable of producing ionization, that there is serious reason to doubt whether it can account for the observed ionization, particularly in the F region.[22,23] As a result it has been concluded that there is an "ultraviolet excess" intensity, far above the value calculated from Planck's formula. This is made plausible by spectroheliograms taken at total eclipse, which show predominantly a line spectrum coming from the chromosphere; most of the intensity comes from H I, He I, and He II. It has been estimated by Saha[22] that, in protuberances, the ratio of He II to He I is 10^{38} times that calculated on the assumption of purely thermal excitation at 6500°K. There is a good chance that, of all the radiation coming from the sun, in the region of wave-lengths shorter than 1000A, by far the greater part is due to the Lyman series (including their continua) of H I and He II, and the $^1S_0-{}^1P_1$ series of He I.[24] Perhaps the escape of this radiation, which of course is strongly absorbed in the sun's atmosphere, is facilitated by convective streaming in which masses of ionized hydrogen and helium from lower regions of high excitation are shot out to great heights.[23]

It is therefore quite possible that the normal ionosphere is largely produced by hydrogen and helium, rather than blackbody, radiation. It has already been stated that the higher members of the Lyman series of hydrogen can ionize O_2 in two possible ways, and the continuum can ionize atomic oxygen. The $^1S_0-{}^1P_1$ series of He I has the wave-lengths 584.4, 537.1, 522.3 etc.; the Lyman series of He II, 303.7, 256.3 etc. Both these series are capable of ionizing N_2, O_2 and O. When the actual values of the absorption coefficients are measured, it will be possible to estimate at what altitude maximum ionization will occur for each line, and the calculations will be much simpler than in the case of radiation with a continuous frequency distribution.

Whatever the source of the extra radiation in the far ultraviolet, some connection must be established between its intensity and the sun-spot cycle. The electron density in the E and F layers varies greatly with the average sun-spot number. Perhaps a considerable portion of the ionization is due to radiation from the bright flocculi normally associated with sun-spots[25] (not to be confused with the transient exceptionally intense flocculi which coincide with radio fade-outs), particularly during the maximum of the sun-spot cycle, while at sun-spot minimum a relatively larger proportion comes from the rest of the chromosphere.

We are now faced with a very definite dilemma. The study of radio fade-outs shows definitely that there is little alteration in the electron density of the E and F layers during a fade-out.[26] This can only mean that the radiation causing fade-outs is *qualitatively* different from that responsible for the normal E and F layers. Suppose we attribute fade-outs to Lyman series radiation from solar eruptive areas. These same areas also emit intensely the helium series starting at 584A. Because the E and F layers are not much disturbed during fade-outs, these two line series cannot be responsible for more than a small fraction of the *normal* E and F layer ionization. This contradicts the considerable evidence that they comprise a large, if not predominant fraction of the intensity in the far ultraviolet. Alternatively, if these series *are* responsible for a considerable part of the normal E and F ionization, they *cannot* cause radio fade-outs.

A way out would be offered if there were evidence for any other radiation from eruptive areas, of a type not normally coming from the sun with appreciable intensity. It seems scarcely possible that the spectrum of any element, other than hydrogen, helium, and ionized calcium, can occur with sufficient intensity to cause fade-outs and yet have been overlooked in studies with the spectroheliograph. Now because of the many processes by which O, O_2 and N_2 can be ionized, it is improbable that the absorption coefficient α (per unit path length, at NTP) of air, which

[22] M. N. Saha, Proc. Roy. Soc. **160**, 160 (1937). We have direct evidence, from the daylight flash spectrum of the upper atmosphere, that one ionization process is $N_2+h\nu(\lambda<661\text{A})\rightarrow N_2^+(\text{excited})+\text{electron}$. Saha has also estimated that if only one-tenth of the measured F region electron density is attributed to this process, the intensity of ultraviolet light in this wave-length region must be of the order of 10^6 times as large as that calculated from the energy distribution of a blackbody.

[23] W. Grotrian, Naturwiss. **27**, 555, 569 (1939).

[24] Professor Donald Menzel, in conversation, emphasized the enormous intensity to be expected from He I, λ 584A, relative to the blackbody continuum.

[25] F. L. Mohler, Science **90**, 137 (1939).

[26] L. V. Berkner and H. W. Wells, Terr. Mag. **42**, 301 (1937) and L. V. Berkner, Phys. Rev. **55**, 536 (1939).

rises to a value of several hundred somewhat beyond 1000A,[27] will fall again to very low values until wave-lengths considerably shorter than the K-absorption limits of oxygen and nitrogen.[28] Hence unless the fade-out producing radiation lies near 1000A, it is probably of much shorter wave-length. If by some means moderately hard x-rays are liberated from eruptive areas, these will only be observed by ionization in the D region. For example, at 2.3A the linear absorption coefficient of air is $\alpha = 0.04$, and 50 percent of radiation of this wave-length would be absorbed in a path of 17 cm at NTP; it would accordingly penetrate somewhat below an altitude of 70 km. A wave-length of 2.3A corresponds to a quantum energy of 5400 electron-volts, and this therefore is a rough lower limit to the energies which would have to be involved.

Korff and Johnson[29] have already made the suggestion that the ionizing radiation which causes fade-outs may lie in the x-ray region. On the chance that it might include a highly penetrating component which could be detected at low altitudes, they measured the ionization at 20 km, by means of a Geiger counter supported by a sounding balloon, before, during, and after a fade-out. The counting rate remained constant within experimental error, from which they concluded that the fade-out producing radiations is predominantly of wave-length greater than 0.1A. From other considerations they set 1.5A as an upper wave-length limit.

Is there any independent evidence that such high energy radiation may be produced in eruptive areas of the sun and escape into space? Vegard[30] has already suggested that soft x-rays may be responsible for part of the *normal* ionosphere, and harder x-rays for fade-out ionization. He assumes that the aurora is caused by high energy electrons, and concludes that these must produce x-rays of comparable energy in the sun's chromosphere. However, most authors have not felt it necessary to evoke x-rays in order to explain the normal ionosphere, and there are grave objections to the theory that the aurora is caused by fast electrons. First, it is questionable whether charged particles of the same sign could continually leave the sun, and whether they could retain the form of a beam in shooting out to great distances, because of electrostatic forces. Moreover, there is a curious puzzle presented by the observation that intense auroral displays and magnetic storms frequently follow, after a period of about 24 hours, solar eruptions which have caused radio fade-out. If we assume that particles, expelled from the eruptive area at the same time as the fade-out producing radiation, cause these aurora, their velocities can be only of the order of 1000 km/sec. For electrons this corresponds to an energy of 3 electron-volts and negligible penetrating power.

A more recent hypothesis[31] is that the rapidly moving gas masses known as protuberances, which usually arch back into the sun, under certain conditions may be expelled into space. Escape may be favored by increased radiation pressure if a protuberance occurs in the neighborhood of an eruptive area. Such a gas mass, containing positive ions, electrons, and neutral atoms, might be electrically neutral as a whole and hence tend to remain together in space. It has been calculated that the slow positive ions would carry the electrons along with them and follow, in the earth's magnetic field, the same type of orbit as the fast electrons assumed by Vegard. Positive ions with velocities of 1000 km/sec. would have much larger energy and penetrating power than electrons of the same velocity, and they could produce aurora at altitudes in the neighborhood of the E region. Since the high energy in this second hypothesis is associated with heavy particles, there is no indication that penetrating x-rays would be produced in the chromosphere.

To summarize our argument: It is very unlikely that Lyα-radiation can produce fade-out ionization. Further experimental work will show whether higher Lyman series members might be responsible, insofar as their penetrating and ionizing power go. But there are strong reasons

[27] E. G. Schneider, forthcoming publication.

[28] The K-absorption limit of N, for example, lies at 31.56A. At a somewhat longer wave-length, 44.5A, $\alpha = 5.0$; at the shorter wave-length 17.67A, $\alpha = 9.1$. (A. H. Compton and S. K. Allison, *X-rays in Theory and Experiment* (Van Nostrand, 1935).)

[29] T. H. Johnson and S. A. Korff, Terr. Mag. **44**, 23 (1939).

[30] L. Vegard, Naturwiss. **26**, 639 (1938).

[31] As a general reference for this and the preceding paragraph, see reference 23.

for supposing that the normal E and F layers are produced to a considerable extent by atomic rather than by blackbody radiation, and this must be attributed largely to hydrogen and helium. If this is so, the absence of any large disturbance of the E and F regions during fade-outs indicates independently that hydrogen or helium radiation *cannot* be responsible for fade-outs. It is then difficult to see to what type of radiation we can attribute fade-outs, unless we consider the possibility of x-rays. However, no independent evidence for the production of x-rays in eruptive areas of the sun seems to be suggested by our present incomplete theories of conditions in the chromosphere and of delayed disturbances in the earth's upper atmosphere following solar eruptions.

I particularly wish to express my appreciation to Professor Otto Oldenberg for many helpful discussions of the subject of this article.

Note: Just before the submission of this article for publication an article appeared by S. E. Williams (Nature **145** 68 (1940)). Williams investigated the absorption of Lyα in oxygen, and found a coefficient approximately 50 times larger than that reported in the present paper. Lacking details of his experimental method, no explanation can be suggested for this huge difference. Nearly any impurity in his absorbing gas, particularly H_2O or CO_2, would result in too large a value for the absorption coefficient.

MAY 15, 1940 PHYSICAL REVIEW VOLUME 57

The Arc Spectrum of Silver*

A. G. SHENSTONE
Palmer Physical Laboratory, Princeton University, Princeton, New Jersey
(Received March 4, 1940)

AMONG all the simpler arc spectra, that of silver has been for years the best example of a badly analyzed spectrum. This is the result of inadequate observation of the spectrum by the many workers who have measured it. The reason for the incompleteness of the observations now appears to be the fact that instruments of too great dispersion were used for the detection of very diffuse lines. Such lines are numerous in silver and attain widths as great as 500 wave numbers.

New observations have been carried out in Princeton with various forms of arc. A preliminary report has been published.[1] The form of arc, which was found by R. Haskins in his senior thesis problem to be the most suitable for observations in the visible and infra-red, was as follows. The electrodes consisted of silver buttons about 5 mm in diameter screwed firmly to water-cooling tubes. The arc was run at 6 to 8 amperes in air or oxygen with the anode down, the cathode being focused on the slit of the spectrograph. Under these conditions the cathode disintegrates by sputtering and the anode increases in weight. The unusual procedure of observing arc lines at the cathode is effective in this case, I believe, because of the high excitation of most of the new lines. It has the added advantage of eliminating the band lines which occur rather strongly at the anode. In the infra-red some exposures were taken with a 20-ampere graphite arc and in the Schumann region small graphite arcs in pure nitrogen were used.[2] This type of arc was necessitated by the fact that silver arcs will hardly run at all in pure nitrogen. The arc observations were made on the following instruments. λ10,000–5000 Steinheil three-prism glass spectrograph; λ5000–2100, Hilger El quartz spectrograph; λ2100–1250, a 30,000 line 2-meter vacuum spectrograph.

In addition the spectra from a hollow cathode argon-filled tube were observed with the 30,000 line 21-ft. grating. The tube was run with the silver in the cathode molten, and very good pictures were obtained in less than an hour.

* When this paper was in preparation there appeared a letter in Phys. Rev. **57**, 243 (1940) from Ebbe Rasmussen in which some of the new levels of AgI, notably $s^3\,{}^2D$, were given.

[1] A. G. Shenstone, Phys. Rev. **56**, 209 (1939).

[2] A. G. Shenstone, Trans. Roy. Soc. **237**, 453 (1938).

TABLE I. *Even levels of* AgI.

ORIGIN	NAME	LEVEL	n^*	ORIGIN	NAME	LEVEL	n^*
$4d^{10}5s$	$5s\,^2S_{\frac{1}{2}}$	61106.50	1.34089	$4d^{10}11d$	$11d\,^2D_{1\frac{1}{2}}$	1355.35?	8.99800
$4d^{9}5s^2$	$5s^2\,^2D_{2\frac{1}{2}}$	30864.40	1.25182	$4d^{10}11d$	$11d\,^2D_{2\frac{1}{2}}$	1354.99?	8.99933
$4d^{9}5s^2$	$5s^2\,^2D_{1\frac{1}{2}}$	26392.5		$4d^{10}12d$	$12d\,^2D$	1098.9	9.994
$4d^{10}6s$	$6s\,^2S_{\frac{1}{2}}$	18550.35	2.43220	$4d^{9}5s(^3D)6s$	$5s6s\,^4D_{3\frac{1}{2}}$	−18306.4	2.293
$4d^{10}5d$	$5d\,^2D_{1\frac{1}{2}}$	12362.50	2.97932	$4d^{9}5s(^3D)6s$	$5s6s\,^4D_{2\frac{1}{2}}$	−19058	2.336
$4d^{10}5d$	$5d\,^2D_{2\frac{1}{2}}$	12342.28	2.98181	$4d^{9}5s(^3D)6s$	$5s6s\,^4D_{1\frac{1}{2}}$	−20159	
$4d^{10}7s$	$7s\,^2S_{\frac{1}{2}}$	9219.52	3.4500	$4d^{9}5s(^3D)6s$	$e\,^2D_{2\frac{1}{2}}$	−20964	
$4d^{10}6d$	$6d\,^2D_{1\frac{1}{2}}$	6903.37	3.98700	$4d^{9}5s(^3D)6s$	$5s6s\,^4D_{\frac{1}{2}}$	−22876.3	
$4d^{10}6d$	$6d\,^2D_{2\frac{1}{2}}$	6892.90	3.99003	$4d^{9}5s(^3D)6s$	$e\,^2D_{1\frac{1}{2}}$	−23487	
$4d^{10}8s$	$8s\,^2S_{\frac{1}{2}}$	5525.21	4.45660	$4d^{9}5s(^1D)6s$	$f\,^2D_{2\frac{1}{2}}$	−25378	
$4d^{10}7d$	$7d\,^2D_{1\frac{1}{2}}$	4406.71	4.99022	$4d^{9}5s(^2D_3)5d$	$11_{3\frac{1}{2},4\frac{1}{2}}$	−25789	2.864
$4d^{10}7d$	$7d\,^2D_{2\frac{1}{2}}$	4400.96	4.99344	$4d^{9}5s(^2D_3)5d$	$12_{3\frac{1}{2},4\frac{1}{2}}$	−26015.5	2.889
$4d^{10}5g$	$5g\,^2G$	4395.4	4.99665	$4d^{9}5s(^2D_3)5d$	$13_{2\frac{1}{2},3\frac{1}{2}}$	−26037	2.891
$4d^{10}9s$	$9s\,^2S_{\frac{1}{2}}$	3681.39	5.45971	$4d^{9}5s(^2D_3)5d$	$14_{2\frac{1}{2}}$	−26116	2.900
$4d^{10}8d$	$8d\,^2D_{1\frac{1}{2}}$	3056.49	5.99190	$4d^{9}5s(^2D_3)5d$	$15_{3\frac{1}{2}}$	−26205.5	2.910
$4d^{10}8d$	$8d\,^2D_{2\frac{1}{2}}$	3053.02	5.99530	$4d^{9}5s(^2D_3)5d$	$16_{3\frac{1}{2},4\frac{1}{2}}$	−26250.1	2.915
$4d^{10}10s$	$10s\,^2S_{\frac{1}{2}}$	2628.37	6.46150	$4d^{9}5s(^2D_2)5d$	$17_{2\frac{1}{2},3\frac{1}{2},4\frac{1}{2}}$	−27487	2.877
$4d^{10}9d$	$9d\,^2D_{1\frac{1}{2}}$	2244.04	6.99400	$4d^{9}5s(^2D_2)5d$	$18_{2\frac{1}{2}}$	−27632	2.893
$4d^{10}9d$	$9d\,^2D_{2\frac{1}{2}}$	2241.84	6.99650	$4d^{9}5s(^2D_2)5d$	$19_{2\frac{1}{2},3\frac{1}{2}}$	−27710	2.902
$4d^{10}11s$	$11s\,^2S_{\frac{1}{2}}$	1970.51	7.46260	$4d^{9}5s(^2D_3)7s$	$5s7s\,^4D_{3\frac{1}{2}}$	−29260	3.329
$4d^{10}10d$	$10d\,^2D_{1\frac{1}{2}}$	1717.53	7.99360	$4d^{9}5s$?	$20_{1\frac{1}{2},2\frac{1}{2}}$	−29506	3.371
$4d^{10}10d$	$10d\,^2D_{2\frac{1}{2}}$	1715.78	7.99725	$4d^{9}5s\,^3D_3$	AgII	−39164	
$4d^{10}12s$	$12s\,^2S_{\frac{1}{2}}$	1531.94	8.46375				

TABLE II. *Odd levels of* AgI.†

ORIGIN	NAME	LEVEL	n^*	ORIGIN	NAME	LEVEL	n^*	ORIGIN	NAME	LEVEL	n^*
$4d^{10}5p$	$5p\,^2P_{\frac{1}{2}}$	31554.45	1.86486	$4d^{9}5s(^3D)5p$	$5s5p\,^4P_{1\frac{1}{2}}$	2601.8		$4d^{9}5s(^3D)5p$	$5s5p\,^4D_{\frac{1}{2}}$	−3469.	
$4d^{10}5p$	$5p\,^2P_{1\frac{1}{2}}$	30633.79	1.89268	$4d^{9}5s(^3D)5p$	$5s5p\,^4F_{3\frac{1}{2}}$	2316.8		$4d^{9}5s(^3D)5p$	$5s5p\,^4F_{3\frac{1}{2}}$	−4531.1	
$4d^{10}6p$	$6p\,^2P_{\frac{1}{2}}$	12809.31	2.92694	$4d^{9}5s(^3D)5p$	$5s5p\,^4F_{4\frac{1}{2}}$	2204.6		$4d^{9}5s(^3D)5p$	$5s5p\,^2P$	−4880	
$4d^{10}6p$	$6p\,^2P_{1\frac{1}{2}}$	12605.90	2.95047	$4d^{9}5s(^3D)5p$	$5s5p\,^4F_{2\frac{1}{2}}$	1785.4		$4d^{9}5s(^3D)5p$	$5s5p\,^2D_{1\frac{1}{2}}$	−5234	
$4d^{10}7p$	$7p\,^2P_{\frac{1}{2}}$	7065.1	3.94111	$4d^{9}5s(^3D)5p$	$5s5p\,^4P_{\frac{1}{2}}$	569.0		$4d^{9}5s(^3D)5p$	$5s5p\,^2D_{2\frac{1}{2}}$	−5865.5	
$4d^{10}7p$	$7p\,^2P_{1\frac{1}{2}}$	6985.6	3.96347	$4d^{9}5s(^3D)5p$	$5s5p\,^4F_{1\frac{1}{2}}$	−135.4		$4d^{9}5s(^1D)5p$	$5s5p\,^2F_2$	1°	−11228
$4d^{10}4f$	$4f\,^2F$	6901.9	3.98743	$4d^{9}5s(^3D)5p$	$5s5p\,^4D_{3\frac{1}{2}}$	−1075.1		$4d^{9}5s(^1D)5p$	$5s5p\,^2P_1$	2°	−12364 ?
$4d^{9}5s(^3D)5p$	$5s5p\,^4P_{2\frac{1}{2}}$	4883.2		$4d^{9}5s(^3D)5p$	$5s5p\,^4F_{2\frac{1}{2}}$	−1827.2		$4d^{9}5s(^1D)5p$	$5s5p\,^2D_2$	3°	−12421
$4d^{10}8p$	$8p\,^2P_{\frac{1}{2}}$	4488.2	4.94472	$4d^{9}5s(^3D)5p$	$5s5p\,^4D_{1\frac{1}{2}}$	−2424.2		$4d^{9}5s^2D_2$			−39164
$4d^{10}8p$	$8p\,^2P_{1\frac{1}{2}}$	4446.1	4.96806								
$4d^{10}5f$	$5f\,^2F$	4397.1 ?	4.99567								
$4d^{10}9p$	$9p\,^2P_{1\frac{1}{2}}$	3079.6	5.96940								

† The symbol for "odd level" has been omitted wherever the prefix based on electron configuration gives the parity.

These observations were chiefly useful in differentiating between types of lines and in determining the series limits very exactly.

The line list, Table III, includes all the lines from λ40,000 to λ1250 which I think can be safely attributed to AgI. There are 243 lines of which 148 are new. Some of the old lines were observed by Kayser, but not again until the present survey was made. The observations of Paul[3] on absorption lines in the Schumann region include, I believe, some impurity lines. My reason for this statement is that Paul failed to observe many certain 5^2S combinations and yet observed other absorptions in the same region. The emission spectrum down to λ1250 definitely includes only three of Paul's lines. Some of his shorter lines may be due to silver but there is no conclusive evidence. I cannot accept his proposed series as real.

The most important term to find is $4d^95s^2\,^2D$, which had been placed, by comparison with similar spectra, almost directly on top of $4d^{10}5p$.[4] This has now proved to be correct, the $^2D_{2\frac{1}{2}}$ being between the components of ^2P and therefore metastable and the $^2D_{1\frac{1}{2}}$ being higher by 4472 cm^{-1}, and therefore not metastable. The correct difference was found by McLennan and McLay[5] in 1928 from three pairs of lines, one pair being very probably fortuitous. The most important combination of the $s^2\,^2D_{2\frac{1}{2}}$ term is that with $6p\,^2P_{1\frac{1}{2}}$ at λ5475. This line is very strong in both arc and Schuler tube and can easily be

[3] F. W. Paul, Phys. Rev. **52**, 923 (1937).

[4] H. A. Blair, Phys. Rev. **36**, 1531 (1930).

[5] J. C. McLennan and A. B. McLay, Trans. Roy. Soc. Can. **22**, 1 (1928).

TABLE III. *Wave-lengths, intensity, and classification of all the lines from λ40000 to λ1250 attributed to* AgI. *A letter n in column one indicates a new line. In column one the symbols have the following meaning: P—F. Paschen, Ann. d. Physik* **33**, *717 (1910); R—H. H. Randall, Astrophys. J.* **34**, *1 (1911); M—W. F. Meggers, letter; S—new observation; H—Hetzler, Bouman and Burns, Phys. Rev.* **48**, *656 (1935); W—F. M. Walters, Sci. Papers, Nat. Bur. Stand. No. 411, 1921; T—*M. I. T. *Wave-length Tables; Av—average of best values; B—H. A. Blair, Phys. Rev.* **36**, *1531 (1930). The wave-length λ was measured on Schuler tube plates where possible. I(arc) and I(ST) are the intensities in the arc and Schuler tube, respectively.*

AUTHORITY (n INDICATES NEW LINE)	λ	$I_{(ARC)}$	$I_{(ST)}$	ν	CLASSIFICATION
P	39951	8		2502.4	$4^3F-7d^3D_3$
P	39889	5		2506.3	4^3F-5^3G
R	18382.3	15		5438.6	$5d^3D_1-4f^3F$
R	18307.9	15		5460.7	$5d^3D_2-4f^3F$
R	17416.7	20		5740.0	$6s^3S_1-6p^3P_2$
R	16819.5	60		5943.9	$6s^3S_1-6p^3P_1$
R	12551.0	10		7965.4	$5d^3D_1-5f^3F$
M n	9001.1	1U		11106.7	
S n	8745.7	1U		11431.	
S n	8704.85	10n		11484.7	$6s^3S_1-7p^3P_2$
S n	8645.70	30n		11563.3	$6s^3S_1-7p^3P_1$
H	8273.519	1000		12083.44	$5p^3P_1-6s^3S_1$
H	7687.779	500		13004.10	$5p^3P_1-6s^3S_1$
S n	7402.96	0		13504.4	
S n	7359.96	20	10	13583.3	$5s^{2\,1}D_2-6p^3P_2$
S n	7297.8	0U		13699.	3^0-14_2
S n	7251.53	5	5	13786.4	$5s^{2\,1}D_2-6p^3P_1$
S n	7109.5	1U		14062.	$6s^3S_1-8p^3P_2$
S n	7088.10	5U	5	14104.3	$6s^3S_1-8p^3P_1$
S n	6861.0	5UU		14571.	1^0-11
S n	6754.5	5UU		14801.	1^0-13
S n	6706.67	5		14904.2	
S n	6655.5	5UU		15021.	1^0-16
S n	6621.08	20		15099.1	$5s5p^3D_2-e^3D_2$
S n	6571.7	2U		15212.6	3^0-18_2
S n	6537.6	2U		15292.	$5s5p^3P-5s6s^4D_1$? 3^0-19 ?
S n	6461.80	0U	2	15471.3	$6s^3S_1-9p^3P_1$
S n	6268.50	10n	20	15948.4	$6s^3S_1-5s5p^4P_1$
S n	6230.63	1		16045.3	
S n	6218.0	2U		16078.	$5s5p^3P-e^3D_2$?
S n	6191.8	0U		16146.	
S n	6141.64	2n		16277.8	
S n	6083.78	10U		16432.6	$5s5p^3F_2-e^3D_2$
S n	6047.6	2U		16531.	
S n	6010.1	5U		16634.	$5s5p^4D_1-5s6s^4D_2$
S n	5989.6	1UU		16691.	$5s5p^4D_1-5s6s^4D_1$
S n	5801.92	5U		17230.9	$5s5p^4D_2-5s6s^4D_2$? $5s5p^3F_2-5s6s^4D_2$
S n	5673.15	5n		17622.0	$5s5p^3D_2-e^3D_1$
W	5667.34	100		17640.1	$5s5p^4D_2-5s6s^4D_2$
S n	5637.01	5U		17735.0	$5s5p^4D_1-5s6s^4D_1$
S n	5609.02	3U		17823.5	$5p^3P_1-6p^3P_2$
S n	5559.58	10U		17982.0	$6s^3S_1-5s5p^4P_2$? $5s5p^4D_2-5s6s^4D_2$
W	5545.67	20U		18027.1	$5p^3P_2-6p^3P_1$
S n	5475.382	20	20	18258.50	$5s^{2\,1}D_2-6p^3P_1$
S	5471.547	50	100	18271.29	$5p^3P_1-5d^3D_2$
S	5465.503	1000	1000	18291.51	$5p^3P_1-5d^3D_2$
S	5436.00	5U		18390.8	$5s5p^4D_2-5s6s^4D_2$
S	5403.22	1n		18502.0	$5s^{2\,1}D_2-5d^3D_1$
S	5400.46	2n		18511.8	
S n	5397.11	0n		18523.3	$5s^{2\,1}D_2-5d^3D_2$
S	5333.62	10U		18743.8	$5p^3P_2-6p^3P_2$
S n	5283.16	1U		18922.8	$5s5p^4F_1-5s6s^4D_2$
S	5276.36	5U		18947.2	$5p^3P_2-6p^3P_1$
S n	5244.40	1n		19062.7	
S n	5238.35	5U		19084.7	$5s5p^4D_2-5s6s^4D_1$
S	5209.078	1000	1000	19191.93	$5p^3P_2-5d^3D_1$
S n	5138.34	5U		19325.6	$5s^{2\,1}D_2-7p^3P_2$
S n	5151.80	2 ?		19405.3	$5s^{2\,1}D_2-7p^3P_1$
S n	5129.30	3U		19490.4	$5s^{2\,1}D_2-4f^3F$
S	5123.50	15n		19512.5	$5s5p^3D_2-f^3D_2$
S n	5032.75	3n		19864.3	
S n	5026.40	3U		19889.4	$5s5p^4D_2-e^3D_2$
S	4992.89	20U		20022.9	$5s5p^4F_1-5s6s^4D_1$
S n	4974.38	1U		20097.4	
S n	4956.18	5		20171.2	$5s5p^3D_2-13$
S n	4937.04	1		20249.4	$5s5p^3D_2-14_2$
S n	4935.75	10		20254.7	
S n	4934.07	5		20261.7	
S n	4925.25	3U		20297.9	$5s5p^4D_2-e^3D_2$
S n	4917.5	10UU		20330.	
S	4888.21	20		20451.7	$5s5p^4D_1-5s6s^4D_1$
S n	4886.27	0		20459.8	
S	4874.100	100	10	20510.90	$5s5p^4F_4-5s6s^4D_2$
S	4847.82	30n(r)		20622.1	$5s5p^4F_2-5s6s^4D_2$
S n	4840.28	0U		20654.2	
S n	4822.79	5UU		20729.	$5s5p^4P_1-5s6s^4D_1$
S	4796.2	20UU(r)		20844.	$5s5p^4F_2-5s6s^4D_2$ $5s5p^3F_2-f^3D_2$
S n	4745.93	2U		21064.8	$5s5p^4D_1-e^3D_1$
S n	4702.3	2UU		21260.	
S	4677.60	30U(r)		21372.5	$5s5p^4F_2-5s6s^4D_2$
S	4668.478	500n	500	21414.28	$5p^3P_1-7s^3S_1$
S	4615.69	30U		21659.2	$5s5p^4P_1-5s6s^4D_2$ $5s5p^3F_2-e^3D_1$
S n	4575.99	2		21847.1	$5s5p^3D_2-19$
S n	4564.02	0U		21904.4	$5s^{2\,1}D_1-8p^3P_2$
S	4556.0	20UU		21943.	$5s5p^4F_2-5s6s^4D_1$
S n	4499.50	1U		22218.5	
S	4476.042	500n	500	22334.92	$5p^3P_1-7s^3S_1$
S	4396.23	20		22740.4	$5s5p^4F_1-5s6s^4D_1$
S n	4394.37	1n		22750.0	$5s5p^4F_2-e^3D_2$
S n	4372.90	3n		22761.7	$5s5p^4P_1-5s6s^4D_1$
S n	4354.7	5UU		22957.	$5s5p^3F_2-17$
T	4311.074	50		23189.58	$5s5p^4P_2-5s6s^4D_2$
S n	4294.27	5n		23280.3	$5s5p^4F_2-e^3D_2$
S n	4281.16	0U		23351.6	$5s5p^4F_1-e^3D_1$
S n	4263.78	1U		23446.8	$5s5p^4P_1-5s6s^4D_1$
S n	4242.19	5n		23566.1	$5s5p^4P_1-e^3D_2$
S n	4228.7	5UU		23641.	$5s5p^3D_2-20$
S	4212.817	100	100	23730.42	$5p^3P_1-6d^3D_2$
S n	4212.520		5	23732.11	$5p^3P_1-4f^3F$
S	4210.960	500	500	23740.89	$5p^3P_2-6d^3D_2$
S n	4186.637	5n	10	23878.81	$5s^{2\,1}D_2-7p^3P_2$
S n	4175.78	3n		23940.9	$5s5p^4P_2-5s6s^4D_2$
S n	4172.016	3n	2	23962.50	$5s^{2\,1}D_2-4f^3F$
S n	4083.43	10U		24482.3	
S n	4062.71	5n		24607.2	$5s^{2\,1}D_2-5s5p^4F_2$
S n	4062.08	5n		24611.0	
S	4055.476	1000	500	24651.08	$5p^3P_2-6d^3D_2$
S n	4055.196		10	24652.78	$5p^3P_2-4f^3F$
S n	4015.68	0n		24895.4	
S n	4012.99	0n		24912.1	
S	3992.15	10U		25042.1	$5s5p^4D_2-14_2$
S	3981.584	100U(r)	100	25108.56	$5p^3P_1-8s^3S_1$
S n	3979.44	5n		25122.1	$5s5p^4D_2-11$
S	3951.28	5n		25301.1	
S	3942.972	10n	1	25354.43	$5s5p^4D_2-12$?
S	3940.43	10U		25370.8	$5s5p^4D_2-13$
S n	3928.01	10U		25451.0	$5s5p^4D_2-14_2$
S n	3923.759	2	15 ?	25478.56	$5s5p^4P_1-5s6s^4D_1$
S	3914.40	50n	3U	25539.15	$5s5p^4D_2-15_2$
S	3907.41	50n		25584.2	$5s5p^4D_2-16$
S n	3847.849	15	50	25981.20	$5s^{2\,1}D_2-5s5p^4P_2$
S	3840.745	100n	100	26029.25	$5p^3P_2-8s^3S_1$
S n	3811.775	50	50	26227.08	$5p^3P_1-7d^3D_2$
S	3810.940	200	200	26232.83	$5p^3P_1-7d^3D_2$
S n	3791.89	1U		26364.6	
S n	3784.183	0U	15	26418.30	$5s^{2\,1}D_2-8p^3P_2$
S n	3771.07	1U		26510.2	
S n	3768.51	5n		26528.2	$5s^{2\,1}D_2-5s5p^4F_1$
S n	3764.53	3U		26556.2	$5s5p^4D_2-18_2$
S n	3753.14	20U		26636.8	$5s5p^4D_2-19$
S n	3727.42	10U		26820.6	$5s5p^4D_2-17$
S n	3723.59	2n		26848.2	
S	3714.28	3n		26915.5	
S	3709.196	50n	30	26952.38	$5p^3P_1-9s^3S_1$
S n	3696.64	2U		27043.9	$5s5p^4D_2-19$
S	3682.505	30	200	27147.73	$5p^3P_2-7d^3D_2$
S n	3654.62	5U		27354.9	$5s5p^4F_1-17$?
S n	3639.578	Pb? 5n		27467.91	$5s^{2\,1}D_2-5s5p^4D_2$
S n	3625.132		5	27577.37	$5p^3P_2-8d^3D_2$
S	3624.684	50n	50	27580.78	$5p^3P_2-8d^3D_2$
S n	3623.49	10n		27589.5	
S n	3598.065	0U	2	27784.81	$5s^{2\,1}D_2-9p^3P_2$
S	3586.672	20n(r)	30	27873.07	$5p^3P_2-9s^3S_1$
S n	3582.78	3Ud		27903.3	
S n	3571.13	0		27994.4	$5s5p^4F_4-11$
S n	3569.722	2	10	28005.42	$5p^3P_2-10s^3S_1$
S	3557.01	10n(r)		28105.5	$5s5p^4F_2-11$
S	3547.16	10n		28183.5	$5s5p^4D_2-5s7s^4D_2$?
S	3542.608	50	100	28219.76	$5s^{2\,1}D_2-5s5p^3F_2$? $5s5p^4F_4-12$?
S n	3537.23	5		28262.7	$5s^{2\,1}D_2-5s5p^4P_2$

TABLE III—*Continued.*

AUTHORITY (n INDICATES NEW LINE)	λ	$I_{(ARC)}$	$I_{(ST)}$	ν	CLASSIFICATION
S n	3533.11	3UU		28296.	
S n	3528.534	3U	5	28332.31	$5s5p^4F_{3\frac{1}{2}}-12$?
S n	3526.01	1n		28352.6	$5s5p^4F_{3\frac{1}{2}}-13$
S n	3524.60	1		28363.9	
S n	3521.393		3	28389.77	$5p^2P_{1\frac{1}{2}}-9d^2D_{1\frac{1}{2}}$
S	3521.122	10	10	28391.95	$5p^2P_{1\frac{1}{2}}-9d^2D_{2\frac{1}{2}}$
S n	3518.900	5n	5	28409.88	$5s5p^4F_{4\frac{1}{2}}-15_{4\frac{1}{2}}$
S	3515.99	2Ud		28433.4	$5s5p^4D_{2\frac{1}{2}}-20$
S	3513.377	15n	3	28454.64	$5s5p^4F_{4\frac{1}{2}}-16$
S	3508.030	20	30	28497.91	$5p^2P_{\frac{1}{2}}-8d^2D_{1\frac{1}{2}}$
S	3505.015	5n	10	28522.42	$5s5p^4F_{3\frac{1}{2}}-15_{3\frac{1}{2}}$
S	3501.921	20n	30	28547.62	$5s^2{}^1D_{2\frac{1}{2}}-5s5p^4F_{3\frac{1}{2}}$
S	3499.668	5n	3	28565.99	
S n	3499.541		2	28567.03	$5s5p^4F_{3\frac{1}{2}}-16$
S	3487.790	5	3	28663.28	$5p^2P_{1\frac{1}{2}}-11s^2S_{\frac{1}{2}}$
S n	3481.22	3n		28717.4	$5s5p^4F_{1\frac{1}{2}}-14_{2\frac{1}{2}}$
S	3469.16	30		28817.2	$5s^2{}^1D_{2\frac{1}{2}}-5s5p^4D_{2\frac{1}{2}}$
S n	3457.276		1	28916.24	$5p^2P_{1\frac{1}{2}}-10d^2D_{1\frac{1}{2}}$
S	3457.066	5	5	28918.01	$5p^2P_{1\frac{1}{2}}-10\,{}^2D_{2\frac{1}{2}}$
S n	3456.102		5	28926.07	$5p^2P_{\frac{1}{2}}-10s^2S_{\frac{1}{2}}$
S n	3435.227		0n	29101.85	$5p^2P_{1\frac{1}{2}}-12s^2S_{\frac{1}{2}}$
S n	3434.665	1	2	29106.61	
S n	3420.41	0U		29227.9	
S n	3414.507		3	29278.44	$5p^2P_{1\frac{1}{2}}-11d^2D_{1\frac{1}{2}}$?
S	3414.464		3	29278.80	$5p^2P_{1\frac{1}{2}}-11d^2D_{2\frac{1}{2}}$?
S	3410.784	8	10	29310.39	$5p^2P_{\frac{1}{2}}-9d^2D_{1\frac{1}{2}}$
S n	3403.78	10U		29370.7	$5s5p^4F_{1\frac{1}{2}}-20$
S n	3398.38	1U		29417.4	$5s5p^4F_{2\frac{1}{2}}-18_{2\frac{1}{2}}$
Av.	3382.893	1000R	1000	29552.04	$5s^2S_{\frac{1}{2}}-5p^2P_{\frac{1}{2}}$
S n	3357.98	1		29771.3	
S	3354.63	5n		29801.0	$5s5p^4F_{2\frac{1}{2}}-17$
S	3350.590	3	3	29836.94	$5p^2P_{\frac{1}{2}}-10d^2D_{2\frac{1}{2}}$
S	3339.20	5n		29938.7	
S n	3329.48	0n		30026.2	$5s5p^4F_{2\frac{1}{2}}-19$
S	3327.70	5n		30042.2	
B	3310.51	2		30198.2	$5p^2P_{\frac{1}{2}}-11d^2D_{1\frac{1}{2}}$
S n	3306.70	1		30233.0	$5s5p^4P_{1\frac{1}{2}}-18_{2\frac{1}{2}}$
S	3305.672	10n		30242.36	$5s^2S_{\frac{1}{2}}-5s^2{}^1D_{2\frac{1}{2}}$
B	3282.53	3		30455.6	$5p^2P_{\frac{1}{2}}-12d^2D_{1\frac{1}{2}}$
Av.	3280.680	1000R	1000	30472.73	$5s^2S_{\frac{1}{2}}-5p^2P_{1\frac{1}{2}}$
S n	3265.72	5		30612.3	
S	3233.18	15		30920.4	$5s5p^4P_{2\frac{1}{2}}-13$
S	3225.15	10		30997.4	$5s5p^4P_{2\frac{1}{2}}-14_{2\frac{1}{2}}$
S	3215.67	15n		31088.8	$5s5p^4P_{2\frac{1}{2}}-15_{2\frac{1}{2}}$
S n	3188.36	2U		31355.0	
S	3186.19	3n		31376.4	
S n	3177.33	5		31463.9	$5s5p^4F_{4\frac{1}{2}}-5s7s^4D_{3\frac{1}{2}}$
T	3170.579	10n		31530.99	$5s^2{}^1D_{2\frac{1}{2}}-5s5p^4D_{2\frac{1}{2}}$
S	3130.02	30U		31939.5	$5s^2{}^1D_{2\frac{1}{2}}-5s5p^4D_{2\frac{1}{2}}$
S	3099.10	20		32258.1	$5s^2{}^1D_{1\frac{1}{2}}-5s5p^4D_{2\frac{1}{2}}$
S n	3034.99	3		32939.5	
S	2938.42	20U		34022.	
S n	2933.00	2n		34084.9	
S n	2928.95	5		34143.6	$5s5p^4P_{2\frac{1}{2}}-5s7s^4D_{2\frac{1}{2}}$
S n	2926.77	10n		34157.4	
S n	2920.70	1n		34228.4	
S n	2919.03	5n		34248.0	
S n	2911.37	0U		34338.	
S n	2909.51	1U		34360.	
S n	2832.27	1U		35297.	
S	2824.39	100U		35395.5	$5s^2{}^1D_{2\frac{1}{2}}-5s5p^2F_{3\frac{1}{2}}$
S	2796.77	3U		35745.	$5s^2{}^1D_{2\frac{1}{2}}-5s5p^2P$
S n	2778.04	1U		35986.	
S n	2775.88	3U		36014.	
S n	2768.88	1U		36105.	
S	2721.77	50		36729.9	$5s^2{}^1D_{2\frac{1}{2}}-5s5p^2D_{2\frac{1}{2}}$
S n	2715.85	3UU		36810.	
S	2595.51	2U		38516.6	
S	2575.63	50U		38813.8	$5s^2{}^1D_{1\frac{1}{2}}-3°$
S	2375.02	50UU		42092.	$5s^2{}^1D_{2\frac{1}{2}}-1°$
S	2312.60	10UU		43228.	$5s^2{}^1D_{2\frac{1}{2}}-2°$
S	2309.56	30U		43285.	$5s^2{}^1D_{2\frac{1}{2}}-3°$
	λ(vac)				
S n	2170.68	15		46068.5	
S n	2167.45	5		46137.2	
S n	2147.40	5U		46567.9	
S n	2143.50	5		46652.7	
S	2070.514	100	100	48297.19	$5s^2S_{\frac{1}{2}}-6p^2P_{\frac{1}{2}}$
S	2061.830	200	200	48500.60	$5s^2S_{\frac{1}{2}}-6p^2P_{1\frac{1}{2}}$
S n	2051.67	5n		48740.8	$5s^2S_{\frac{1}{2}}-5d^2D_{1\frac{1}{2}}$?
S n	1850.47	5		54040.3	$5s^2S_{\frac{1}{2}}-7p^2P_{\frac{1}{2}}$
S n	1847.73	20		54120.5	$5s^2S_{\frac{1}{2}}-7p^2P_{1\frac{1}{2}}$
S n	1766.20	10n		56618.7	$5s^2S_{\frac{1}{2}}-8p^2P_{\frac{1}{2}}$
S n	1763.69	0		56699.4	$5s^2S_{\frac{1}{2}}-7d^2D_{1\frac{1}{2}}$?
S n	1763.55	1		56703.8	$5s^2S_{\frac{1}{2}}-7d^2D_{2\frac{1}{2}}$?
S n	1759.68	5		56828.5	
S	1709.26	50		58504.9	$5s^2S_{\frac{1}{2}}-5s5p^4P_{1\frac{1}{2}}$
S n	1708.11	10		58544.2	
S n	1651.87	100n		60537.4	$5s^2S_{\frac{1}{2}}-5s5p^4P_{\frac{1}{2}}$
S n	1632.88	5		61241.5	$5s^2S_{\frac{1}{2}}-5s5p^4F_{1\frac{1}{2}}$
S n	1574.02	5		63531.6	$5s^2S_{\frac{1}{2}}-5s5p^4D_{1\frac{1}{2}}$
S	1548.58	50RUU		64575.	$5s^2S_{\frac{1}{2}}-5s5p^4D_{\frac{1}{2}}$
S	1515.63	100RUU		65979.	$5s^2S_{\frac{1}{2}}-5s5p^2P$
S	1507.37	50RUU		66341.	$5s^2S_{\frac{1}{2}}-5s5p^2D_{1\frac{1}{2}}$

observed visually. It appears in no published lists but was observed some years ago in this laboratory. It was so strong that, at that time, it was not thought that it could possibly be a silver line which had escaped previous observation.

The structure $4d^95s5p$ is partly positive and partly negative, and includes in its combinations with $4d^{10}5s$ the three widest lines I have ever observed. One of them is about 500 cm^{-1} wide with a central reversal about 100 cm^{-1} wide, and it serves as a continuum for the absorption of the lines of a nitrogen band.

The term $4d^95s6s^4D$ was found in its predicted position and it accounts for most of the strongest lines by its combinations with $4d^95s5p$. As in CuI, the outer components $4D_{3\frac{1}{2}}$ and $^4D_{\frac{1}{2}}$ give sharp lines and the inner two give diffuse lines. In addition one and possibly both of the ^2D terms from $4d^95s6s$ have been discovered, as well as a number of levels of $4d^95s5d$. A possible series member $4d^95s7s^4D_{3\frac{1}{2}}$ falls in the correct position. It is of interest to notice that the majority of the newly classified lines are between negative levels. It is surprising that the spectrum is as well developed as it is.

The numerical values of the levels are based on a new calculation of the ^2S series limit. From the accurate grating wave-lengths, the series was recalculated to fit the extended Ritz formula[6]

$$n^*=n+\mu+\alpha T+\beta T^2.$$

With the constants $\mu=-3.53427$, $\alpha=-1.600\times10^{-6}$, $\beta=-1.11\times10^{-12}$, all the levels except the lowest are represented quite accurately by

[6] A. G. Shenstone, Trans. Roy. Soc. **235**, 195 (1936).

the formula. The ^2D series is also nearly Ritzian but was not used because of the possibility of a perturbation due to $4s^2\,{}^2D$.

All the even levels are collected in Table I and all the odd in Table II. Their combinations are given in Table III.

There are a number of peculiarities in the spectrum which should be noticed. Perhaps the most important of these is the rather large intensity of several ordinarily prohibited combinations. The best known are the $5p^2P-6p^2P$ lines, which have been dealt with theoretically by Sambursky.[7] That theory should now be modified in the light of the more complete analysis available. Lines which contravene both the parity and J rules and yet appear in the practically field free Schuler tube are $5s^2S-5s^2\,{}^2D_{2\frac{1}{2}}$ and $5p^2P-4^2F$. The former line is, like its counterpart in HgII observed by Paschen,[8] a "nebular line." Other prohibited lines which appear faintly in the arc are $5s^2S-5d^2D$, $5s^2S-7d^2D$ and $5s^2\,{}^2D_{2\frac{1}{2}}-5d^2D$.

The intensities in the principal series show an unusual anomaly. The first two pairs of lines have about correct relative intensities, but in the third pair $5^2S-7^2P_{1\frac{1}{2}}$ is relatively much too strong. In the fourth pair, $5^2S-8^2P_{1\frac{1}{2}}$ is entirely missing and $5^2S-8^2P_{\frac{1}{2}}$ is stronger than the preceding $5^2S-7^2P_{\frac{1}{2}}$. It is possible but improbable that these anomalies are caused by absorption in the lines of the bands of nitrogen, because the series 6^2S-n^2P seems quite normal.

Attention should be drawn to the following doubtful points.

$5g^2G$. The value of ^2G depends on a new identification of the two longest of Paschen's infra-red lines.

$11d^2D_{1\frac{1}{2}}$, $^2D_{2\frac{1}{2}}$. These levels may be incorrect by a fraction of a wave number. The lines from which they were calculated have wrong intensities and may be spurious.

$y^2D_{2\frac{1}{2}}$. This level may be spurious. It is based on two lines only and one of those is used elsewhere. It does, however, account for one strong line which has been tried as every other possible combination.

$5f^2F$ is doubtful. It is based on the combination $5d^2D_{1\frac{1}{2}}-5f^2F$ with no line to represent the stronger combination $5d^2D_{2\frac{1}{2}}-5f^2F$. If the line is assigned in the other way, 5^2F has a value far from the one expected.

$5s5p^4D_{\frac{1}{2}}$, ^2P, $^2D_{1\frac{1}{2}}$ are based on the three extraordinarily wide lines observed in the Schumann region. There is no doubt of the reality of the levels, but the naming is arbitrarily made to agree best with the equivalent levels in CuI.

The level $5s5p^2F_{3\frac{1}{2}}$ at 4531.1 is one that would be found from one of McLennan's three $s^2\,{}^2D$ differences. The two lines are, however, of completely different character and one of them is quite definitely assigned elsewhere. On that evidence it is not considered to be a combination with $s^2\,{}^2D_{1\frac{1}{2}}$.

1^0, 2^0, 3^0 are probably the equivalent of the levels 6278, 5964, 5656, in CuI. Whether it is correct to connect these levels with the limit ^1D rather than with ^3D is doubtful.

Attention has been called to the extreme width of many of the silver arc lines. This width is, of course, an effect due to auto-ionization, but why is it so extreme in silver? Auto-ionization should theoretically be greatest quite close to the ionization point which initiates it, but this does not seem to be true in silver. A thorough experimental examination of the line widths might be well worth while.

[7] S. Sambursky, Zeits. f. Physik **68**, 774 (1931).
[8] F. Paschen, Berichte d. Preuss. Akad. d. Wiss. **32**, 536 (1928).

Thermal Separation of Isotopes

WILLIAM W. WATSON
Sloane Physics Laboratory, Yale University, New Haven, Connecticut

(Received February 29, 1940)

The performance of a simple, multi-stage apparatus for the separation of isotopes by thermal diffusion is discussed. All parts are built of copper pipe, each unit being based on a ½-inch G.E. Calrod heater of 2 meters effective heating length. Tests with a CH_4-N_2 mixture show that convective coupling of the bottom of one unit with the top of the next functions well. In the case of CH_4, with two units preceded by a scrubber which maintains economically normal CH_4 at the "light" end, and with $\Delta T=370°C$ between the two surfaces, the C^{13} content at the "heavy" end at equilibrium is 2.77 times the normal amount. A single unit with $\Delta T=400°C$ filled with neon at 1.5−1 atmosphere gives a separation factor of 8 for Ne^{22}/Ne^{20}. The relative separations produced in CH_4 and Ne are shown to be in agreement with the theory.

THE theory of the separation of isotopes by the thermal diffusion process has been discussed in detail by Furry, Jones and Onsager,[1] Debye,[2] and Waldmann.[3] Comparison of experimental results with theoretical expectations has been made by Clusius and Dickel[4] in the report of their original work on the separation of N_2-O_2 mixtures and Cl isotopes with long hot-wire columns. Using a column with methane between concentric cylinders, Nier[5] has shown that the separation factor for various pressures is in quantitative agreement with the theory of Furry, Jones and Onsager. Results with short concentric cylinder columns under various operating conditions have been reported by Bramley and Brewer.[6]

Guided by the Furry, Jones and Onsager calculations, we have been experimenting with multi-stage all-metal apparatus of the vertical concentric cylinder type. This has been used chiefly for the concentration of C^{13} in methane, but the performance of the apparatus has also been investigated with N_2-CH_4 mixtures and a single 2-meter column has been employed in the separation of the neon isotopes. The multi-stage feature has been used from the start in these experiments not only as a matter of convenience, since the total length of column needed for a considerable concentration of the C^{13} isotope is large, but also because of the possibility of decreasing the gap space between the hot and cold cylindrical surfaces in successive stages. In this way one can obtain in the first stages a transport of the heavy carbon comparable to that in the last stage, thereby increasing the speed of production.

APPARATUS

All surfaces are copper both because of its good heat conductivity and because radiation losses are minimized, copper retaining its polish in the methane atmosphere. The bottom of a column is connected to the top of the next one in the series by means of two ½-inch or ¾-inch pipes, one of which is heated in order to set up convective circulation. In our first model[7] two one-meter units were followed by a three-meter column, each unit consisting of a ½-inch O.D. pipe concentrically mounted by means of fine centering pins inside a 1-inch I.D. pipe. The two shorter units had their inner surfaces heated by means of inside spiral Chromel ribbon heaters, while the three-meter unit was heated on the outside. With methane gas at atmospheric pressure circulating in this apparatus 2 kw of power were consumed to maintain the hot surfaces at 330°C with one gallon of water per minute to cool the other surfaces. As reported, this apparatus doubled the C^{13} content of the methane, although the calculations of Furry, Jones and Onsager would lead one to expect at least three

[1] W. Furry, R. Jones and L. Onsager, Phys. Rev. **55**, 1083 (1939).
[2] P. Debye, Ann. d. Physik **56**, 284 (1939).
[3] L. Waldmann, Zeits. f. Physik **114**, 53 (1939).
[4] K. Clusius and G. Dickel, Zeits. f. physik. Chemie **B44**, 397 (1939).
[5] A. O. Nier, Phys. Rev. **57**, 30 (1940).
[6] A. Bramley and A. K. Brewer, Science **90**, 165 (1939).
[7] W. W. Watson, Phys. Rev. **56**, 703(L) (1939).

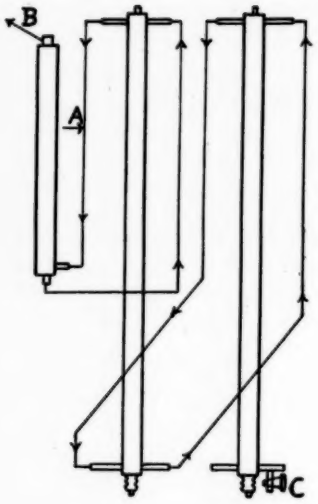

FIG. 1. Schematic drawing showing assembly and operation of two-stage apparatus for thermal separation of isotopes.

times this concentration. The lowered coefficient of thermal diffusion measured for methane by Nier[8] accounts well for the discrepancy.

To increase the efficiency and separation factor it was decided to abandon heating of the outer cylindrical surface and to have the inner surfaces heated as uniformly and economically as possible. In the next model, therefore, two columns based on ½-inch G.E. Calrod heaters of 2 meters effective heating length were constructed. The heater is mounted concentrically in a water-cooled 1-inch I.D. copper pipe, the differential extension of the two surfaces being taken up by a sylphon bellows at the lower end. Every 50 cm along the length of the heaters narrow copper fins are silver-soldered on to insure centering within the larger pipes. The two columns are connected together convectively and ahead of the first one is placed one of the 1-meter units as a scrubbing column. A schematic drawing of the assembly is given in Fig. 1. Fresh methane gas is introduced into a coupling pipe at the bottom of the scrubber and gas slightly enriched in C^{12} is valved-off at the top.

Tank methane (92 percent in these experiments) is purified by the method of Storch and Golden[9] and stored in a water-sealed gasometer of 30 liters capacity from which it is introduced, thoroughly dried, into the apparatus at a pressure about 2 mm above that of the atmosphere. We have recently begun using tank methane 99½ percent pure, and can thus be assured, with treatment, of 100 percent CH_4 in quantities for a larger apparatus with more stages. The flow of fresh gas into the apparatus is controlled by the rate of valving-off at the top of the scrubber, somewhat less than 100 cc/hr. The gas at the top of the first Calrod unit is thus maintained at normal composition and the separation factor of the apparatus gives the maximum enrichment in C^{13} at the "heavy" end.

NITROGEN-METHANE SEPARATION

To test the relative performance under several different operating conditions a 50 percent-50 percent mixture of N_2 and CH_4 was introduced into the apparatus. At the end of a column where the degree of separation was to be measured the gas mixture circulated convectively through a glass volume of about 130 cc in the manner indicated in Fig. 4 below. Additional convective circulation was maintained through a liquid-air trap attached to this end volume. The procedure was to close off this volume from the column, freeze down the CH_4 with liquid air, and read the residual pressure with a Hg manometer. The liquid air was then removed and the stopcocks opened, thus returning the trapped gas to the circulation with the end of the column. Each such measurement required 20 minutes. A calibration curve was obtained for each end volume from

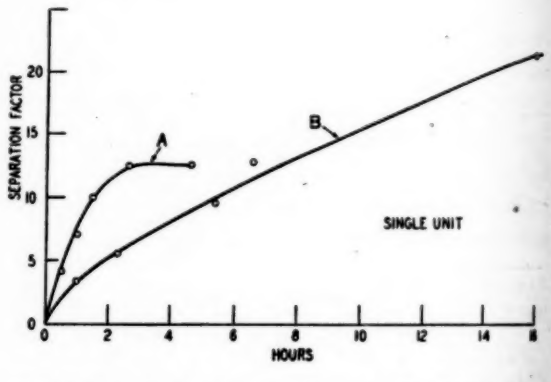

FIG. 2. Separation factor *vs.* time for N_2-CH_4 mixture in single 2-meter unit, *A*, without valving-off gas at top, *B*, with valving-off.

[8] A. O. Nier, Phys. Rev. **56**, 1009 (1939).
[9] H. H. Storch and P. L. Golden, J. Am. Chem. Soc. **54**, 4662 (1932).

determinations of the residual pressures for different known N_2-CH_4 mixtures. The temperature difference between the two surfaces was kept at 300°C.

In Fig. 2 is plotted the separation factor (ratio of the N_2/CH_4 ratio at the bottom to that at the top) for a single Calrod unit, A, without valving-off gas at the top and B, with valving-off at the top, i.e., maintainance of a 50/50 ratio at the top throughout the run. Despite the lack of high accuracy in these determinations, the approximate exponential rise of the factor to its equilibrium value and the relative slowness of the rise under the condition of valving-off gas at the top are evident. These facts are quite in agreement with the theory.

With the two units connected convectively the separation of this gas mixture was tested simultaneously at both ends at 50 minute intervals after introduction of the gas into the already heated apparatus. The results are shown in Fig. 3. Quite apparently disturbing influences are affecting the measured values, but it is evident that the factor is approximately the square of that found for a single column. It is to be concluded that this method of coupling units together works well.

This same separation experiment was performed at $\frac{1}{2}$ and $\frac{1}{4}$ atmos. pressure in the apparatus. As compared to the factors at atmos. pressure those at $\frac{1}{4}$ atmos. were considerably lower, while at $\frac{1}{2}$ atmos. the separation was found to rise at a slightly faster rate, with an equilibrium value a little above that at atmospheric pressure. Now Nier[5] has found that for a column with a gap space $d=0.712$ cm using methane the maximum equilibrium separation factor occurs at a pressure of 0.6 atmosphere. Since according to the Furry, Jones and Onsager theory p^2d^3 should be approximately constant for maximum factor, all other variables remaining fixed, for our $d=0.61$ cm this optimum pressure for methane should be 0.76 atmosphere. However, in view of the convenience of using atmospheric pressure and being able to maintain normal isotope concentration at the "light" end by simply valving-off, it was decided to continue operating at the higher pressure. The resulting lowering of the factor may be offset by merely increasing the length of the column slightly.

C^{13} Concentration

The two-columns plus scrubber with convective coupling were operated with methane for four days after which samples were withdrawn at the "heavy" end through a variable metal-taper leak at the rate of 3 cc per hour. The temperature difference was 370°C. Mass spectrographic analysis of CO_2 made from one of these samples showed a C^{13} content 2.77 times the normal amount. The other samples have been used in a

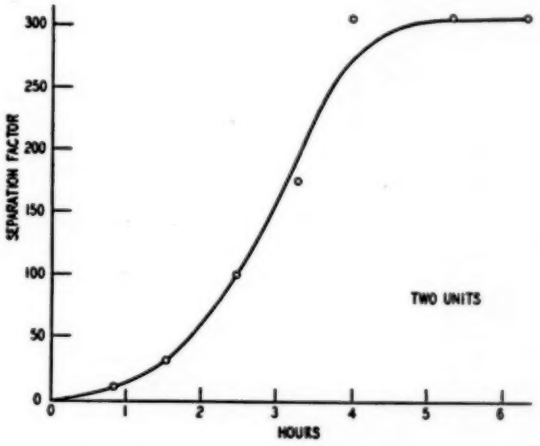

FIG. 3. Separation factor *vs.* time for N_2-CH_4 mixture in two 2-meter units connected convectively.

gas target of our cyclotron for the purpose of enhancing activities arising from C^{13} bombardment.

The power consumption in this carbon isotope separation was 1300 watts. Now according to Eq. (67) of reference 1, the power expended because of conduction in the methane gas should be 800 watts in the two Calrod columns and the scrubber. About 100 watts are taken by the coupling pipe heaters and probably some 200 watts would be the radiation loss, the latter being relatively small because of the fact that the copper walls retain their polish in this reducing atmosphere. The remainder of the power input is apparently being lost by conduction through the copper and brass end plates silver-soldered on to the heaters. This loss is now being minimized by end-connectors made of four inches of stainless steel tubing.

For an apparatus made of six of these identical 2-meter Calrod columns this 2.77 factor should be cubed, a factor of 21. In collaboration with Professor Onsager, the writer has designed such a

six-unit model, but with decreasing gap spaces and coupling pipe sizes for successive units. It is to be hoped that its factor is better than this 21 estimate. We expect to have this apparatus in operation soon.

Separation of Neon Isotopes

One of these Calrod units has been used very successfully in separating the neon isotopes. The manner of operation is indicated schematically in Fig. 4. Two liters of pure neon gas were pumped into the column with a Toeppler pump to a pressure of $1\frac{1}{2}$ atmospheres. The gas was circulated convectively through the lower end volume of about 300 cc. Between the hot and cold surfaces a temperature difference of 400°C was maintained. After two days, gas was bled off at the top at the rate of about 20 cc an hour into several glass containers until the pressure in the column had dropped to atmospheric. The lower end volume was then cut off and, with little waste, the contents of the column pumped back into the original flask. Mass-spectrographic analyses of the heavy and light samples gave the following results:

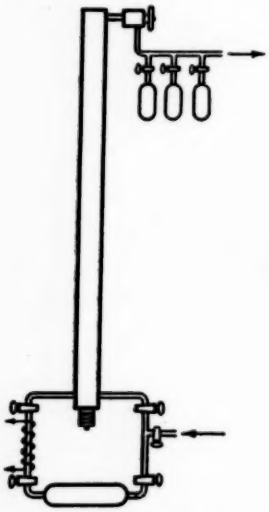

FIG. 4. Diagram illustrating operation of single unit for separating neon isotopes.

	Heavy	Light	Ratio
Ne^{20}	84%	97.6%	0.86
Ne^{21}	0.43%	0.163%	2.64
Ne^{22}	15.7%	2.28%	6.88

The factor for Ne^{22}/Ne^{20} separation is thus about 8. It is of interest to compare this with the C^{13} enrichment produced by the same apparatus. Our factor for methane in a single column would be $2.77^{\frac{1}{2}}=1.67$, with ΔT lower by 30°C than that used for neon. Nier[10] has recently measured the coefficient of thermal diffusion for neon. He finds that for end temperatures close to those used here this quantity is 0.71 times the value computed from Enskog's equation for elastic spheres, whereas for methane it is 0.3 of the hard sphere value. The $(m_2-m_1)/(m_2+m_1)$ factor is 1/33 for CH_4 and 2/42 for Ne, the ratio being 11/7 in favor of Ne. Thus although the varying pressure in the neon experiments makes exact calculation impossible, it is evident that the relative performance of the apparatus for these two gases is about that to be expected. These neon samples have been used in deuteron bombardment experiments by Professor Pollard and the writer. There is an indication that a subsequent separation of the neon isotopes was even better than the values just mentioned.

I wish to thank Dr. David W. Stewart, Dr. Albert Keston and Professor H. C. Urey for the mass spectrometer analyses, and Professor L. Onsager for much valuable discussion on applications of the theory of the thermal separation of isotopes.

[10] A. O. Nier, Phys. Rev. **57**, 338 (1940).

Field Theories for Charged Particles of Arbitrary Spin

L. I. SCHIFF
Department of Physics, University of California, Berkeley, California
(Received February 13, 1940)

A class of field theories that are invariant under the complete Lorentz and gauge groups is discussed. These theories employ wave fields that provide irreducible representations of the space rotation group, so that the particles described by them have a definite spin. The Pauli-Weisskopf and Dirac theories are of this type, and apart from them there is just one theory for each value of the spin $\geqq\frac{1}{2}$ (the present theory for spin $\frac{1}{2}$ is different from the Dirac theory). There are in each of these cases four states of the field for a given momentum and spin orientation: both signs of energy and both signs of charge. Quantization according to the exclusion principle can be made to result in a positive definite energy, but this prevents the charge densities from commuting outside the light cone. It seems therefore that these theories do not correspond to reality.

I

THE problem of constructing relativistic field theories for particles of arbitrary spin has been considered recently by several writers. Dirac[1] set up relativistic wave equations that did not, as pointed out by Kemmer[2] and by Taub,[3] transform covariantly under reflections of the space coordinates. Fierz[4] was able to find equations that met this difficulty, but they were not gauge covariant. He found, however, that even in the force-free case it was desirable to have a particular theory describe particles of only one spin, since otherwise there was a tendency for both the charge and energy of the field to be indefinite.

Fierz and Pauli,[5] using the Lagrangian formalism to guarantee the consistency of their equations, have now found reflection and gauge invariant relativistic theories that describe particles of definite but arbitrary spin. They have used as their wave fields quantities that provide irreducible representations of the Lorentz group, but that are not irreducible under the space rotation group. Thus the wave fields do not in themselves describe particles of a definite spin or satisfy the Klein-Gordon equation in the absence of electromagnetic fields. These difficulties were met by adjoining auxiliary fields in such a way that the Lagrangian equations of motion provide a sufficient number of supplementary identities to eliminate all but the particles of the highest spin capable of being described by the original wave fields. This technique is an extension of that followed in the Proca (spin 1) theory; in that relatively simple case it is unnecessary to adjoin auxiliary fields. For if the Lagrangian is written in terms of the four-vector wave field alone, a suitable choice of the coefficients of its various invariant parts provides an identity that suffices to eliminate the particles of spin 0 that would otherwise appear.[6]

Another method for constructing suitably invariant theories describing particles of a definite spin consists in using from the outset only wave fields that provide irreducible representations of the space rotation group, in which case the Klein-Gordon equation is satisfied in the absence of electromagnetic fields and no supplementary identities are needed. Well-known examples of this method are the Pauli-Weisskopf (spin 0) and Dirac (spin $\frac{1}{2}$) theories. The application of the method can be extended; it is shown below that in the absence of electromagnetic fields there exists just one other theory for each value of the spin $\geqq\frac{1}{2}$ (the present theory for spin $\frac{1}{2}$ is different from the Dirac theory), and that these together with the two older theories exhaust the possibilities of this method. Investigation of these theories shows that the unquantized field energy is indefinite in each case. Quantization according

[1] P. A. M. Dirac, Proc. Roy. Soc. **A155**, 447 (1936).
[2] N. Kemmer, Proc. Roy. Soc. **A166**, 127 (1938).
[3] A. H. Taub, Phys. Rev. **56**, 799 (1939).
[4] M. Fierz, Helv. Phys. Acta **12**, 3 (1939).
[5] M. Fierz and W. Pauli, Proc. Roy. Soc. **A173**, 211 (1939).

[6] It is worth noting that the interaction with electromagnetic radiation can be chosen differently from that of the usual Proca theory without destroying the supplementary identity.

to the Fermi-Dirac statistics can be made to result in a positive definite energy, but then requires that the charge densities at different places and the same time fail to commute. Therefore these theories do not seem to describe physical particles.

On the basis of former theories, one might conclude that the definiteness of the field energy and charge depends essentially on the order of the wave equations; the charge is definite and the energy not when the equations are of first order, and the opposite is true when they are of second order. However, this conclusion is correct only when the wave fields are multiplied by their complex conjugates in the momentum terms of the Lagrangian and Hamiltonian. For in the present theories, the wave fields are multiplied by the complex conjugates of their space reflections in the momentum terms; this results in both the energy and charge being indefinite, even though the wave equations are of second order. We shall see that there are *four* states of a free particle of given momentum and spin orientation: both signs of energy and both signs of charge. This doubling of the number of states can be inferred from an examination of the unquantized field. Thus in the older theories, one could specify at any time the wave fields and their space reflections when the equations are of first order (half-integer spin), or the wave fields and their time derivatives when the equations are of second order (integer spin); in all of the present theories, one can specify at any time the wave fields, their space reflections and the time derivatives of both, thus doubling the number of degrees of freedom of the field.

II

It is known that the two-component spinors containing all primed or all unprimed indices, and symmetric in all of them, provide all the irreducible representations of finite rank of the space rotation group.[7] We therefore use the n-index spinor $\psi_{\mu\nu\cdots}$ and its space reflection $\phi^{\mu'\nu'\cdots}$ to describe a particle of spin $n/2$. Since it is only necessary to consider the present theories in the absence of electromagnetic fields in order to show that they probably cannot describe physical particles, we shall need in addition only the momentum spinor $p_{\alpha'\beta}$, for which $\frac{1}{2}p_{\alpha'\beta}p^{\alpha'\beta}=p_t^2-p_x^2-p_y^2-p_z^2\equiv\hbar^2\Box$. It is then clear that the only real invariant Lagrangian densities, other than those of the Pauli-Weisskopf and Dirac theories, that give wave equations of the first degree and of not higher than the second order are (velocity of light set equal to unity):

$$L=\theta[\bar{\psi}_{\mu'\nu'\cdots}(\tfrac{1}{2}p_{\alpha'\beta}p^{\alpha'\beta}-m^2)\phi^{\mu'\nu'\cdots}\pm\bar{\phi}^{\mu\nu\cdots}(\tfrac{1}{2}p_{\alpha'\beta}p^{\alpha'\beta}-m^2)\psi_{\mu\nu\cdots}],\quad n\geqq 1.$$

Here, the bars denote complex conjugates; θ stands for 1 or i, and $\pm$ stands for 1 or -1 according as n is even or odd. The p operators above may be regarded as operating either to the right or to the left since this does not affect the total Lagrangian.

It is now convenient to define new field variables:

$$\xi_\lambda\equiv[n!/\lambda!(n-\lambda)!]^{\frac{1}{2}}\psi_{\mu\nu\cdots},$$
$$\eta_\lambda\equiv[n!/\lambda!(n-\lambda)!]^{\frac{1}{2}}\phi^{\mu'\nu'\cdots},$$

where $\lambda=0, 1, 2, \cdots n$ is the number of indices of ψ or ϕ equal to 1 or 1′, respectively. In terms of these, we have for the Lagrangian equations of motion:

$$(\hbar^2\Box-m^2)\xi_\lambda=0,\quad(\hbar^2\Box-m^2)\eta_\lambda=0,$$

and for the canonical momenta to the field variables:

$$\xi_\lambda^*=\pm i\theta\hbar(\bar{\eta}_\lambda p_t),\quad \eta_\lambda^*=i\theta\hbar(\bar{\xi}_\lambda p_t),$$

where p_t operates to the left in these relations and to the right in their complex conjugate relations. To find the normal coordinates of the field, we first make an expansion in plane waves (box of unit volume):

$$\xi_\lambda=\sum_k a_{\lambda k}\exp[i\mathbf{kx}],$$
$$\xi_\lambda^*=\sum_k a_{\lambda k}^*\exp[-i\mathbf{kx}],$$
$$\eta_\lambda=\sum_k b_{\lambda k}\exp[i\mathbf{kx}],$$
$$\eta_\lambda^*=\sum_k b_{\lambda k}^*\exp[-i\mathbf{kx}],$$
$$E_k=+(\hbar^2k^2+m^2)^{\frac{1}{2}},$$

[7] B. L. van der Waerden, *Die Gruppentheoretischen Methode in der Quantenmechanik* (Springer, 1932), p. 78. The notation of the present paper agrees with the standard spinor notation except for the typographically advantageous replacement of dotted indices by primed indices.

in terms of which the Hamiltonian and total charge become:

$$H=\theta\sum[\hbar^{-2}(a^*\bar{b}^*\pm b^*\bar{a}^*)+E^2(\bar{a}b\pm\bar{b}a),$$

$$q=-ie\hbar^{-1}\sum(a^*a+b^*b-\bar{a}\bar{a}^*-\bar{b}\bar{b}^*),$$

where the indices k and λ have been dropped. The change of variables:

$$a=\tfrac{1}{2}E^{-\frac{1}{2}}(A+\bar{B}+\bar{C}+D),$$

$$a^*=\tfrac{1}{2}i\hbar E^{\frac{1}{2}}(\bar{A}-B-C+\bar{D}),$$

$$b=\pm\tfrac{1}{2}\theta E^{-\frac{1}{2}}(A+\bar{B}-\bar{C}-D),$$

$$b^*=\tfrac{1}{2}i\theta\hbar E^{\frac{1}{2}}(\bar{A}-B+C-\bar{D}),$$

then brings the energy and charge into the "normal" form:

$$H=\sum E(\bar{A}A+B\bar{B}-C\bar{C}-\bar{D}D),$$

$$q=e\sum(\bar{A}A-B\bar{B}-C\bar{C}+\bar{D}D).$$

Regarding this change of variables as a contact transformation from $(a, b, \bar{a}, \bar{b}, a^*, b^*, \bar{a}^*, \bar{b}^*)$ to $(A, B, C, D, A^*, B^*, C^*, D^*)$, we see that the canonical momentum $A^*=i\hbar\bar{A}$, etc., and that the Hamiltonian equations of motion for the normal coordinates are:

$$dA/dt=-iE\hbar^{-1}A,\quad dB/dt=-iE\hbar^{-1}B,$$

$$d\bar{A}/dt=iE\hbar^{-1}\bar{A},\quad d\bar{B}/dt=iE\hbar^{-1}\bar{B},$$

$$dC/dt=iE\hbar^{-1}C,\quad dD/dt=iE\hbar^{-1}D,$$

$$d\bar{C}/dt=-iE\hbar^{-1}\bar{C},\quad d\bar{D}/dt=-iE\hbar^{-1}\bar{D}.$$

The four states of the field for given momentum $\hbar\mathbf{k}$ and spin orientation λ represent particles of both signs of energy and of charge. Thus second quantization according to Einstein-Bose statistics results in an indefinite energy. It is nevertheless possible to introduce the exclusion principle through the anticommutation laws:

$$[A_{\lambda k}, \bar{A}_{\mu l}]^+=[B_{\lambda k}, \bar{B}_{\mu l}]^+=[C_{\lambda k}, \bar{C}_{\mu l}]^+$$
$$=[D_{\lambda k}, \bar{D}_{\mu l}]^+=\delta_{\lambda\mu}\delta_{kl},$$

with all other anticommutators vanishing. The operator for the number of particles in a state then has only the eigenvalues 0 and 1, so that one could make hole theory and secure a positive definite energy. Another immediate consequence, however, is that the commutation laws for the wave fields and their complex conjugates lose their usual infinitesimal character, so that the charge densities at different places and the same time fail to commute. Further, it is necessary to give up either the canonical Hamiltonian formalism or the covariance of the theory. For the equations of motion $\dot{f}=i\hbar^{-1}[H, f]$, with the H given above, do not agree with the unquantized Hamiltonian equations, and in order to preserve the Hamiltonian formalism it would be necessary to replace H by $H'=\Sigma E(\bar{A}A+\bar{B}B-\bar{C}C-\bar{D}D)$. Although the c number Hamiltonians corresponding to H and H' are the same, the q number Hamiltonians differ by certain commutators of the wave fields that are not Lorentz covariant.[8]

In spite of the indefiniteness of the energy when quantization is made according to Einstein-Bose statistics, one could perhaps still interpret the theory reasonably if there were no means by which the occupation numbers of the C and D states could change if they were all initially set equal to zero. However, the generalization of the original Lagrangian to the presence of electromagnetic fields, which is straightforward although not unique, shows that it is impossible to avoid electromagnetic coupling terms that would cause radiative transitions and pair-production in the negative energy states.

[8] Compare with the Fermi-Dirac quantization of the Pauli-Weisskopf theory, W. Pauli, *Princeton mimeographed notes* (1936), p. 15; Annales Poincaré **6**, 137 (1936).

On the Time Distribution of So-Called Random Events

WILLY FELLER
Brown University, Providence, Rhode Island

(Received February 10, 1940)

This paper contains a discussion and complete solution of a problem treated recently by A. Ruark.

1

UNDER the same title, A. Ruark[1] recently discussed a statistical problem which seems frequently encountered in analyzing the results of some counting experiments and which "appears to have an interest far transcending its immediate applications." In mathematical terms Ruark's problem is the following one.

Consider a sequence of "random events," that is to say, suppose that the probability $W_n(t)$ of the occurrence, in a run of duration t, of exactly n events is given by the Poisson formula:[2]

$$W_n(t)=(ft)^n e^{-ft}/n! \quad W_0(t)=e^{-ft}, \tag{1}$$

where $f>0$ is a constant characteristic for the process. Now, out of a series of observations, pick out at random[3] some time-interval of length D; let n be the number of actually observed events during that time. Pick out, again at random, two consecutive events among these. What is the probability that the time elapsed between their occurrence will exceed a given number $T<D$? In other words: we wish to calculate the conditional probability $P(T; n, D)$ that the interval between two consecutive events will exceed T, under the hypothesis that it is known that these events occurred in a run of duration D during which there occurred exactly $n\geq 2$ events.

Using Bayes' theorem, Ruark finds for this probability the expression

$$\frac{1}{1-e^{-fD}}\frac{n}{fD}\left(1-\frac{T}{D}\right)^{n-1}. \tag{2}$$

But by definition $P(0; n, D)=1$, for all possible n, D, whereas the expression (2) may take on any value between 0 and ∞. In an actual counting experiment, the probability that (2) will largely exceed 1 is small, because the probability that $n\sim fD$ is overwhelming. Still it is clear that (2) is not the correct expression for any probability distribution. We propose to show that the correct solution of our problem is

$$P(T; n, D)=(1-T/D)^n. \tag{3}$$

Now Ruark considers $P(T; n, D)$, or (2), only as an approximation to another conditional probability $P_1(T; n, D)$, with which he was primarily concerned: the n events divide the whole interval D into $n+1$ sub-intervals (the probability of an event occurring exactly in an end-point being 0). In the above formulation we considered only $n-1$ of them, namely, those between two consecutive events. In the original problem, as formulated by Ruark, we are to pick out at random any of the $n+1$ intervals; the probability of its length exceeding T is $P_1(T; n, D)$. Ruark considers $P(T; n, D)$ as an approximative value of $P_1(T; n, D)$. It will be shown, however, that

$$P(T; n, D)\equiv P_1(T; n, D). \tag{4}$$

More precisely, our calculations will show that it is not necessary to choose the interval at random: $P(T; n, D)$ can be interpreted also as the conditional probability that, for any fixed $k\leq n$, the length of the kth among the said intervals will

[1] A. Ruark, Phys. Rev. **56**, 1165 (1939).

[2] Sometimes also called after Bateman. The assumptions leading to (1) are: (i) the probability of the occurrence of an event in any time-interval $(t, t+\Delta t>t)$ is, independently of the previous events, $f\cdot\Delta t+o(\Delta t)$, where $o(\Delta t)$ stands for terms of order negligible as compared with Δt; (ii) the probability of the occurrence of more than one event during $(t, t+\Delta t)$ is $o(\Delta t)$. Obviously the second assumption cannot be deduced from the first one and is essential for the deduction of (1).

[3] This assumption is essential for Ruark's problem: the calculation would be different if we were to consider e.g. time intervals of duration D starting with some actually observed event (in which case n would be replaced by $n-1$). For the reader's convenience we follow Ruark's notations as far as possible. D is used both to denote our time-interval and its length.

exceed T, under assumption that the interval $(0, D)$ contains exactly n events.

There is a third interpretation of $P(T; n, D)$, which is the simplest and, perhaps, the most natural one: $P(T; n, D)$ is also the conditional probability that if we pick out at random any point t of our interval D, there is no event between t and $t+T$. The interpretation given above for (3) can be considered as a consequence of this. Similarly, in Poisson's original formula (1) $W_0(t)$ gives the probability that the interval between two consecutive events will exceed t, but that is only a consequence of the primary definition. We proceed now to the actual computations.

2

The conditional probability $P_B(A)$ of an event A under the hypothesis of another event B is computed directly from the definition

$$P_B(A)=P(AB)/P(B), \tag{5}$$

where $P(B)$ is the absolute probability of the event B, $P(AB)$ the probability of the combination of both events A and B. For all conditional probabilities which we require, the hypothesis B consists in the occurrence of exactly n events in a run of duration D; hence by (1)

$$P(B)=(fD)^n e^{-fD}/n! \tag{6}$$

Now let $(0, D)$ be the given interval and denote by $E_1, \cdots, E_n$ the $n\geq 2$ events which are to occur in it. Let us first fix some k $(1\leq k\leq n-1)$, and denote by A the event that the time interval between E_k and E_{k+1} exceeds a given number T with $0\leq T\leq D$. Suppose the times of occurrence of E_k and E_{k+1} to be t and τ. Then the realization of the event A requires that $0<t<D-T$ and $t+T<\tau<D$. In addition, the simultaneous realization of A and B means: (i) during $(0, t)$ there are exactly $k-1$ events; (ii) an event occurs at the moment t; (iii) no events between t and τ; (iv), an event at the moment τ; (v) exactly $n-k-1$ events during (τ, D). The probability of this event is:

$$e^{-ft}\frac{(ft)^{k-1}}{(k-1)!}fdt\cdot e^{-f(\tau-t)}fd\tau\cdot e^{-f(D-\tau)}\frac{\{f(D-\tau)\}^{n-k-1}}{(n-k-1)!}$$
$$=e^{-fD}f^n\frac{t^{k-1}(D-\tau)^{n-k-1}}{(k-1)!(n-k-1)!}dtd\tau.$$

Thus, summing over the possible values of t and τ

$$P(AB)=e^{-fD}\frac{f^n}{(k-1)!(n-k-1)!}$$
$$\times\int_0^{D-T}t^{k-1}dt\int_{t+T}^{D}(D-\tau)^{n-k-1}d\tau$$
$$=e^{-fD}\frac{\{f(D-T)\}^n}{n!}.$$

Finally by (5) and (6) the Eq. (3) results. Thus the conditional probability distribution for the interval sizes is the same for the time-intervals between any E and the next. Hence, we may fix k arbitrarily or choose E_k at random among $E_1, \cdots, E_{n-1}$: the conditional probability distribution of the time to wait for the next event is in both cases given by (7).

So far, the assertion (3) has been proved. In Ruark's original problem, we have also to consider the intervals from the E_1 to D, and from the beginning to the occurrence of E_1 and from E_n to D. Consider, e.g., the first one, and let E_1 occur at the time τ. The realization of the event A means $\tau\geq T$. The realization of AB requires: (i) no event occurs during $(0, \tau)$; (ii) an event occurs at τ; (iii) $(n-1)$ events occur during (τ, D). The elementary probability of this event is

$$e^{-f\tau}fd\tau\cdot e^{-f(D-\tau)}\frac{\{f(D-\tau)\}^{n-1}}{(n-1)!},$$

and hence

$$P(AB)=e^{-fD}\frac{f^n}{(n-1)!}\int_T^D(D-\tau)^{n-1}d\tau$$
$$=e^{-fD}\frac{\{f(D-T)\}^n}{n!},$$

which again coincides with the common probability for the intervals between any E_k and E_{k+1}. The same argument applies for the interval between E_n and D. Hence, if we are to choose at random any of the $n+1$ sub-intervals of D, we still fall back on (3). This again proves (4),

though this identity was to be expected *a priori*.

The same argument holds also for the last and simplest of the three problems mentioned above: if x is any fixed or randomly chosen point in $0<x<D-T$, the conditional probability that the next event will occur between $x+\tau$ and $x+\tau+d\tau$ is obviously

$$e^{-\int_\tau^{\tau+d\tau} f d\tau}\cdot e^{-\int_{\tau+d\tau}^{D} f d\tau}\{f(D-\tau)\}^{n-1}/(n-1)!P(B)$$

$$=\frac{n}{D}\left(1-\frac{\tau}{D}\right)^{n-1}$$

and hence we get by a single integration again the correct answer (3).

MAY 15, 1940 PHYSICAL REVIEW VOLUME 57

On the Deviations from Ohm's Law at High Current Densities

EUGENE GUTH, *University of Notre Dame, Notre Dame, Indiana*
AND
JOSEF MAYERHÖFER,* *University of Vienna, Vienna*

(Received March 2, 1940)

The deviations from Ohm's law at high current densities are calculated on the basis of the wave-mechanical theory of conductivity. A current density of 10^9 amp./cm² causes a 1 percent deviation only. No observable deviations are to be expected at the experimental current densities available at present (10^6 amp./cm²). This is in agreement with the experiments of Barlow, neither does it contradict those of Bridgman, if the effects found by him are due to secondary factors. The method used consists in the actual solving of the fundamental equation for conductivity in a higher approximation. It is proved that in the Lorentz model (fixed metal ions) the fundamental equation is not soluble in the second approximation in the field strength. A solution in this approximation can be obtained only by assuming inelastic collisions between the electrons and the metal ions. The analogy between the distribution function containing the influence of the electric field and a distribution function found by Pidduck for the motion of ions in gases is pointed out. A generalization of the present theory is indicated by taking into account the influence of the external field on the lattice waves.

INTRODUCTION

OHM'S law has been extraordinarily successful for many decades; but our present knowledge makes it clear that this law can be, not a fundamental law (such as Coulomb's law), but a derived law, which describes reality only to a first approximation. Therefore, attempts have been made to fix its limits experimentally. As early as 1876, Maxwell made observations up to a current density of 5×10^4 amp./cm², but obtained only negative results. Later, measurements by Lecher and Rausch von Traubenberg also gave negative results up to current densities of 10^7 amp./cm² within the limits of error of their experiments. Bridgman[1] performed more accurate experiments using Ag and Au foils of 10^{-5} cm thickness, and his measurements seemed to indicate that deviations from Ohm's law existed at current densities of 10^6 amp./cm². His results, however, are contested by Barlow,[2] who considers Ohm's law valid up to 2×10^6 amp./cm².

Until the present time all theories of metals consider only the first approximation of the dependence of the current upon the electric field, and it is supposed that deviations from Ohm's law can be explained without further assumptions by simply computing higher approximations. This has been carried out in this paper, and the deviations from Ohm's law which are automatically obtained at high current densities show

* The joint investigations of the authors, on which this paper is based took place in 1936–38. The present article has been prepared by the senior author (E. G.).

[1] P. W. Bridgman, Phys. Rev. **19**, 387 (1922); Proc. Am. Acad. Arts **57**, 131 (1922). Professor Bridgman, in a conversation, pointed out that the effects he observed were certainly real, but at that time the question had not been settled as to whether the effects could be accounted for by some minute phenomena not yet studied in detail. Such phenomena are, for instance, (a) time lag in the thermal conductivity, (b) some kind of electromotive forces connected with a change in temperature (cf. Bridgman, second reference above, p. 145).

[2] H. M. Barlow, Phil. Mag. **9**, 1041 (1931).

the possible limitations of this law. While detailed treatment is given only to the region of high temperatures, the only region in which the whole theory of metallic conduction has a safe foundation, indications will be made as to how the theory could be extended to the region of low temperatures.

Our result is that deviations should be observable at a current density of $\sim 10^9$ amp./cm^2 only. Thus, Ohm's law should hold for all present available experimental current densities. In order to obtain this result, a general method of solving the wave-mechanical equation for conductivity which is applicable for the case of a strong electric field was developed. The distribution function showing the influence of the field is compared with Pidduck's distribution function obtained for the problem of motions of ions in gases.

The Validity of Lorentz' Approximation

H. A. Lorentz[3] first established a systematic theory of metals in terms of the "electron-gas" picture. He considered the metal to consist of a mixture of two gases, an electron gas and a gas of metal ions, and applied the kinetic theory of gases to this model. The problem was simplified by Lorentz in making the assumption that the mass of an ion is infinitely large in comparison with the mass of an electron, thus allowing one to consider the ions as being practically immovable in electron-ion collisions.

The following notations used in describing the motion of the electrons are due to Lorentz:

(x, y, z) = a point in position space,
(ξ, η, ζ) = a point in velocity space before collision,
$r = (\xi^2+\eta^2+\zeta^2)^{\frac{1}{2}}$,
(ξ', η', ζ') = a point in velocity space after collision,
n = number of atoms per unit volume,
R = radius of sphere of action of an electron for a collision with an atom,
φ = azimuth around the ξ axis,
$X = eF/m$ = force acting on electron,
F = electric field strength assumed to act in the x direction.

[3] H. A. Lorentz, *Theory of Electrons* (Leipzig, 1909), p. 266.

The motion of the electrons is describable by a distribution function $f(x, y, z, \xi, \eta, \zeta)$. If there is no temperature gradient, f reduces to a function of the velocity coordinates alone, and the following equation of Lorentz[3] holds:

$$nR^2r\int_0^{\pi/2}\int_0^{2\pi}\{f(\xi', \eta', \zeta')-f(\xi, \eta, \zeta)\} \times\cos\vartheta\sin\vartheta d\vartheta d\varphi = X\frac{\partial f}{\partial \xi}. \quad (1)$$

The left side represents the change of the distribution function by the impacts of electrons with the ions. The right side is the change due to the electric field. To integrate over total solid angle, a new variable $\theta = 2\vartheta$ is introduced:

$$\frac{nR^2r}{4}\int_0^{\pi}\int_0^{2\pi}\{f(\xi', \eta', \zeta')-f(\xi, \eta, \zeta)\} \times\sin\theta d\theta d\varphi = X\frac{\partial f}{\partial \xi}. \quad (2)$$

Lorentz obtains an approximate solution of this equation by substituting

$$f = f_0(r)+g; \quad g \ll f_0.$$

He shows that $g \sim X$; therefore, f may be expanded in powers of the parameter X

$$f = f_0+Xf_1+X^2f_2+\cdots. \quad (3)$$

Substituting this in (2) and comparing the coefficients of X, we obtain the following equations:

$$\frac{nR^2r}{4}\int_0^{\pi}\int_0^{2\pi}(f_1'-f_1)\sin\theta d\theta d\varphi = X\frac{\partial f_0}{\partial \xi}, \quad (4)$$

$$\frac{nR^2r}{4}\int_0^{\pi}\int_0^{2\pi}(f_2'-f_2)\sin\theta d\theta d\varphi = X\frac{\partial f_1}{\partial \xi}. \quad (5)$$

. . . . . .

If we put $X = 0$, any function of r alone will solve Eq. (2), so that f_0 is not determined by this equation. It was this very fact that allowed Sommerfeld to reconstruct the theory of metals by assuming the Fermi distribution instead of the Maxwell distribution for the electrons without any change in the Lorentz equation itself.

If f_0 is given, the necessary and sufficient

condition for the solubility of the equation

$$\int\int (f'-f)\sin\theta d\theta d\varphi=\Phi$$

is that the right-hand side Φ be orthogonal to the solutions of the homogeneous equation. It can be shown that (4) has only solutions which are functions of r alone. The condition for solubility is, therefore,

$$\int_0^\pi\int_0^{2\pi}\Phi f(r)\sin\psi d\psi d\epsilon=0 \qquad (6)$$

and applying this condition to (4)

$$\int_0^\pi\int_0^{2\pi}\frac{\partial f_0}{\partial\xi}\sin\psi d\psi d\epsilon =\frac{df_0}{dr}\int_0^\pi\int_0^{2\pi}\sin\psi\cos\epsilon\sin\psi d\psi d\epsilon=0.$$

Hence (4) has a solution. The result of the first approximation, as obtained by Lorentz,[4] is:

$$f=f_0-\frac{eF}{m}\frac{\xi}{r}\frac{l}{r}\frac{df_0}{dr}\quad(l=1/nR^2r). \qquad (7)$$

To obtain a higher approximation, we calculate the right side of (5)

$$\frac{\partial f_1}{\partial\xi}=-\frac{l}{r^2}\frac{df_0}{dr}-\frac{\xi^2}{r}\frac{d}{dr}\left(\frac{l}{r^2}\frac{df_0}{dr}\right). \qquad (8)$$

From the condition of solubility (6) follows a restriction for f_0 which cannot possibly be fulfilled. Therefore, Eq. (5) cannot be solved, and consequently (1) has physical sense only in the first approximation.[5]

The reason for the insolubility of (1) in the second approximation for the field strength may be ascertained by an examination of the fundamental restriction, which Lorentz took as a basis for his calculations. If the ratio of the mass of the metal ion to the mass of the conduction electron does not have a finite value, then there can occur no transfer of energy during collision. In the first approximation this does not matter. However, in the second approximation a stationary state does not exist because the electrons continually absorb energy from the electric field, the absorption being proportional to F^2, and are therefore accelerated more and more. This absorption of energy is easily seen to be simply the Joulean heat. According to the Lorentz model, all this heat would be stored in kinetic energy of the electrons. Actually, this is not the case. The electron-ion collisions are not elastic. Consequently, in virtue of the small specific heat of the electrons as compared to that of the ions, in thermal equilibrium practically all Joulean heat will be received by the ions.

Because of these limitations, Lorentz' equation cannot be used for our case, and one must look for a generalization of it in which the above assumption is not made. In the theory of metals, only those generalizations are useful which lead to the Fermi distribution in the zero-order approximation: either a generalization of Nordheim's equation[6] for the mixture of two Fermi gases or the wave-mechanical one of Bloch. On account of the uncertainty of the limits of the electron-gas picture, the wave-mechanical theory will be considered.

The Wave-Mechanical Theory of Conductivity

If one considers the interaction of the electrons with the lattice, the following equation for the distribution function is valid:

$$(\partial f/\partial t)_{\text{impact}}+(\partial f/\partial t)_{\text{field}}=0.$$

According to Sommerfeld and Bethe,[7] the first term is

$$\left(\frac{\partial f}{\partial t}\right)_{\text{impact}}=\frac{2C^2G^{-3}}{9M\hbar}\frac{\partial}{\partial t}\sum_{\mathbf{q}}\frac{q^2}{\omega_q}\{\Omega(E_{\mathbf{k}+\mathbf{q}}-E_{\mathbf{k}}-h\nu)[(1-f(\mathbf{k}))f(\mathbf{k}+\mathbf{q})(N_{\mathbf{q}}+1)-f(\mathbf{k})(1-f(\mathbf{k}+\mathbf{q}))N_{\mathbf{q}}] +\Omega(E_{\mathbf{k}+\mathbf{q}}-E_{\mathbf{k}}+h\nu)[1-f(\mathbf{k})f(\mathbf{k}+\mathbf{q})N_{\mathbf{q}}-f(\mathbf{k})(1-f(\mathbf{k}+\mathbf{q}))(N_{\mathbf{q}}+1)]],$$

[4] Reference 3, p. 269.
[5] B. Davydow, Physik. Zeits. Sowjetunion **8**, 59 (1935) is not correct in stating that the expansion into powers of the field diverges and that the second approximation becomes infinite.
[6] L. W. Nordheim, Proc. Roy. Soc. **A119**, 689 (1928).
[7] Sommerfeld-Bethe, *Handbuch der Physik*, Vol. 24/2. formula (34,40).

where $f(\mathbf{k})$ is the number of electrons having the wave vector $\mathbf{k}$. N is the number of quanta of the elastic vibrations of the lattice in the state

$$h\nu=\hbar\omega_{\mathbf{q}};\quad \text{i.e.,}^{8}\quad N=\frac{1}{e^{h\nu/kT}-1}.$$

$\mathbf{q}$ is the vector by which $\mathbf{k}$ is changed in a transition: $\mathbf{k}'=\mathbf{k}+\mathbf{q}$. The prime designates, as previously, the state after an impact. For other abbreviations we refer to Sommerfeld-Bethe.[9] Furthermore, it is always assumed that: $E=\hbar^2k^2/2m$.

Instead of summing, one can integrate, and there follows:

$$\sum_{\mathbf{q}}=\left(\frac{G}{2\pi}\right)^3\cdot\frac{1}{n}\int_0^{q_0}q^2dq\int_0^{2\pi}d\varphi\int_0^{\pi}\sin\vartheta d\vartheta.$$

Only when energy is conserved will the function Ω not vanish, and therefore the integral can be evaluated:

$$\frac{\partial}{\partial t}\int_0^{\pi}\Omega\sin\vartheta d\vartheta=\frac{2\pi\hbar}{qdE/dk}.$$

If $\omega=u_0q$, there results

$$\left(\frac{\partial f}{\partial t}\right)_{\text{impact}}=\frac{2C^2}{9M}\frac{2\pi}{u_0dE/dk}\frac{1}{2\pi^3}\frac{1}{n}\int_0^{q_0}q^2dq\int_0^{2\pi}d\varphi J,$$

where

$$J=(1-f(\mathbf{k}))f(\mathbf{k}+\mathbf{q},E+h\nu)(N_{\mathbf{q}}+1)-f(\mathbf{k})(1-f(\mathbf{k}+\mathbf{q},E+h\nu))N_{\mathbf{q}}$$
$$+(1-f(\mathbf{k}))f(\mathbf{k}+\mathbf{q},E-h\nu)N_{\mathbf{q}}-f(\mathbf{k})(1-f(\mathbf{k}+\mathbf{q},E-h\nu))(N_{\mathbf{q}}+1)$$
$$=\frac{1}{e^{h\nu/kT}-1}\{(1-f_k)f^+{}_{k+q}e^{h\nu/kT}-f_k(1-f^+{}_{k+q})-(1-f_k)f^-{}_{k+q})-f_k(1-f^-{}_{k+q})e^{h\nu/kT}\}.$$

Here $f^+{}_{k+q}$ denotes $f(\mathbf{k}+\mathbf{q})\Big|_{E_{\mathbf{k}+\mathbf{q}}=E_{\mathbf{k}}+h\nu}$.

Finally, we obtain

$$\frac{2C^2}{18Mu_0(dE/dk)\pi^2}\frac{1}{n}\int_0^{q_0}q^2dq\int_0^{2\pi}d\varphi J=+\frac{eF}{\hbar}\frac{\partial f}{\partial k_x},\tag{9}$$

where the right-hand side represents the field term. This is a functional equation, for the unknown function f not only appears for the energy E, but also for $E\pm h\nu$. To solve this equation, the distribution functions are developed into spherical harmonics:

$$f(\mathbf{k})=\psi_0+P_1\psi_1+P_2\psi_2+\cdots;\quad f(\mathbf{k}+\mathbf{q})=\psi_0+\mathcal{P}_1\psi_1+\mathcal{P}_2\psi_2+\cdots,$$

where

$$P_1=\frac{k_x}{k};\quad P_2=\tfrac{1}{2}(3P_1{}^2-1);\quad \mathcal{P}_1=\frac{k_x+q_x}{|\mathbf{k}+\mathbf{q}|};\quad \mathcal{P}_2=\tfrac{1}{2}(3\,\mathcal{P}_1{}^2-1).$$

Since the values of $\mathcal{P}_1,\mathcal{P}_2$ are different for emission and absorption of sound quanta a distinction will be made between these two cases by upper indices $\mathcal{P}_1{}^+$, $\mathcal{P}_1{}^-$. The same notation will be used for the ψ: $\psi_0{}^+$, $\psi_0{}^-$ $\cdots$. Collecting the coefficients of spherical harmonics on the left-hand side, the coefficient of P_0 becomes:

$$(1-\psi_0)\psi_0{}^+e^{h\nu/kT}-\psi_0(1-\psi_0{}^+)+(1-\psi_0)\psi_0{}^--\psi_0(1-\psi_0{}^-)e^{h\nu/kT}.\tag{10}$$

[8] Boltzmann's constant k should not be mistaken for $k=|\mathbf{k}|$ because it is nearly always with T: kT.
[9] Sommerfeld-Bethe, reference 7.

Further, we have

$$e^{h\nu/kT}[-P_1\psi_1\psi_0^+ + \mathcal{P}_1^+(1-\psi_0)\psi_1^+] - P_1\psi_1(1-\psi_0^+) + \mathcal{P}_1^+\psi_0\psi_1^+ - P_1\psi_1\psi_0^- \times\mathcal{P}_1^-(1-\psi_0)\psi_1^- - [P_1\psi_1(1-\psi_0^-) - \mathcal{P}_1^-\psi_0\psi_1^-]e^{h\nu/kT}. \quad (11)$$

On the right-hand side we obtain

$$\frac{eF}{\hbar}\frac{\partial f}{\partial k_x} = \frac{eF}{\hbar}\left(\frac{\partial\psi_0}{\partial k_x} + \psi_1\left[\frac{1}{k} - \frac{k_x}{k^2}\frac{k_x}{k}\right] + \frac{k_x}{k}\frac{\partial\psi_1}{\partial k_x} + \cdots\right)$$

$$= \frac{eF}{\hbar}\left\{\frac{2}{3}\frac{E}{k}P_0\left(\frac{\partial\psi_1}{\partial E} + \frac{1}{E}\psi_1\right) + \frac{\hbar^2}{m}P_1 k\frac{\partial\psi_0}{\partial E} + \cdots\right\}. \quad (12)$$

The Case for Zero Electric Field

When the electric field is zero, the right-hand side of (9) vanishes, so that the integrand of the left-hand side must vanish. If the coefficient of P_0 (10) is set equal to zero, we obtain the functional equation for ψ_0:

$$(1-\psi_0(E))\psi_0(E+h\nu)e^{h\nu/kT} - \psi_0(E)(1-\psi_0(E+h\nu)) + (1-\psi_0(E))\psi_0(E-h\nu) - \psi_0(E)(1-\psi_0(E-h\nu))e^{h\nu/kT} = 0,$$

which may be solved by expanding into a Taylor series

$$\psi_0(E+h\nu) = \psi_0 + h\nu\frac{d\psi_0}{dE} + \frac{(h\nu)^2}{2!}\frac{d^2\psi_0}{dE^2} + \cdots \frac{h\nu}{E} \approx \frac{1}{1000}.$$

It is advantageous to change the variables by introducing

$$x = E/kT; \quad \alpha = h\nu/kT; \quad \psi_0(E+h\nu) = \psi_0 + \alpha\frac{d\psi_0}{dx} + \frac{\alpha^2}{2}\frac{d^2\psi_0}{dx^2} + \cdots. \quad (13)$$

When the coefficients of the various powers of α are set equal to zero, each gives an equation for ψ_0, provided they do not vanish identically. The first and second coefficients vanish; the third coefficient gives

$$(1-\psi_0)\left(\frac{\psi_0}{2} + \psi_0' + \frac{\psi_0''}{2}\right) + \frac{\psi_0\psi_0''}{2} + \frac{(1-\psi_0)\psi_0''}{2} - \psi_0\left(-\frac{\psi_0''}{2} + \psi_0' + \frac{1-\psi_0}{2}\right) = 0$$

or

$$\psi_0'' + \psi_0'(1-2\psi_0) = 0. \quad (14)$$

This equation is the derivative of

$$\psi_0' + \psi_0 - \psi_0^2 = 0. \quad (14a)$$

The constant of integration is equal to zero. Making use of the transformation $(\psi_0 \neq 0) z = 1/\psi_0$ we obtain

$$z' - z + 1 = 0.$$

The general solution is

$$z = Ce^x + 1; \quad \text{or} \quad \psi_0 = 1/Ce^{E/kT} + 1.$$

All solutions of (14) are Fermi distributions and differ only in the values of the constant C which is usually written as $1/A$. The other coefficients of α give equations of the Fermi distributions also, but of higher order. The Fermi distribution is the result of the interaction between the electron-waves and the impacts alone. It is not necessary to consider the whole impact term (10) in order to obtain the Fermi distribution; we may use one-half of the expression on the left and equate to zero. The same method of expansion into a power series of α may be employed, and we obtain a differential equation of every order of the Fermi distribution.

The distribution function of the electrons is determined by (10) alone. This is also valid if Pauli's principle is neglected, but then one obtains the Maxwell distribution:

$$\psi_0^+ e^{h\nu/kT} - \psi_0 + \psi_0^- - \psi_0 e^{h\nu/kT} = 0; \quad \psi_0'' + \psi_0' = 0; \quad \psi_0 = Ae^{-z} = Ae^{-E/kT}. \tag{15}$$

The essential point is that an exchange of energy between the electrons and the lattice must take place. If the impacts are elastic and the lattice is rigid ($h\nu = 0$), then in the case of zero field, (10) vanishes identically, and the approximation of order zero remains indefinite. Again we arrive at Lorentz' approximation, where the ratio of the masses of metal ions to electrons is infinite.

Thus, one can say that in any kinetic theory of gases and metals the distribution function of order zero is determined only if the impacts are not elastic.

General Case

Considering (11) and expanding, we obtain:

$$\psi_0^{\pm} = \psi_0 \pm \alpha \frac{d\psi_0}{dx} + \frac{\alpha^2}{2}\frac{d^2\psi_0}{dx^2} \pm \cdots; \quad \alpha = h\nu/kT$$

$$\left(1+\alpha+\frac{\alpha^2}{2}+\cdots\right)\left\{-P_1\psi_1\left(\psi_0+\alpha\psi_0'+\frac{\alpha^2}{2}\psi_0''+\cdots\right)+\mathfrak{P}_1^+(1-\psi_0)\left(\psi_1+\alpha\psi_0'+\frac{\alpha^2}{2}\psi_1''+\cdots\right)\right\}$$

$$-P_1\psi_1\left(1-\psi_0-\alpha\psi_0'-\frac{\alpha^2}{2}\psi_0''+\cdots\right)+\mathfrak{P}_1^+\psi_0\left(\psi_1+\alpha\psi_1'+\frac{\alpha^2}{2}\psi_1''+\cdots\right)$$

$$-P_1\psi_1\left(\psi_0-\alpha\psi_0'+\frac{\alpha^2}{2}\psi_0''+\cdots\right)+\mathfrak{P}_1^-(1-\psi_0)\left(\psi_1-\alpha\psi_1'+\frac{\alpha^2}{2}\psi_1''+\cdots\right)$$

$$-\left(1+\alpha+\frac{\alpha^2}{2}+\cdots\right)\left\{P_1\psi_1\left(1-\psi_0+\alpha\psi_0'-\frac{\alpha^2}{2}\psi_0''+\cdots\right)-\mathfrak{P}_1^-\psi_0\left(\psi_1-\alpha\psi_1'+\frac{\alpha^2}{1}\psi_1'''+\cdots\right)\right\}.$$

Collecting the coefficients of the powers of α:

coefficient of

$$\alpha^0: \quad -2P_1\psi_1+(\mathfrak{P}_1^+ + \mathfrak{P}_1^-)\psi_1,$$

coefficient of

$$\alpha^1: \quad \psi_1'(\mathfrak{P}_1^+ - \mathfrak{P}_1^-)+\psi_1(\mathfrak{P}_1^+ - \mathfrak{P}_1^-)+\psi_0\psi_1(\mathfrak{P}_1^- - \mathfrak{P}_1^+).$$

Inserting this into the expression for J and having expanded also the Bose-Planck distribution of lattice vibrations, we have:

$$J = \frac{kT}{h\nu}[(\psi_0''+\psi_0'(1-2\psi_0))\alpha^2 P_0+\psi_1(-2P_1+\mathfrak{P}_1^+ + \mathfrak{P}_1^- + ((\alpha))+\cdots].$$

The symbol $((\alpha))$ means that there are terms of order α^1 still present, but that they can be neglected. We may now integrate over φ and obtain approximately

$$\int_0^{2\pi}\mathfrak{P}_1^+ d\varphi \approx \frac{1}{k}\left(1-\frac{h\nu}{2E}\right)2\pi k_z\left(1+\left[-\frac{q^2}{2k^2}+\frac{h\nu}{2E}\right]\right);$$

$$\int_0^{2\pi}\mathfrak{P}_1^- d\varphi \approx \frac{1}{k}\left(1+\frac{h\nu}{2E}\right)2\pi k_z\left(1+\left[-\frac{q^2}{2k^2}-\frac{h\nu}{2E}\right]\right).^{10}$$

If terms of higher order are neglected, there results

$$\int_0^{2\pi}(\mathfrak{P}_1^+ + \mathfrak{P}_1^-)d\varphi = \frac{2\pi k_z}{k}\cdot 2.$$

[10] Reference 7 (35,15).

Using the abbreviation

$$R=C^2\Omega_0 m/18\pi^2 M u_0\hbar^2,$$

we have

$$\left(\frac{\partial f}{\partial t}\right)_{\text{impact}}=\frac{R}{k}\int_0^{q_0} q^2dq\left[P_0(\psi_0''+\psi_0'(1-2\psi_0))\alpha^2\cdot 2\pi+P_1\frac{-q^2}{2k^2}4\pi\psi_1\right]\frac{kT}{h\nu}$$

and since

$$\alpha=h\nu/kT=\hbar\omega_0/kT=\hbar u_0 q/kT,$$

$$\left(\frac{\partial f}{\partial t}\right)_{\text{impact}}=\frac{R}{k}\left\{P_0\cdot 2\pi\frac{\hbar u_0}{kT}\frac{q_0^4}{4}(\psi_0''+\psi_0'(1-2\psi_0))-P_1\frac{4\pi}{2k^2}\frac{kT}{\hbar u_0}\frac{q_0^4}{4}\psi_1\right\}.$$

Finally, comparing the coefficients of α of the impact term and the field term

$$-\left(\frac{\partial f}{\partial t}\right)_{\text{field}}=\frac{eF}{\hbar}\left\{P_0\cdot\frac{2}{3}\cdot\frac{1}{|\mathbf{k}|}(x\psi_1'+\psi_1)+P_1\frac{\hbar^2}{m}|\mathbf{k}|\frac{1}{kT}\psi_0'\right\},$$

$$\psi_0''+\psi_0'(1-2\psi_0)=eF\cdot A(x\psi_1'+\psi_1);\quad A=4\cdot(2/3)kT/\hbar R\cdot 2\pi q_0^4\hbar u_0,$$

$$\psi_1=-eFBx^2\psi_0';\qquad B=4m\cdot 2u_0/\hbar^2 R\pi q_0^4,$$

we obtain

$$\psi_0''(1+\beta x^3)+\psi_0'(1-2\psi_0+3\beta x^2)=0;\quad \beta=(eF)^2AB. \tag{16}$$

This equation determines that part of the distribution function of the electrons which does not depend on direction. (16) differs from the differential equation of the Fermi distribution (14) by an additional term proportional to $\beta\approx F^2$. For weak electric fields it is permissible to equate this term to zero and then the Fermi distribution is obtained.

Equation (16) is the derivative of the following:

$$\psi_0'(1+\beta x^3)+\psi_0-\psi_0^2=0. \tag{16a}$$

Let us compare this equation with the differential equation of first order, which the distribution function of Pidduck[11] obeys:

[11] F. B. Pidduck, Proc. Lond. Math. Soc. (11) **15**, 89 (1915). Pidduck treats the mixture of two gases according to the classical kinetic theory of gases applying Boltzmann's equations. He starts with the equation

$$\int\int\int_{-\infty}^{+\infty}d\omega\int_0^{\infty}bdb\int_0^{2\pi}d\varphi\cdot r(f'F'-fF)=X\frac{\partial f}{\partial\xi},$$

taking for F the Maxwellian distribution and assuming a finite ratio of the masses. After transforming this equation into one with a symmetric kernel, he deduces a series of equations by expansion into spherical harmonics. These equations are solved then by another expansion into the ratio of the masses. In this way the following distribution function as modified by the influence of the electric field is obtained:

$$f_0=Ae^{-E/kT}(E/kT+b)^b$$
$$b=(eF/kT)^2\cdot l/6;\ l\text{: mean free path.}$$

The same distribution function was rediscovered twenty years later by B. Davydow (Physik. Zeits. Sowjetunion **9**, 433 (1936)) who started from a different equation. The identity of the results of Pidduck and Davydow was first pointed out by Mayerhöfer (Thesis, Vienna, June 1937). Pidduck himself noticed it (Phys. Rev. **53**, 197 (1938)).

$$f=Ae^{-E/kT}(E/kT+b)^b;\quad f'(1+b/x)+f=0;$$
$$x=E/kT.$$

Both equations refer to relatively strong electric fields, but one from the classical point of view, the other from the quantum point of view. We know from the preceding section that in the case of $\beta=0$, by omitting $-\psi_0^2$, the differential equation of first order for the Fermi distribution reduces to that of the Maxwell distribution. The only difference, therefore, lies in the form of the dependence of the additional term upon the energy. According to Pidduck b is proportional to the square of the mean free path of an electron, but according to wave mechanics l depends on the square of energy. So b is proportional to the fourth power of x, $b/x\sim x^3$ and the conformity is clear.

To obtain the solution of (16a) we proceed as in the case of zero field. The general solution is:

$$\psi_0=1/C\exp\left[\int\frac{dx}{1+\beta x^3}\right]+1.$$

Practically, βx^3 is always very small compared to 1, and the denominator may be expanded, obtaining

$$\psi_0\approx 1/Ce^{x-(\beta x^4/4)}+1.$$

To compute the current, we start from the Sommerfeld-Bethe equation (36.9) and replace f

by ψ_0:

$$J=-(2/3)e^2F\int_0^\infty \frac{1}{\hbar}\frac{1}{(2\pi)^3}4\pi\frac{2m}{\hbar^2}E\frac{d\psi_0}{dE}l(E)dE,$$

where

$$\frac{d\psi_0}{dE}=-\psi_0{}^2C\exp\left[\frac{E}{kT}-\frac{\beta}{4}\left(\frac{E}{kT}\right)^4\right]\times\frac{1}{kT}\left(1-\beta\left(\frac{E}{kT}\right)^3\right).$$

It is not necessary to compute the integral exactly. If we neglect the terms in the exponential function and denote by f_0 the Fermi function, we have

$$\frac{d\psi_0}{dE}\approx\frac{df_0}{dE}[1-\beta(E/kT)^3].$$

Furthermore, the bracket and just as well E and $l(E)$ may be factored out of the integral, if their value is taken at the point ζ_0, and the current becomes

$$J=J_0[1-\beta(E_0/kT)^3],$$

where J_0 is the current for very small fields, or explicitly

$$J=\sigma_0F\left(1-\frac{ABe^2F^2}{(kT)^3}E_0{}^3\right). \qquad (17)$$

This formula gives the dependence of the current upon higher powers of the electric field in the case where the second term is relatively small compared to the first.

If the second term of (17) is small, then Ohm's law is valid. If it is not small, then the limits of Ohm's law have been reached. To evaluate it numerically we take[12]

$$\theta=217;\quad C=6.7\text{ ev};\quad E_0=5.5\text{ ev}$$

and calculate the field strength at which the additional term amounts to 1 percent. We obtain about 5 abs. e.s.u. corresponding to a current density of[13]

$$J=\sigma F=6\times7\times10^{17}\times5\text{ e.s.u.}\approx10^9\text{ amp./cm.}^2$$

This then is the current density at which the deviation from Ohm's law is of the order of 1 percent. Since this current density is almost 1000 times greater than those applied by Bridgman and Barlow, no observable deviations from Ohm's law should occur in their experiments, a fact which is in agreement with Barlow who states that Ohm's law is valid for current densities up to 2×10^6 amp./cm^2.

Influence of the Electric Field on the Lattice Waves

In the present theory of conductivity as used in this paper, the influence of the electric field only upon the distribution function of the electrons is considered. In a more consistent theory the equilibrium of the electron waves and the lattice waves must be considered. This is analogous to the case of a mixture of two gases where (according to Boltzmann) a system of two simultaneous integro-differential equations holds. If we denote the distribution functions of electrons and lattice waves by f and N, respectively, then the fundamental equations written symbolically would be as follows:

$$(f,f)+(f,N)=(\partial f/\partial t)_{\text{field}},$$
$$(N,N)+(N,f)=(\partial N/\partial t)_{\text{dissipation}}.$$

In the first approximation the perturbation of the lattice waves is small. Consequently, in the first equation f may be assumed to be constant and in the second equation, N. The two equations are not coupled then. The first equation reduces to the fundamental equation of the present theory, the second being omitted.

In the second approximation, however, the two equations are simultaneous. For a solution we may start from the first approximation considering the coupling as a perturbation. The influence of the external field on the lattice may be connected with the problem of the so-called "Umklapp-Prozesse."[14]

[12] According to E. L. Peterson and L. W. Nordheim, Phys. Rev. **51**, 355 (1937). Cf. also J. Bardeen, Phys. Rev. **52**, 688 (1937).

[13] A very crude estimate can be obtained as follows: For Lorentz' development: $f=f_0+f_1$, the condition $f_1\ll f_0$ must hold, because f_1 on the right-hand side of his equation can be neglected only in this case. Assuming

$$\frac{f_1}{f_0}=-\frac{1}{f_0}\frac{l}{r}\frac{eF}{m}\frac{df_0}{dr}\frac{\xi}{r}=(1-f_0)\frac{leF}{3kT}=10^{-2},$$

we obtain $J=\sigma F\sim10^8$ amp./cm^2. Such an estimate was also made by Dr. Nordheim.

[14] Cf. also W. V. Houston, Phys. Rev. **55**, 1255 (1939).

Galvano- and Thermomagnetic Phenomena in Iron and Nickel*

E. H. Butler, Jr. and E. M. Pugh,
Physics Department, Carnegie Institute of Technology, Pittsburgh, Pennsylvania
(Received June 19, 1939)

The four transverse galvano- and thermomagnetic effects (Hall, Ettingshausen, Nernst, and Righi-Leduc), the Thomson coefficient, and the thermal and electrical conductivities have been measured in bars of nickel and electrolytic iron. Three independent relations between the effects, derived by Sommerfeld on the basis of the Fermi statistical theory of metallic conduction, are verified within a factor of 3. It is shown further that this theory does not account for the size of an individual effect unless the average field for the conduction electrons in the iron is twice the measured value of the magnetic induction, and that in nickel some fifteen times the measured value. Two possible explanations are suggested.

Introduction

THE four transverse galvano- and thermomagnetic effects, the Hall potential gradient and Ettingshausen temperature gradients with electric current flow and the Nernst potential gradient and Righi-Leduc temperature gradient with heat flow, have been treated in a thorough fashion by Sommerfeld and Frank.[1] A quantitative relation between the four effects was derived on the basis of the Fermi statistical theory of metallic conduction under the following assumptions: that the interaction between the electrons and nuclei can be treated in terms of the electron mean free path, that the electron spin energy term in the distribution function can be neglected, that the number of free electrons in a metal is independent of the temperature, that the dependence of the electron mean free path on the temperature can be neglected, and that the magnetic fields are weak. These relations have been approximately verified for the normal metals. For the normal metals the effects are proportional to the magnetic induction B. However, Kundt,[2] Pugh,[3] and Pugh and Lippert[4] have shown that the Hall potential gradient for a ferromagnetic substance is a single-valued function only of the intensity of magnetization I and not of the magnetic induction B or of the magnetic field H. An estimate of the internal field actually acting on the conduction electrons and causing the transverse effects can be made from measured values of the potential gradients *if* the ferromagnetics can first be shown to obey the same relations that the normal metals obey.

The purpose of the work reported in the present paper has been first, to measure the four transverse effects, the Thomson coefficient, the thermal conductivity, and the electrical resistivity in two ferromagnetic substances, iron and nickel, in order to check the theoretical relations derived by Sommerfeld[1] for the normal metals; and second, to estimate the magnitude of the internal field acting on the conduction electrons.

Relations Between the Transverse Effects

Each pair of effects, galvano- and thermomagnetic, occurs simultaneously. In the case of the flow of electricity the current, not the potential gradient, can be arbitrarily prescribed; but in the case of the flow of heat exactly the opposite is true. Hence an inherent asymmetry exists which prevents the elimination of one effect without disturbing the other.

We consider a metallic plate lying in the xy plane, through which a primary current may flow in the x direction, and which lies in a homogeneous magnetic field in the z direction. Two types of effects are distinguished, isothermal and adiabatic. By an isothermal effect is meant a galvano- or thermomagnetic effect so produced that the temperature in the y direction (perpendicular to the primary current) is uniform. By an

* Abstracted from the thesis submitted by E. H. Butler, Jr. to the Committee on Graduate Instruction of Carnegie Institute of Technology in partial fulfilment of the requirements for the degree of Doctor of Science.

[1] Sommerfeld and Frank, Rev. Mod. Phys. **3**, 1 (1931).
[2] A. Kundt, Wied. Ann. **49**, 257 (1893).
[3] E. M. Pugh, Phys. Rev. **32**, 824 (1928); **36**, 1503 (1930).
[4] Pugh and Lippert, Phys. Rev. **42**, 709 (1932).

adiabatic effect is meant one produced when no heat is allowed to flow in the y direction. In the latter case, with a primary electric current flowing, it is impossible to prevent a flow of heat along the direction of the electric current because in a closed electric circuit heat is inevitably convected along with the current. It is possible, however, to set the temperature gradient along the direction of current flow equal to zero, since the temperature gradient is small to begin with, and the conductivity is so large for most metals that a small amount of heat, if conducted away rapidly enough, leaves the temperature essentially uniform.

With each effect is associated a constant, the proportionality factor between gradient and product of current density and magnetic field. The following three equations[1] are the relations between the four effects. Subscripts a and i refer, respectively, to the adiabatic and isothermal coefficients.

$$R_i=\rho S_a, \tag{1}$$

$$Q_i=KP_a/T, \tag{2}$$

$$Q_a-Q_i=\sigma R_i/\rho. \tag{3}$$

Here R is the Hall coefficient; P, the Ettingshausen coefficient; Q, the Nernst coefficient; S, the Righi-Leduc coefficient; K, the thermal conductivity; ρ, the electric resistivity; T, the absolute temperature; and σ, the Thomson coefficient. This particular Thomson coefficient is defined as the ratio of the electric field to the temperature gradient, both along the direction of the primary current.

The isothermal coefficients appearing in these equations cannot be measured because the inherent asymmetry in electric current and heat flow prevents the attainment of the boundary conditions defining isothermal effects. Hence, additional appeal to some theory must be made to obtain relations between the isothermal and adiabatic coefficients. Sommerfeld[1] gives these relations as:

$$Q_a=2Q_i, \tag{4}$$

$$R_a=R_i. \tag{5}$$

These relations are derived from a second approximation in the Fermi statistical theory of metallic conduction under the following assumptions: (1) The interaction between electrons and nuclei can be treated in terms of the electron mean free path. (2) The electron spin energy term in the distribution function can be neglected. (3) The number of free electrons in a metal is independent of the temperature. (4) The dependence of the mean free path of the electron on its velocity can be neglected. (5) The magnetic fields are weak.

This second approximation, necessary for any adiabatic phenomena, takes into account deviations from complete degeneracy of the electron gas. The last assumption may be the least acceptable when considering a ferromagnetic substance. The two macroscopic quantities, the magnetic induction B or the intensity of magnetization I, do fall into the category of "weak" fields, but the actual internal field producing the effects is certainly neither of these. The field that a conduction electron experiences in a metal is probably proportional to the intensity of magnetization but its magnitude is unknown.

From a consideration of Eqs. (4) and (5) the relations between the coefficients become:

$$R_a=\rho S_a, \tag{6}$$

$$Q_a=2KP_a/T, \tag{7}$$

$$Q_a=2\sigma R_a/\rho. \tag{8}$$

The last equation is the one usually called Moreau's relation. It has always appeared previously in its present form *without* the factor 2 and with Q_i instead of Q_a. However, the Thomson coefficient appearing in it was twice as large as the one considered here and was a coefficient not even appearing in the transverse phenomena.[1] All previous "verifications" of it have been purely accidental, depending solely upon the appearance of the factor 2 on both sides of the equation.

Description of the Measurements

The specimens used were bars machined from electrolytic iron and commercially pure nickel. The impurities present were unknown, and a knowledge of them was not necessary because the relations between the effects, if at all fundamental, will be true for any single specimen regardless of the variation of any one effect from specimen to specimen.

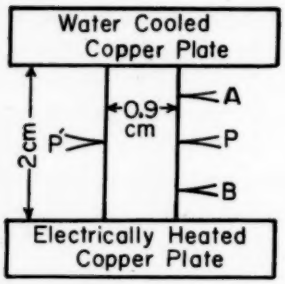

FIG. 1. Cross section through center of test bar (0.9×2 ×9 cm) arranged for measuring the Nernst and Righi-Leduc effects. Thermocouples A, P, B, determine the temperature gradient of the primary heat current, and thermocouples P and P' are temperature and electric potential probes for measuring the transverse effects.

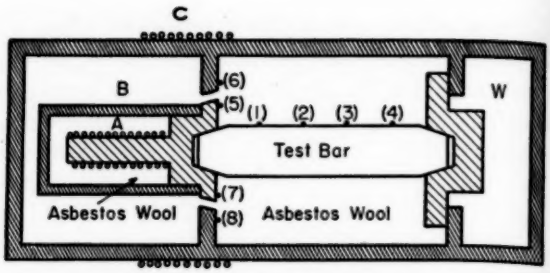

FIG. 2. Apparatus for measuring the thermal conductivity of the test bars. Beveled ends of bars are fitted into copper blocks. One block is heated electrically (coil A). The other is cooled by water in chamber W. Compensating coil C maintains temperatures at points (6) and (8) equal to those at points (5) and (7).

Strains set up in the bars by machining were removed by annealing in an atmosphere of hydrogen. Each bar was heated beyond its Curie point and then allowed to cool slowly. Such treatment is known to render a homogeneous specimen isotropic and also to remove some of the impurities.

The arrangements for measuring all four transverse effects were similar to the arrangement used by Pugh[3] and by Pugh and Lippert[4] for measuring the Hall effect. The test bars were the same shape, rectangular bars (0.9 cm×2 cm ×9 cm) with ends beveled to fit into the electromagnet. In each case the effect was measured, after temperature equilibrium had been established, by magnetically saturating the bar parallel to its length and then reversing the magnetization. In each case the primary current, electric or thermal, was caused to flow parallel to the 2-cm dimension of the bar. Fig. 1 shows the arrangement for measuring the Nernst and Righi-Leduc effects. The two copper plates were carefully fitted to and covered most of the top and bottom (0.9 cm×9 cm) surfaces of the bar. One plate was heated and the other cooled in a manner to insure a uniform steady flow of heat through the middle of the bar. The copper-constantan thermocouples P and P' measured the Righi-Leduc temperature differences, and the copper legs of these couples measured the Nernst e.m.f. Thermocouples A, P, and B measured the temperature gradient of the primary heat current.

The arrangement for measuring the Hall and Ettingshausen effects was the same as shown in Fig. 1 with the copper plates replaced by the copper wire electrodes used by Pugh and Lippert.[4] These electrodes provided a large, steady, essentially uniform electric current density at the center of the bar. Thermocouples A and B were eliminated, but P and P' were retained to measure both the Ettingshausen temperature difference and the Hall e.m.f.

All of the transverse effects were measured with a Wolff potentiometer which, combined with a high sensitivity galvanometer, was sensitive to 10^{-8} volt. To obtain the transverse temperature differences, P and P' had to be read separately (not combined into one differential couple) to avoid errors due to the transverse e.m.f.'s. The errors in the transverse e.m.f. readings due to the simultaneous occurrence of the transverse temperature differences could not be eliminated, but corrections were easily obtained. For this correction it was necessary to calibrate a couple consisting of the thermocouple copper and the test bar. Such a calibration was obtained from the arrangement of Fig. 1. Since the temperatures of the thermocouples A, P, and B were already known, readings of the potentiometer when it was connected to the copper legs of A and P, P and B, A and B gave the desired information. The calibration of this couple was needed also to determine the Thomson coefficient σ of the test bar.

This Thomson coefficient σ is the one used in obtaining the e.m.f. of a thermocouple. If a and b are the two metals of a thermocouple $\sigma_b - \sigma_a = \theta(dH/d\theta)$, where H is the thermoelectric power of the couple and θ the absolute temperature. Since σ for lead is zero, the σ for the thermocouple

copper was obtained by calibrating a copper-lead thermocouple. The σ for the test bar was then obtained from the calibration of the test bar-copper thermocouple already mentioned. The thermal e.m.f. *vs.* temperature curves were assumed to be parabolic.

The intensity of magnetization of the bars at the different temperatures was measured in the same way as described in reference 3 by the use of a high sensitivity galvanometer greatly overdamped to act as a fluxmeter.

The method of measuring the thermal conductivity of the bars is shown in Fig. 2. The beveled ends of the bar were fitted into copper blocks of which one was heated electrically by the resistance coil *A* and the other was cooled by a steady flow of water through the chamber *W*. Thermocouples at (1), (2), (3), and (4) measured the temperature gradient along the bar which was observed to be practically constant. The space between the brass shell *B* and the heating coil *A* was packed with asbestos wool. The whole apparatus was surrounded by another brass shell from which it was insulated by asbestos at all points except at the water end. A compensating coil *C* maintained a temperature gradient in the outer shell which corresponded closely with the temperature gradient in the test bar. The input to *C* was adjusted so that thermocouples at points (6) and (8) showed the same temperature as those at points (5) and (7). This made the temperature of that portion of the outer shell which surrounded *B*, practically the same as that of *B* and thus prevented loss of heat from coil *A*. The heat flow along the bars was calculated from the electric power input to coil *A*. A correction was made for the small amount of heat conducted out along the leads.

In all the experiments temperature equilibrium was established before observations were made. This usually required twenty hours or more. Many precautions were required and were taken to obtain constant heater currents and steady flow of constant temperature cooling water. Fluctuations were reduced so that in the worst cases (Nernst and Righi-Leduc) the temperature of the bar varied less than 0.007°C/min.

Results

The results are given in Tables I, II, III, and IV.

The Eqs. (6), (7), and (8) to be verified show that, in Tables III and IV, the figures in the first row should equal those in the second row, and the figures in the third row should equal

TABLE I. *Coefficients (c.g.s.) units for a bar (0.9×2×9 cm) of commercial nickel annealed in hydrogen. The first four, the transverse coefficients, were obtained with the nickel saturated at the given temperature and were calculated with B–H (or 4πI) in the place of the usual B. The average values of B, H, and 4πI for these temperatures were 6670, 1000, and 5670, respectively.*

		40°C	50°C	60°C	70°C	Mean Error %
Righi-Leduc	$S_a\times10^7$	−6.87	−6.65	−6.47	−6.38	4
Nernst	$Q_a\times10^3$	5.93	6.62	7.31	8.00	3
Ettingshausen	$P_a\times10^7$	0.67	1.07	1.27	1.48	8
Hall	$R_a\times10^2$	−1.53	−1.60	−1.66	−1.72	3
Resistivity	$\rho\times10^{-3}$	12.15	12.63	13.04	13.46	0.5
Thomson Coef.	$\sigma\times10^{-2}$	−9.33	−9.63	−9.92	−10.22	6
Thermal Con.	$K\times10^{-6}$	6.78	6.78	6.78	6.78	6

TABLE II. *Coefficients for a bar (0.9×2×9 cm) of electrolytic iron annealed in hydrogen. The first four, the transverse coefficients, were obtained with the iron saturated at the given temperature and were calculated with B–H (or 4πI) in place of the usual B. The average values of B, H, and 4πI for these temperatures were 23,000, 930, and 22,100, respectively.*

		40°C	50°C	60°C	70°C	Mean Error %
Righi-Leduc	$S_a\times10^7$	3.28	3.39	3.50	3.61	3
Nernst	$Q_a\times10^3$	−2.04	−2.06	−2.08	−2.10	3
Ettingshausen	$P_a\times10^8$	−2.03	−2.08	−2.14	−2.20	12
Hall	$R_a\times10^3$	6.43	7.27	8.10	8.94	3
Resistivity	$\rho\times10^{-3}$	11.65	12.21	12.77	13.33	0.5
Thomson Coef.	$\sigma\times10^{-2}$	−9.55	−9.88	−10.3	−10.6	6
Thermal Con.	$K\times10^{-6}$	7.45	7.45	7.45	7.45	6

TABLE III. *Experimental test of the theoretical Eqs. (6), (7), and (8) from the data on nickel, Table I. At each temperature the theory predicts that*

$$R_a/\rho = S_a \text{ and } Q_a/2 = KP_a/T = \sigma R_a/\rho.$$

	40°C	50°C	60°C	70°C	MEAN ERROR %
$R_a/\rho \times 10^7$	−12.6	−12.7	−12.7	−12.8	3
$S_a \times 10^7$	− 6.87	− 6.65	− 6.47	− 6.28	4
$Q_a/2 \times 10^3$	2.97	3.31	3.66	4.00	3
$KP_a/T \times 10^3$	1.61	1.91	2.20	2.49	10
$\sigma R_a/\rho \times 10^3$	1.17	1.22	1.26	1.32	7

those in the last two rows. Obviously the experimental figures do not check the theory within the limits of error of the experiments, but they do check as far as the signs and orders of magnitude of the results are concerned. Taking ratios between figures which the theory predicts should be equal, we find the largest ratio is 3.0 and the smallest 1.3. The three relations are therefore verified within a factor 3. If one considers the assumptions made in the theory and the impossibility of experimentally imposing the conditions required by the theory, these results are probably as good as could be expected.

A closer verification is not necessary to confirm one's belief in the validity of the relations. It must be emphasized that it is *impossible* to realize the boundary conditions defining an adiabatic coefficient. Heat will inevitably be conducted away by any probe applied to a specimen. It is also equally impossible to measure an isothermal coefficient because of the inherent asymmetry in electric current and heat flow. Any attempt to regulate one upsets the other and prevents the attainment of the initial goal. Any measurement is a compromise, but fortunately the difference is small between the quantities desired and the ones actually measured. The factors 1 and 2 giving the ratios between the adiabatic and isothermal coefficients according to the statistical theory actually give only an order of magnitude when neither of the coefficients in the ratio can be measured accurately.

Thermodynamic reasoning does not aid in this instance.[5] The essence of such an argument would be to set up a reversible cycle wherein a thermomagnetic effect supplied energy for a galvanomagnetic effect. This means isolation of the individual effects and hence isothermal phenomena which never exist.

Sommerfeld's paper[1] gives an expression for the Hall coefficient in terms of the electron free path and the Fermi critical velocity for an electron. This critical velocity can be calculated from known constants for a metal and the number of free electrons per atom. These values for iron and nickel were taken from Mott and Jones.[6] The coefficients calculated in this way are comparable with the ones measured *only* if there exists in the iron an effective field of 45,000 gauss and in the nickel an effective field of 100,000 gauss, both much larger than the measured values of the magnetic induction, 23,000 for iron and 6600 for nickel.

Two possible explanations of this discrepancy are suggested. The first explanation assumes that the average field "seen" by the conduction electrons actually is much greater than the measured induction B. Certainly the magnetic field in a ferromagnetic crystal is quite inhomogeneous, and the average[7] may depend upon factors, such as the probable paths of the electrons, which do not affect the measured value of B. Some evidence for this point of view is found in the fact that the transverse effects are proportional to the intensity of magnetization I instead of the magnetic induction B. The inhomogeneous field is obviously a function of I. Superimposed upon this inhomogeneous field is

TABLE IV. *Experimental test of the theoretical Eqs. (6), (7), and (8) from the data on iron, Table II. At each temperature the theory predicts that*

$$R_a/\rho = S_a \text{ and } Q_a/2 = KP_a/T = \sigma R_a/\rho.$$

	40°C	50°C	60°C	70°C	MEAN ERROR %
$R_a/\rho \times 10^7$	5.52	5.95	6.34	6.70	3
$S_a \times 10^7$	3.28	3.39	3.50	3.61	3
$Q_a/2 \times 10^3$	−1.02	−1.03	−1.04	−1.05	3
$KP_a/T \times 10^3$	− .483	− .480	− .477	− .473	14
$\sigma R_a/\rho \times 10^3$	− .527	− .588	− .653	− .710	7

[5] P. W. Bridgman, Phys. Rev. **24**, 644 (1924).

[6] N. F. Mott and H. Jones, *Theory of the Properties of Metals and Alloys* (Oxford University Press, 1936).

[7] The estimates of the effective internal field in iron from neutron polarization experiments (Frisch, von Halban, and Koch, Phys. Rev. **53**, 719 (1938); P. N. Powers, Phys. Rev. **54**, 827 (1938)) do not agree and should not be expected to agree with this average. The average field experienced by an electron may be quite different from the average field for a neutron, since the paths of the two particles will be very different through this inhomogeneous magnetic field.

a uniform field equal to H. A change in the uniform field H must make an *equal* change in any average field acting upon the electrons. However, when I is kept constant and H is changed, no change is observed[2–4] in the transverse effects. This seems to indicate that the average field "seen" by the conduction electrons must be so large that changes due to H are negligible by comparison.

The second explanation would assume that the difficulty lies in the treatment of the interaction between electrons and the nuclei entirely in terms of the electron mean free path. Jones and Zener[8] have had considerable success in clearing up a similar discrepancy found in the change of resistance with magnetic field by more exact treatment of the interaction between electrons and nuclei. It is probable that both effects are responsible for the discrepancy.

The authors are indebted to L. A. Young for helpful advice and criticism.

[8] Jones and Zener, Proc. Roy. Soc. **A145**, 268 (1934).

MAY 15, 1940 PHYSICAL REVIEW VOLUME 57

Fresnel Formulae Applied to the Phenomena of Nonreflecting Films

KATHARINE B. BLODGETT
Research Laboratory, General Electric Company, Schenectady, New York

(Received March 18, 1940)

The Fresnel formulae are applied to the calculations of the amplitudes of rays reflected and transmitted by nonreflecting films of transparent isotropic substances. Two cases are considered. In the first, the film of refractive index n_0 is bounded on both sides by a medium of refractive index n_0. In the second, the film is bounded by media of refractive indexes n_0 and n_2. It is shown how in the first case these formula lead to zero reflection when the thickness t of the film is given by $n_1 t \cos r_1 = (2n+2)\lambda/4$. In the second case for zero reflection the thickness must be given by $n_1 t \cos r_1 = (2n+1)\lambda/4$.

SEVERAL workers[1–3] have coated glass with films for the purpose of diminishing or extinguishing the reflection of light from the glass. Their published papers have given the following analysis of the requirements which must be met in order that a film shall reflect no light of wave-length λ. A film which meets these requirements is called a nonreflecting film.

There are two types of nonreflecting films made of transparent substances: *Type (a)*. A film having a refractive index n_1 bounded on both sides by a medium of refractive index n_0. (Example: wall of a soap-bubble.) *Type (b)*. A film having a refractive index n_1, bounded by media of refractive indices n_0 and n_2, where $n_0 < n_1 < n_2$. (Example: film of fluorite on glass.) The requirements for the extinction of reflected light are given by the following equations.

[1] J. Strong, J. Opt. Soc. Am. **26**, 73 (1936).
[2] K. B. Blodgett, Phys. Rev. **55**, 391 (1939).
[3] C. H. Cartwright and A. F. Turner, Phys. Rev. **55**, 595(A) (1939).

THICKNESS

The film must have a thickness t which is given by the equations

$$n_1 t \cos r_1 = (2n+2)\lambda/4 \text{ for Type (a)}, \quad (1)$$

$$n_1 t \cos r_1 = (2n+1)\lambda/4 \text{ for Type (b)}, \quad (2)$$

where r_1 is the angle of refraction of light in the film, and n has the values 0, 1, 2, $\cdots$.

REFRACTIVE INDEX OF FILM

Type (a). The film may have any value of refractive index.

Type (b). Case (1). Film viewed by perpendicular light, $i=0$. The film must have a refractive index which satisfies the equation

$$n_1^2 = n_0 n_2. \quad (3)$$

Case (2). Film viewed at an angle of incidence $i \neq 0$. The refractive index must satisfy one of

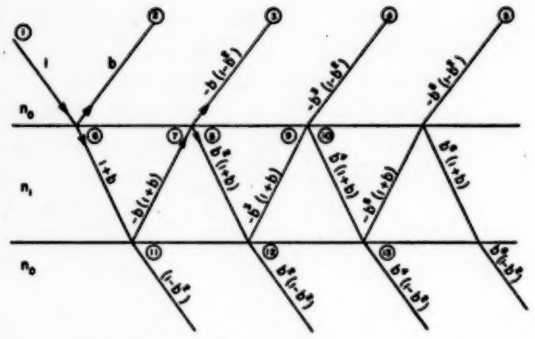

FIG. 1. Paths of a ray of light polarized perpendicular to the plane of incidence. The film of refractive index n_1 is bounded on both sides by a medium of refractive index n_0.

the following equations:

$$\text{For the } R_s \text{ ray} \quad \tan i \tan r_2 = \tan^2 r_1, \tag{4}$$

$$\text{For the } R_p \text{ ray} \quad \sin^2 r_1 \cos^2 r_1 = \sin i \cos i \sin r_2 \cos r_2, \tag{5}$$

where R_s and R_p are the polarized rays having the plane of polarization perpendicular and parallel, respectively, to the incident plane; and r_1 and r_2 are the angles of refraction of light in the media of refractive indices n_1 and n_2.

The present paper will apply the Fresnel formulae to calculations of the amplitudes of the rays reflected and transmitted by nonreflecting films of transparent isotropic substances. The Fresnel formulae are[4]

$$R_s = -E_s \frac{\sin (i-r)}{\sin (i+r)}, \tag{6}$$

$$D_s = E_s \frac{2 \cos i \sin r}{\sin (i+r)}, \tag{7}$$

$$R_p = -E_p \frac{\tan (i-r)}{\tan (i+r)}, \tag{8}$$

$$D_p = E_p \frac{2 \cos i \sin r}{\sin (i+r) \cos (i-r)}, \tag{9}$$

where E_s, R_s, D_s represent the amplitudes of the incident ray, reflected ray, and transmitted ray, respectively, for R_s-polarized light (as defined above), and E_p, R_p, D_p have corresponding values for R_p-polarized light.

Equations (6), (7), (8) and (9) are in agreement with the requirement imposed by energy relationships between the three rays. The energy of a light wave per unit volume is $na^2/8\pi$ where a is the amplitude of the wave. Therefore the energy per unit time of a wave having a wave front of cross section A and traveling with the velocity c is $Acna^2/8\pi$. From this we obtain the following value for the energy of the ray D,

$$D^2 = (E^2 - R^2) A_0 n_0 / A_1 n_1, \tag{10}$$

where A_0 and A_1 represent the cross sections of the waves in the media in which the light is reflected and refracted, respectively. This equation may be written

$$D^2 = (E^2 - R^2) \cos i \sin r / (\cos r \sin i). \tag{11}$$

The values of D_s, E_s and R_s from Eqs. (6) and (7) satisfy Eq. (11); also the values of D_p, E_p and R_p from Eqs. (8) and (9).

From Eqs. (6) and (7) we obtain the result

$$E_s + R_s = D_s. \tag{12}$$

That is, the sum of the amplitudes of the incident and reflected rays on one side of a boundary is equal to the amplitude of the refracted ray on the opposite side of the boundary.

From Eqs. (8) and (9) we obtain

$$E_p - R_p = D_p \sin i / \sin r, \tag{13}$$

which can be written $E_p - R_p = n_1 D_p / n_0$ where $n_1/n_0 = \sin i / \sin r$.

Figure 1 represents the paths which a ray of R_s-polarized light takes when it strikes a film of Type (a). The amplitude of the incident ray is taken as unity. The diagram shows the amplitude

TABLE I. *Amplitudes of reflected and transmitted rays for incident light polarized both perpendicular (R_s) and parallel (R_p) to the plane of incidence. The film of refractive index n_1 is bounded on both sides by a medium of refractive index n_0.*

RAY	R_s-POLARIZED	R_p-POLARIZED
1	1	1
2	b	d
3	$-b(1-b^2)$	$-d(1-d^2)$
4	$-b^3(1-b^2)$	$-d^3(1-d^2)$
5	$-b^5(1-b^2)$	$-d^5(1-d^2)$
6	$1+b$	$(1-d)n_0/n_1$
7	$-b(1+b)$	$-d(1-d)n_0/n_1$
8	$b^3(1+b)$	$d^3(1-d)n_0/n_1$
9	$-b^5(1+b)$	$-d^5(1-d)n_0/n_1$
10	$b^7(1+b)$	$d^7(1-d)n_0/n_1$
11	$1-b^2$	$1-d^2$
12	$b^2(1-b^2)$	$d^2(1-d^2)$
13	$b^4(1-b^2)$	$d^4(1-d^2)$

[4] *Handbuch der Physik*, Vol. 20, p. 211.

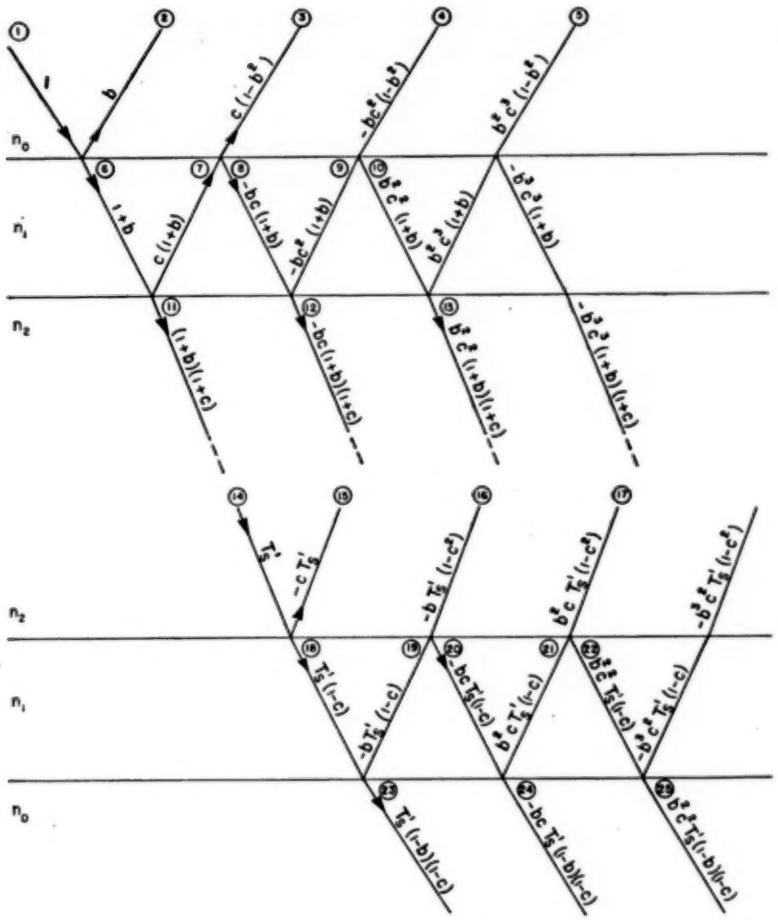

FIG. 2. Paths of a ray of light polarized perpendicular to the plane of incidence. The film of refractive index n_1 is bounded by media of refractive indexes n_0 and n_2.

of the fraction of the light which follows each path. Ray (1) is split into the following components.

(A) Ray (2) reflected from the upper surface of the film. The amplitude of (2) is $b=\sin(i-r)/\sin(i+r)$ from Eq. (6).

(B) Ray (6) refracted in the film. From Eq. (12) ray (6) has the value $1+b$.

(C) Ray (7) reflected from the second surface of the film, with the value $-b(1+b)$, since the values of R_s given by Eq. (6) are equal in value and opposite in sign for rays striking the inner and outer surfaces of a film of Type (a).

(D) Ray (8), and other successively reflected rays (9), (10) $\cdots$ having the values given on the diagram.

(E) Ray (3) refracted with the value $-b(1-b^2)$ calculated from rays (7) and (8) by Eq. (12). Other refracted rays are (4), (5) $\cdots$.

(F) Transmitted ray (11) calculated from rays (6) and (7) by Eq. (12). Other transmitted rays are (12), (13) $\cdots$.

When the thickness of a film of Type (a) is given by Eq. (1), the path difference between the successive reflected rays (2), (3), (4) $\cdots$ is λ, and also between the successive transmitted rays (11), (12), (13) $\cdots$. Therefore the amplitude of the sum of the rays is

$$\begin{aligned} R&=b-b(1-b^2)(1+b^2+n^4\cdots)\\ &=b-b(1-b^2)/(1-b^2)\\ &=0. \end{aligned} \tag{15}$$

The amplitude of the sum of the transmitted rays is

$$\begin{aligned} T&=(1-b^2)(1+b^2+b^4\cdots)\\ &=(1-b^2)/(1-b^2)\\ &=1. \end{aligned} \tag{16}$$

TABLE II. *Amplitudes of reflected and transmitted rays for incident light polarized both perpendicular (R_s) and parallel (R_p) to the plane of incidence. The film of refractive index n_1 is bounded by media of refractive indexes n_0 and n_2.*

RAY	R_s-POLARIZED	R_p-POLARIZED
1	1	1
2	b	d
3	$c(1-b^2)$	$e(1-d^2)$
4	$-bc^2(1-b^2)$	$-de^2(1-d^2)$
5	$b^2c^3(1-b^2)$	$d^2e^3(1-d^2)$
6	$1+b$	$(1-d)n_0/n_1$
7	$c(1+b)$	$e(1-d)n_0/n_1$
8	$-bc(1+b)$	$-de(1-d)n_0/n_1$
9	$-bc^2(1+b)$	$-de^2(1-d)n_0/n_1$
10	$b^2c^2(1+b)$	$d^2e^2(1-d)n_0/n_1$
11	$(1+b)(1+c)$	$(1-d)(1-e)n_0/n_2$
12	$-bc(1+b)(1+c)$	$-de(1-d)(1-e)n_0/n_2$
13	$b^2c^2(1+b)(1+c)$	$d^2e^2(1-d)(1-e)n_0/n_2$
14	T_s'	T_p'
15	$-cT_s'$	$-eT_p'$
16	$-bT_s'(1-c^2)$	$-dT_p'(1-e^2)$
17	$b^2cT_s'(1-c^2)$	$d^2eT_p'(1-e^2)$
18	$T_s'(1-c)$	$T_p'(1+e)n_0/n_1$
19	$-bT_s'(1-c)$	$-dT_p'(1+e)n_0/n_1$
20	$-bcT_s'(1-c)$	$-deT_p'(1+e)n_0/n_1$
21	$b^2cT_s'(1-c)$	$d^2eT_p'(1+e)n_0/n_1$
22	$b^2c^2T_s'(1-c)$	$d^2e^2T_p'(1+e)n_0/n_1$
23	$T_s'(1-b)(1-c)$	$T_p'(1+d)(1+e)$
24	$-bcT_s'(1-b)(1-c)$	$-deT_p'(1+d)(1+e)$
25	$b^2c^2T_s'(1-b)(1-c)$	$d^2e^2T_p'(1+d)(1+e)$

This means that when parallel rays of light of unit amplitude strike the surface of the film, the rays which leave the film also have unit amplitude since each ray is the sum of a series of rays, the sum being unity. The successive members of the series usually diminish very rapidly in value. For example, when light strikes a film of refractive index $n=1.50$ at an angle $i=30°$, the value of b calculated by Eq. (6) is 0.240. Therefore the rays (11), (12), and (13) $\cdots$ have the values 0.9422, 0.0545, 0.0031, 0.0002, $\cdots$. Table I gives the corresponding values of the amplitudes of the rays for R_p-polarized light. The value of d can be calculated from Eq. (8). In this case also the sum of the reflected rays is zero, and of the transmitted rays is unity.

Figure 2 gives the paths of the rays and their formulae for a film of Type (b). The formulae are listed in Table II. The values of b and d in the formulae can be calculated by means of Eqs. (6) and (8) for the upper boundary of the film which separates the media of refractive indices n_0 and n_1, and c and e for the lower boundary between n_1 and n_2.

When a film satisfies Eq. (2) the path difference between the successive reflected rays is $\lambda/2$. Therefore in writing the sum of the reflected rays (2), (3), (4), (5) $\cdots$, alternate members of the series must be written with the sign opposite to that which appears in Fig. 2 and in Table II. The sum R is

$$\begin{aligned} R&=b-c(1-b^2)(1+bc+b^2c^2+\cdots)\\ &=b-c(1-b^2)/(1-bc). \end{aligned} \tag{18}$$

Eqs. (4) and (5) were derived from Eqs. (6), (7), (8), (9) for the cases $b=c$ and $d=e$. When Eq. (4) is satisfied, Eq. (18) becomes

$$R=0. \tag{19}$$

The path difference between the rays (11), (12), (13) transmitted in the medium n_2 is also $\lambda/2$. Therefore the sum T_s' of these rays is

$$\begin{aligned} T_s'&=(1+b)(1+c)(1+bc+b^2c^2\cdots)\\ &=(1+b)(1+c)/(1-bc)\\ &=(1+b)/(1-b) \text{ when } b=c. \end{aligned} \tag{20}$$

For R_p-polarized light, the sum is

$$T_p'=n_0(1-b)/n_2(1+b). \tag{21}$$

Figure 2 shows the paths of the rays into which a ray T_s' [ray (14)] is split when it strikes the second boundary of the medium n_2. The sum of the rays (15), (16), (17) $\cdots$ is zero. The sum T of the rays (23), (24), (25) $\cdots$ is

$$T=T_s'(1-b)(1-c)/(1-bc).$$

When $b=c$ and $T_s'=(1+b)/(1-b)$ from Eq. (20), we have the result

$$T=1.$$

Similarly the equations for the case of R_p-polarized light give the result $T=1$.

The writer is indebted to Dr. F. Seitz for assistance in deriving some of the formulae in this paper.

A New Method for Investigating the Refractive Index and the Thickness of Thin Interference Films on Glass*

ANTONIN VAŠIČEK
Czech Technical College, Brno, Bohemia
(Received February 8, 1940)

If plane polarized light falls on lead glass the surface of which had been chemically changed to be covered with an interference film, the reflected light is in general elliptically polarized. If, however, the path difference of reflected rays from the air-film boundary and from the film-glass boundary is $2n_0 d \cos r + \frac{1}{2}\lambda = k\lambda$, where k gives the order of the maximum, the first maximum for $k=1$ being $d(n_0^2 - \sin^2\varphi)^{\frac{1}{2}} = \frac{1}{4}\lambda$, and where n_0 is the refractive index of the film, d its thickness, φ the angle of incidence, r the angle of refraction and λ the wave-length of the monochromatic light, then the reflected light is plane polarized. For this angle of incidence, φ, the plane of polarization of the reflected plane polarized light will be the same as if the polarized light were reflected from an ideal surface of glass (not covered with a film). From the angle between the plane of polarization of the analyzer and the plane of incidence the refractive index of the glass, n, can be calculated according to the formula deduced from Fresnel's relations: $n^2 = \sin^2\varphi[1 + \mathrm{tg}^2\varphi\,\mathrm{tg}^2(\psi + 45°)]$, where φ is the angle of incidence, ψ the angle between the plane of polarization of the analyzer and the plane of incidence (the angle between the plane of polarization of the polarizer and the plane of incidence is 135°). We can calculate the refractive index, n_0, and thickness, d, of the surface film from the formula for the maxima if we determine two angles of incidence, φ_1 and φ_2 for two different wave-lengths. The refractive index of the film, n_0, is given by the formula:

$$n_0 = \left(\frac{\lambda_1^2 \sin^2\varphi_2 - \lambda_2 \sin^2\varphi_1}{\lambda_1^2 - \lambda_2^2}\right)^{\frac{1}{2}}.$$

The results of the measurements are given in tables.

IN a previous paper[1] artificial surface films on glass were studied for the first time. The present communication is concerned with the results of a study proposed in that paper of the elliptical polarization of light reflected from such thin films on glass. As these results are in good accord with those obtained with similar films by K. B. Blodgett[2] and described in the paragraph "etching of glass" of her paper published in this journal, and were besides this obtained quite independently, their communication may not be out of place here.

Thin films are formed on certain kinds of lead glass by action of dilute sulphuric acid. The surface of the glass is thereby covered with a dust of lead sulphate which can be easily removed. The sulphuric acid penetrates only to a certain depth, and on a soft lead glass a thin, but very hard, superficial film is formed, which is, as the measurement of its refractive index shows, substantially a film of quartz glass.

The object of the present paper is the description of a new method for measuring the refractive index and the thickness of these interference films on glass; it is thus a supplement to the present author's previous paper, as well as to that by K. B. Blodgett already quoted, with which he became acquainted only after completion of his experiments.

APPARATUS

The polarimetric measurements of the refractive index and of the thickness of the superficial film on glass were made with a Fuess (Berlin) polarization spectrometer. Focal length of the collimator and telescope object-lenses is 180 mm (diameter 18 mm). The circle of the spectrometer has a diameter of about 165 mm, the smallest division being 10 minutes of arc. With a lens 10 seconds of arc can be read on a vernier. In front of the collimator is placed a polarizer and similarly an analyzer in front of the telescope (see the schematic diagram in Fig. 1). The polarizer and analyzer (Glan-Thomson's Nicols, square section 14×14 mm) are placed in a rotating circle (diameter about 130 mm); the circles are divided in 15 minutes of arc. With a lens 30 seconds of arc can be read on a vernier. The rotating circles of the analyzer and polarizer can be moved either by hand or by means of

* A preliminary notice on the present investigation has been presented before the Česká akad. Praha, December 15, 1939.
[1] Stornik české vysoké škely technické v Brně **12**, 45 (1938); Kolloid Zeits. **86**, 288 (1939).
[2] K. B. Blodgett, Phys. Rev. **55**, 391 (1939).

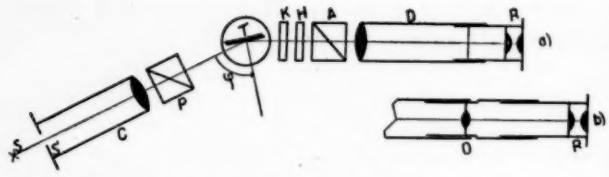

FIG. 1. The sketch of the polarization spectrometer. S the source of monochromatic light, S' the slit, C the collimator, P the polarizer, T the rotating table, K the compensator, D Nakamura's double-plate, A the analyzer, D the telescope, R eyepiece for measurements in a dark field (a) and the telescope O with eyepiece R (for measurements in half-shade (b)).

micrometric screws for fine adjustment. In front of the analyzer is placed the circle of the compensator with a similar outfit as the polarizer or analyzer. The Sénarmont's compensator (a quarter-wave mica plate) is placed so that it is possible to put it in an oriented position in front of the analyzer and to take it out again. Between the analyzer and the compensator Nakamura's double-plate of quartz is placed in a fixed position for half-shade measurements.

As a source of monochromatic light a sodium vapor discharge tube emitting wave-length 5893A or a mercury high pressure lamp with a special green filter for monochromatic light of wave-length 5461A was used. Both sources were manufactured by Philips, Eindhoven.

The polarimetric measurements can be made in two ways. In the first, a dark field in the telescope is used. The telescope is to be focused on the slit (or to infinity) of the collimator. The analyzer is rotated until the image of the slit vanishes on the dark background, the Nicols being crossed. In the second method, the measurements are made in half-shade. Nakamura's double-plate is placed in front of the analyzer, the eyepiece of the telescope being replaced by a telescope focused on the boundary-line of the double-plate. The analyzer is rotated until both halves of the double-plate are equally shaded.

When studying polarized light with a weak ellipticity by the half-shade method Sénarmont's compensator is the most suitable one. The measurement is made as follows:[3] Sénarmont's compensator is at first not introduced, so that the rays of light pass directly into the Nakamura's plate and into the analyzer. The analyzer is rotated until we get half-shade. This adjustment of the analyzer is made easily if the ratio of the semi-axes of the ellipse is less than $\frac{1}{10}$. In this position the plane of vibration of the analyzer is perpendicular to the semi-major axis of the ellipse, indicating thus the angle, χ, between the semi-major axis and the plane of incidence. This plane is given by the axis of the collimator and that of the telescope. Then the Sénarmont's compensator is oriented so that its directions of vibration coincide with the directions of the semi-axes of the ellipse, that is with the direction of vibration of the analyzer, is put in front of the analyzer.

The half-shade is thus destroyed, and with plane polarized light we have to rotate the analyzer through a certain angle, γ, to get the half-shade again (Fig. 2). This angle indicates the so-called ellipticity $\lg\gamma = b/a$, which is equal to the ratio of the semi-axes of the ellipse.

Sénarmont's compensator is placed so that at positive ellipticity, that is, when the light vector describes an ellipse in the positive direction, the analyzer is rotated in the positive direction. This is to the left when we look into the telescope. At negative ellipticity the analyzer is rotated in the opposite direction. The angle of the polarizer is at 45°. In the fundamental position the data read on the circles of the analyzer and compensator are nearly the same—the difference being only a few minutes. Thus the adjustment of the compensator is made very easy.

By measuring the angle, χ, between the semi-major axis of the ellipse and the plane of incidence, and the angle γ giving the ellipticity of light, the light vector describing the ellipse is completely determined. Because in the formulae for optical constants there is usually given the

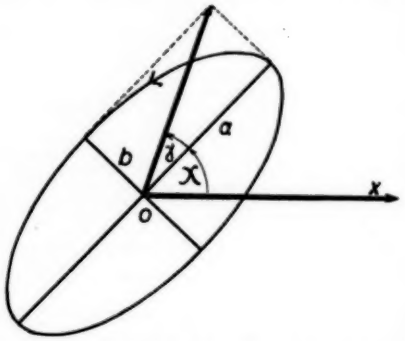

FIG. 2. The axis x is the plane of incidence.

[3] Geiger-Scheel, *Handbuch der Physik* (Berlin, 1928), Vol. 19, p. 955.

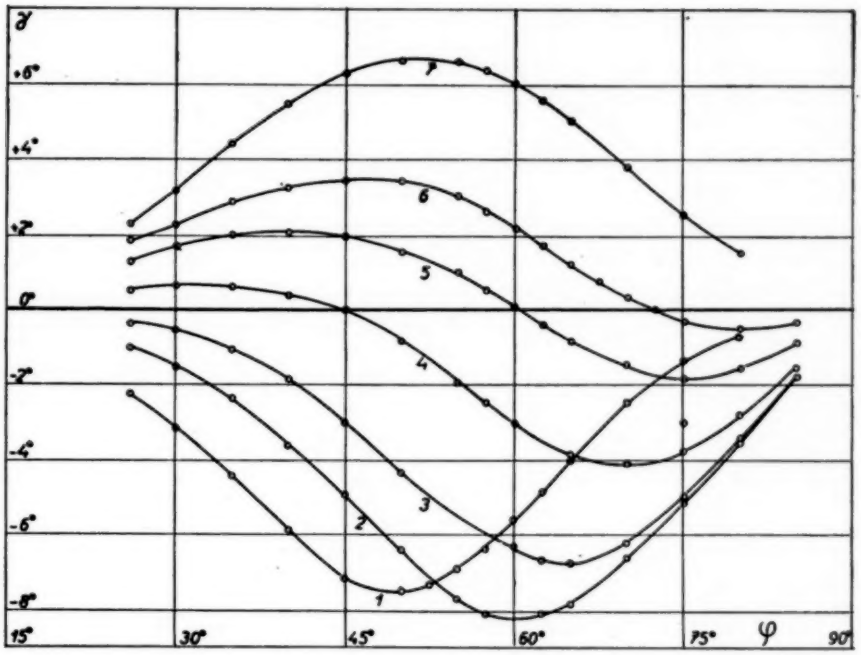

FIG. 3. The angle γ indicating the ellipticity as a function of the angle of incidence φ. The curves were obtained for white-blue (1), white-yellow (2), yellow (3), yellow-brown (4), red (5), purple (6), and blue (7).

ratio of the amplitudes, $\operatorname{tg}\psi$, and the phase difference, Δ, the ψ and Δ are calculated from the formulae

$$\cos^2\psi = \cos^2\gamma\cos^2\chi, \qquad (1)$$

$$\operatorname{tg}\Delta = \operatorname{tg}^2\gamma/\sin^2\chi. \qquad (1')$$

THE MEASUREMENTS

The plane of polarization of the polarizer includes with the plane of incidence an angle of 135°. Thus many errors in measurement are eliminated, especially the systematic error in adjustment of the compensator, if the directions of vibration of the compensator do not coincide exactly with the semi-axes of the ellipse. When plane-polarized light falls on glass covered with a thin interference film, the reflected light is in general weakly elliptically polarized—the light vector describing a very narrow ellipse approaching a straight line. Fig. 3 represents graphically the dependence of the angle γ indicating the ellipticity on the angle of incidence, φ. The curves were obtained for the following interference colors: white-blue, white-yellow, yellow, yellow-brown, red, purple, and blue. Fig. 3 gives the best idea about the course of those curves for various interference colors of the film. Fig. 4 gives similarly the dependence of the angle χ between the semi-major axis of the ellipse and the plane of incidence on the angle of incidence, φ, for the same yellow-brown, interference color (curve 4). The curve 0 corresponds to the ideal surface of glass without the superficial film.

In Fig. 3 attention is called to the curves, which turn from positive values to negative ones, in other words, to those angles of incidence, where the ellipticity or the angle γ is zero. At this angle of incidence the reflected light is strictly plane polarized. With the color corresponding to a greater thickness of the film in white light (from yellow-brown to red and to purple) these points are shifted to greater angles of incidence. Note in Fig. 4 the angle of incidence corresponding in Fig. 3 to the angle of incidence for zero ellipticity. At this angle of about 45° for zero ellipticity the experimental curve touches the curve corresponding to the ideal surface of glass without the film, or the reflecting glass covered with the film behaves in the same way as glass without any such film.

The angle of incidence for the zero ellipticity has the following significance: the rays of light reflected on the air-film boundary and on the film-glass boundary meet at this angle of incidence in the same phase—or this angle of incidence determines the maximum of reflected

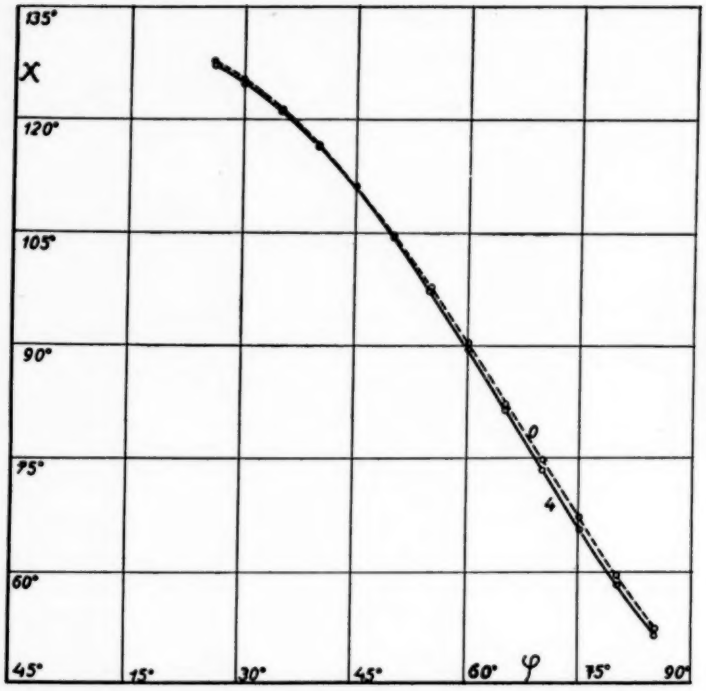

FIG. 4. The angle χ between the semi-major axis of the ellipse and the plane of incidence as a function of the angle of incidence φ. The curve O is calculated for the ideal surface of glass without film; (4) is the experimental curve for yellow-brown color. The angle between the plane of polarization of the polarizer and the plane of incidence is 135°.

monochromatic light of the wave-length λ used. The condition for this maximum on a film of the refractive index n_0 and the thickness d, if the angle of refraction in the film is r, is

$$2n_0 d \cos r + \tfrac{1}{2}\lambda = k\lambda, \qquad (2)$$

where k is the order of the maximum. The additional term $\frac{1}{2}\lambda$ on the left side of Eq. (2) is connected with the change of phase into the opposite one for the case of reflection on a medium with a greater refractive index.

For the first-order maximum ($k=1$)

$$2n_0 d \cos r = \tfrac{1}{2}\lambda. \qquad (3)$$

Taking instead of the angle of refraction, r, the angle of incidence, φ, we have

$$\cos r = (n_0^2 - \sin^2 \varphi)^{\frac{1}{2}}/n_0$$

and

$$d(n_0^2 - \sin^2 \varphi)^{\frac{1}{2}} = \tfrac{1}{4}\lambda. \qquad (4)$$

If the angle of incidence corresponds to zero ellipticity of the reflected light—the reflected light being then strictly plane polarized—the film behaves as a plate with a path difference equal to λ for the first-order maximum. (The actual path difference in the volume is $\frac{1}{2}\lambda$ but an additional $\frac{1}{2}\lambda$ must be introduced because of the change of phase for a reflection on a medium of greater refractive index.) Such a superficial film has no influence upon the plane polarized light reflected on the unchanged surface of the glass.

The plates with a path difference λ, 2λ, $3\lambda\cdots$ are made usually of a doubly refracting material such as mica or quartz. If n_0 and n_e denote the two refractive indices of the ordinary and extraordinary rays, the thickness d of the plate with path difference λ is given by the relation

$$(n_0 - n_e)d = \lambda. \qquad (5)$$

Such a plate with path difference λ has no influence when it is placed between the reflecting surface and the polarizer (or the analyzer). In the doubly refracting plate the ray is divided into two rays which after passing through the plate combine and interfere with a certain path difference. The thin film on glass behaves quite similarly if the path difference of the light reflected on the air-film and on the film-glass boundary is λ for the first-order maximum or 2λ, $3\lambda\cdots$ for higher orders. Such films have no influence upon plane polarized light reflected on the unchanged surface of the glass. The angle between the plane of polarization of the plane polarized light and the plane of incidence is the same as if

the plane polarized light were reflected from an unchanged surface of glass without a film. In addition to Eq. (4) which may relate to the angle of incidence for zero ellipticity, we have also the formula for the refractive index of glass n deduced from Fresnel's relations:

$$n^2=\sin^2\varphi[1+\mathrm{tg}^2\,\varphi\,\mathrm{tg}^2\,(\psi+45°)], \qquad (6)$$

where ψ is the angle between the plane of polarization of the analyzer and the plane of incidence. We assume that this angle between the plane of polarization of the polarizer and the plane of incidence is 135°. The value of the refractive index of the glass, n, calculated from formula (6) is identical with that obtained by the method of minimum deviation.

If the angle of incidence for zero ellipticity is measured only for one wave-length, e.g., for the sodium line $\lambda=5893$A, only the refractive index of the glass, n, can be calculated from formula (6). If, however, the refractive index of the film, n_0, is known, it is possible to calculate from the formula (4) also the thickness, d, of the film. Because the refractive index of the film, n_0, is not known usually, it is necessary to determine for two wave-lengths λ_1 and λ_2 the angles of incidence, φ_1 and φ_2 for zero ellipticity. Then we have for the wave-length λ_1

$$d(n_0^2-\sin^2\varphi_2)^{\frac{1}{2}}=\lambda_1/4 \qquad (7)$$

and for the wave-length λ_2

$$d(n_0^2-\sin^2\varphi_2)^{\frac{1}{2}}=\lambda_2/4. \qquad (8)$$

TABLE I. *Measurements of the reflection of the sodium line and mercury line from the film on glass. The mean of the values of n_0 given in column 4 is 1.462±0.002.*

Investigated Surface No.	φ_1	φ_2	n_0	d(A)	n_0d(A)
1					
1st meas.	30°00′	46°01′	1.465	1073±1	1568±1
1					
2nd meas.	30°00′	45°53′	1.459	1072±1	1567±1
2					
1st meas.	30°25′	46°17′	1.463	1079±1	1570±1
2					
2nd meas.	30°31′	46°19′	1.461	1075±2	1571±1
3					
1st meas.	35°00′	49°50′	1.461	1095±2	1602±1
3					
2nd meas	34°49′	49°47′	1.465	1095±2	1601±1
4	35°36′±7′	50°23′±5′	1.463±0.007	1106±2	1606±1
5	38°38′±7′	52°57′±4′	1.463±0.007	1114±2	1629±1
6	41°59′±6′	55°54′±6′	1.461±0.008	1133±2	1657±1

The refractive index of the film is then

$$n_0\left(\frac{\lambda_1^2\sin^2\varphi_2-\lambda_2^2\sin^2\varphi_1}{\lambda_1^2-\lambda_2^2}\right)^{\frac{1}{2}}. \qquad (9)$$

The thickness of the film, d, may be calculated according to one of the formulae (7) and (8).

With regard to dispersion the refractive index of the film calculated according to formula (9) is the mean of the refractive indices of the film for the wave-lengths λ_1 and λ_2. The measurements summarized in Tables I and II were made for the sodium line $\lambda_1=5893$A and mercury green line $\lambda_2=5461$A. The temperature of the room changed between 18°–20°C.

TABLE II. *Data on films which show colors when white light is incident on the film. Measurements are made for $\lambda=5893$A, and the value of n_0 is taken as 1.462±0.002. The mean of the value of n given in column 5 is 1.7390±0.0003. This is to be compared with the value of n obtained by the method of minimum deviation which is 1.7393±0.0001.*

Investigated Surface No.	Color	φ	$\psi+45°$†	n	d(A)	n_0d(A)	n_0d*(A)
1	yellow-brown	45°00′	66°00′	1.7385	1151±2	1683±1	1680
2		45°14′	65°44′	1.7393	1153±2	1685±1	
3	red	59°35′	45°47′	1.7386	1248±3	1824±1	2450
4		60°21′	44°37′	1.7392	1253±3	1832±1	
5	purple	70°25′	28°54′	1.7392	1318±3	1927±2	2570
6		72°03′	26°22′	1.7390	1327±3	1940±2	

* According to the literature.
† The angle of the polarizer is 135°.

Column 1 gives the number of the measured surface. At a perpendicular incidence of white light on the reflecting surface covered with an interference film one sees when observing the vertically reflected light, a yellow-brown interference color. Surface No. 1 shows the lightest shade. Columns 2 and 3 give the measured angles of incidence for zero ellipticity, φ_1, for the sodium line $\lambda_1=5893$A, and φ_2, for the mercury green line $\lambda_2=5461$A.

The angles of incidence, φ_1 and φ_2, for zero ellipticity were determined by interpolation. In the neighborhood of the angle of incidence for zero ellipticity, the angle γ indicating the ellipticity is determined for 3 to 4 angles of incidence, e.g., for 27.5°, 30.0°, 32.5°, and 35.0°. If, for example, for the angle of incidence $\varphi=30.0°$ the ellipticity is zero, the angle indicating the ellipticity is positive for $\varphi=27.5°$,

whereas it is negative for $\varphi = 32.5°$. Then the dependence of the angle γ on the angle of incidence, φ, is represented graphically, and the angle of incidence for zero ellipticity determined from this graph by interpolation. The angles γ indicating the ellipticity are reproducible to 0.5, this being also the smallest division, which we can read by means of the vernier on the circle of the compensator. To this error of measurement in the angle of incidence for zero ellipticity corresponds a maximum error 7′ for the sodium line (at smaller angles of incidence it is larger) and up to 6′ for the mercury green line. Note the measurements on surfaces Nos. 4, 5, and 6. With the surfaces Nos. 1, 2, 3 two independent series of measurements were made on the same reflecting surface, from which the reproducibility of the measurements by this method can be well estimated.

The refractive index of the film, n_0, calculated according to the formula (9) is given in column 4. The exactness of the measurement of the refractive index is about 0.5 percent as can be judged from the results obtained on surfaces Nos. 4, 5, and 6. If the measurements are made on several surfaces, we can reduce this error to 0.2 percent.

The mean value of the refractive index n_0 measured for $\lambda_1 = 5893$A and $\lambda_2 = 5461$A corresponds to the refractive index of fused quartz. K. B. Blodgett in her communication gives an approximate value of 1.46 for the refractive index of this film. According to Landolt-Börnstein,[4] the refractive index of fused quartz is 1.4585, for $\lambda = 5893$A and 1.4607 for $\lambda = 5330$A, the mean being 1.4595. This result is an important criterion for the chemical composition of the thin superficial film on the glass, formed artificially by chemical treatment. The thin film is of fused quartz. This was to be expected from the chemical point of view. The lead atoms have been extracted from the surface layer of the glass and precipitated by sulphuric acid in the form of lead sulphate.

Column 5 gives the thicknesses of the film, d, and finally column 6 gives the optical paths, $n_0 d$, which are from an optical point of view more important.

[4] Landolt-Börnstein, *Handbuch der Physik* (Berlin, 1923), Table II, p. 915.

Table II gives the results of measurements on surface films, which show at perpendicular incidence of white light and perpendicular reflection a yellow-brown, red and purple color. The measurements were made only for sodium light $\lambda = 5893$A. The refractive index of the film is known from measurements given in Table I; $n_0 = 1.462 \pm 0.002$.

Column 1 gives again the number of the measured surface. For each of the three mentioned colors two surfaces showing approximately the same interference color were measured. Column 2 gives again the interference color. Column 3 gives the angles of incidence, φ, for zero ellipticity of the reflected light, and column 4 the angle ψ between the plane of polarization of the analyzer and the plane of incidence corresponding to the mentioned angle of incidence, φ. Column 5 gives the values of the refractive index of the glass, n, calculated by formula (6). Below the table the refractive index of the glass measured by the method of the minimum deviation is given for comparison. The value of the refractive index of glass obtained by reflection agrees with that from refraction of light within the limits of experimental error.

Column 6 gives the thicknesses of the interference films, d, and column 7 the optical paths $n_0 d$. Finally, column 8 gives, for purpose of comparison, the thicknesses, $n_0 d$, of the air-layer according to Müller-Pouillet,[5] which, at perpendicular incidence of white light and when observing the light reflected perpendicularly, would show the same interference colors (as far as it is possible to compare the interference colors). For the yellow-brown color the results are in good accord. There is a striking difference in the values of the optical paths for the red and purple colors, where the results given by the present author are substantially lower. It is worth mentioning that the difference of optical paths for the red and the purple color is in both instances the same. It is to be noted that Newton originally estimated the thickness of the air-layer for the red color lower than is given in the above-mentioned *Lehrbuch der Physik*.[5] (See, also, a paper by A. Rollet.[6]) Also according to the experimental curves, the values given by the present author are correct;

[5] Müller-Pouillet, *Lehrbuch der Physik*, tenth edition (Braunschweig, 1909), "Optik," p. 744.

[6] A. Rollet, Akad. Wiss. Wien, 3, No. 77, 177 (1878), see especially pp. 229 and 230.

values mentioned heretofore in the literature are too high.

It would be a useful task to measure by this method the thicknesses of thin interference surface films by using maxima not only of the first order, but mainly those of higher orders. Films on glass offer only limited possibilities in this respect since they give only maxima of the first and partially of the second order. More suitable for this study would be monomolecular films as produced and studied by K. B. Blodgett, for it is possible to lay these monomolecular layers on each other to any thickness.

In conclusion some practical consequences following from the study of physical properties, such as refractive index and thickness, of films on lead glass may be mentioned. By an optical method this superficial film was identified as a film of quartz glass. This thin, but very hard film of quartz glass can give good protection against mechanical damage to the soft lead glass (for example, of lenses). Another question is, whether the vessels of various types of lead glass, for example dishes, can be dangerous to life or not owing to chemical reaction with an acid. Finally, thin surface films on glass may be used in practice for producing glass articles showing iridescent colors.

MAY 15, 1940 PHYSICAL REVIEW VOLUME 57

A Direct Comparison on a Crystal of Calcite of the X-Ray and Optical Interferometer Methods of Determining Linear Thermal Expansion

Evidence of Differences Among Calcite Crystals*

J. B. AUSTIN, *Research Laboratory, United States Steel Corporation, Kearny, New Jersey*

H. SAÏNI, J. WEIGLE, *Institut de Physique, Université de Genève, Switzerland*

AND

R. H. H. PIERCE, JR., *Research Laboratory, United States Steel Corporation, Kearny, New Jersey*

(Received March 11, 1940)

Measurements by the x-ray and optical interferometer methods on the same specimen of calcite gave values for the coefficient of linear expansion which agree within the limit of measurement. Comparison of these results with data for other crystals of calcite shows that there is a significant difference in the expansion of different crystals. The spacing between the (211) [((100))] planes is also measurably different.

IN a recent determination of the thermal dilatation of calcite, Weigle and Saïni,[1] using an x-ray powder method, obtained coefficients for the expansion along the two principal crystallographic axes which were approximately 20 percent lower than those obtained by Benoit,[2] whose data, obtained by means of an optical interferometer, have hitherto been regarded as among the best available. This discrepancy, which is many times greater than the combined experimental error, indicates either that the two methods do not give comparable results or that there is a significant difference in the expansion of different crystals of calcite. As measurements of the dilatation of sodium nitrate by the same x-ray method[3] had given values in satisfactory agreement with data obtained by means of the interferometer,[4] it seemed likely that the discrepancy with calcite was due to a difference in the specimens tested, a view which is supported by the difference in density among calcite crystals observed by DeFoe and Compton.[5]

* A preliminary note describing these results has been given by Saïni, Compte rendu des Séances, Société de physique et d'histoire naturelle de Genève **52**, 108 (1935).

[1] J. Weigle and H. Saïni, Helv. Phys. Acta **7**, 257 (1934).

[2] J. R. Benoit, Trav. Bur. Int. Poids et Mesures **6**, 190 (1888).

[3] H. Saïni and A. Mercier, Helv. Phys. Acta **7**, 267 (1934).

[4] J. B. Austin and R. H. H. Pierce, Jr., J. Am. Chem. Soc. **55**, 661 (1933).

[5] O. K. DeFoe and A. H. Compton, Phys. Rev. **25**, 618 (1925).

If such a difference exists it is important that it be established beyond doubt and that its magnitude be determined, since calcite is commonly used as a standard grating in x-ray spectroscopy and the change in lattice spacing with temperature must be accurately known. For example, the coefficient of linear thermal expansion perpendicular to the (211) planes should be known to better than 1 percent if full advantage is to be taken of the precision of present x-ray technique.[6]

In order to determine to what extent the discrepancy between the data of Benoit and those of Weigle and Saïni is caused by the use of different experimental methods, measurements have been made by both x-ray and interferometer methods on the *same* crystal of calcite. The specimen selected, a large clear crystal from Big Timber, Montana, contained the following known impurities:

MgO less than 0.03 percent
MnO less than 0.06 percent
Fe less than 0.01 percent.

Small pieces were carefully cut from this block so that the linear expansion in four different directions within the crystal could be determined in an interferometer which has been described.[4] The small pieces used in these determinations were then ground into powder and the expansion determined by the x-ray method used in the earlier measurements on calcite.[1]

TABLE I. *Mean coefficients of linear thermal expansion between 18° and t°C. ($\alpha \times 10^6$.) The accuracy of coefficients determined optically is $\pm 0.5 \times 10^{-6}$, determined by x-rays it is 1.5×10^{-6}.*

	Parallel to a axis Perpendicular to $(11\bar{2})$		Perpendicular to ((011))	Perpendicular to rhombohedral face ((100)) (211)	Parallel to c axis Perpendicular to (111)	
t°C	Interferometer	X-rays	Interferometer	Interferometer	Interferometer	X-rays
50	−4.9		0.1	10.8	25.1	
100	−4.8	−3.4	0.2	11.1	25.9	26.8
150	−4.8		0.4	11.4	26.8	
200	−4.8		0.6	11.6	27.4	
250	−4.8		0.8	11.8	27.8	
300	−4.7		0.9	12.0	28.1	

The results of the two sets of measurements, shown in Table I and Fig. 1, agree within the limit of accuracy of measurement, thus demonstrating that the methods are comparable and should, in general, give the same values for the several coefficients. Since the x-ray method gives directly the expansion along the a and c axes, and does not give directly the expansion along the other directions studied with the interferometer, only the two coefficients for the axes are included in Table I. Coefficients for other directions as calculated from the x-ray data are given in Fig. 1, in which the several coefficients are plotted as a function of the square of the cosine of the angle between the c axis and the direction in which the expansion was determined, a method of plotting which gives a straight line for rhombohedral crystals. Planes perpendicular to the direction in which the expansion was measured are indicated by Miller indices with parentheses used according to the convention of Ewald and Hermann.[7] It will be observed that although the difference between the two sets of measurements always lies within the experimental error, the coefficients determined by the x-ray method are consistently the higher, which may indicate a significant difference between the methods, but if so, the difference is small and can be established only by more accurate determinations. In any case, a possible difference of this sort is very much

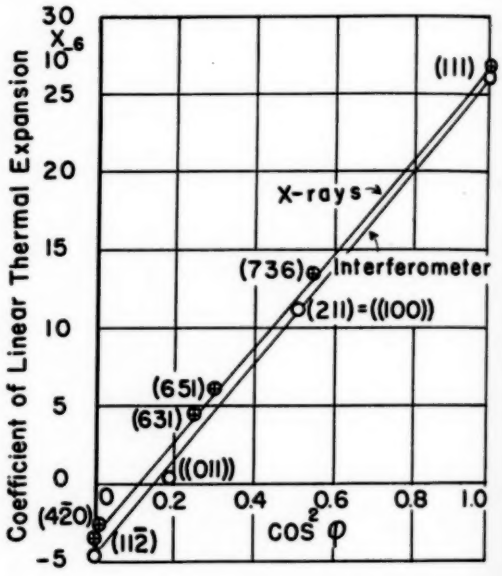

FIG. 1. Thermal expansion coefficients for different directions in a crystal of calcite as determined by x-ray and optical interferometer measurements on the same sample.

[6] Cf. C. D. Cooksey and D. Cooksey, Phys. Rev. **36**, 85 (1930).

[7] P. P. Ewald and C. Hermann, *Strukturbericht*, 1913–26 (Akademisches Verlagsgesellschaft, Leipzig, 1931), p. 293.

TABLE II. *Thermal expansion coefficients of calcite as reported in the literature*

INVESTIGATOR	TEMP. RANGE °C	LINEAR EXPANSION COEFFICIENT $\times 10^6$ PERPENDICULAR TO (111)	PERPENDICULAR TO (112)
Mitscherlich[1]	Room Temp. to 100°	28.6	−5.6
Fizeau[2]	0 to 100°	26.4	−5.3
Pfaff[3]	0 to 100°	26.3	−3.1
Benoit[4]	18° to 100°	25.7	−5.5
Kozu, Masuda and Ueda[5]	20° to 100°	22.5	−6
Kozu, Masuda and Ueda[5]	20° to 100°	21.2	−6
Weigle and Saïni[6]	18° to 100°	21.0	−3.8
Austin and Pierce[7]	20° to 100°	28.0	−5.0
Adenstedt[8]	−20° to 0°	24.6	−5.6
This research—x-ray	18° to 100°	26.8	−3.4
Interferometer	18° to 100°	25.9	−4.8

[1] E. Mitscherlich, cf. C. Hintze, *Handbuch der Mineralogie* (Walter de Gruyter & Co., Berlin, 1930), Vol. 1, Part 3, p. 2859.
[2] H. Fizeau, cf. C. Hintze, *Handbuch*, reference 1.
[3] F. Pfaff, Pogg. Ann. **104**, 171 (1858); **107**, 148 (1859).
[4] J. R. Benoit, Trav. Bur. Int. Poids et Mesures **6**, 190 (1888).
[5] Kozu, Masuda and Ueda, Sci. Reports, Tohoku Imp. Univ. [III] **3**, 247 (1929).
[6] J. Weigle and H. Saïni, Helv. Phys. Acta **7**, 257 (1934).
[7] J. B. Austin and R. H. H. Pierce, Jr., unpublished data for a sample used for analytical standardizations.
[8] H. Adenstedt, Ann. d. Physik [5] **26**, 69 (1936).

smaller than the observed differences among samples. For example, the coefficients for the sample from Big Timber are in fair agreement with those reported by Benoit[2] but differ by over 20 percent from those for the sample previously studied by Weigle and Saïni, a difference which can only be accounted for as a difference between the samples.

As further evidence for the existence of differences among samples, we have collected the several sets of data reported in the literature and have in Table II compared them with our results and with another set of hitherto unpublished measurements obtained by means of the interferometer. The coefficient for the direction perpendicular to the *a* axis is small, in fact, its magnitude is only two or three times the experimental error in some cases, hence, a relatively large variation is to be expected, but the expansion along the *a* axis is so large that the observed variation of nearly 30 percent among the values for this coefficient cannot be ascribed to any error of measurement. It should be noted in particular that there are significant differences among the coefficients obtained with different samples by the same investigators using the same method. Thus, Weigle and Saïni obtained $21.0\pm1.5\times10^{-6}$ for their first sample as compared with $26.8\pm1.5\times10^{-6}$ for the sample from Big Timber and Austin and Pierce obtained $28.0\pm0.5\times10^{-6}$ for a sample used as an analytical standard as compared with $25.9\pm0.5\times10^{-6}$ for the sample from Big Timber.

The coefficient for the direction perpendicular to the (211) [or ((100))] planes, derived from the several sets of data for the expansion along the *a* and *c* axes by means of a cosine plot similar to Fig. 1, varies from 7.8×10^{-6} to 12.0×10^{-6}, a variation much greater than is permissible in x-ray measurements of the highest precision. These are, of course, mean coefficients for the range 18° to 100°C and it is not impossible that the coefficient for a smaller range, say 18° to 25°C, would show a smaller variation, yet even so, the variation is certain to be larger than 1 percent which is the desired accuracy.

It is also of interest to compare the distance between the (211) [or ((100))] planes at 18°C for different samples. The value for the sample studied previously by Weigle and Saïni is 3.0262×10^{-8} cm, whereas that determined on the present sample is 3.0290×10^{-8}. The value recommended by Siegbahn is 3.02904×10^{-8} cm for small Bragg angles and 3.02945 for a limiting angle of 90°. As the present measurements were made with a Bragg angle of 75°, the value for the sample from Big Timber differs by 1 part in 10,000 from the Siegbahn value whereas the parameter of the Weigle and Saïni sample shows a difference of 1 part of 1000. There appears, therefore, to be a difference in grating space as well as in the coefficient of linear expansion.

LETTERS TO THE EDITOR

Prompt publication of brief reports of important discoveries in physics may be secured by addressing them to this department. Closing dates for this department are, for the first issue of the month, the eighteenth of the preceding month, for the second issue, the third of the month. Because of the late closing dates for the section no proof can be shown to authors. The Board of Editors does not hold itself responsible for the opinions expressed by the correspondents.

Communications should not in general exceed 600 words in length.

Note on the Ends of the Mesotron Tracks Observed in an Expansion Chamber

In recent literature we find the reproduction of a number of photographs showing the ends of mesotron tracks.[1]

If it is assumed that the mesotron undergoes disintegration, it might be expected that every track will terminate in an electron track, but this is nowhere to be seen on the photographs. It must, however, be borne in mind that a mesotron, after it has ceased to produce appreciable ionization, still possesses sufficient energy to move by diffusion, and traverse a certain distance from the end-point of the track before it undergoes disintegration.

Unfortunately, an exact estimate of the diffusion range is impossible, since this latter depends on the velocity of the mesotron at the end of the track. From Bohr's condition for ionization this velocity should amount to several units multiplied by 10^8 cm/sec.

After the ionization has ceased, the mesotron begins to move more and more slowly because of elastic collisions with nuclei. Thus the energy of the mesotron decreases, and the diffusion coefficient becomes a function of the time.

From the equation for diffusion

$$\partial F/\partial t = D\Delta F \tag{1}$$

we obtain the following expression for the probability F that a unit volume will contain a mesotron:[2]

$$F=[3/2\pi\langle r^2\rangle_{Av}]^{\frac{1}{2}} \exp\left[-3r^2/2\langle r^2\rangle_{Av}\right], \tag{2}$$

where

$$\langle r^2\rangle_{Av}=6\int_0^\infty D dt.$$

The diffusion coefficient D is usually expressed as

$$D=V\lambda/3=V/3\sigma_{eff}N$$

where V is the velocity of the mesotron and N the number of atoms in unit volume. The effective cross section σ_{eff} for diffusion can be represented as follows[2]

$$\sigma_{eff}=\int\sigma(1-\cos\theta)d\Omega=\frac{2\pi Z^2e^4}{(2mV^2)^2}\int_{\theta_0}^{\pi}\frac{1-\cos\theta}{\sin^4\frac{1}{2}\theta}\sin\theta d\theta \tag{3}$$

where θ_0 is an angle determined by the screening of the atomic electrons, its value being of the order of magnitude

$$\theta_0\sim\frac{Ze^2/\mu V^2}{a_0/Z^{1/3}}=\frac{Z^{4/3}m}{\mu}\left(\frac{e^2}{\hbar V}\right)^2.$$

With the aid of (3) we obtain

$$\sigma_{eff}=\frac{\pi Z^2e^4}{E^2}\lg\frac{2}{\theta_0}. \tag{4}$$

The energy lost by a mesotron along unit path is

$$-\frac{dE}{dx}=N\int\sigma\frac{(2p\sin\frac{1}{2}\theta)^2}{2M}d\Omega=N\frac{2\mu}{M}\sigma_{eff}E=N\sigma_{eff}E\delta \tag{5}$$

where μ is the mass of the mesotron, p its momentum, and M the mass of the atom.

Since $\delta=2\mu/M\ll1$, a great many collisions are required before the mesotron will suffer an appreciable loss of energy. The use of the above equation for diffusion is therefore quite legitimate.

Let us now calculate the quantity $\langle r^2\rangle_{Av}$ in the distribution function (2):

$$r^2=6\int_0^\infty Ddt=6\int_{E_0}^0 D(E)\frac{dE}{(dE/dt)}=6\int_0^{E_0}\frac{DdE}{N\delta\sigma_{eff}EV}=\frac{\lambda_0^2}{2\delta}, \tag{6}$$

where $\lambda_0=1/N\sigma_{eff}(E_0)$; E_0 is the energy of the mesotron corresponding to the moment when the diffusion starts.

For $E_0=10$ kev we obtain in air under normal conditions: $\langle r^2\rangle_{Av}^{\frac{1}{2}}\geqq1.0$ cm (if we put $\mu=160m$, where m is the mass of the electron).

Let us further calculate the time during which the mesotron slows down

$$\tau=\int_{E_0}^0\frac{dE}{dE/dt}=\int_0^{E_0}\frac{dE}{\delta\sigma_{eff}VEN}=\frac{2\lambda_0}{3\delta V_0}. \tag{7}$$

In our case $\tau\geqq10^{-8}$ sec.

For energies corresponding to $\theta_0\sim1$ Eq. (4) is no longer correct. However, at those energies for which this condition is fulfilled, the diffusion is negligibly small. The total diffusion range can therefore be calculated from Eq. (6).

It must be noted that in determining the energy of any particle from its range in an expansion chamber or from the total ionization in an ionization chamber, the loss of energy due to elastic collisions with nuclei, after the ionization has ceased, must be taken into consideration. In particular, an energy of the order of one million volts is spent on nuclear collisions by every fragment resulting from the fission of uranium.

In conclusion, we wish to express our sincere thanks to A. T. Kirichenko and N. L. Ostrover for many interesting discussions of the problem.

A. MIGDAL
J. POMERANCHUK

Physico-Technical Institute,
Leningrad, U. S. S. R.,
March 25, 1940.

[1] H. Meier-Leibnitz, Zeits. f. Physik **112**, 569 (1939); Y. Nishina, M. Takeuchi and T. Ichimiya, Phys. Rev. **55**, 585 (1939).
[2] Bethe, Rose and Smith, Proc. Am. Phil. Soc. **78**, 573 (1938).

Experiments on the Periodic Deviation From the "Schottky Line"

Measurements made with extreme care have verified the discovery made by Seifert and Phipps[1] that the thermionic emission from a heated filament does not increase linearly with the square root of the electric intensity as called for by the Schottky mirror image theory. The maxima and minima which have been checked are near *25.6*, 40, *65.5*, 121 and *255* kv per cm (italicized numbers for minima). Seifert and Phipps[1] state that "the heights of the maxima and minima for a given filament decrease slightly with increasing temperature" while Turnbull and Phipps[2] state that "the magnitude of the percent deviation, δ, increases with temperature." There is agreement that within experimental error the location of the maxima and minima is independent of the temperature. My observations show that the amplitude of the deviations are *independent* of the temperature except at the lower fields where the non-periodic deviations are greater the lower the temperature, as has already been pointed out.[3]

The principal object of this letter is to stress the importance of this temperature independence of both the amplitude of the effect and the position of the maxima and minima on the electric intensity scale. The results impose serious limitations on any theory which tries to explain the periodic deviations observed as a change in the transmission properties of the surface barrier unless the theory incorporates a temperature factor exactly compensating for the difference in the electron energy distribution which is a necessary consequence of the change in temperature or else the transmission function must change with the electric field in such a way that its alteration is independent of the energy of the electron transmitted through the surface of the metal. It does not appear that either of the theories[4] so far suggested are capable of explaining the observed facts.

WAYNE B. NOTTINGHAM

Massachusetts Institute of Technology,
Cambridge, Massachusetts,
April 24, 1940.

[1] R. L. E. Seifert and T. E. Phipps, Phys. Rev. **56**, 652 (1939).
[2] D. Turnbull and T. E. Phipps, Phys. Rev. **56**, 663 (1939).
[3] W. B. Nottingham, Phys. Rev. **49**, 78 (1936).
[4] H. M. Mott-Smith, Phys. Rev. **56**, 668 (1939); C. J. Mullin and E. Guth, Phys. Rev. **57**, 349 (1940).

Erratum: On the Yield of Nuclear Reactions with Heavy Elements

(Phys. Rev. **57**, 472 (1940))

The relations given in the caption of Fig. 1 of the above-named paper contain an error in exponent of the numerical factors, 10^{26} appearing instead of 10^{24}. They should read: $(2me/\pi\hbar^2)S_p = 1.52\times10^{24}S_p$ for protons and $(2me/\pi\hbar^2)S_\alpha = 6.08\times10^{24}S_\alpha$ for α-particles. The other two relations in the caption remain unchanged.

V. F. WEISSKOPF
D. H. EWING

University of Rochester,
Rochester, New York,
April 23, 1940.

Notes on the Separation of Alloys and Isotopes by the Centrifuge

Density differences of two percent were produced by Joly and Poole[1] in liquid alloys of lead, tin, and bismuth by use of a centrifuge. With a Beams ultracentrifuge I have changed the density of liquid Wood's metal by as much as 13 percent.

The centrifuge consisted of two hardened steel rotors held together by a bolt as indicated in Fig. 1. Opposite faces of the rotors were ground and polished to almost optical flatness. Four radial slots in the lower rotor held ingots of the alloy. The vacuum chamber containing the rotor was heated to 100°C and then the rotor run at 500 r.p.s. The hydrostatic pressure at this speed forced the rotors apart slightly so that some metal leaked out. With the removal of material, the pressure was reduced and the leakage stopped. The remaining metal (about 25 percent) in the four slots had densities of 8.40, 8.33, 8.29, and 8.33 g/cc. The original material (Pb 50 percent, Bi 25 percent, Sn 12.5 percent, Cd 12.5 percent) had a density of 9.57 g/cc.

Separation by use of the centrifuge of the constituents of an alloy in the liquid state is possible but any attempt to separate isotopes in a liquid, without counter-currents, seems futile because of the slowness of the molecular sedimentation. This limitation exists even though vibrations and temperature inequalities, to which earlier failures have been attributed,[1-4] can be removed. For mercury, the sedimentation velocity under unit force is about 10^{-14} cm/sec., if one calculates by the classical hydrodynamic method. With a force field as high as 500,000 g the velocity imposed on a heavy molecule, 5×10^{-9} cm/sec., is still negligible. If the "cage model" of a liquid[5] is used, the influence of the field on a single molecule is again found to be small in a force field of 500,000 g. The ratio of the energy an atom might acquire in moving freely as far as 3×10^{-8} cm under the influence of this field to its thermal energy is about 7×10^{-8}. So separation in the field would be negligible in comparison with mixing due to diffusion.

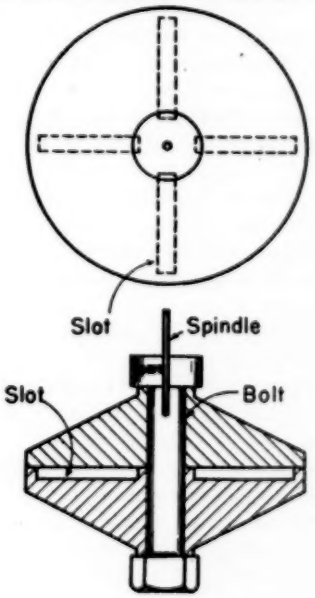

FIG. 1. Compound rotor.

Separation of isotopes in the gas phase is possible by the method of "evaporative centrifuging" used by Beams and Skarstrom[6] and by Humphreys.[4] The Lindemann-Aston separation factor is proportional to $\exp[1/T]$. I have therefore attempted to obtain a relatively large separation of the chlorine isotopes by using hydrogen chloride just above its melting point in a Beams centrifuge. The rotor was cooled to $-98°C$ and the vapor from the liquid HCl was pumped through the hollow spindle which formed the axle. (See reference 6 for details.) Although no analysis by the mass spectrograph of the fractions was made, the operation of the centrifuge at low temperature was demonstrated. The theoretical isotopic separation coefficient which is 1.11 at room temperature, becomes 1.25 just above the solidification temperature of hydrogen chloride if the rotor velocity is 5×10^4 cm/sec. at the boundary of the liquid-gas phase. This velocity is the highest practical in "evaporative centrifuging" with hollow rotors.

The substitution of hydrogen chloride for carbon tetrachloride results in a decrease in molecular mass and a three-hundred-fold increase in ratio of gas pressure at the rotor center to that at the gas-liquid boundary. Under these conditions the time for equilibrium across a radial sector of the rotor is reduced and an increased rate of removal seems practical. If then the centrifuge is employed to separate isotopes, it would appear advantageous to use the hydrogen halides near their melting points to effect a partial separation of large amounts of chlorine and bromine isotopes.

Research Laboratory,
General Electric Company,
Schenectady, New York,
February 7, 1940.

H. C. POLLOCK

[1] J. Joly and J. H. J. Poole, Phil. Mag. **39**, 372 (1920).
[2] R. S. Mulliken, J. Am. Chem. Soc. **44**, 1033 (1922); **44**, 1729 (1922).
[3] J. H. J. Poole, Phil. Mag. **41**, 818 (1921).
[4] R. F. Humphreys, Phys. Rev. **56**, 684 (1939).
[5] M. J. Polissar, J. Chem. Phys. **6**, 833 (1938).
[6] J. W. Beams and C. Skarstrom, Phys. Rev. **56**, 266 (1939).

Observations on the Dark Current of a Willemite Crystal

Some time ago the photoconductivity of a single crystal of willemite was investigated at low temperatures.[1] Several times during this study it was noticed that the dark current showed a sudden large increase at about $-60°C$ while the crystal was warming up with the field on, and then fell to its very low initial value. Subsequent studies on this crystal showed that this effect is obtained when the crystal is illuminated with ultraviolet light at low temperatures with field on (in our case 2000 volts/cm) and then allowed to warm up in the dark. However, if the crystal is depolarized and then warmed up in the dark with the field on, the effect observed was only about 1/100 of that obtained when the crystal was initially illuminated as described above. This small effect is probably due to the fact that the crystal was not completely depolarized. Since the rate of warming up could not be controlled conveniently with the present arrangement for cooling the crystal, no quantitative measurements were made concerning the dependence of dark current on temperature, time, and exposure to ultraviolet light. This phenomenon was observed for both λ 2537A and λ 3125A. It would doubtless occur for the whole range of wave-lengths for which the crystal exhibits photoconductivity. Similar results were found when electrical contact was made with either gold (sputtered) or Aquadag electrodes.

We feel that this dark current effect is probably connected with the emission of trapped light reported by Johnson.[2] Further experiments are indicated, such as simultaneous observations of dark current and fluorescence.

We hope to publish a more detailed account of experiments on photoconductivity and absorption of crystalline willemite in the near future.

Palmer Physical Laboratory,
Princeton, New Jersey,

R. C. HERMAN

Randal Morgan Laboratory of Physics,
University of Pennsylvania,
Philadelphia, Pennsylvania,
April 29, 1940.

R. HOFSTADTER

[1] R. Hofstadter and R. C. Herman, Phys. Rev. **56**, 212 (1939).
[2] R. P. Johnson, J. Opt. Soc. Am. **29**, 387 (1939).

Resonance Scattering of Neutrons in Helium

Experiments of Staub and Stephens[1] on the scattering of neutrons in helium have shown that resonance occurs for neutrons of about one Mev, arising from the existence of a virtual P level of He^5.[2] This resonance raises the ratio of the forward scattering cross sections of helium and hydrogen from 1.4 to 2.5 Mev to about 9 at 1 Mev. We have investigated the resonance scattering more closely by using a continuous neutron spectrum. This was produced by allowing the monochromatic neutrons of a *dd* generator to strike a paraffin howitzer of suitable shape, where, by elastic collision the neutrons lost part of their original energy. The howitzer was shaped so as to give a continuous neutron distribution which was almost uniform from 0.6 to 2.0 Mev. This distribution was determined by the scattering of the neutrons in a cloud chamber filled with methane. The shape of the resonance curve over this region has been measured in 0.1-Mev intervals by using the same cloud chamber technique as described by Staub and Stephens. From our results we conclude that the level of He^5 has a width at half-maximum of 0.4 Mev. The shape of the resonance peak of the scattering cross-section curve indicates a doublet structure of the two levels $J=\frac{3}{2}$ and $J=\frac{1}{2}$ with a splitting of 0.24 ± 0.1 Mev. Since the more intense peak occurs at the lower energy and corresponds to $J=\frac{3}{2}$ the doublet is inverted. The $\frac{3}{2}$ level is unstable against decay into a neutron and an α-particle by 0.76 Mev and the $\frac{1}{2}$ level by 1.0 Mev. The shape and the absolute values of the resonance scattering cross-section curve are within the experimental error in agreement with the predictions of the dispersion theory derived for this particular case by Bloch.[3] The previous experimental data of Staub and Stephens fit into the present curve within the statistical error. A full account of the experiments will be published shortly.

Stanford University,
Stanford University, California,
April 21, 1940.

H. STAUB
H. TATEL

[1] H. Staub and W. E. Stephens, Phys. Rev. **55**, 131 (1939).
[2] J. H. Williams, W. G. Shepherd and R. O. Haxby, Phys. Rev. **52**, 390 (1937).
[3] F. Bloch, to be published soon.

Evidence for a New Type of Nuclear Reaction

A 33-minute period was observed when sulphur was bombarded with 0.1μa of 22-Mev He^{++} ions accelerated by the Harvard cyclotron. This was identified as a chlorine activity by dissolving the irradiated sulphur in CS_2, adding dilute HNO_3 and a drop of HCl, and precipitating the chlorine as AgCl by the addition of $AgNO_3$. By bending the electrons in a magnetic field their sign was found to be positive. This test excludes all chlorine isotopes that might be formed by an (α, p) reaction with the exception of Cl^{36}. However, the latter is known to have a period greater than 1 year.[1]

Radioactive Cl^{34} is a positron emitter of 33-min. half-life.[1] It can be formed from phosphorus by the reaction $P^{31}(\alpha, p)Cl^{34}$ and from sulphur by $S^{33}(d, n)Cl^{34}$. Phosphorus was bombarded with α-particles and an absorption curve was obtained for the 33-min. activity. Similar data were taken for the 33-min. activity induced in sulphur by α-particles. A comparison of the two absorption curves showed that the two were identical within the limits of experimental error.

A series of tests were then made to show that the observed activity in sulphur was not due to phosphorus contamination. Chemical analysis of the sulphur indicated that there was less than 0.001 percent of phosphorus. By comparing the relative strengths of the 33-min. period in sulphur and in phosphorus, it was concluded that at least 1.5 percent contamination in the sulphur would be required to yield the observed activity. To eliminate the possibility of deuteron contamination in the He^{++} ion beam, sulphur was bombarded with 11-Mev deuterons. The resulting 33-min. activity when compared with the α-particle induced activity indicated that 50 to 100 percent of the He^{++} ion beam must have been D^+ ions if the latter were responsible for the observed activity. However, visual observations of the He^{++} ion beam and tests with carbon as a monitor showed that there was less than 1 percent of deuteron contamination. Furthermore, the $S+He^{++}$ and $S+D^+$ total decay curves are quite distinct.

These tests indicate that the 33-min. period is to be identified as Cl^{34}. Since the lightest stable sulphur isotope is 32, the most reasonable assumption seems to be that Cl^{34} is formed from S^{32} by the reaction $S^{32}(\alpha, d)Cl^{34}$ or $S^{32}(\alpha, pn)Cl^{34}$.

Reactions of the (α, d) or (α, pn) type are highly endoergic with thresholds in the neighborhood of 10 Mev. It should be possible to decide between the two types by threshold measurements, since the latter requires 2.2 Mev more energy than the former (corresponding to the binding energy of the deuteron).

No evidence has been found for a 1.1-hour period reported by King, Henderson, and Risser.[2] Two very weak activities of 3.3 hours and >8 days were observed but have not been identified.

It is a pleasure to thank Professor K. T. Bainbridge and the members of the cyclotron laboratory for their interest and cooperation. We are indebted to Professor G. P. Baxter for the chemical analysis of the sulphur, to Dr. A. K. Solomon for performing the chlorine separation, and to Dr. I. A. Getting for the use of his magnet and Geiger counter.

R. SHERR

Research Laboratory of Physics,
Harvard University,
Cambridge, Massachusetts,
April 30, 1940.

[1] J. J. Livingood and G. T. Seaborg, Rev. Mod. Phys. 12, 35 (1940).
[2] King, Henderson and Risser, Phys. Rev. 55, 1118 (1939).

The Production and Half-Life of Chlorine 33

The series of radioactive elements characterized by the formula $Z-N=1$ is of importance to the theory of nuclear structure since, as Wigner[1] has shown, it is possible to calculate on simple assumptions, the energy release in the positron decay, and further by the use of the Sargent relationship, the half-life may be predicted. The properties of the members of the series have been studied[2] (with a few exceptions) up to $Z=14$. We have recently measured the half-life of a short-lived radioactive element which is almost certainly $_{17}Cl^{33}$, a high member of the series. The measured half-life of 2.8 seconds[3] is too short to allow a chemical verification of the assignment to be made, so one must rely on physical evidence, which is presented below.

Sulphur of high purity was bombarded with 8-Mev deuterons in an atmosphere of helium (to eliminate recoil products from the disintegration of air atoms). A swinging arm carried the target from the bombarding chamber to an ionization chamber and Dershem electrometer located behind the yoke of the 37″ cyclotron in less than one second after the end of the activation. Readings were permanently recorded on a kymograph.

The record showed a decay curve which could be analyzed into two components of 2.5 min. and 2.8 sec. The former is P^{30} formed in the known reaction $S^{32}+d \rightarrow P^{30}+\alpha$. The short period gives an exponential decay over a factor of 100 in intensity. The saturation activities of the two periods are almost the same, which would rule out the possibility that the short one was due to a contamination or to any of the rare sulphur isotopes. The only other common type of reaction to be expected is $S^{32}+d \rightarrow Cl^{32}+n$. A $(d, 2n)$ reaction giving rise to Cl^{32} can almost be ruled out on energetic grounds. We therefore conclude that the 2.8-sec. period is due to the decay of Cl^{33} in the reaction $Cl^{33} \rightarrow S^{33}+e^+$.

I wish to express my thanks to Professor E. O. Lawrence and the staff of the Radiation Laboratory for their hospitality and for the use of the laboratory facilities made possible by grants from the Rockefeller Foundation and the Research Corporation, and, in particular, I wish to thank Professor L. W. Alvarez who suggested the experiment and followed its development closely.

J. BARTON HOAG

Radiation Laboratory,
Department of Physics,
University of California,
Berkeley, California,
April 15, 1940.

[1] E. P. Wigner, Phys. Rev. 56, 519 (1939).
[2] M. G. White, L. A. Delsasso, J. G. Fox and E. C. Creutz, Phys. Rev. 56, 512 (1939).
[3] A more exact value, together with the details of the experiment will be published later.

Magnetic Storm Effect on Cosmic Rays at High Latitudes

The beginning of the recent magnetic storm at 8:49 A.M. E.S.T. on March 24, 1940[1] was accompanied by a sudden decrease in cosmic-ray intensity of about 2 percent at 58° N. magnetic latitude. The occurrence of such an effect in a region well above the "knee" of the latitude curve is difficult to interpret in terms of a change in the earth's magnetic field. The results were obtained by a Carnegie, Model C cosmic-ray meter mounted on board the *M. S. Northland* during a south-bound trip from Juneau to Seattle. The results are shown on the lower curve in the

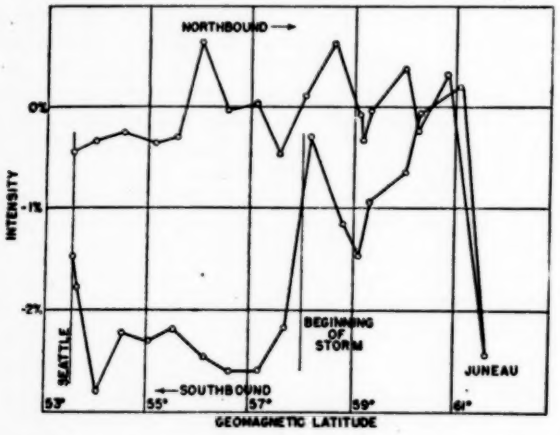

FIG. 1. Effect of recent magnetic storm on cosmic-ray intensity.

accompanying Fig. 1. The upper curve is for the northbound half of the same trip and may be taken as a typical curve with which the lower one may be compared. The drop at Juneau occurs on every trip and cannot be assigned to the magnetic storm. We wish to thank Dr. A. H. Compton for pointing out the significance of such an effect at so high a latitude.

DONALD H. LOUGHRIDGE
PAUL FREDERICK GAST

University of Washington,
Seattle, Washington,
May 1, 1940.

[1] Reported in Science, April 5, 1940.

The Effect of the Coulomb Force on Binding Energies of Light Nuclei

It has been pointed out[1-4,13,15] that the observed difference in binding energy between nuclei differing by interchange of a neutron and a proton was at least consistent with the equality of n-n and p-p forces and probably indicated the amount of Coulomb repulsion of the interchanged proton. The recent accurate measurement of Be, Li, and B (p, n) thresholds[10] and n and p scattering in helium[8,9] makes it possible to present a complete list of the experimentally observed differences in binding energy between pairs of isobaric light nuclei for which $Z=\frac{1}{2}A\pm\frac{1}{2}$. The experimentally observed values of the difference in mass of these pairs plus the $(n$-$H)$ mass difference is given in Table I, together with some theoretically calculated values.[1-3] It is interesting to note that the two new pairs (Li^5-He^5) and (B^9-Be^9) have distinctly smaller Coulomb repulsions than are calculated on the assumption that the radius of the nucleus varies as $A^{\frac{1}{3}}$ and that the particles are distributed homogeneously in the nucleus.[3] Much better agreement is obtained with the values calculated on the central model, taking into account the binding of the extra neutron.[3] However, for pairs with 11 or more particles, the homogeneous model agrees much better with experiment than the central model. The (Be^7-Li^7) difference is best accounted for on the alpha-triton model[3] of which it is the simplest example.

TABLE I. *Coulomb differences, observed and computed. A: Hartree-Fock model, fitted at O^{15} and He^4. B: Alpha-triton model, fitted at He^3 and Cl^{35}. C: Homogeneous distribution model, fitted to average of heavier nuclei. D: Central nucleus model, fitted at N^{13}.*

PAIR	EXPERIMENTAL VALUE (MEV)	REF.	COMPUTED VALUES (MEV) A	B	C	D
$_2He^3-_1H^3$	0.74±0.05	(6)	0.70	0.74*	0.825	0.78
$_3Li^5-_2He^5$	0.8 ±0.2	(7, 8, 9)			1.39	0.88
$_4Be^7-_3Li^7$	1.62±0.06	(10)		1.75	1.86	1.85
$_5B^9-_4Be^9$	1.81±0.05	(10)	1.58		2.28	1.83
$_6C^{11}-_5B^{11}$	2.75±0.07	(10)	2.07	2.75*	2.68	2.84
$_7N^{13}-_6C^{13}$	2.97±0.05	(10, 11)	2.35		3.03	2.98*
$_8O^{15}-_7N^{15}$	3.47±0.10	(12, 13)	2.82	3.75	3.38	3.6
$_9F^{17}-_8O^{17}$	3.87±0.10	(14)	2.86		3.71	3.6
$_{10}Ne^{19}-_9F^{19}$	3.97±0.10	(15)		4.76	4.0	4.28
$_{11}Na^{21}-_{10}Ne^{21}$	4 to 5	(16)			4.3	4.6
$_{12}Mg^{23}-_{11}Na^{23}$	4.59±0.10	(15)			4.6	5.02
$_{13}Al^{25}-_{12}Mg^{25}$	4.76±0.10	(15)			4.88	

* Calculated values fitted here.

A "nuclear radius" can be defined from the simple formula of the Coulomb repulsion of the extra proton $C=6(Z-1)e^2/5R$ (Z atomic number of the nucleus with the extra proton). This R calculated from the observed values of C is plotted in Fig. 1, as a function of A. The dotted line is the curve $R=1.45\times10^{-13}A^{\frac{1}{3}}$ cm. The marked de-

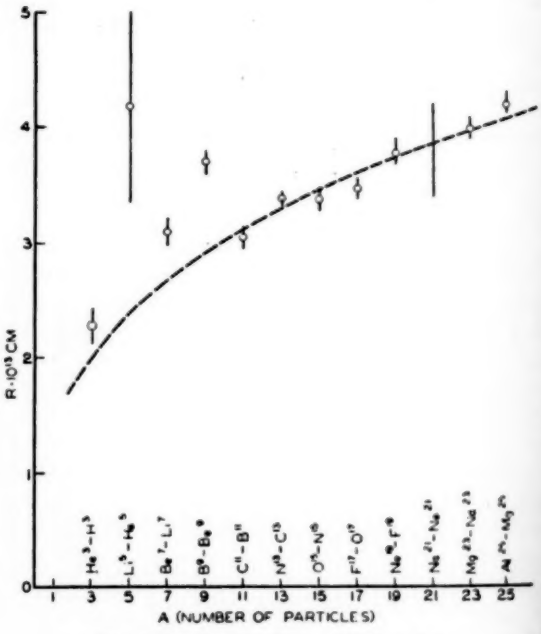

FIG. 1. "Coulomb radius" for light nuclei.

parture of B^9 and Li^5 from the dotted line is especially noticeable on this plot. The close fit of the heavier nuclei to the dotted line is also clearly shown. The large radius of B^9 and Li^5 is consistent with the simple picture of the extra proton in a p state around a closed α-particle shell.

W. E. STEPHENS*

Westinghouse Research Laboratories,
East Pittsburgh, Pennsylvania,
May 1, 1940.

* Westinghouse Research Fellow.

[1] E. Feenberg and E. Wigner, Phys. Rev. **51**, 104 (1937).
[2] H. Brown and D. R. Inglis, Phys. Rev. **55**, 1182 (1939) (fitted to newer values of He^3-H^3 and $B^{11}-C^{11}$).
[3] H. A. Bethe, Phys. Rev. **54**, 436 (1938) (fitted to new $N^{13}-C^{13}$ value for central model and to average of heavier nuclei for homogeneous model).
[4] W. H. Barkas, Phys. Rev. **55**, 691 (1939).
[5] H. A. Bethe, Phys. Rev. **53**, 313 (1938).
[6] L. W. Alvarez and R. Cornog, Phys. Rev. **57**, 248 (1940).
[7] Williams, Shepherd, and Haxby, Phys. Rev. **51**, 888 (1937).
[8] H. Staub and W. E. Stephens, Phys. Rev. **55**, 131 (1939).
[9] N. P. Heydenburg and N. F. Ramsey, Bull. Am. Phys. Soc., Vol. 15, No. 2, Abstract 112, April 10 (1940).
[10] Haxby, Shoupp, Stephens and Wells, Phys. Rev. **57**, 348 and 567 (1940).
[11] E. M. Lyman, Phys. Rev. **55**, 234 (1939).
[12] Stephens, Djanab and Bonner, Phys. Rev. **52**, 1079 (1937).
[13] Fowler, Delsasso and Lauritsen, Phys. Rev. **49**, 561 (1936).
[14] Kurie, Richardson and Paxton, Phys. Rev. **49**, 368 (1936).
[15] White, Delsasso, Fox and Creutz, Phys. Rev. **56**, 513 (1939).
[16] White (not published).

MAY 15, 1940 PHYSICAL REVIEW VOLUME 57

Proceedings of the Southeastern Section of the American Physical Society

MINUTES OF THE CHARLESTON, SOUTH CAROLINA, MEETING, MARCH 22–23, 1940

THE sixth annual meeting of the Southeastern Section of the American Physical Society was held at The Citadel, Charleston, South Carolina, on Friday and Saturday, March 22–23, 1940. Approximately one hundred and sixty-five members and guests attended the meeting. Local arrangements were made by a committee headed by Professor N. F. Smith.

The regular program consisted of thirty-one papers, abstracts for twenty-four of which are appended hereto. Abstracts of the other papers will be found in the August issue of the *American Journal of Physics*. There was a special program of invited papers on applied physics as follows:

Gasoline, from the Point of View of the Physicist.—PAUL D. FOOTE, *Gulf Research and Development Company.*

Physical Methods of Determining Atmospheric Contaminations.—A. H. PFUND, *Johns Hopkins University.*

Physical Problems in the Textile Industry.—K. L. HERTEL, *University of Tennessee.*

Home Insulation.—S. J. BRODERICK, *Southern Experiment Station, U. S. Bureau of Mines, Tuscaloosa, Alabama.*

Spectro-Chemical Analysis in Agricultural Research.—L. H. ROGERS, *Florida Agricultural Experiment Station.*

At the business meeting the election of the following officers for the year 1940–41 was announced: Chairman, F. G. Slack; Vice Chairman, Fred Allison; Secretary, E. S. Barr; Treasurer, C. B. Crawley; Members of the Executive Committee, F. L. Brown (4 years) and L. W. Morris (1 year).

The invitation extended by Vanderbilt University to hold the 1941 annual meeting at Nashville, Tennessee, was accepted.

E. S. BARR, *Secretary*

ABSTRACTS

1. Impulsive Electrical Discharge Through a Conducting Liquid. HUGH F. HENRY, *University of Virginia.*—The discharge which takes place between Cu electrodes in a $CuSO_4$ solution is produced in a manner similar to that previously described.[1] Impulsive potential is applied to the electrodes from a $\frac{1}{4}$-mf condenser with a series spark gap for a switch. Electrodes of various shapes were used and the discharge characteristics determined as a function of applied voltage and solution concentration. With one of the electrodes conical with a rounded end ($\frac{1}{4}$ mm radius) and the other flat, rotating mirror photographs show that luminosity first appears at the conical electrode regardless of polarity and then progresses across the gap. With each electrode pointed, luminosity appears at both anode and

cathode. To study the progress of the discharge, a circuit was placed in parallel with the discharge cell to remove the potential at times from 2 to 20×10^{-6} sec. after the spark gap switch closed. From Schlieren photographs the speed of progression from cathode toward anode was found to be approximately 180 m/sec. in fair agreement with rotating mirror determinations. The time lag between the application of potential and the appearance of luminosity at an electrode is decreased by forming very small bubbles on the electrode surface by electrolysis immediately before the discharge. With identical electrodes, luminosity appears first at the cathode.

[1] L. B. Snoddy and J. W. Beams, Phys. Rev. **55**, 879 (1939).

2. The Leader Process in a Long Discharge Tube. F. H. MITCHELL, *University of Virginia.*—Current and speed characteristics of discharges due to negative impulsive potentials applied to an electrode in one end of a glass tube 14 cm in diameter and 12 meters long, containing dry air, were determined with a high speed cathode-ray oscillograph. The average speed over a distance of 6.4 meters was found as a function of pressure (0.006 to 8.0 mm Hg) and applied potential (25 to 115 kv). Since the maximum current at the input circuit was limited under most conditions by the tube length, current measurements were made in a section halfway down the tube rather than at the input circuit. Cylindrical wire mesh cages 100 cm in diameter and 60 to 360 cm long, placed concentrically around the tube, were connected to ground through a low resistance. The potential difference across this resistance due to return current in the cage was used to compute the current in a short length of tube, independent of limitations due to finite tube length and without appreciable effect on the discharge itself. The current varied from 35 to 100 amperes, approximately the value necessary to charge a conducting tube of this size to the applied potential. The rate of increase of current in this section was obtained from the slope of these oscillograms.

3. A Theoretical Analysis of Surface Energy as a Cause of Phagocytosis. R. H. LYDDANE AND O. STUHLMAN, JR., *University of North Carolina.*—From a consideration of the free surface energy of a hypothetical cell it will be shown that conditions of equilibrium between a cell and a particle immersed in plasma about to be ingested can be completely described in terms of the contact angle between cell and body when immersed in a given medium. The mathematical analysis shows that the cosine of the contact angle equals $-m/n$ where m is equal to the difference between the surface tensions of the interfaces solid-cell and solid-plasma, and n is the surface tension of the cell-plasma interface. This also describes the relative position of the body with respect to the cell at all times. The cell continues to ingest the particle until the surface energy of the cell has sunk to a minimum.

4. The Construction of an Electron Microscope and Auxiliary Equipment. WM. HURST, *Duke University.*—A magnetic electron microscope is being constructed at Duke University for application to the study of viruses and other biological material. A description is given of the high voltage source, electron beam source, geometry and certain characteristics of the magnetic lens, method of photographing image, pump data, magnetic lens testing equipment and a general outline of the electron microscope assembly.

5. Composition of Mixed Vapors in Cloud Chambers. T. N. GAUTIER AND ARTHUR RUARK, *University of North Carolina.*—The composition of vapors in contact with a liquid mixture is in general not the same as the composition of the liquid; the discrepancy in fact may be large. Data on the composition of the vapor must be employed in getting cross sections for events occurring in cloud chambers. The interesting case is that of ethyl alcohol-water mixtures, because of their relatively large vapor pressures and their frequent use in cloud-chamber work. Curves based on data from the *International Critical Tables* will be presented, giving the vapor pressures of ethyl alcohol and water over mixtures containing various percentages of alcohol by volume. If the cycle of operation of the chamber is relatively short, it is both possible and probable that the evaporation of condensed vapor from the walls and floor of the chamber is not rapid enough to give a close approach to the equilibrium concentrations.

6. Methods of Increasing the Resolving Power of an Ultracentrifuge. J. W. BEAMS, *University of Virginia.*—Mason and Weaver and Svedberg have shown that the resolving power of an ultracentrifuge is proportional to $4\pi^2n^2rh$, where n is the revolutions per second, r the radius, and h the length of the column of solution that can be observed. For large molecular weight substances this resolving power is greatly increased by flowing the solvent through the cell from the periphery toward the axis at the same rate as the material sediments out toward the periphery. This allows the sedimenting boundary to be observed for long periods of time and thus h is effectively increased. If the material being centrifuged is not at the isoelectric point, the resolving power may be increased by passing an electrical current through it in such a direction that the centrifugal and electric forces acting on the particles or molecules balance, thus holding the sedimenting boundary in the field of view for a long period. The apparatus used in the above experiments will be described and the results obtained discussed.

7. X-Ray Diffraction in Cellosolves. THOMAS D. CARR AND A. A. BLESS, *University of Florida.*—X-ray diffraction patterns of methyl, ethyl, and butyl cellosolves have been obtained with an ionization spectrometer using monochromatic x-rays from molybdenum. The patterns show two peaks greatly different in intensity. The principal peak occurs at the same angle for the series, while the secondary peak shifts to smaller angles as the number of carbon atoms increases. The diffraction patterns of these liquids thus resemble the patterns of alcohols as obtained by Stewart

and Morrow,[1] and not those of the ethers, which show only a single peak.[2,3] The similarity of cellosolves to the alcohols thus agrees with the results obtained from dielectric constant measurements.[4] The thickness of the molecules, assuming that it is related to the main peak is found to be 5.26A, while the lengths of the molecules obtained from the secondary peaks are 5.11, 6.36, and 9.66A for methyl, ethyl, and butyl cellosolves, respectively.

[1] Stewart and Morrow, Phys. Rev. **30**, 232 (1927).
[2] W. Noll, Phys. Rev. **42**, 336 (1932).
[3] R. D. Spangler, Phys. Rev. **46**, 698 (1934).
[4] W. H. Byers, J. Chem. Phys. **7**, 175 (1939).

8. The Mechanical Characteristics of the Human Stapes. OTTO STUHLMAN, JR., *University of North Carolina.*—Recent work by the writer has shown that the stapes possesses a superior arch approximately classified as Gothic and an inferior arch of parabolic shape. The data to be presented will show that the superior arch is under tension and the two crura are symmetrical in curvature conforming to the curve y^2 proportional to $x^{1.15}$. The posterior arch is in compression and more parabolic with its posterior crus and anterior crus conforming to the curves y^2 proportional to $x^{0.84}$ and $x^{0.93}$, respectively. Their relation to the non-linear transmission characteristic and aural responses will be pointed out.

9. A Method for Measuring the Optical Rotatory Power of Crystals in the Ultraviolet. NEWTON UNDERWOOD AND CLIFFORD BECK, *Vanderbilt University.*—Light from a mercury arc passes through a monochromator, a Glan-Thompson polarizer, removable 45° glass plate (used in orienting the crystal), the crystal under observation, a Wollaston double-image prism, and falls on a photographic film. If the two images are made of equal intensities by adjusting the plane of polarization of the light incident on the Wollaston to 45° azimuth from an extinction point, the insertion of the crystal into the optical path will change the relative intensities; but the balance may be restored by a compensating rotation of the polarizer. Instead of attempting to make a photograph on a match-point with or without the crystal, exposures are made with the polarizer settings near the expected match-point, which point is then found by graphical interpolation. The microphotometer used to measure the relative density of the images consists of a photo-cell mounted over the eyepiece of a microscope having an illumination system designed for illuminating moving picture sound tracks. The less dense image is placed under the microscope, the amplifier adjusted until the galvanometer reads 100, then when the more dense image is moved into place the galvanometer reads directly its relative density.

10. Precision of a Photoelectric Spectrophotometer in Absorption Measurements. W. C. BOSCH AND K. D. COLEMAN, *Tulane University.*—A multi-range photoelectric spectrophotometer, utilizing electrometer tube amplification, was used to study absorption in various solutions in the 300 to 800-mμ region. The precision of the instrument in locating absorption bands, and in measuring intensity values used in the Beer-Lambert equation, was determined. For substances having sharp absorption bands, such as the dye light green SF yellowish which has a series of sharp multiple frequency bands, band positions were determined to within 1 or 2 mμ. Without observing precautions against stray light, specific and molecular extinction coefficients of materials which, in solution, follow Beer's law, were determined to within ± 2 percent of a mean value for the extinction range 0.1 to 0.8. With suitable selected filters in the incident light beam, stray light error was materially reduced. Extinction coefficients measured in the extinction range 0.1 to 1.0 then showed a deviation from a mean value of approximately ± 1 percent, and values in the 1.0 to 1.5 range were determined with a maximum error of ± 4 percent and an average deviation of ± 2 percent.

11. Infra-Red Absorption of Methyl Alcohol in the Liquid State. D. R. MCMILLAN, JR., *University of North Carolina.*—Recently the infra-red absorption of methyl alcohol vapor has been measured by Borden and Barker.[1] A series of bands was observed and attributed to the various CH and OH vibrations of the molecule. The present work was undertaken to observe the changes in various bands due to associational effects. The region studied has extended from 6μ to 16μ. In the region from 6μ to 8μ the absorption of the liquid is similar in appearance to that of the vapor and two maxima appear at 1467 and 1430 cm^{-1}. These frequencies correspond to 1477 and 1455 cm^{-1} observed in the vapor. The CO vibration that appears at 1034 cm^{-1} for the vapor, appears at 1029 cm^{-1} in the liquid showing that the frequency is practically the same in the two cases. An additional band in the liquid has been observed at 1120 cm^{-1} which is produced by the OH blending vibration. This band cannot be well observed in the vapor state on account of overlapping.

[1] A. Borden and E. F. Barker, J. Chem. Phys. **6**, 553 (1938).

12. A Device for the Preparation of Thin Absorption Cells. E. S. BARR, *Tulane University.*—The observation of infra-red absorption spectra of many liquids involves the use of cell thicknesses of the order of a few hundredths of a millimeter. For the comparison of spectra, it is highly desirable that cell thicknesses be reproducible and of known values. The use of washers between transparent plates, a common procedure, may involve an error due to the film between washer and plate. Furthermore, the preparation of washers of a desired thickness is difficult. In order to facilitate spectral measurements, a device has been constructed which permits the rapid preparation of such thin cells of any desired thickness. This consists of two fluorite plates mounted on heavy brass supports which are accurately parallel to each other and perpendicular to the direction of their motion. The separation of the plates is regulated readily and accurately by means of a calibrated micrometer screw and a small-angle wedge arrangement. The correlation of plate-separation and screw head reading was checked by means of a filar micrometer microscope. Constructional details and technique of use will be discussed.

13. Note on the Ultraviolet Absorption Systems of Benzene Vapor. H. SPONER AND G. NORDHEIM, *Duke University*, AND E. TELLER, *George Washington University*.—It had been shown[1] that the near ultraviolet absorption spectrum at 2700–2200A represents an electronic transition $^1A_{1g}\rightarrow{}^1B_{2u}$ which is forbidden by symmetry and is made allowed when vibrations of type e_g^+ are excited. The transition can be described by the excitation of a double bond electron of character e_g^- into an e_u^+ level. The resulting electronic configuration yields, besides B_{2u}, molecular wave functions of symmetry B_{1u} and E_u^-. A forbidden transition $^1A_{1g}\rightarrow{}^1B_{1u}$ is now suggested for the bands at 2050–1850A and an allowed $^1A_{1g}\rightarrow E_u^-$ transition for the much more intense bands[2] at 1850–1650A. Structural regularities in the first system are discussed. The somewhat irregular vibrational structure of the latter may be due to a slight change in equilibrium configuration because of the degenerate character of the upper level. The continuous absorption underlying this region corresponds perhaps to another electronic transition involving a rupture of one C−H bond. It is assumed that this respulsive state is also responsible for the diffuseness of the $^1A_{1g}\rightarrow{}^1B_{1u}$ system and the predissociation in the $^1A_{1g}\rightarrow{}^1B_{2u}$ transition. The observed two Rydberg series[3] can both be assigned to allowed transitions of symmetry $^1A_{1g}\rightarrow{}^1E_u^-$.

[1] A. L. Sklar, J. Chem. Phys. **5**, 669 (1937); H. Sponer, G. Nordheim, A. L. Sklar and E. Teller, J. Chem. Phys. **7**, 207 (1939).
[2] E. P. Carr and H. Stücklen, J. Chem. Phys. **6**, 55 (1938).
[3] W. C. Price and R. W. Wood, J. Chem. Phys. **3**, 439 (1935).

14. A Linear Densitometer. JOHN A. TIEDEMAN, *Woman's College, University of North Carolina*.—The logarithmic circuit of Meagher and Bentley[1] is used in conjunction with a vacuum photoelectric cell. A bridge circuit employing two balanced amplifier tubes is arranged so that the zero and full scale deflections may be set rapidly. The logarithmic response is obtained from the emission of the hot cathode, with no plate voltage, and a fixed positive voltage on the several grids. The linearity of the device is fixed by the choice of this voltage, and other types of response, not linear, are possible. The device can be made linear within the limits of experimental error for a density range of 0 to 2.7 (which is a transmission range of 500 to 1), and is within 15 percent of linearity for a density range of 0 to 3.2 (which is a transmission range of 1600 to 1). Design considerations for rapid measurement, its use in measuring reflection density and considerations important in calibration are discussed.

[1] R. E. Meagher and E. P. Bentley, Rev. Sci. Inst. **10**, 336 (1939).

15. Discharges Through Oxygen Gas Flames. FREDERICK L. BROWN, *University of Virginia*.—Beams and Snoddy[1] have reported a high voltage discharge between two gas flames. The phenomenon suggested an investigation of the spectra shown in similar discharges. This is a preliminary report on such a survey. As would be expected the oxygen gas flame without discharge shows the OH bands strongly and with varying conditions bands of CH, CN and C_2, but in general, there are no atomic lines. When a discharge is passed through the flame the OH bands are strengthened in the flame and atomic lines of C, O, N, and H appear. Hα is generally strong, especially in a noisy spark, Hβ may be missing or weak, or else strong and partly reversed, depending on voltage, oxygen content and position relative to burner. The spark between the flames shows primarily the nitrogen second positive bands and Hα. Some direct photographs were made of the flames and discharges using a quartz fluorite lens with filters to differentiate between the red and the ultraviolet. These show marked differences.

[1] J. W. Beams and L. B. Snoddy, Phys. Rev. **57**, 63 (1940).

16. A Vibrationless Support for Galvanometers. DUDLEY WILLIAMS, *University of Florida*.—A support of the type described by Strong[1,2] has been constructed. The platform supporting the galvanometer has a 2.0-sec. period of vibration in a horizontal plane and a 0.3-sec. period of torsional vibration about a vertical axis. Since perfectly symmetrical support of the galvanometer platform is difficult to achieve, ordinary building vibrations with horizontal components sometimes produce torsional vibrations of the platform. This difficulty has been minimized by suspending from the galvanometer platform a metal ring with large moment of inertia. The period of torsional oscillation is thereby increased to 1.5 sec. The natural vibrations of the system are damped by oil pans as in Strong's support and also by a set of vanes submerged in an oil reservoir. Methods of suppressing vertical oscillations are discussed.

[1] J. Strong, *Procedures in Experimental Physics* (Prentice-Hall, 1938) pp. 590–592.
[2] R. Müller, Ann. d. Physik **1**, 613 (1929).

17. Probable Error for Poisson Distributions. ERIC RODGERS, *University of Alabama*.—It is shown for Poisson distributions that the probability of obtaining an arbitrary deviation from the average approaches rather rapidly the corresponding probability for normal distributions provided the deviation in each case is expressed in terms of the standard deviation as a unit. Some curves have been plotted showing the manner of approach.

18. Temperature Variation in the Specific Heat of Some Bases by a New Method. R. A. WEISS, *University of Virginia*.—Results using a new method of continuous flow calorimetry[1] are presented. Essentially the apparatus consists of two calorimeters connected in series through which the same fluid flows and the measurements give the relative variation of c_p under differing conditions. Absolute measurement of the fluid flow and the power input are unnecessary. Ratios of resistances only need be determined. The influence of errors is minimized. Application is here made to gases in which the changes in c_p, under varying temperatures from 42°C to 150°C and approximately atmospheric pressure, are compared. The essential features of the calorimeter design of Osborne, Stimson and Sligh[2] are incorporated. This relative method is applicable to other thermal properties of fluids and to varying pressures.

[1] L. G. Hoxton, Proc. Virginia Academy of Science, p. 28 (1931-32).
[2] N. S. Osborne, H. F. Stimson, T. S. Sligh, Jr., Nat. Bur. Stand. J. Research **20**, 119 (1925).

19. Graphs of Hypergeometric Functions Occurring in Continuous Hydrogen Wave Functions. JAMES G. BECKERLEY, *University of Georgia.*—The confluent hypergeometric function

$$ {}_1F_1(a, b, z) = 1 + \frac{a}{b}z + \frac{a(a+1)}{b(b+1)}\frac{z^2}{2!} \cdots $$

has been tabulated for certain real values of a and b, but not for complex values of these parameters. This is inconvenient for problems involving the numerical calculation of continuous hydrogen functions, since these latter contain hypergeometric functions of the type ${}_1F_1(i\alpha+n, 2n, ix)$, where $-1 \leq \alpha \leq 1$ and $n = 1, 2, 3, \cdots$. This paper shows that in order to calculate these functions it is only necessary to compute numerically the real part of ${}_1F_1(i\alpha+n, 2n, ix)$ and this only for two values of n. The imaginary part may then be computed by Kummer's formula. The functions for other values of n may be computed by means of recursion formulas. Numerical results are given in graphical form for ${}_1F_1(i\alpha+1, 2, ix)$ and ${}_1F_1(i\alpha+2, 4, ix)$ for $\alpha = 0$, 0.2, 0.4, 0.6, 0.8, 1.0 and for $-10 \leq x \leq +10$. Comparisons with various asymptotic formulas are given as well as some new formulas for shortening the labors of such numerical calculations. The numerical results can be used for calculating any of the continuous hydrogen functions in repulsive as well as in attractive Coulomb fields. It is also shown that the numerical results may be used in the calculation of any confluent hypergeometric function of the form ${}_1F_1(i\alpha+n, m, ix)$ where n and m are any positive integers and $m = 0$.

20. The Determination of Auroral Intensity by a Photometric Method. L. B. SNODDY AND V. C. SNODDY, *University of Virginia.*—The determination of sky brightness during auroral displays started in the summers of 1937 and 1938[1] were continued at Churchill in Northern Manitoba during this last summer. A visual photometer of the Lummer-Brodhun type was used. The positions of the standard lamp were recorded as dots on a moving paper tape. In this way quite rapid variations in brightness could be followed, since readings could be taken and recorded at less than five-second intervals. Sky brightness in isolated regions was determined as well as the illumination due to large auroral forms. The most important result appears to be the slow decay of sky brightness after all distinct auroral forms have disappeared. This method also enables exact correlation to be made between auroral intensity variations and any accompanying changes in the earth's magnetic field.

[1] L. B. Snoddy and V. C. Snoddy, Trans. Am. Geophys. Union, p. 368 (1939).

21. The Absorption of Cosmic-Ray Shower Particles. W. M. NIELSEN, *Duke University.*—Previous work[1] on the Rossi transition curves at large thickness (lead to iron and iron to lead) has shown that such cosmic-ray showers are electronic in character. G-M counter measurements have now been made of the absorption in lead and in iron of such shower particles. The character of the absorption curves gives new evidence for the electronic character of the showers produced under large depths of absorbing material.

[1] Karl Z. Morgan and W. M. Nielsen, Phys. Rev. **52**, 564 (1937).

22. A Thermionic Milliammeter for Radiofrequency Currents. J. C. MOUZON, *Duke University.*—The use of a filament type radio tube in conjunction with a low range d.c. milliammeter for measuring radiofrequency currents will be discussed. The r.f. current is used to heat the filament of a vacuum tube and the thermionic emission measured with a d.c. meter is used as an indication of the r.f. current.

23. Maximum Temperature Differences Obtained by Radiation to Space Through the Atmosphere. CHARLES M. HECK, *North Carolina State College.*—The average rate of radiation of terrestrial objects toward a clear sky at night (0.02 g cal. per sq. cm per minute) gives no hint as to the maximum temperature differences that can be produced between bodies so radiating but differently insulated from the direct radiation of the earth. The minimum temperatures observed over snow fields and on mountain peaks is compared with results the author obtained using various insulating means and with nested cones. The nested cones produced temperature differences as great as any recorded over snow fields during continuous northern nights. However, the temperature gradients produced with nested cones were some thousand times greater than those produced in nature by radiation to the sky.

24. Flow of Air Through Porous Media. R. R. SULLIVAN AND K. L. HERTEL, *University of Tennessee.*—The value of k, when Kozeny's equation is written,

$$ Q = \frac{2k}{9\mu}\frac{A}{\sigma^2}\frac{(1-c)^2}{c^2}\frac{\Delta p}{X}, $$

has been determined for the flow of air through a porous medium composed of small glass beads. Pressure difference across the bed was of the order of 10^{-2} atmosphere. Thus compression of the air was negligible. k was found to be unity with an uncertainty of less than one percent. It is recognized that this value is not in agreement with that indicated by Carman.[1] In the above equation Q = rate of flow of air in cc/sec., A = area of cross section of porous medium, X = length of porous medium, μ = coefficient of viscosity of air, σ = surface of beads per unit volume of beads, c = volume of beads per unit volume of medium, Δp = pressure drop across plug. All values are in c.g.s. units.

[1] P. C. Carman, Trans. Inst. Chem. Eng. **16**, 168 (1938).

Proceedings of the New York State Section of the American Physical Society

Minutes of the Spring Meeting at Buffalo, New York, April 6, 1940

THE Spring Meeting of the New York State Section of the American Physical Society was held at the University of Buffalo on Saturday, April 6, 1940. The attendance was about 125. The following program of invited papers was presented:

Address of Welcome.—Chancellor S. P. Capen, *University of Buffalo.*

Why Teach Physics in High Schools.—Arthur A. Hammond, *Lafayette High School, Buffalo.*

Measurements in Architectural Acoustics (with Demonstrations).—L. Grant Hector, *University of Buffalo.*

What is News in Physics.—Robert D. Potter, *Science Service.*

Effect of Short Wave Radiation on Trichinella Spiralis.—Frederick J. Holl and L. Grant Hector, *University of Buffalo.*

Some Educational Applications of Optical Instruments.—Harold Osterberg, *Spencer Lens Company.*

At the business session the following officers were elected: Chairman, R. C. Gibbs, Cornell University; Vice Chairman, C. W. Hewlett, General Electric Company; Treasurer, G. H. Cameron, Hamilton College; Secretary, P. R. Gleason, Colgate University; Members of Executive Committee, L. A. DuBridge, University of Rochester and E. L. Manning, State Education Department.

An inspection of the various laboratories of the Physics Department was enjoyed by a large group after the formal meeting had adjourned.

Paul R. Gleason, *Secretary*